bioRxiv preprint doi: https://doi.org/10.1101/2025.05.02.651978; this version posted May 3, 2025. The copyright holder for this preprint (which was not certified by peer review) is the author/funder. All rights reserved. No reuse allowed without permission.

Specialized high-capacity mitochondria fuel cell invasion

Isabel W. Kenny-Ganzert[1], Lena P. Basta[1], Lianzijun Wang[1], Qiuyi Chi[1], Caitlin Su[1], Katherine S. Morton[2,3], Joel N. Meyer[2], David. R Sherwood[1*]

[1]Department of Biology, Duke University, Durham, NC 27708, USA
[2]Nicholas School of the Environment, Duke University, Durham, NC 27708, USA
[3]University of Rochester Medical Center, University of Rochester, Rochester, NY 14642, USA

*Lead contact and correspondence: David. R. Sherwood (david.sherwood@duke.edu)

Keywords: cell invasion; mitochondria; ATP; electron transport chain; biosensor; endogenous tagging; basement membrane

bioRxiv preprint doi: https://doi.org/10.1101/2025.05.02.651978; this version posted May 3, 2025. The copyright holder for this preprint (which was not certified by peer review) is the author/funder. All rights reserved. No reuse allowed without permission.

Abstract

Cell invasion through basement membrane (BM) is energetically intensive, and how an invading cell produces high ATP levels to power invasion is understudied. By generating 20 endogenously tagged mitochondrial proteins, we identified a specialized mitochondrial subpopulation within the *C. elegans* anchor cell (AC) that localizes to the BM breaching site and generates elevated ATP to fuel invasion. These ETC-enriched high-capacity mitochondria are compositionally unique, harboring increased protein import machinery and dense cristae enriched with ETC components. High-capacity mitochondria emerge at the time of AC specification and depend on the AC pro-invasive transcriptional program. Finally, we show that netrin signaling through a Src kinase directs microtubule polarization, which facilitates metaxin adaptor complex dependent ETC-enriched mitochondrial trafficking to the AC invasive front. Our studies reveal that an invasive cell produces high ATP by generating and localizing high-capacity mitochondria. This might be common strategy used by other cells to meet energy demanding processes.

bioRxiv preprint doi: https://doi.org/10.1101/2025.05.02.651978; this version posted May 3, 2025. The copyright holder for this preprint (which was not certified by peer review) is the author/funder. All rights reserved. No reuse allowed without permission.

Introduction

Cell invasion through basement membranes (BMs), a dense sheet-like extracellular matrix (ECM) that surrounds and separates tissues[1], is crucial for development and immune cell trafficking. Despite the formidable barrier formed by BMs, many cells acquire the specialized ability to invade and transmigrate BMs. This includes trophoblasts during embryo implantation, neural crest cells that populate diverse, mesodermal cells during gastrulation, neuronal axons that breach BM to innervate the spinal cord, and immune cells trafficking to sites of infection and injury[2-6]. Dysregulation of cell invasion also underlies many human diseases, such as rheumatoid arthritis, pre-eclampsia, and endometriosis[7-10]. Most notably, the acquisition of invasive behavior initiates cancer metastasis, which is the primary cause of cancer lethality[11]. Despite the physiological and clinical importance of BM invasion, the molecular and cellular mechanisms that drive this specialized behavior are not fully understood.

A unique feature of invasive cells is the ability to form F-actin-rich invadosomes. These membrane-associated protrusive structures harbor and secrete matrix metalloproteinases (MMPs) to breakdown and physically displace BM barriers[12-14]. To develop invasive capabilities, cells require upregulation of ribosome biogenesis, translation of numerous pro-invasive proteins, and de novo lipid synthesis to form dynamic invadosome membrane structures[15-18]. Protein translation, lipid biogenesis, membrane trafficking, and F-actin turnover, all require significant energy in the form of ATP[19-25]. Thus, another distinctive trait of invasive cells that breach BMs are mechanisms to generate high ATP levels to fuel the many molecular and cellular processes required to breakdown BM[26].

Studies in cancer cell lines and tumor samples have revealed that metastatic cancers largely depend on mitochondrial OXPHOS to power invasion[26-29]. For example, there is an upregulation of OXPHOS and mitochondrial biogenesis genes in invasive circulating cancer cells, a decrease in breast and melanoma cancer cell invasion *in vitro* and suppression of metastasis

bioRxiv preprint doi: https://doi.org/10.1101/2025.05.02.651978; this version posted May 3, 2025. The copyright holder for this preprint (which was not certified by peer review) is the author/funder. All rights reserved. No reuse allowed without permission.

in vivo after blocking OXPHOS, and a reliance on OXPHOS for proper invasion of invasive lung cancer leader cells *in vitro*[30]. Mitochondria are also localized to the leading edge of many cancer cells, such as pancreatic, prostate, ovarian, breast, glioblastoma, lung, and hepatocellular, and mitochondria enrich at the leading edge of migrating fibroblasts[31-35]. Work in several cancer cell lines and migrating fibroblasts has found that mitochondrial localization to the leading edge is dependent on kinesin-mediated trafficking along microtubules, although the signals that direct transport and many of the mechanisms mediating trafficking remain poorly understood[31,34,36]. Mitochondrial enrichment is thought to ensure high levels of localized ATP production to fuel F-actin polymerization, membrane dynamics, actomyosin contractility, and focal adhesion turnover required for cell movement and invasion[26,37]. Studies in pancreatic ductal carcinoma cells have further revealed that mitochondria fuse, increase in size and generate more ATP within protrusions invading through artificial matrices[32]. Emerging evidence indicates that mitochondria are uniquely tailored for distinct functions[38-40], whether mitochondria that localize to the leading edge of invasive cells have other unique attributes that facilitate production of high ATP levels required for cell invasion, however, is unknown.

Anchor cell (AC) invasion through BM in *C. elegans* is a visually accessible, highly stereotyped, and genetically tractable *in vivo* model of cell invasion[41,42]. The AC is a specialized uterine cell that invades through the underlying linked gonadal and ventral epithelial BMs to initiate uterine-vulval attachment[43,44]. During AC invasion, a netrin (*C. elegans* UNC-6) cue secreted from the underlying vulval cells polarizes F-actin-rich invadosomes to the invasive front of the AC, where they dynamically assemble and disassemble and depress the BM until one breaches the BM[14,45]. At the site of BM breaching, a large invasive protrusion forms via lysosome exocytosis to expand the BM opening[14,16]. The AC's pro-invasive transcriptional program, including the proto-oncogenes Fos and MECOM transcription factors (*C. elegans* FOS-1 and EGL-43, respectively), and BM breaching machinery, including actin regulators Arp2/3, cofilin, and matrix-degrading MMPs, are shared with invasive metastatic cancer cells[43,46,47]. The AC also harbors a robust

bioRxiv preprint doi: https://doi.org/10.1101/2025.05.02.651978; this version posted May 3, 2025. The copyright holder for this preprint (which was not certified by peer review) is the author/funder. All rights reserved. No reuse allowed without permission.

energy acquisition and delivery system to fuel the invasive machinery, including polarized glucose transporters, glycolytic enzymes, and mitochondria that enrich at the AC's invasive front and provide high levels of ATP to fuel invadosomes and the invasive protrusion[48,49]. The visual and molecular genetic accessibility of AC invasion, combined with a recently completed AC transcriptome[43], provide a powerful model to establish the cellular and molecular underpinnings of mitochondria formation and composition within invasive cells.

Here, using whole-body ATP biosensors, we show that the AC harbors elevated ATP levels during its differentiation as an invasive cell and that ATP peaks and is enriched at the invasive front during BM invasion. By examining AC mitochondrial gene expression, we reveal that genes encoding components of the electron transport chain (ETC) complexes, which work to establish the electrochemical gradient that drives OXPHOS, are highly expressed and enriched in the AC. We endogenously tagged 15 components across all five ETC complexes as well as 5 mitochondrial proteins involved in import and cristae formation with mNeonGreen (mNG). These strains along with electron microscopy, dyes for mitochondrial transmembrane potential and mitochondrial lipid composition, and targeted disruptions, revealed that the AC contains a population of specialized, ETC-enriched, transport enhanced, and cristae dense, mitochondria that are preferentially localized to the invasive front and are required for the high ATP levels for BM invasion. We show these high-capacity mitochondria are specified early during AC invasive differentiation by the AC's proto-oncogenic transcription factor network and reveal that netrin signaling guides their trafficking to the site of BM breaching through mitochondrial metaxin adaptor complexes, microtubules, and the Src family kinase, SRC-1. Together, we present the first extensive endogenously tagged mitochondrial component toolkit and discover a specialized subset of high-capacity mitochondria with increased OXPHOS capability that are preferentially trafficked to the BM breach site to fuel invasion.

bioRxiv preprint doi: https://doi.org/10.1101/2025.05.02.651978; this version posted May 3, 2025. The copyright holder for this preprint (which was not certified by peer review) is the author/funder. All rights reserved. No reuse allowed without permission.

Results

AC mitochondria produce high ATP without increasing volume, number or morphology

Anchor cell (AC) invasion is a highly stereotyped basement membrane (BM) transmigration that can be staged with the underlying 1° fated P6.p vulval precursor cell (VPC) divisions[41,42,50]. The AC is a specialized uterine cell, which is specified between the L2/L3 larval stages (early P6.p 1-cell stage, Figure 1A)[51]. During the L3 stage, the AC grows and expresses many pro-invasive proteins (P6.p 1-cell stage)[52-54]. At the P6.p early 2-cell stage many protrusive F-actin rich invadosomes rapidly form and turn over until one penetrates the BM, which triggers the exocytosis of lysosomes and focused F-actin generation at the breach site to form a single large protrusion[45,55,56]. The protrusion clears a path through the BM, allowing the AC to contact the underlying VPCs and initiate direct uterine-vulval contact (Figure 1A). Mitochondria polarize towards the AC invasive front and generate ATP required to fuel the invasion process[49,57,58]. We previously used an AC-expressed ratiometric ATP:ADP biosensor, PercevalHR[58,59], which revealed a dramatic increase in the ATP:ADP ratio at the site of mitochondria enrichment when BM breaching and protrusion formation occur[58]. This suggested that ATP generation might be uniquely regulated in the AC.

To compare AC ATP metabolism with neighboring non-invasive uterine cells, we expressed the genetically encoded biosensors PercevalHR and iATPSnFR1.0 under the ubiquitous *eef-1a.1* promoter[60]. PercevalHR measures the ATP:ADP ratio, which reflects the free energy of ATP hydrolysis available for driving energy demanding processes[61]. iATPSnFR1.0 is formed from circularly permuted superfolder GFP inserted between the ATP-binding helices of the ε-subunit of a bacterial F0-F1 ATPase and is responsive to physiological levels of cytoplasmic ATP, but not ADP[62]. Interestingly, we found an increase in the ATP:ADP ratio in the AC compared to neighboring uterine cells at the P6.p 1-cell stage (n = 20/20 animals examined) several hours prior to invasion when the AC is growing and translating pro-invasive proteins (Figure 1B). This ratio peaked and was polarized toward the invasive front at the time of BM breaching (Figure 1B,

bioRxiv preprint doi: https://doi.org/10.1101/2025.05.02.651978; this version posted May 3, 2025. The copyright holder for this preprint (which was not certified by peer review) is the author/funder. All rights reserved. No reuse allowed without permission.

2-cell n = 27/27 and 2-4-cell stage, n = 21/21). We similarly found that the fluorescence levels of iATPSnFR1.0 were elevated at the P6.p 1-cell stage and increased ~50% at the time of BM breaching (Figure 1C). Given the known dynamic response range of iATPSnFR1.0 fluorescence to ATP *in vitro*, this likely represents over a 3-fold increase in ATP in the AC at the time of breaching[63]. We also found a ~40% increase in AC iATPSnFR1.0 fluorescence compared to neighboring uterine cells (Figure 1D). Importantly, we have previously shown that *eef-1a.1* drives similar expression levels in the AC and uterine cells and expression does not increase at the time of AC invasion (Figure S1A)[60]. Unlike PercevalHR, which has rapid fluorescence kinetics with exposure to ATP:ADP[61], iATPSnFr1.0 takes up to 10 seconds to return to baseline fluorescence after ATP exposure[63]. This likely accounts for the uniform cytosolic florescence and nuclear localization of iATPSnFR1.0 in the AC[64]. iATPSnFR1.0 is a GFP based sensor and, like GFP, is sensitive to pH[63]. Importantly, we have previously shown that GFP does not show pH sensitivity in the AC[58]. Together, both PercevalHR and iATPSnFR1.0 show that the AC uniquely produces high ATP levels prior to invasion that peak during BM transmigration.

Cellular ATP can be produced via mitochondrial oxidative phosphorylation (OXPHOS) or glycolysis[65]. To establish the contribution of glycolytic metabolism to ATP production during AC invasion, we used the glycolysis ratiometric biosensor HYlight[66]. The fluorescence ratio emitted by HYlight serves as a proxy for glycolytic activity, as it measures the glycolytic metabolite fructose 1, 6-biphosphate (FBP), which is the glycolysis commitment step[66,67]. We found that glycolytic activity as measured by HYlight was the same in the AC as neighboring non-invasive uterine cells (Figure S1B), suggesting that the AC uses OXPHOS to generate higher ATP levels. To directly test this, we reduced OXPHOS by treating worms with rotenone, a potent mitochondrial toxin [68]. Rotenone treatment caused a significant decrease in iATPSnFR1.0 fluorescence (~40%), similar to the reduction in the ATP:ADP ratio we previously reported using PercevalHR[58], and penetrant invasion defects (Figures 1E and 1F; Table S1). In addition, we dissipated the AC's mitochondrial proton gradient by generating transgenic animals with AC-specific overexpression of the

bioRxiv preprint doi: https://doi.org/10.1101/2025.05.02.651978; this version posted May 3, 2025. The copyright holder for this preprint (which was not certified by peer review) is the author/funder. All rights reserved. No reuse allowed without permission.

mitochondrial uncoupling protein UCP-4 (*lin-29p::UCP-4::SL2::mKate2::PH*)[69,70], which also reduced the ATP:ADP AC ratio (Figure S1C). Impaired mitochondria respiration shifts neuronal metabolism towards glycolysis[67]. We thus examined HYlight after rotenone treatment and similarly found increased glycolysis (30% increase in HYlight ratio, Figure 1G, HYlight-Reduced Affinity (-RA) control Figure S1D). This might explain the residual ATP production in AC and moderate invasion defect after OXPHOS inhibition (Figures 1E and 1F). Together, these results implicate a key role for mitochondrial OXPHOS in the increased ATP production necessary for AC invasion.

Mitochondria polarize to the AC invasive front and associate with glycolytic enzymes[58]. Whether AC mitochondria have other features that contribute to high ATP levels is unknown. Increased mitochondrial biogenesis, increased mitochondrial volume, and alterations in mitochondrial morphology are implicated in enhanced ATP production[71-74]. We examined mitochondrial volume and network morphology but found no differences between the AC and neighboring uterine cells (Figure S1E and S1F). Further, we examined the localization of mitochondrial transcription factor-A (TFAM::GFP, *C. elegans* HMG-5::GFP)[75]. TFAM drives mtDNA replication during mitochondrial biogenesis, compacts mitochondrial nucleoids, and TFAM puncta mark mitochondrial nucleoids[75-78]. There was no difference, however, in the number of TFAM puncta in the AC compared to neighboring uterine cells (Figure S1G), strongly suggesting a lack of enhanced AC mitochondrial biogenesis. Together these results offer compelling evidence that the AC does not require greater mitochondria number, volume, or network morphology to drive higher OXPHOS dependent ATP levels required for invasion.

AC mitochondria are enriched for electron transport chain components

We were next interested in determining if AC mitochondria have a distinct molecular composition that might facilitate high ATP production. Mitochondria have two phospholipid bilayers, an outer membrane (OMM) that separates the mitochondria from the cytoplasm, and a

bioRxiv preprint doi: https://doi.org/10.1101/2025.05.02.651978; this version posted May 3, 2025. The copyright holder for this preprint (which was not certified by peer review) is the author/funder. All rights reserved. No reuse allowed without permission.

folded inner membrane (IMM) that encloses the mitochondrial matrix (Figure 2A)[79].These mitochondrial compartments house diverse proteins that perform a variety of functions, including OXPHOS, apoptosis, and calcium regulation[79]. To determine if any mitochondrial molecular functions might be augmented in the AC, we referenced Human MitoCarta3.0, a publicly available dataset of 1136 mitochondrially-associated genes with mitochondrial pathway annotations[80] and identified 1076 known or predicted *C. elegans* orthologs (Table S2). From the *C. elegans* mitochondrial genes, we found genes in 7 mitochondrial pathways were enriched in a recently published AC transcriptome (Figure S2A)[52]. Of those, six pathways encoded proteins involved in the electron transport chain (ETC) and OXPHOS (Figure S2A; Table S2), suggesting that increased levels of ETC components might contribute to elevated AC ATP production.

The ETC is comprised of five multi-protein complexes (CI-V) localized to the IMM and generates an electrochemical proton gradient that is used to drive the rotational catalysis mechanism of ATP synthase (Figure 2A)[81]. RNAi mediated reduction of the transcriptionally enriched complexes I-IV ETC components resulted in invasion defects (Figures 2B and S2B; Table S1), consistent with an important role for the ETC in AC invasion. As components of the OXPHOS complexes might have modulatory roles in ATP production[82], we also used RNAi to target *ant-1.1*, which encodes the dominant *C. elegans* adenosine nucleotide transporter (ANT) that transports ATP out of the mitochondria to the cytoplasm[83-85]. RNAi mediated depletion of ANT-1.1 resulted a strong invasion defect (60%) (Figures 2B and S2B, Table S1). Using the PercevalHR ATP:ADP biosensor, we further found that RNAi mediated reduction of *nuo-1, nduv-2,* and *ucr-2.1* decreased the ATP:ADP ratio in the AC (Figures 2C and S2C). As with rotenone treatment, HYlight revealed increased glycolysis after RNAi mediated reduction to *nuo-1* (Figure S2D).

To determine whether the transcriptional enrichment of ETC components correlated with protein abundance in mitochondria, we used genome-editing to insert mNeonGreen (mNG) at the C-terminus of 15 ETC proteins (Methods). This included genes encoding 4 Complex I (CI) *(nduv-*

bioRxiv preprint doi: https://doi.org/10.1101/2025.05.02.651978; this version posted May 3, 2025. The copyright holder for this preprint (which was not certified by peer review) is the author/funder. All rights reserved. No reuse allowed without permission.

2, nduf-7, nuo-1, nuo-6), 2 Complex II (CII) (*sdhb-1, mev-1*), 3 Complex III (CIII) (*ucr-2.1, isp-1, cyc-1*), 5 Complex IV (CIV) (*cox-10, cox-5a, cox-5b, cox-6a, cox-4*) proteins, and 1 Complex V (CV) (*atp-4*) protein. We assessed the knock-in lines for viability, mitochondrial respiratory capacity, and AC invasion. Of the 15 tagged strains, 4 (*nuo-6, isp-1, cyc-1, atp-4*) were homozygous sterile. Interestingly, when maintained as heterozygotes, progeny of these lines were viable through adulthood (Table S3; see Methods), suggesting a sensitive mitochondrial germline requirement where mitochondria have high activity[86,87]. The growth rates of 7 of the 11 homozygous strains were like wild-type animals, however, 4 were slower growing (Table S3). Seahorse analysis for mitochondrial respiratory capacity of 8 homozygous viable strains revealed normal mitochondria health, with the exception of COX-4::mNG and SDHB-1::mNG, with only COX-4::mNG showing impaired basal function (Figure S2E)[88,89]. Importantly in all 15 tagged strains, homozygous animals displayed normal AC invasion, suggesting ETC function in the AC was largely unaffected (Table S1).

We next measured the fluorescence intensity of each mNG tagged ETC component per mitochondrion and compared ETC component abundance in the AC versus neighboring uterine cell mitochondria at the P6.p 2-cell stage (Figure 2D, 2E, S2F, and S2G). To control for mitochondrial density, we utilized adaptive thresholding and quantified ETC component intensity per mitochondrion (Methods). Strikingly, we found that 14 of the 15 ETC proteins were enriched (~1.2 to 2.1-fold) in the AC mitochondria compared to non-invasive neighboring uterine cell mitochondria (Figures 2D and S2G). One of the main functions of the ETC is to generate the mitochondrial membrane potential ($\Delta\psi$), which is harnessed for ATP production. Using a mitochondrial membrane potential sensitive dye, Tetramethylrhodamine Ethyl Ester (TMRE), we found that the AC has a higher membrane potential than neighboring uterine cells (Figure S2H). We conclude that the AC has ETC-enriched mitochondria that generate an increased membrane potential and produce higher ATP levels. We hereafter refer to these as high-capacity mitochondria.

bioRxiv preprint doi: https://doi.org/10.1101/2025.05.02.651978; this version posted May 3, 2025. The copyright holder for this preprint (which was not certified by peer review) is the author/funder. All rights reserved. No reuse allowed without permission.

High-capacity AC mitochondria have elevated protein import machinery and dense cristae

We next investigated the cellular and molecular composition of the high-capacity AC mitochondria. The ETC localizes to inner mitochondrial membrane (IMM) folds, or cristae, which increase surface area and allow for the dense packing of ETC proteins[90,91]. To assess cristae architecture, we used transmission electron microscopy (TEM) and found that AC mitochondria contain a higher density of cristae per mitochondrion than neighboring non-invasive uterine cells (43% versus 34%, respectively, Figure S3A).

We next asked if there were molecular differences that support high ETC enriched AC mitochondria. We reasoned that high-capacity mitochondria would require greater import of nuclear encoded ETC proteins and mechanisms to support dense cristae. We thus examined the requirement of the mitochondrial protein translocases (*C. elegans* TOMM and TIMM complexes) that facilitate the import of proteins from the cytoplasm, mitochondrial contact site and cristae organizing system (MICOS) components that stabilize cristae, and the cardiolipin synthase (CRLS) enzyme that synthesizes cardiolipin, which stabilizes cristae structure (Figure 3A)[92-94]. We performed an RNAi screen targeting these genes and found that knockdown of nearly all decreased AC mitochondria enrichment of the ETC components NUO-1::mNG (CI), NDUV-1::mNG (CI) and UCR-2.1::mNG (CIII) (Figures 3B, S3B, and S3C; Table S4). Furthermore, RNAi knockdown of *tomm-20* (TOMM complex), *immt-1* (MICOS component), *crls-1* (cardiolipin synthase), disrupted AC invasion and decreased the AC ATP:ADP ratio (Figures 3C and 3D; Table S1). We created endogenous mNG knock-ins in TOMM-20, IMMT-1, and CRLS-1 and found each were enriched in the AC mitochondria compared to the neighboring uterine cells (1.3-1.6-fold, Figures 3E, 3F, and S3D). Similarly, nonyl acridine orange (NAO), which stains for cardiolipin[95], showed ~2-fold more cardiolipin accumulation in AC mitochondria compared with uterine mitochondria (Figure S3E). We conclude that the AC high-capacity mitochondria are built with

bioRxiv preprint doi: https://doi.org/10.1101/2025.05.02.651978; this version posted May 3, 2025. The copyright holder for this preprint (which was not certified by peer review) is the author/funder. All rights reserved. No reuse allowed without permission.

dense cristae and an increased import system to harbor ETC enriched mitochondria that increase ATP production for invasion.

High-capacity mitochondria are established early during AC invasive differentiation

We next wanted to determine if the ETC enriched mitochondria are specified by the AC pro-invasive transcriptional program[96]. EGL-43 (MECOM oncogene) is a core transcription factor of the AC transcriptional network that is crucial to specifying invasive differentiation [43]. RNAi targeting *egl-43* dramatically reduced AC mitochondrial ETC enrichment of NUO-1::mNG and UCR-2.1::mNG, indicating high-capacity mitochondria are a component of the invasive program (Figures 4A and S4A).

To determine when high-capacity mitochondria are formed in the AC, we examined the timing of the molecular enrichment of ETC components, cristae components, and mitochondrial import machinery. The AC and neighboring ventral uterine cells are stochastically specified from two proto-uterine cells (α1 and α2, Figure 4B) that both have the potential to become an AC or VU (ventral uterine cell). The earliest marker of AC fate is upregulation of the LIN-12 (Notch) ligand LAG-2 in the AC (Figure 4B)[97]. We examined AC mitochondrial components that were required for ETC enrichment (TOMM-20::mNG, IMMT-1::mNG, CRLS-1::mNG), as well as ETC components (NDUV-2::mNG, and UCR-2.1::mNG) in combination with *lag-2*p::mCherry::PH (Figures 4C and S4B). We correlated the *lag-2p::*mCherry::PH signal α1:α2 ratio, with the mitochondrial component α1:α2 ratio in proto-uterine cells at the time of AC/VU specification. The non-zero slope, a measure of regression, was only significant for the relationship between TOMM-20::mNG and the *lag-2* driven signal (*i.e.* they both increased in the early specified AC at the same time). This indicates that TOMM-20 is the first component of AC mitochondria to become enriched and that this occurs at the time of AC specification. We next quantified the levels of TOMM-20::mNG, IMMT-1::mNG, CRLS-1::mNG, NDUV-2::mNG, and UCR-2.1::mNG per mitochondrion

bioRxiv preprint doi: https://doi.org/10.1101/2025.05.02.651978; this version posted May 3, 2025. The copyright holder for this preprint (which was not certified by peer review) is the author/funder. All rights reserved. No reuse allowed without permission.

after AC specification (E1C) and leading up to (1C-2C) and after (4C) AC invasion. We found that all components at the E1C stage were elevated compared to neighboring uterine cells and that TOMM-20 remained stable across time, IMMT-1 peaked at the E1C, CRLS-1 increased over time, and both ETC proteins peaked between 1C and 2C (Figures 4D, S4C, and S4D). Transcriptional reporters of *nuo-1* and *nduv-2* (*nuo-1*p::mNG; *nduv-2*p:mNG) confirmed an increase in expression after AC specification at the E1C stage (Figure S4E). Together, these results indicate that high-capacity AC mitochondria are specified by the pro-invasive transcriptional network and begin forming during AC specification.

Basal AC mitochondria are high-capacity and distinct from apical mitochondria

We have previously reported that mitochondria polarize at the AC invasive front [58]. To better quantify this enrichment, we determined the volume of mitochondria in the apical and basal portions of the AC and found that ~70% of the total mitochondria are basally localized at the 2-cell stage, while neighboring uterine cells showed equal apical/basal distribution (Figure S5A). Additionally, we found that the basal mitochondria population had higher mitochondrial membrane potential ($\Delta\psi$m, TMRE staining) compared to apical mitochondria (Figure S5B). This suggested that basal AC mitochondria might be distinct from the apical mitochondria.

To determine if the composition of basal mitochondria is distinct from apical mitochondria we utilized adaptive thresholding and quantified ETC component intensity per mitochondrion of endogenously tagged ETC components (as in Figure 2) and TOMM-20, IMMT-1, and CRSL-1 (Figure 3). We found that all but one was significantly enriched (1.5-2.0-fold) in the basal mitochondria compared to apical mitochondria (Figures 5A, 5B, and S5C). We also discovered that mitochondria are initially uniformly distributed in the AC shortly after AC specification (early-1-cell stage), but segregate into two populations at the late 1-cell stage (Figure 5C).

To ascertain if these two populations of mitochondria intermix or remain distinct once established, we performed fluorescence recovery after photobleaching (FRAP) on mitochondria

bioRxiv preprint doi: https://doi.org/10.1101/2025.05.02.651978; this version posted May 3, 2025. The copyright holder for this preprint (which was not certified by peer review) is the author/funder. All rights reserved. No reuse allowed without permission.

marked with endogenous NUO-1::mNG at the 2-cell stage prior to invasion. A portion of basal invasive mitochondria were photobleached, then the change in fluorescence intensity in the bleached and non-photobleached apical and neighboring basal mitochondria was measured to determine if, and from where, mitochondria moved into the bleached region (Figure 5D). We found that following photobleaching, the mitochondrial signal in the bleached basal mitochondria recovered and that the mitochondrial signal in the non-photobleached adjacent basal region decreased, while the apical signal was unchanged (Figures 5E and S5D). In contrast, similar photobleaching of neighboring non-invasive uterine cells revealed exchange between all mitochondria in the cell (Figures 5E and S5D). We conclude that the AC contains two spatially and compositionally distinct mitochondrial populations, with a specialized high-capacity basal mitochondria population with a higher membrane potential isolated from an apical population with lower ETC levels and decreased membrane potential.

High-capacity mitochondria localize to the BM breach site and are polarized by netrin

We next wanted to examine high-capacity mitochondrial behavior during BM breaching and protrusion formation. Using endogenously-tagged type IV collagen to mark the BM (EMB-9::mRuby)[98] with NUO-1::mNG to image high-capacity mitochondria in the AC, we performed time-lapse imaging of BM breaching and protrusion formation. In all cases we observed high-capacity mitochondria at breach site and concentrated within the emerging invasive protrusion (n = 6/6; Figures 6A, S6A, and S6B; Movie S1-3). Netrin (*C. elegans* UNC-6) secreted from the underlying 1° fated P6.p VPCs polarizes invadosomes, the invasive protrusion, and prenylation enzymes towards the invasive plasma membrane[16,45,56,58,99]. To determine if netrin signaling also polarizes high-capacity mitochondria towards the invasive front at the time of BM breaching, we examined high-capacity mitochondria (marked with NUO-1::mNG) in an *unc-6 (ev400)* null mutant. Loss of netrin disrupted high-capacity mitochondria basal enrichment and the basal enrichment of the ATP:ADP ratio (measured by PercevalHR) (Figures 6B and 6C). We conclude

bioRxiv preprint doi: https://doi.org/10.1101/2025.05.02.651978; this version posted May 3, 2025. The copyright holder for this preprint (which was not certified by peer review) is the author/funder. All rights reserved. No reuse allowed without permission.

that netrin signaling directs high-capacity mitochondria to the invasive front and that mitochondria dynamically concentrate at the BM breach site and in the protrusion.

Netrin/Src polarizes microtubules to direct high-capacity mitochondria via metaxin adaptors to the invasive front

Microtubules transport mitochondria to areas of high ATP demand in neurons and migrating cells in culture[31,32,35,100,101]. Netrin regulates microtubule dynamics, stability, and elongation to attract and direct growing neuronal axons[102]. We have previously shown that microtubules are enriched at the invasive front[58]. To determine if netrin regulates microtubules in the AC, we visualized AC microtubules using an endogenously tagged microtubule-binding domain of ensconsin (*lin-29p*::EMTB::GFP) in wild-type animals and *unc-6* mutants and found that microtubule basal enrichment was greatly reduced (Figure 7A). Microtubules have two functionally distinct ends – the plus end with β-tubulin exposed which polymerizes/depolymerizes faster than the minus end with α-tubulin exposed[103]. To determine if microtubules are polarized in the AC, we examined the endogenously-tagged plus-end protein (EBP-2::GFP) and minus-end protein (GFP::GIP-1)[104], and found that microtubules in the AC are oriented with the plus-end at the basal end of the cell and the minus-end at the apical (Figures 7B). These observations suggest that trafficking along polarized microtubules could direct high-capacity mitochondria to the invasive front.

Microtubules serve as tracks for motor proteins and their adaptors to transport cargo. Notably, genes encoding mitochondrial trafficking proteins were among the upregulated MitoCarta pathways in the AC transcriptome (Table S2). Of these mitochondrial associated proteins, we were particularly interested in MTX-1, a metaxin, which functions as an OMM mitochondrial adaptor for plus ended directed mitochondrial trafficking[105,106]. The two *C. elegans* metaxin homologs, MTX-1 and MTX-2, have functionally distinct roles in trafficking. MTX-2 works with the known microtubule adaptor, MIRO-1, as part of the core adaptor complex for both microtubule

bioRxiv preprint doi: https://doi.org/10.1101/2025.05.02.651978; this version posted May 3, 2025. The copyright holder for this preprint (which was not certified by peer review) is the author/funder. All rights reserved. No reuse allowed without permission.

plus-end and minus-end transport, whereas MTX-1 only serves as an adaptor for plus-end transport[106]. RNAi-mediated loss of *mtx-1* and *mtx-2*, significantly reduced the basal polarity of high-capacity mitochondria (Figures 7C and S7A). Furthermore, we endogenously-tagged both *mtx-1* and *mtx-2* with mNG and found MTX-1::mNG and MTX-2::mNG are basally enriched in the AC and thus enriched in the high-capacity mitochondria (Figure 7D). We also found that metaxin localization was dependent on netrin signaling and loss of netrin (*unc-6* mutant) resulted in a loss of basal metaxin enrichment (Figure S7B). We conclude that high-capacity mitochondrial enrichment at the site of invasion is netrin dependent and that basally localized mitochondria are trafficked on plus-end microtubules using the metaxin adaptor complex.

We next wanted to determine what links the netrin (*unc-6*) directional cue to polarized microtubule transport. Evidence suggests that Src family kinases couple netrin signaling to microtubule dynamics through phosphorylation of β-tubulin, which regulates microtubule dynamics[102,107]. *C. elegans* harbor two *src* genes*, src-1* and *src-2*[108] and *src-1* is expressed at high levels in the AC transcriptome[52]. We examined endogenously-tagged SRC-1::GFP and found basal AC enrichment in an *unc-6* dependent manner (Figure 7E). Further, the basal enrichment of both mitochondria and microtubules was reduced in a *src-1(lq185)* mutant background (Figures 7F and 7G), indicating that SRC-1 polarizes microtubules and mitochondria to the basal invasive front.

AMPK, an energy sensor and metabolic regulator, has been shown in ovarian cancer cells to direct mitochondria to the leading edge of lamellipodia[31]. RNAi knockdown of four AMPK components (*aak-1*, *aak-2*, *aakb-1*, and *aakb-2)*, however, did not disrupt mitochondrial localization (Figure S4D). Interestingly, previous studies in neurons and several cancer cell lines have shown that loss of ATP production reduces mitochondrial trafficking along microtubules[31,35,109-111]. suggesting that ATP output could be used as a mechanism that preferentially traffics high-capacity AC mitochondria along polarized microtubules to the invasive front. Consistent with this notion, both pharmacological (rotenone treatment) and genetic (*nuo-1*

bioRxiv preprint doi: https://doi.org/10.1101/2025.05.02.651978; this version posted May 3, 2025. The copyright holder for this preprint (which was not certified by peer review) is the author/funder. All rights reserved. No reuse allowed without permission.

RNAi) perturbation of ETC function resulted in a loss in the basal enrichment of high-capacity mitochondria (Figures 7H and S7C). Taken together, our results suggest a model where netrin (UNC-6) signaling through SRC-1 polarizes microtubules towards the invasive front. This facilitates trafficking of high-capacity mitochondria harboring the metaxin adaptor complex to supply high levels of ATP for BM breaching (Figure S7E).

Discussion

There is an emerging notion that mitochondria specialize to meet the functional needs of different cells and tissues[38,112]. Tissue level biochemical studies provided the first evidence of specialized mitochondria and showed distinct mitochondrial proteomes in the mouse brain, liver, heart, and kidney[113]. This was followed by findings that identified distinct mitochondria within different cell types, including mitochondria in oocytes lacking assembled ETC complex I to mitigate damaging ROS production[114], mitochondria within fibroblasts that lack ATP synthase and are specialized to produce proline and ornithine[115], and mitochondria with decreased matrix proteins and mitochondrial DNA and an upregulated Ca^{2+} uniporter that regulate filipodia length in osteosarcoma cells[40].

Here we show that the *C. elegans* AC has specialized mitochondria that produce high levels of ATP to fuel invasion through BM. Transcriptomic analysis revealed broad enrichment of ETC components and examination of 15 endogenous mNeonGreen (mNG) tagged ETC components identified a distinct subpopulation of mitochondria localized to the invasive front of the AC. In these high-capacity mitochondria, increased TOM complex transport proteins and dense cristae facilitate import and housing of higher levels of ETC components that produce an elevated mitochondrial membrane potential driving high ATP production at the site of BM breaching. Notably, these mitochondria form shortly after AC specification, and this coincides with increased ATP levels a full ~5 hours before AC invasion. The elevated ATP prior to invasion likely supports energy demanding cellular processes necessary for invasion, such as increased

bioRxiv preprint doi: https://doi.org/10.1101/2025.05.02.651978; this version posted May 3, 2025. The copyright holder for this preprint (which was not certified by peer review) is the author/funder. All rights reserved. No reuse allowed without permission.

translation of pro-invasive proteins and de novo lipid synthesis[16-18,52]. Further, we found mitochondrially produced ATP peaked at the time of BM breaching when energy consuming invasive protrusion dynamics occur[58]. Notably, there was also heterogeneity in the upregulation of different ETC components within the high-capacity mitochondria, both within ETC complexes and between complexes. The difference in stoichiometry between components may indicate further specialization of ETC function and highlights an unknown complexity of the ETC.

The AC high-capacity mitochondria appear to be built for heightened ATP generation, which modeling experiments suggest is the rate limiting step for supplying cytosolic ATP[116]. ETC-enriched mitochondria might be a common strategy for cells to support energetically demanding processes. For example, proteomic studies of mitochondria in the heart and synapse, which both are energy intensive, have shown mitochondria contain higher levels of some ETC components[117,118]. Further, imaging studies at the synapse, have revealed these mitochondria contain dense cristae and elevated cytochrome C (complex III)[119]. [120]. Adipocyte mitochondria associated with lipid droplets also have dense cristae, elevated levels of the ETC complex IV component Cox4 and elevated respiratory capacity, which is thought to support ATP-dependent triacylglyceride synthesis[121]. In addition, high levels of ETC might be a common feature of invasive cells, as studies in aggressive ovarian, breast, pancreatic, and lymphoma cancers have revealed upregulation of various ETC components and complexes[122-129].

Mitochondria traffic on microtubules to areas of high energy demand, including to the leading edge of invasive and migrating cells and to neuronal synapses and dendrites[31,36,37,100,110,130,131]. However, the cues and mechanisms that direct trafficking are largely unknown. Our studies indicate that netrin signaling is a key component of high-capacity mitochondria trafficking to the site of BM invasion through polarization of microtubules to the invasive front. It's been proposed that netrin signaling polarizes microtubules to redirect microtubules towards sources of netrin by balancing both the promotion of microtubule dynamics and stabilization[132,133]. Evidence suggests that netrin might stabilize microtubules through Src

bioRxiv preprint doi: https://doi.org/10.1101/2025.05.02.651978; this version posted May 3, 2025. The copyright holder for this preprint (which was not certified by peer review) is the author/funder. All rights reserved. No reuse allowed without permission.

family kinase mediated phosphorylation of tubulin[133]. Consistent with Src acting downstream of netrin to polarize microtubules, we discovered that SRC-1 is upregulated in the AC and localized to the invasive front in a netrin dependent manner. Further, loss of *src-1* disrupted microtubule and high-capacity mitochondria polarization.

We also show that high-capacity mitochondrial trafficking is dependent on metaxin adaptors. Metaxins were first identified as mitochondrial proteins in the sorting and assembly machinery (SAM) complex and have been separately found to be essential in TNF-induced apoptosis[134,135]. Evidence from *C. elegans*, *Drosophila*, and human neurons suggests that metaxin-2 is also a core component of a mitochondrial transport adaptor complex and in combination with either metaxin-1 or TRAK-1 directs plus end or minus end mitochondrial movements, respectively[105,106]. Our work extends the function of metaxins beyond neurons to invasive and migratory cells. In the AC we found that the plus-ends of microtubules are oriented towards the site of BM invasion. Consistent with studies in neurons, loss of *mtx-1* (plus-end adaptor) and *mtx-2* (core adaptor) dramatically perturbed basal (plus-end directed) enrichment of high-capacity mitochondria. Further, we previously found that loss of TRAK-1 alone does not alter basal mitochondria enrichment[58], suggesting a minor or absent function for minus end directed movement in high-capacity mitochondria positioning.

An open question is how high-capacity mitochondria preferentially localize to the invasive front over mitochondria that have reduced ETC components and ATP production and remain apically in the AC. AMPK, an energy sensor, has been shown to direct mitochondria to leading edge of lamellopodia in ovarian cancer cells, although the molecular targets of this kinase for directing trafficking are not known[31]. However, we did not observe defects in high-capacity mitochondrial trafficking after knockdown of four AMPK components, suggesting AMPK does not regulate mitochondrial trafficking in the AC. Reduction of the ETC component NUO-1 and inhibition of OXPHOS with rotenone, which both reduced ATP production, however, perturbed high-capacity mitochondrial enrichment to the invasive front. Thus, when high-capacity

bioRxiv preprint doi: https://doi.org/10.1101/2025.05.02.651978; this version posted May 3, 2025. The copyright holder for this preprint (which was not certified by peer review) is the author/funder. All rights reserved. No reuse allowed without permission.

mitochondria no longer produce elevated ATP, they appear not to be basally trafficked. As ATP diffusion is limited in cells[136] and trafficking on microtubules is energy intensive[31,137], one possible explanation is a competitive self-organizing system, where high-capacity mitochondria with MTX-1 (plus ended directed adaptor) and increased ATP output are more competitive in moving along microtubules, and thus preferentially traffic to the ends of microtubules at the invasive front. Consistent with this model, disruption of ATP production in mitochondria limits their trafficking in cancer cells and neurons[35,109-111]. Molecular competition of shared limited resources is known to govern a number of biological processes, such as preference for mRNA competition to be translated by ribosomes, sigma factor competition to bind with RNA polymerase to dictate gene transcription, and competition between RNA binding proteins that drives localized phase separation in *C. elegans* embryos[137-139]. As metaxins are also enriched on high-capacity mitochondria, this could bestow the high-capacity mitochondria an additional competitive advantage in loading on to microtubules.

Mitochondria are responsible for numerous cellular processes beyond ATP production, including fatty acid synthesis, stress response, cell-cell signaling, and calcium homeostasis[140,141]. Thus, specialized mitochondria might be a common, but hidden feature of cells. A key impediment in assessing mitochondrial diversity is the challenge of detecting differences in individual mitochondrial molecular composition within and between cells. By endogenously editing 20 genes with mNG tags whose encoded proteins are components of mitochondria—15 ETC, two cristae, two metaxins and a TOMM complex component—our studies have greatly expanded the toolkit of live cell reagents to examine mitochondrial diversity. Our endogenously tagged strains have revealed ETC-enriched high-capacity mitochondria in the AC and led to insights into single cell mitochondrial heterogeneity, specialization, specification, and trafficking. As the lineages and differentiation programs for *C. elegans* cells are known in detail[142], this emerging toolkit can be used and expanded to investigate mitochondrial specialization in other cell types, how mitochondria are regulated in cell division, apoptosis, and oogenesis, how mitochondria respond

bioRxiv preprint doi: https://doi.org/10.1101/2025.05.02.651978; this version posted May 3, 2025. The copyright holder for this preprint (which was not certified by peer review) is the author/funder. All rights reserved. No reuse allowed without permission.

to environmental changes, and how mitochondria are altered during aging. Our Mitocarta-based curation indicate approximately 1000 known proteins associated with *C. elegans* mitochondria. Ultimately, it should be possible to endogenously tag most of these mitochondrial components, which offers to reveal the breadth of mitochondrial diversity and lead to new insights into unknown mitochondrial functions.

Limitations of this study

Our studies indicate that the AC has ETC enriched mitochondria that generate a higher membrane potential and ATP to drive cell invasion. The ETC is composed of over 100 components that are subdivided into five complexes, each with unique functions[143]. Testing the function of the entire upregulated ETC complex was not possible. Instead, we relied on a diverse approach and targeted individual ETC components, chemically inhibit complex I, reduce mitochondrial membrane potential, and decrease ATP release from mitochondria. While our data demonstrate that the ETC is upregulated to generate more ATP, we cannot rule out upregulation enhances or alters other functions of the ETC, such as ROS signaling, metabolite transport, Ca^{2+} regulation, and regeneration of electron carriers[140,141]. A related limitation is that we could weaken ETC upregulation but not eliminate it. Thus, while we were able to target the enriched ETC by knocking down individual components, reduce the membrane potential with the uncoupler UCP-4, and target the ATP transporter *ant-1.1*, we could not completely reduce the upregulated ETC and thus cannot assess its full contribution to breaching the BM and cell invasion.

Methods

Experimental Model Details

Caenorhabditis elegans (*C. elegans*) were maintained at 20°C on nematode growth media (NGM) plates and fed *Escherichia coli* strain OP50. In text and figures, wild-type refers to N2 Bristol strain *C. elegans,* and standard *C. elegans* nomenclature is used to convey genotypes of

bioRxiv preprint doi: https://doi.org/10.1101/2025.05.02.651978; this version posted May 3, 2025. The copyright holder for this preprint (which was not certified by peer review) is the author/funder. All rights reserved. No reuse allowed without permission.

553 strains. Promoter-driven transgenes are denoted by the italicized gene name followed by “p”, “::”
554 signifies an adjoining protein, and italicized mutant alleles are enclosed within parentheses
555 following the gene name. As previously described, anchor cell (AC) invasion was scored in L3
556 hermaphrodites and staged in reference to the number of vulval precursor cells (VPCs) (Figure
557 1)(Sherwood and Sternberg, 2006). Synchronization of L1 animals was performed using
558 standard hypochlorite treatment for all RNAi and rotenone experiments[144]. All endogenously
559 tagged strains in this study were generated by injecting into the gonads of wild-type *C. elegans*.
560 Endogenous strains that were homozygous infertile were either maintained by picking animals
561 with the fluorescent signal of interest or crossed with a balancer strain (detailed in Key
562 Resources Table). Measurements of fluorescence intensity in all strains were done in
563 homozygous animals (See Table S3 for details on the health of endogenous tagged strains). All
564 animals were well-fed (3+ generations without starvation) prior to any experimentation or
565 imaging to control for nutrient-dependent phenotypes. All genotypes of all strains were verified
566 by genotyping PCR and/or plate-level phenotype, such as “unc” – uncoordinated animals that
567 are unable to crawl. All strains used in this study are listed in the key resources table.
568
569 **Construction of endogenously-tagged strains**
570 CRISPR-Cas9 mediated genome editing with a self-excising hygromycin selection cassette
571 (SEC) was used to generate endogenously tagged strains[145]. In brief, optimal location to insert
572 the fluorescent protein was identified based on the tertiary and quaternary structure of the
573 protein and any protein cleavage sites were accounted for (such as mitochondrial localization
574 sequences that get cleaved). To generate the SEC repair plasmids, N2 gDNA was used as a
575 template to amplify ~2KB homology arms upstream and downstream of the PAM site. To ensure
576 the Cas9 doesn’t subsequently cut the PAM site after the initial insertion cut, the mNeonGreen
577 (mNG) was inserted in between the guide sequence and PAM or silent mutations to the guide
578 sequence were made in the homology arms. The homology arms were inserted into the vector

bioRxiv preprint doi: https://doi.org/10.1101/2025.05.02.651978; this version posted May 3, 2025. The copyright holder for this preprint (which was not certified by peer review) is the author/funder. All rights reserved. No reuse allowed without permission.

mNG-C1^SEC^bothlink SEC repair template[146] and confirmed correct assembly by colony PCR and sequencing. PureLink™ HiPure Plasmid Miniprep (Invitrogen #K210002) was used to isolate high purity sgRNA plasmid DNA and SEC repair plasmid DNA for injection. https://crispor.gi.ucsc.edu/ was used to identify short guide sequences where the fluorescent protein should be inserted and PAM sites where the Cas9 protein cleaves. The short guide RNA (sgRNA) plasmid was generated by cutting the Cas9 guide plasmid, pDD122 (Addgene, #47550), with NheI and EcoRV, then using HiFI assembly (New England Biolabs, #E2621L) to insert the respective sgRNA sequences into the plasmid. For each strain the germline of 10-30 young adult N2 hermaphrodites were injected with a mixture containing 100ng/µL of the SEC repair plasmid DNA, 50ng/µL of the sgRNA plasmid DNA, and 2.5 ng/ul of co-injection markers (pCFJ90 *myo*-2p::mCherry, pCFJ104 *myo*-3p::mCherry). After 3-4 days at 20°C, F1 progeny of singled-out injected animals were treated with 500µl of 2mg/ml Hygromycin B (Sigma-Aldrich #H3274). Candidate knockin animals exhibited rolling (due to *sqt-1(e1350)* within the SEC), survived Hygromycin B treatment, and lacked the red fluorescent co-injection markers. F2 rolling (*sqt-1(e1350)*+) animals were singled, confirmed homozygous knockin through roller phenotypes and presence of consistent fluorescence signals. To excise the SEC, we heat shocked about 6 L3/L4 homozygous rollers at 34°C in a water bath for 4 hours. After 3-4 days, adult non-rolling animals were singled to check for homozygous excision by confirming loss of rolling in all progeny. Successful genome editing was verified by visualizing fluorescence and PCR genotyping. See Table S5 for list of oligonucleotides used in strain generation and genotyping and See Key Resources Table for all strains.

Construction of promoter-driven transgenic strains

Promoter-driven transgenic strains were generated through the Mos single copy insertion (MosSCI) on Chromosome I or Chromosome II or extrachromosomal array integration.

bioRxiv preprint doi: https://doi.org/10.1101/2025.05.02.651978; this version posted May 3, 2025. The copyright holder for this preprint (which was not certified by peer review) is the author/funder. All rights reserved. No reuse allowed without permission.

Promoters and fusion proteins were either amplified from N2 gDNA (*nuo-1* promoter, *nduv-2* promoter, *ucp-4*, *tomm-20*), another plasmid (*eef-1A.1* promoter, *lin-29* promoter, *GFP, mNeonGreen, mKate2, PercevalHR, HYlight, HYlight-RA*), or a *C. elegans* codon-optimized gene block (*iATPSnFR1.0*). The Cas9 guide plasmid, pCFJ352, which is targeted near the ttTi4348 Mos insertion site, was used to generate transgenes via the Mos single copy insertion (MosSCI) on chromosome I. pCFJ352 was a gift from Erik Jorgensen (Addgene plasmid # 30539; http://n2t.net/addgene:30539; RRID:Addgene_30539). The Cas9 guide plasmid, pDD122, which is targeted near the ttTi5605 Mos insertion site, was used to generate transgenes via the Mos single copy insertion (MosSCI) on chromosome II[147].The SEC repair plasmids for MosSCI chromosome I (pAP088) and MosSCI chromosome II (pAP087) were cut with restriction enzymes, NheI and NotI, then the respective promoter and fusion protein were cloned into the cut SEC repair plasmid backbone using NEBuilder HiFi DNA Assembly master mix (NEB, #E2621L). Injection, selection, excision, and genotyping were performed as described above. The following strains were generated by MosSCI: The biosensors (iATPSnFR1.0 and HYlight) and their controls (cytosolicGFP and HYlight-RA) were driven by the *eef-1A.1* ubiquitous promoter. Ubiquitous mitochondrially-localized mKate2 to visualize all mitochondria independent of endogenous fluorescence intensity (driven by *rpl-28* ubiquitous promoter) and AC-specific overexpression of UCP-4::SL2::mKate2 (driven by the AC promoter *lin-29*). See Key Resources Table for all strains.

To generate strains using extrachromosomal array integration, *unc-119(ed4)* hermaphrodites were injected with promoter-driven fusion protein plasmids, 50 ng/ml *unc-119*+ rescue DNA, 50ng/ml pBsSK, and 25 ng/ml EcoRI cut salmon sperm DNA. Stable extrachromosomal lines were established and then integrated using gamma radiation[148]. To reduce the possibility of background mutations resulting from radiation, integrated lines were backcrossed three times with N2 animals. See Key Resources Table for all strains.

bioRxiv preprint doi: https://doi.org/10.1101/2025.05.02.651978; this version posted May 3, 2025. The copyright holder for this preprint (which was not certified by peer review) is the author/funder. All rights reserved. No reuse allowed without permission.

630

631 **Feeding RNAi**

632 RNA interference (RNAi) was performed by feeding animals *Escherichia coli* strain HT115
633 containing the L4440 RNAi vector targeting genes of interest or the empty L4440 vector. RNAi
634 clones were sourced from either the Vidal or Ahringer feeding RNAi libraries, then streaked out
635 on LB plates containing tetracycline and ampicillin. A single RNAi colony was inoculated in LB
636 with 100 µL/mL Ampicillin (Sigma-Aldrich #A0166) and grown overnight (12-16 hours) at 37°C in
637 an incubator with a shaker. To induce double-stranded RNA expression, 1 µL/mL isopropyl β-d-
638 1-thiogalactopyranoside (IPGT, Sigma-Aldrich #I6758) was added to RNAi cultures and placed
639 back in the 37°C shaker for 1 h. After initial dsRNA induction, RNAi cultures were seeded on
640 NGM plates containing topically applied 1mM IPTG and 100-mg/ml ampicillin and allowed to dry
641 at room temperature overnight for further induction. All RNAi clones were sequenced to confirm
642 correct target gene.
643 Synchronized L1 animals were plated on RNAi NGM plates, fed for 39 hours for imaging P6.p 2-
644 cell stage or 42 hours to score invasion at the P6.p late 4-cell stage. For every RNAi
645 experiment, a negative control (empty L4440 RNAi vector) and either knockdown efficiency
646 measurement (Table S6) or positive control (*fos-1a* RNAi that causes a penetrant invasion
647 defect) was used to ascertain RNAi activity.

648

649 **Rotenone Treatment**

650 Rotenone (EMD Millipore #557368) was reconstituted in DMSO to make a 20mM stock solution
651 and stored at -20°C. Synchronized L1 animals were plated on NGM plates seeded with *E. coli*
652 OP50 and allowed to grow for 34 hours at 20°. Early L3 larvae were washed off from NGM
653 plates with M9 solution and collected into 1.5 mL canonical tubes. 20mM rotenone (final
654 working concentration 40 µM) were added to the collecting tube and placed on a rocker or
655 rotator (to avoid hypoxia) for 2-hours at room temperature. The same volume of DMSO in M9

bioRxiv preprint doi: https://doi.org/10.1101/2025.05.02.651978; this version posted May 3, 2025. The copyright holder for this preprint (which was not certified by peer review) is the author/funder. All rights reserved. No reuse allowed without permission.

was used on control animals for the equivalent amount of time. Before imaging, animals were recovered from the incubation onto fresh OP50 NGM plates.

Seahorse Extracellular Flux Analyzer-based measurements of mitochondrial respiration

All experiments were performed with bleach synchronized L3 *C. elegans* from wild-type N2 lines and 8 endogenously tagged ETC component lines (*nuo-1::mNG*, *nduv-2::mNG*, *sdhb-1::mNG*, *mev-1::mNG*, *ucr-2.1::mNG*, *cox-4::mNG*, *cox-6A::mNG*, *cox-10::mNG*). L3 *C. elegans* were washed from OP50 plates and transferred into each well of a 24-well Seahorse plate. The Seahorse Extracellular Flux Bioanalyzer was used to quantify oxygen consumption rate (OCR) as described in previous studies[149]. The number of individual animals per well were counted using confocal imaging of the plate to normalize the OCR measurements per individual worm. For each of the 9 lines, 5-10 L3 animals per strain were used and four technical replicates were done for each strain.

Assessment of AC invasion

Assessment of anchor cell (AC) invasion was performed as previously described[42]. In brief, synchronized L3 animals at the VPC P6.p late 4-cell stage were mounted onto 5% agar with 1% sodium azide to anesthetize the worms and imaged on a Ziess upright compound microscope equipped with 488 and 561 nm filters and a Nomarski prism for differential interference contrast (DIC). The assessment of AC invasion was based on two indicators: loss of the DIC phase dense BM line and absence of the fluorescence BM marker underneath the AC. Complete removal of the BM resulting in a gap of the width of anchor cell nucleus is scored as normal invasion. Incomplete or blocked invasion is scored if the size of the BM gap is less than the width of the AC nucleus or fully intact respectively. The sensitized strain referred to in Table S1

bioRxiv preprint doi: https://doi.org/10.1101/2025.05.02.651978; this version posted May 3, 2025. The copyright holder for this preprint (which was not certified by peer review) is the author/funder. All rights reserved. No reuse allowed without permission.

is null for matrix metalloproteases (MMPs) *zmp-1, 3, 4, 5, 6*. Loss of MMPs delays invasion and requires more ATP to breach the BM[49].

Mitochondria import and cristae screen

Candidate genes for the mitochondrial import and cristae screen were compiled by finding *C.elegans* orthologs of mammalian genes annotated as having a role in mitochondrial protein import and cristae formation[80] for which RNAi clones were available and sequenced correctly. RNAi plates were made according to the RNAi protocol described above. Screening was conducted with the strain (NK2657) with co-labeled endogenous NUO-1::mNG (mNeonGreen) and AC-specific plasma membrane marker (mCherry). Animals were synchronized by hypochlorite treatment, plated on RNAi or L4440 control, and grown until the VPC P6.p 2-cell stage. Screening was performed on a Ziess upright compound microscope equipped with 488 and 561 nm filters. We scored animals for the loss of NUO-1::mNG fluorescence enrichment in the AC compared to the uterine cell within the same animal. Systematic effects of the RNAi were evaluated by comparing signal of the promoter driven AC-specific mCherry to the control. RNAi treatment that led to a decrease in the mCherry signal would suggest a nonspecific effect. All genes that decreased the enrichment of NUO-1::mNG in the AC subsequent to knockdown were reported as hit (Table S) and each hit was repeated three times to validate the effect.

AC-specific UCP-4 Overexpression

The plasmid containing the AC-specific overexpression of UCP-4 also contained a membrane-localized mKate2 (mKate2::PLC∂P). When imaging the effects of UCP-4 on the ATP:ADP ratio, we confirmed expression of the mKate2.

Microscopy and image acquisition

bioRxiv preprint doi: https://doi.org/10.1101/2025.05.02.651978; this version posted May 3, 2025. The copyright holder for this preprint (which was not certified by peer review) is the author/funder. All rights reserved. No reuse allowed without permission.

Confocal images were acquired on a Ziess Axioimager microscope equipped with either a Yokogawa CSU-10 or CSU- W1 spinning disk confocal controlled by Micromanager Software vv1.4.23 or v2.0.1 using a Zeiss 100x Plan-Apochromat 1.4NA oil immersion objective and with either a Hamamatsu ORCA-Fusion sCMOS camera, Hamamatsu ORCA-Quest qCMOS camera, or ImageEM EMCCD camera. Animals were mounted on 5% noble agar pads and anesthetized with either 0.01M sodium azide (Sigma-Aldrich #S2002) or 5mM Levamisole (Millipore Sigma #L9756). Time-lapse imaging of AC invasion was performed as previously described on a Ziess Axioimager microscope with a Yokogawa CSU-W1 spinning disk and Hamamatsu ORCA-Fusion sCMOS camera [150]. Fluorescence recovery after photobleaching (FRAP) was done on a Ziess Axioimager microscope equipped with an iLas targeted laser system from BioVision using an Omicron Lux 60mW 405nm laser, Yokogawa CSU- W1 spinning disk confocal controlled by Metamorph imaging software, a Zeiss 100x Plan-Apochromat 1.4NA oil immersion objective and Hamamatsu ORCA-Fusion sCMOS camera.

All quantitative mitochondrial protein measurements of endogenously tagged strains (Figures 2D and 3E) were imaged using identical acquisition settings (488nm laser at 0.6 laser power, 150ms exposure, 128eGain, relative z-stack from -3.5µmto 3.5um, z-step size 0.37um) along with a control strain to confirm reproducibility across multiple imaging sessions. PercevalHR was imaged as previously described[57]. Briefly, optimal acquisition settings for both the ATP (488nm excitation and 525nm emission) and ADP (405nm excitation and 525nm emission) channels were determined to be 488nm laser at 2.5 laser power with 500ms exposure and 405nm laser at 3.0 laser power with 1000ms exposure. To prevent photobleaching from 405nm laser from effecting 488nm excitation, multidimensional acquisition parameters were set to acquire in order of channel then z-slice, meaning all z-slices of the ATP channel were acquired before the ADP channel. HYlight was imaged as previously described[67]. Using the published physiological ratio for the HYlight-RA control (FBP-bound/FBP-unbound ratio of ~0.4)[67],

bioRxiv preprint doi: https://doi.org/10.1101/2025.05.02.651978; this version posted May 3, 2025. The copyright holder for this preprint (which was not certified by peer review) is the author/funder. All rights reserved. No reuse allowed without permission.

appropriate acquisition settings were determined as 488nm laser at 2.5 laser power with 800ms exposure and 405nm laser at 3.0 laser power with 800ms exposure. For all experiments measuring glycolysis, both HYlight and HYlight-RA were imaged and with the same acquisition settings. Due to the photosensitivity of the sensor HYlight(-RA) one z-plane was imaged per animal. Quantitative imaging of iATPSnFr1.0, cytosolic GFP, and ETC promoter driven fluorescent expression, was carefully acquired with standardized acquisition settings to assure intensiometric measurements were reproducible across developmental time and experimental condition.

Staining with mitochondrial dyes

Tetramethylrhodamine, Ethyl Ester, Perchlorate (TMRE, ThermoFisher Scientific #T669) was reconstituted in DMSO and diluted to 1µM in M9 buffer. A mixed population of animals were added to fresh OP50 NGM plates with 400µL of 1µM TMRE. Animals were stained and allowed to continue to grow overnight in the dark at room temperature before imaging. Nonyl Acridine Orange (NAO, ThermoFisher Scientific #A1372) was reconstituted in M9 then diluted to 5µM in M9 buffer. As with the TMRE protocol, 100µL of 5µM NAO was added to OP50 NGM plates with a mixed population of animals. The NAO treated animals were grown overnight at room temperature before imaging. To account for variability in the uptake of dyes, AC mitochondrial measurements of TMRE and NAO were internally controlled by either measuring neighboring uterine cells or measuring both apical and basal mitochondria within the same cell.

Assembling *C. elegans* MitoCarta

MitoCarta is a compendium of human and mouse mitochondrial genes coding for proteins in the 149 annotated mitochondrial pathways[80]. The current version of MitoCarta3.0 includes 1136 human mitochondrial genes. Using OrthoList2.0, a comparative orthologs prediction tool between *C. elegans* and human genome[151], we identified 824 *C. elegans* orthologs to the

bioRxiv preprint doi: https://doi.org/10.1101/2025.05.02.651978; this version posted May 3, 2025. The copyright holder for this preprint (which was not certified by peer review) is the author/funder. All rights reserved. No reuse allowed without permission.

human MitoCarta3.0 genes. Out of the 312 human genes that Ortholist2.0 did not annotate, orthologs for an additional 131 genes were retrieved manually from the Alliance of Genome Resources[152]. In total, 84% of the Human MitoCarta genes had orthologous genes in *C. elegans* (955 out of 1136 genes) and 16% of the Human genes did not have known *C. elegans* orthology (181 out of 1136). Ortholist2.0 and Alliance of Genome Resources cross reference 6 andd 9 different gene ortholog databases, respectively, accounting for the discrepancies in ortholog annotations. The number of databases confirming orthologs for each gene is reported in Table S2. The number of databases confirming the orthology is reported in the Table to represent the source, either from Alliance or from Ortholist2.0. A total of 1094 (including duplicates of any *C. elegans* orthologs) *C. elegans* mitochondrial genes were compiled (Table S2).

Transcriptome analysis of the *C.elegans* MitoCarta

The *C. elegans* MitoCarta (CMC) genes were cross-referenced with a recently generated AC transcriptome[52] to determine the transcriptional enrichment of each gene in the AC compared to the whole animal (as measured by Log2-fold change). Gene Set Enrichment Analysis (GSEA) was conducted based on the data set of the transcriptional enrichment (log2-fold change) of each CMC genes and the gene set of 149 mitochondria pathways[153-155]. The GSEA algorithm filters the gene set size and removes all mitochondrial pathways where the number of genes is less than 2[155]. A list of 145 gene sets/mitochondrial pathways were analyzed and sorted based on the normalized enrichment score (NES). The significance of the enrichment was interpreted with a false discovery rate (FDR) Q-value that is less than 0.05. Plotting for the GSEA (Figure S2) was conducted in R studio (version 4.4.0).

Quantification and Statistical Analysis

Quantitative Mitochondrial Protein Measurements

bioRxiv preprint doi: https://doi.org/10.1101/2025.05.02.651978; this version posted May 3, 2025. The copyright holder for this preprint (which was not certified by peer review) is the author/funder. All rights reserved. No reuse allowed without permission.

All acquired images of endogenously-tagged mitochondrial proteins were processed using ImageJ/Fiji. Mitochondria signal within the cell of interest (either AC or UC) was analyzed using 3-slice sum projections (0.2 µm z-step size) confocal z-stacks (with background subtraction, 6.7 pixel rolling ball radius). A mask for each mitochondria in the cell of interest was generated using the adaptive thresholding plugin[156]. This mask was used as a region of interest and the mean fluorescence intensity was measured to determine the "total" fluorescence per mitochondria for all mitochondria in the cell. The cell was then manually subdivided into apical and basal regions and the mean fluorescence intensity per mitochondria was measured in each region. Polarity was then calculated using the following ratio:

$$polarity = \frac{basal\ mean\ fluorescence\ intensity\ per\ mitochondria}{apical\ mean\ fluorescence\ intensity\ per\ mitochondria}$$

Mitochondrial volume quantification

Using a mitochondrially localized mKate (*rpl-28p::tomm-20::mKate*), a confocal z-stack was acquired through the entire uterus (51 slices, 0.2 µm step size) and the images were background subtracted using 6.7 pixel rolling ball radius. To generate an accurate projection of all mitochondria in each analyzed cell (both AC and uterine cell), regions of interest around the boundary of each cell were manually drawn and any signal outside of this ROI was removed for each z-slice. The new compiled stack for each cell of interest was subsequently analyzed using Imaris Version 9.9.1 to generate a 3D isosurface rendering. 3D isosurface renderings relied on adaptive thresholding as described above and were used to determine the volume of the mitochondria within each cell.

Mitochondrial Morphology Assessment

bioRxiv preprint doi: https://doi.org/10.1101/2025.05.02.651978; this version posted May 3, 2025. The copyright holder for this preprint (which was not certified by peer review) is the author/funder. All rights reserved. No reuse allowed without permission.

Z-stacks of all the mitochondria within the cell of interest were generated as described above. Using the ImageJ plugin "Mitochondrial Analyzer[156]", each z-stack was thresholded and mitochondrial sphericity and branch number were measured.

HMG-5 puncta

Using animals with endogenously tagged HMG-5 (*hmg-5::GFP*)[157], a confocal z-stack was collected through the entire uterus (51 slices, 0.20 µm step size). 4 central slices of the AC or UC were sum z-projected and the number of puncta were manually counted.

Transmission Electron Microscopy cristae analysis

Using transmission electron microscopy (TEM) images from a depositary of images from previously published work[44], boundaries around individual mitochondria were manually drawn and annotated as either AC or UC. Those images were then assigned random numbers to blind the analysis. For each blinded image the freehand selection tool was used to circle and measure both the outer perimeter of the mitochondria (OMM) and the inner membrane (IMM) folds/cristae. The total area of the IMM and OMM were individually measured. The ratio of IMM to OMM were obtained by dividing the total area of IMM by the total area of the OMM.

Analysis of ratiometric biosensors

Ratiometric biosensors PercevalHR and HYlight(-RA) were used to determine the ATD:ADP ratio and FBP-bound:FBP-unbound ratio, respectively. As described above (See Microscopy and Image Acquisition), the imaging data for these biosensors were acquired as two-channel images. To transform the two-channel images into ratiometric images, the "Imaging Calculator > Divide" function in Fiji was used to divide the signal of the 488nm-excitation channel (ATP for PercevalHR and FBP-bound for HYlight(-RA)) by the 405nm-excitation channel (ADP for PercevalHR and FBP-unbound for HYlight(-RA)). The divided ratiometric images were used for

bioRxiv preprint doi: https://doi.org/10.1101/2025.05.02.651978; this version posted May 3, 2025. The copyright holder for this preprint (which was not certified by peer review) is the author/funder. All rights reserved. No reuse allowed without permission.

quantification. Representative images for figures were displayed as the spectral intensity map using the “Fire” look-up table in Fiji (LUT).

Spectral representation of fluorescence intensity

Spectral intensity maps were used to emphasize differences in fluorescent intensity. Using the “Fire” look-up table (LUT) in Fiji, the spectral intensity map and corresponding calibration bar were applied to representative images shown in figures. In instances where all representative images within the panel were constrained to the same minimum and maximum pixel intensity, exact values were displayed at the bottom and top of the calibration bar, respectively. Calibration bars were annotated with “hi” and “lo” (represent high and low intensity pixel values) for representative images that were displayed with different minimum and maximum pixel intensity either due to variation in the image acquisition settings or normalization of ATP:ADP ratios.

Statistical Analysis

For all experiments, the sample size (*n*) of animals, cells, or mitochondria measured was listed in the figure legend or table, along with the statistical tests used and the p-values. All statistical analyses and graph generation were done in GraphPad Prism (Version 10). Normality of each experimental data set was evaluated using the Shapiro-Wilk test. Comparisons across multiple time-points were performed using a one-way ANOVA with Tukey’s post hoc test for multiple comparisons. Comparisons of fluorescence intensity between two cells in the same animal (AC vs US)or between two mitochondrial populations within the same cell (apical vs basal) were conducted using paired t-test or mixed-effects ANOVA with Geisser-Greenhouse correction and uncorrected Fisher’s LSD to allow for comparison between designated pairs. Comparisons of fluorescence intensity between a control and treatment were made using a two-tailed unpaired t-test with Welch’s correction if the variance was unequal between the two groups. Comparisons

bioRxiv preprint doi: https://doi.org/10.1101/2025.05.02.651978; this version posted May 3, 2025. The copyright holder for this preprint (which was not certified by peer review) is the author/funder. All rights reserved. No reuse allowed without permission.

of fluorescence intensity between a single control and two or more treatments were performed by one-way ANOVA with Dunnett's test for multiple comparisons. When assessing AC invasion defects based on invasion scoring, a Fisher's exact 2x2 test was used to compare the treatment verses the control. When determining if there was a statistically significant relationship between the lag2 ratio and the mitochondrial component fluorescence intensity per mitochondria ratio between the α1 and α2 cells, measure of non-zero slope was used to interpret the results of the simple linear regression analysis.

Acknowledgements

We wish to thank Jake Leyhr for assistance with MitoCarta data curation and presentation, Siddharthan Balachandar Thendral for movie processing, Meghan Morrissey for generation of the TEM image repository, and Delaney Graham for help with RNAi screening. Additionally, we would like to thank Laura Kelley for helpful discussions throughout the project. We gratefully thank the Pablo Lara-Gonzalez lab for the SRC-1::GFP strain and the Colón-Ramos lab for supplying the HYlight and HYlightRA plasmids. The Caenorhabditis Genetics Center, supported by the National Institutes of Health Office of Research Infrastructure Programs (P40 OD01044), provided some of the *C. elegans* strains. I.W.K., L.P.B., Q.C., L.W., and D.R.S. were supported by R35GM118049 and a Department of Biology Hargitt fellowship. J.M., and K.M. were supported by P42ES010356 and T32ES021432.

Author contributions

Conceptualization: I.W.K. and D.R.S.; Data curation: I.W.K.; Formal analysis: I.W.K., L.P.B., K.M., L.W.; Funding acquisition: D.R.S.; Investigation: I.W.K., L.P.B, L.W., K.M., C.S.; Methodology: I.W.K., L.P.B., Q.C., K.M.; Project administration: I.W.K., D.R.S.; Resources: J.N.M. and D.R.S.; Supervision: D.R.S.; Visualization: I.W.K., L.P.B., L.W., K.M.; Writing – original draft: I.W.K., L.P.B., D.R.S.; Writing – review & editing: I.W.K., L.P.B., D.R.S.

bioRxiv preprint doi: https://doi.org/10.1101/2025.05.02.651978; this version posted May 3, 2025. The copyright holder for this preprint (which was not certified by peer review) is the author/funder. All rights reserved. No reuse allowed without permission.

References

1. Jayadev, R., and Sherwood, D.R. (2017). Basement membranes. Current Biology *27*, R207-R211. 10.1016/j.cub.2017.02.006.
2. Moser, G., Windsperger, K., Pollheimer, J., de Sousa Lopes, S.C., and Huppertz, B. (2018). Human trophoblast invasion: new and unexpected routes and functions. Histochem Cell Biol *150*, 361-370. 10.1007/s00418-018-1699-0.
3. Bronner, M.E., and LeDouarin, N.M. (2012). Development and evolution of the neural crest: an overview. Dev Biol *366*, 2-9. 10.1016/j.ydbio.2011.12.042.
4. Nichols, E.L., and Smith, C.J. (2019). Pioneer axons employ Cajal's battering ram to enter the spinal cord. Nature Communications *10*, 562. 10.1038/s41467-019-08421-9.
5. Bahr, J.C., Li, X.Y., Feinberg, T.Y., Jiang, L., and Weiss, S.J. (2022). Divergent regulation of basement membrane trafficking by human macrophages and cancer cells. Nat Commun *13*, 6409. 10.1038/s41467-022-34087-x.
6. Kyprianou, C., Christodoulou, N., Hamilton, R.S., Nahaboo, W., Boomgaard, D.S., Amadei, G., Migeotte, I., and Zernicka-Goetz, M. (2020). Basement membrane remodelling regulates mouse embryogenesis. Nature *582*, 253-258. 10.1038/s41586-020-2264-2.
7. Han, S.J., Jung, S.Y., Wu, S.-P., Hawkins, S.M., Park, M.J., Kyo, S., Qin, J., Lydon, J.P., Tsai, S.Y., Tsai, M.-J., et al. (2015). Estrogen receptor β modulates apoptosis complexes and the inflammasome to drive the pathogenesis of endometriosis. Cell *163*, 960-974. 10.1016/j.cell.2015.10.034.
8. Pan, H., Sheng, J.-Z., Tang, L., Zhu, R., Zhou, T.-H., and Huang, H.-F. (2008). Increased expression of c-fos protein associated with increased matrix metalloproteinase-9 protein expression in the endometrium of endometriotic patients. Fertil Steril *90*, 1000-1007. 10.1016/j.fertnstert.2007.07.1386.
9. Jiang, S., Chen, Q., Liu, H., Gao, Y., Yang, X., Ren, Z., Gao, Y., Xiao, L., Zhong, M., Yu, Y., and Yang, X. (2020). Preeclampsia-Associated lncRNA INHBA-AS1 Regulates the Proliferation, Invasion, and Migration of Placental Trophoblast Cells. Mol Ther Nucleic Acids *22*, 684-695. 10.1016/j.omtn.2020.09.033.
10. Gathiram, P., and Moodley, J. (2016). Pre-eclampsia: its pathogenesis and pathophysiolgy. Cardiovasc J Afr *27*, 71-78. 10.5830/cvja-2016-009.
11. Gerstberger, S., Jiang, Q., and Ganesh, K. (2023). Metastasis. Cell *186*, 1564-1579. 10.1016/j.cell.2023.03.003.
12. Hey, S., and Linder, S. (2024). Matrix metalloproteinases at a glance. J Cell Sci *137*. 10.1242/jcs.261898.
13. Cambi, A., and Chavrier, P. (2021). Tissue remodeling by invadosomes. Fac Rev *10*, 39. 10.12703/r/10-39.
14. Naegeli, K.M., Hastie, E., Garde, A., Wang, Z., Keeley, D.P., Gordon, K.L., Pani, A.M., Kelley, L.C., Morrissey, M.A., Chi, Q., et al. (2017). Cell Invasion In Vivo via Rapid Exocytosis of a Transient Lysosome-Derived Membrane Domain. Developmental Cell *43*, 403-417.e410. 10.1016/j.devcel.2017.10.024.

bioRxiv preprint doi: https://doi.org/10.1101/2025.05.02.651978; this version posted May 3, 2025. The copyright holder for this preprint (which was not certified by peer review) is the author/funder. All rights reserved. No reuse allowed without permission.

15. Costa, D.S., Kenny-Ganzert, I.W., Chi, Q., Park, K., Kelley, L.C., Garde, A., Matus, D.Q., Park, J., Yogev, S., Goldstein, B., et al. (2023). The C. elegans Anchor Cell Transcriptome: Ribosome Biogenesis Drives Cell Invasion through Basement Membrane. BioRxiv, 2022.2012.2028.522136. 10.1101/2022.12.28.522136.
16. Park, K., Garde, A., Thendral, S.B., Soh, A.W.J., Chi, Q., and Sherwood, D.R. (2024). De novo lipid synthesis and polarized prenylation drive cell invasion through basement membrane. Journal of Cell Biology *223*. 10.1083/jcb.202402035.
17. Martin-Perez, M., Urdiroz-Urricelqui, U., Bigas, C., and Benitah, S.A. (2022). The role of lipids in cancer progression and metastasis. Cell Metab *34*, 1675-1699. 10.1016/j.cmet.2022.09.023.
18. Prakash, V., Carson, B.B., Feenstra, J.M., Dass, R.A., Sekyrova, P., Hoshino, A., Petersen, J., Guo, Y., Parks, M.M., Kurylo, C.M., et al. (2019). Ribosome biogenesis during cell cycle arrest fuels EMT in development and disease. Nat Commun *10*, 2110. 10.1038/s41467-019-10100-8.
19. Estévez-Herrera, J., Domínguez, N., Pardo, M.R., González-Santana, A., Westhead, E.W., Borges, R., and Machado, J.D. (2016). ATP: The crucial component of secretory vesicles. Proceedings of the National Academy of Sciences *113*, E4098-E4106. doi:10.1073/pnas.1600690113.
20. Marshansky, V., and Futai, M. (2008). The V-type H+-ATPase in vesicular trafficking: targeting, regulation and function. Curr Opin Cell Biol *20*, 415-426. 10.1016/j.ceb.2008.03.015.
21. Shah, N., Colbert, K.N., Enos, M.D., Herschlag, D., and Weis, W.I. (2015). Three αSNAP and 10 ATP molecules are used in SNARE complex disassembly by N-ethylmaleimide-sensitive factor (NSF). J Biol Chem *290*, 2175-2188. 10.1074/jbc.M114.620849.
22. Solinas, G., Borén, J., and Dulloo, A.G. (2015). De novo lipogenesis in metabolic homeostasis: More friend than foe? Mol Metab *4*, 367-377. 10.1016/j.molmet.2015.03.004.
23. Princiotta, M.F., Finzi, D., Qian, S.B., Gibbs, J., Schuchmann, S., Buttgereit, F., Bennink, J.R., and Yewdell, J.W. (2003). Quantitating protein synthesis, degradation, and endogenous antigen processing. Immunity *18*, 343-354. 10.1016/s1074-7613(03)00051-7.
24. Li, Y., Yao, L., Mori, Y., and Sun, S.X. (2019). On the energy efficiency of cell migration in diverse physical environments. Proc Natl Acad Sci U S A *116*, 23894-23900. 10.1073/pnas.1907625116.
25. Dunn, J., and Grider, M.H. (2025). Physiology, Adenosine Triphosphate. In StatPearls, (StatPearls Publishing
Copyright © 2025, StatPearls Publishing LLC.).
26. Garde, A., and Sherwood, D.R. (2021). Fueling Cell Invasion through Extracellular Matrix. Trends Cell Biol *31*, 445-456. 10.1016/j.tcb.2021.01.006.
27. Zhang, L., Chen, X., Wang, J., Chen, M., Chen, J., Zhuang, W., Xia, Y., Huang, Z., Zheng, Y., and Huang, Y. (2024). Cysteine protease inhibitor 1 promotes metastasis by mediating an oxidative phosphorylation/MEK/ERK axis in esophageal squamous carcinoma cancer. Sci Rep *14*, 4985. 10.1038/s41598-024-55544-1.

bioRxiv preprint doi: https://doi.org/10.1101/2025.05.02.651978; this version posted May 3, 2025. The copyright holder for this preprint (which was not certified by peer review) is the author/funder. All rights reserved. No reuse allowed without permission.

28. Porporato, P.E., Filigheddu, N., Pedro, J.M.B.-S., Kroemer, G., and Galluzzi, L. (2018). Mitochondrial metabolism and cancer. Cell Research *28*, 265-280. 10.1038/cr.2017.155.
29. Porporato, P.E., Payen, V.L., Pérez-Escuredo, J., De Saedeleer, C.J., Danhier, P., Copetti, T., Dhup, S., Tardy, M., Vazeille, T., Bouzin, C., et al. (2014). A mitochondrial switch promotes tumor metastasis. Cell Rep *8*, 754-766. 10.1016/j.celrep.2014.06.043.
30. Commander, R., Wei, C., Sharma, A., Mouw, J.K., Burton, L.J., Summerbell, E., Mahboubi, D., Peterson, R.J., Konen, J., Zhou, W., et al. (2020). Subpopulation targeting of pyruvate dehydrogenase and GLUT1 decouples metabolic heterogeneity during collective cancer cell invasion. Nat Commun *11*, 1533. 10.1038/s41467-020-15219-7.
31. Cunniff, B., McKenzie, A.J., Heintz, N.H., and Howe, A.K. (2016). AMPK activity regulates trafficking of mitochondria to the leading edge during cell migration and matrix invasion. Mol Biol Cell *27*, 2662-2674. 10.1091/mbc.E16-05-0286.
32. Papalazarou, V., Zhang, T., Paul, N.R., Juin, A., Cantini, M., Maddocks, O.D.K., Salmeron-Sanchez, M., and Machesky, L.M. (2020). The creatine-phosphagen system is mechanoresponsive in pancreatic adenocarcinoma and fuels invasion and metastasis. Nat Metab *2*, 62-80. 10.1038/s42255-019-0159-z.
33. Caino, M.C., Seo, J.H., Aguinaldo, A., Wait, E., Bryant, K.G., Kossenkov, A.V., Hayden, J.E., Vaira, V., Morotti, A., Ferrero, S., et al. (2016). A neuronal network of mitochondrial dynamics regulates metastasis. Nat Commun *7*, 13730. 10.1038/ncomms13730.
34. Zhao, J., Zhang, J., Yu, M., Xie, Y., Huang, Y., Wolff, D.W., Abel, P.W., and Tu, Y. (2013). Mitochondrial dynamics regulates migration and invasion of breast cancer cells. Oncogene *32*, 4814-4824. 10.1038/onc.2012.494.
35. Caino, M.C., Ghosh, J.C., Chae, Y.C., Vaira, V., Rivadeneira, D.B., Faversani, A., Rampini, P., Kossenkov, A.V., Aird, K.M., Zhang, R., et al. (2015). PI3K therapy reprograms mitochondrial trafficking to fuel tumor cell invasion. Proc Natl Acad Sci USA *112*, 8638-8643. 10.1073/pnas.1500722112.
36. Madan, S., Uttekar, B., Chowdhary, S., and Rikhy, R. (2021). Mitochondria Lead the Way: Mitochondrial Dynamics and Function in Cellular Movements in Development and Disease. Front Cell Dev Biol *9*, 781933. 10.3389/fcell.2021.781933.
37. Altieri, D.C. (2017). Mitochondria on the move: emerging paradigms of organelle trafficking in tumour plasticity and metastasis. Br J Cancer *117*, 301-305. 10.1038/bjc.2017.201.
38. Monzel, A.S., Enríquez, J.A., and Picard, M. (2023). Multifaceted mitochondria: moving mitochondrial science beyond function and dysfunction. Nat Metab *5*, 546-562. 10.1038/s42255-023-00783-1.
39. Benador, I.Y., Veliova, M., Mahdaviani, K., Petcherski, A., Wikstrom, J.D., Assali, E.A., Acín-Pérez, R., Shum, M., Oliveira, M.F., Cinti, S., et al. (2018). Mitochondria Bound to Lipid Droplets Have Unique Bioenergetics, Composition, and Dynamics that Support Lipid Droplet Expansion. Cell Metab *27*, 869-885.e866. https://doi.org/10.1016/j.cmet.2018.03.003.

bioRxiv preprint doi: https://doi.org/10.1101/2025.05.02.651978; this version posted May 3, 2025. The copyright holder for this preprint (which was not certified by peer review) is the author/funder. All rights reserved. No reuse allowed without permission.

40. Marlar-Pavey, M., Tapias-Gomez, D., Mettlen, M., and Friedman, J.R. (2025). Compositionally unique mitochondria in filopodia support cellular migration. Curr Biol *35*, 1227-1241.e1226. 10.1016/j.cub.2025.01.062.
41. Sherwood, D.R. (2006). Cell invasion through basement membranes: an anchor of understanding. Trends Cell Biol *16*, 250-256. 10.1016/j.tcb.2006.03.004.
42. Sherwood, D.R., and Sternberg, P.W. (2003). Anchor cell invasion into the vulval epithelium in C. elegans. Developmental Cell *5*, 21-31. 10.1016/s1534-5807(03)00168-0.
43. Kenny-Ganzert, I.W., and Sherwood, D.R. (2024). The C. elegans anchor cell: A model to elucidate mechanisms underlying invasion through basement membrane. Semin Cell Dev Biol *154*, 23-34. 10.1016/j.semcdb.2023.07.002.
44. Morrissey, M.A., Keeley, D.P., Hagedorn, E.J., McClatchey, S.T.H., Chi, Q., Hall, D.H., and Sherwood, D.R. (2014). B-LINK: a hemicentin, plakin, and integrin-dependent adhesion system that links tissues by connecting adjacent basement membranes. Developmental Cell *31*, 319-331. 10.1016/j.devcel.2014.08.024.
45. Hagedorn, E.J., Ziel, J.W., Morrissey, M.A., Linden, L.M., Wang, Z., Chi, Q., Johnson, S.A., and Sherwood, D.R. (2013). The netrin receptor DCC focuses invadopodia-driven basement membrane transmigration in vivo. J Cell Biol *201*, 903-913. 10.1083/jcb.201301091.
46. Hagedorn, E.J., Kelley, L.C., Naegeli, K.M., Wang, Z., Chi, Q., and Sherwood, D.R. (2014). ADF/cofilin promotes invadopodial membrane recycling during cell invasion in vivo. The Journal of Cell Biology *204*, 1209-1218. 10.1083/jcb.201312098.
47. Linder, S., Wiesner, C., and Himmel, M. (2011). Degrading devices: invadosomes in proteolytic cell invasion. Annu Rev Cell Dev Biol *27*, 185-211. 10.1146/annurev-cellbio-092910-154216.
48. Garde, A., Kenny, I.W., Kelley, L.C., Chi, Q., Mutlu, A.S., Wang, M.C., and Sherwood, D.R. (2022). Localized glucose import, glycolytic processing, and mitochondria generate a focused ATP burst to power basement-membrane invasion. Developmental Cell *57*, 732-749.e737. 10.1016/j.devcel.2022.02.019.
49. Kelley, L.C., Chi, Q., Caceres, R., Hastie, E., Schindler, A.J., Jiang, Y., Matus, D.Q., Plastino, J., and Sherwood, D.R. (2019). Adaptive F-Actin Polymerization and Localized ATP Production Drive Basement Membrane Invasion in the Absence of MMPs. Dev Cell *48*, 313-328 e318. 10.1016/j.devcel.2018.12.018.
50. Sherwood, D.R., and Plastino, J. (2018). Invading, Leading and Navigating Cells in Caenorhabditis elegans: Insights into Cell Movement in Vivo. Genetics *208*, 53-78. 10.1534/genetics.117.300082.
51. Kimble, J. (1981). Alterations in cell lineage following laser ablation of cells in the somatic gonad of Caenorhabditis elegans. Dev Biol *87*, 286-300. 10.1016/0012-1606(81)90152-4.
52. Costa, D.S., Kenny-Ganzert, I.W., Chi, Q., Park, K., Kelley, L.C., Garde, A., Matus, D.Q., Park, J., Yogev, S., Goldstein, B., et al. (2023). The Caenorhabditis elegans anchor cell transcriptome: ribosome biogenesis drives cell invasion through basement membrane. Development *150*. 10.1242/dev.201570.

bioRxiv preprint doi: https://doi.org/10.1101/2025.05.02.651978; this version posted May 3, 2025. The copyright holder for this preprint (which was not certified by peer review) is the author/funder. All rights reserved. No reuse allowed without permission.

53. Sherwood, D.R., Butler, J.A., Kramer, J.M., and Sternberg, P.W. (2005). FOS-1 promotes basement-membrane removal during anchor-cell invasion in C. elegans. Cell *121*, 951-962. 10.1016/j.cell.2005.03.031.
54. Kenny-Ganzert, I.W., and Sherwood, D.R. (2023). The C. elegans anchor cell: A model to elucidate mechanisms underlying invasion through basement membrane. Semin Cell Dev Biol. 10.1016/j.semcdb.2023.07.002.
55. Park, K., Garde, A., Thendral, S.B., Soh, A.W.J., Chi, Q., and Sherwood, D.R. (2024). De novo lipid synthesis and polarized prenylation drive cell invasion through basement membrane. J Cell Biol *223*. 10.1083/jcb.202402035.
56. Naegeli, K.M., Hastie, E., Garde, A., Wang, Z., Keeley, D.P., Gordon, K.L., Pani, A.M., Kelley, L.C., Morrissey, M.A., Chi, Q., et al. (2017). Cell Invasion In Vivo via Rapid Exocytosis of a Transient Lysosome-Derived Membrane Domain. Dev Cell *43*, 403-417 e410. 10.1016/j.devcel.2017.10.024.
57. Garde, A., and Sherwood, D.R. (2022). Visualizing cytoplasmic ATP in C. elegans larvae using PercevalHR. STAR Protoc *3*, 101429. 10.1016/j.xpro.2022.101429.
58. Garde, A., Kenny, I.W., Kelley, L.C., Chi, Q., Mutlu, A.S., Wang, M.C., and Sherwood, D.R. (2022). Localized glucose import, glycolytic processing, and mitochondria generate a focused ATP burst to power basement-membrane invasion. Dev Cell *57*, 732-749 e737. 10.1016/j.devcel.2022.02.019.
59. Tantama, M., Martínez-François, J.R., Mongeon, R., and Yellen, G. (2013). Imaging energy status in live cells with a fluorescent biosensor of the intracellular ATP-to-ADP ratio. Nature Communications *4*, 2550. 10.1038/ncomms3550.
60. Kenny-Ganzert, I., Chi, Q., and Sherwood, D. (2023). Differential production rates of cytosolic and transmembrane GFP reporters in C. elegans L3 larval uterine cells. microPublication Biology.
61. Tantama, M., Martinez-Francois, J.R., Mongeon, R., and Yellen, G. (2013). Imaging energy status in live cells with a fluorescent biosensor of the intracellular ATP-to-ADP ratio. Nat Commun *4*, 2550. 10.1038/ncomms3550.
62. Lobas, M.A., Tao, R., Nagai, J., Kronschläger, M.T., Borden, P.M., Marvin, J.S., Looger, L.L., and Khakh, B.S. (2019). A genetically encoded single-wavelength sensor for imaging cytosolic and cell surface ATP. Nature Communications *10*, 711. 10.1038/s41467-019-08441-5.
63. Lobas, M.A., Tao, R., Nagai, J., Kronschlager, M.T., Borden, P.M., Marvin, J.S., Looger, L.L., and Khakh, B.S. (2019). A genetically encoded single-wavelength sensor for imaging cytosolic and cell surface ATP. Nat Commun *10*, 711. 10.1038/s41467-019-08441-5.
64. Seibel, N.M., Eljouni, J., Nalaskowski, M.M., and Hampe, W. (2007). Nuclear localization of enhanced green fluorescent protein homomultimers. Anal Biochem *368*, 95-99. 10.1016/j.ab.2007.05.025.
65. Wilson, D.F. (2017). Oxidative phosphorylation: regulation and role in cellular and tissue metabolism. J Physiol *595*, 7023-7038. 10.1113/jp273839.
66. Koberstein, J.N., Stewart, M.L., Smith, C.B., Tarasov, A.I., Ashcroft, F.M., Stork, P.J.S., and Goodman, R.H. (2022). Monitoring glycolytic dynamics in single cells using a

bioRxiv preprint doi: https://doi.org/10.1101/2025.05.02.651978; this version posted May 3, 2025. The copyright holder for this preprint (which was not certified by peer review) is the author/funder. All rights reserved. No reuse allowed without permission.

fluorescent biosensor for fructose 1,6-bisphosphate. Proceedings of the National Academy of Sciences *119*, e2204407119. doi:10.1073/pnas.2204407119.

67. Wolfe, A.D., Koberstein, J.N., Smith, C.B., Stewart, M.L., Gonzalez, I.J., Hammarlund, M., Hyman, A.A., Stork, P.J.S., Goodman, R.H., and Colón-Ramos, D.A. (2024). Local and dynamic regulation of neuronal glycolysis in vivo. Proceedings of the National Academy of Sciences *121*, e2314699121. 10.1073/pnas.2314699121.

68. Heinz, S., Freyberger, A., Lawrenz, B., Schladt, L., Schmuck, G., and Ellinger-Ziegelbauer, H. (2017). Mechanistic Investigations of the Mitochondrial Complex I Inhibitor Rotenone in the Context of Pharmacological and Safety Evaluation. Sci Rep *7*, 45465. 10.1038/srep45465.

69. Pfeiffer, M., Kayzer, E.B., Yang, X., Abramson, E., Kenaston, M.A., Lago, C.U., Lo, H.H., Sedensky, M.M., Lunceford, A., Clarke, C.F., et al. (2011). Caenorhabditis elegans UCP4 protein controls complex II-mediated oxidative phosphorylation through succinate transport. J Biol Chem *286*, 37712-37720. 10.1074/jbc.M111.271452.

70. Cho, I., Hwang, G.J., and Cho, J.H. (2016). Uncoupling Protein, UCP-4 May Be Involved in Neuronal Defects During Aging and Resistance to Pathogens in Caenorhabditis elegans. Mol Cells *39*, 680-686. 10.14348/molcells.2016.0125.

71. Pacelli, C., Giguère, N., Bourque, M.J., Lévesque, M., Slack, R.S., and Trudeau, L. (2015). Elevated Mitochondrial Bioenergetics and Axonal Arborization Size Are Key Contributors to the Vulnerability of Dopamine Neurons. Curr Biol *25*, 2349-2360. 10.1016/j.cub.2015.07.050.

72. Bennett, C.F., Latorre-Muro, P., and Puigserver, P. (2022). Mechanisms of mitochondrial respiratory adaptation. Nat Rev Mol Cell Biol *23*, 817-835. 10.1038/s41580-022-00506-6.

73. Pekkurnaz, G., and Wang, X. (2022). Mitochondrial heterogeneity and homeostasis through the lens of a neuron. Nat Metab *4*, 802-812. 10.1038/s42255-022-00594-w.

74. Faitg, J., Lacefield, C., Davey, T., White, K., Laws, R., Kosmidis, S., Reeve, A.K., Kandel, E.R., Vincent, A.E., and Picard, M. (2021). 3D neuronal mitochondrial morphology in axons, dendrites, and somata of the aging mouse hippocampus. Cell Rep *36*, 109509. 10.1016/j.celrep.2021.109509.

75. Schwartz, A.Z.A., Tsyba, N., Abdu, Y., Patel, M.R., and Nance, J. (2022). Independent regulation of mitochondrial DNA quantity and quality in Caenorhabditis elegans primordial germ cells. Elife *11*. 10.7554/eLife.80396.

76. Kukat, C., Davies, K.M., Wurm, C.A., Spahr, H., Bonekamp, N.A., Kuhl, I., Joos, F., Polosa, P.L., Park, C.B., Posse, V., et al. (2015). Cross-strand binding of TFAM to a single mtDNA molecule forms the mitochondrial nucleoid. Proc Natl Acad Sci U S A *112*, 11288-11293. 10.1073/pnas.1512131112.

77. Picca, A., and Lezza, A.M. (2015). Regulation of mitochondrial biogenesis through TFAM-mitochondrial DNA interactions: Useful insights from aging and calorie restriction studies. Mitochondrion *25*, 67-75. 10.1016/j.mito.2015.10.001.

78. Kukat, C., Wurm, C.A., Spahr, H., Falkenberg, M., Larsson, N.G., and Jakobs, S. (2011). Super-resolution microscopy reveals that mammalian mitochondrial

bioRxiv preprint doi: https://doi.org/10.1101/2025.05.02.651978; this version posted May 3, 2025. The copyright holder for this preprint (which was not certified by peer review) is the author/funder. All rights reserved. No reuse allowed without permission.

nucleoids have a uniform size and frequently contain a single copy of mtDNA. Proc Natl Acad Sci U S A *108*, 13534-13539. 10.1073/pnas.1109263108.

79. Chen, W., Zhao, H., and Li, Y. (2023). Mitochondrial dynamics in health and disease: mechanisms and potential targets. Signal Transduction and Targeted Therapy *8*, 333. 10.1038/s41392-023-01547-9.

80. Rath, S., Sharma, R., Gupta, R., Ast, T., Chan, C., Durham, T.J., Goodman, R.P., Grabarek, Z., Haas, M.E., Hung, W.H.W., et al. (2021). MitoCarta3.0: an updated mitochondrial proteome now with sub-organelle localization and pathway annotations. Nucleic Acids Res *49*, D1541-d1547. 10.1093/nar/gkaa1011.

81. Martin, F.J.O., Santiveri, M., Hu, H., and Taylor, N.M.I. (2024). Ion-driven rotary membrane motors: From structure to function. Curr Opin Struct Biol *88*, 102884. 10.1016/j.sbi.2024.102884.

82. Tang, J.X., Thompson, K., Taylor, R.W., and Oláhová, M. (2020). Mitochondrial OXPHOS Biogenesis: Co-Regulation of Protein Synthesis, Import, and Assembly Pathways. Int J Mol Sci *21*. 10.3390/ijms21113820.

83. Bround, M.J., Bers, D.M., and Molkentin, J.D. (2020). A 20/20 view of ANT function in mitochondrial biology and necrotic cell death. Journal of Molecular and Cellular Cardiology *144*, A3-A13. https://doi.org/10.1016/j.yjmcc.2020.05.012.

84. Ruprecht, J.J., King, M.S., Zögg, T., Aleksandrova, A.A., Pardon, E., Crichton, P.G., Steyaert, J., and Kunji, E.R.S. (2019). The Molecular Mechanism of Transport by the Mitochondrial ADP/ATP Carrier. Cell *176*, 435-447.e415. 10.1016/j.cell.2018.11.025.

85. Farina, F., Alberti, A., Breuil, N., Bolotin-Fukuhara, M., Pinto, M., and Culetto, E. (2008). Differential expression pattern of the four mitochondrial adenine nucleotide transporter ant genes and their roles during the development of Caenorhabditis elegans. Dev Dyn *237*, 1668-1681. 10.1002/dvdy.21578.

86. Charmpilas, N., and Tavernarakis, N. (2020). Mitochondrial maturation drives germline stem cell differentiation in Caenorhabditis elegans. Cell Death Differ *27*, 601-617. 10.1038/s41418-019-0375-9.

87. Kirillova, A., Smitz, J.E.J., Sukhikh, G.T., and Mazunin, I. (2021). The Role of Mitochondria in Oocyte Maturation. Cells *10*. 10.3390/cells10092484.

88. Yoo, I., Ahn, I., Lee, J., and Lee, N. (2024). Extracellular flux assay (Seahorse assay): Diverse applications in metabolic research across biological disciplines. Mol Cells *47*, 100095. 10.1016/j.mocell.2024.100095.

89. Mello, D.F., Perez, L., Bergemann, C.M., Morton, K.S., Ryde, I.T., and Meyer, J.N. (2024). Comprehensive characterization of mitochondrial bioenergetics at different larval stages reveals novel insights about the developmental metabolism of Caenorhabditis elegans. PLoS ONE *19*, e0306849. 10.1371/journal.pone.0306849.

90. Leveille, C.F., Mikhaeil, J.S., Turner, K.D., Silvera, S., Wilkinson, J., and Fajardo, V.A. (2017). Mitochondrial cristae density: a dynamic entity that is critical for energy production and metabolic power in skeletal muscle. J Physiol *595*, 2779-2780. 10.1113/jp274158.

91. Heine, K.B., Parry, H.A., and Hood, W.R. (2023). How does density of the inner mitochondrial membrane influence mitochondrial performance? Am J Physiol Regul Integr Comp Physiol *324*, R242-r248. 10.1152/ajpregu.00254.2022.

bioRxiv preprint doi: https://doi.org/10.1101/2025.05.02.651978; this version posted May 3, 2025. The copyright holder for this preprint (which was not certified by peer review) is the author/funder. All rights reserved. No reuse allowed without permission.

92. Ikon, N., and Ryan, R.O. (2017). Cardiolipin and mitochondrial cristae organization. Biochim Biophys Acta Biomembr *1859*, 1156-1163. 10.1016/j.bbamem.2017.03.013.

93. Benaroya, H. (2024). Mitochondria and MICOS - function and modeling. Rev Neurosci *35*, 503-531. 10.1515/revneuro-2024-0004.

94. den Brave, F., Pfanner, N., and Becker, T. (2024). Mitochondrial entry gate as regulatory hub. Biochim Biophys Acta Mol Cell Res *1871*, 119529. 10.1016/j.bbamcr.2023.119529.

95. Saunders, J.E., Beeson, C.C., and Schnellmann, R.G. (2013). Characterization of functionally distinct mitochondrial subpopulations. J Bioenerg Biomembr *45*, 87-99. 10.1007/s10863-012-9478-4.

96. Medwig-Kinney, T.N., Smith, J.J., Palmisano, N.J., Tank, S., Zhang, W., and Matus, D.Q. (2020). A developmental gene regulatory network for C. elegans anchor cell invasion. Development *147*. 10.1242/dev.185850.

97. Seydoux, G., and Greenwald, I. (1989). Cell autonomy of lin-12 function in a cell fate decision in C. elegans. Cell *57*, 1237-1245. https://doi.org/10.1016/0092-8674(89)90060-3.

98. Srinivasan, S., Ramos-Lewis, W., Morais, M., Chi, Q., Soh, A.W.J., Williams, E., Lennon, R., and Sherwood, D.R. (2025). A collagen IV fluorophore knock-in toolkit reveals trimer diversity in C. elegans basement membranes. J Cell Biol *224*. 10.1083/jcb.202412118.

99. Wang, Z., Linden, L.M., Naegeli, K.M., Ziel, J.W., Chi, Q., Hagedorn, E.J., Savage, N.S., and Sherwood, D.R. (2014). UNC-6 (netrin) stabilizes oscillatory clustering of the UNC-40 (DCC) receptor to orient polarity. J Cell Biol *206*, 619-633. 10.1083/jcb.201405026.

100. Misgeld, T., and Schwarz, T.L. (2017). Mitostasis in Neurons: Maintaining Mitochondria in an Extended Cellular Architecture. Neuron *96*, 651-666. 10.1016/j.neuron.2017.09.055.

101. Schuler, M.-H., Lewandowska, A., Caprio, G.D., Skillern, W., Upadhyayula, S., Kirchhausen, T., Shaw, J.M., and Cunniff, B. (2017). Miro1-mediated mitochondrial positioning shapes intracellular energy gradients required for cell migration. Mol Biol Cell *28*, 2159-2169. 10.1091/mbc.E16-10-0741.

102. Huang, H., Majumder, T., Khot, B., Suriyaarachchi, H., Yang, T., Shao, Q., Tirukovalluru, S., and Liu, G. (2024). The role of microtubule-associated protein tau in netrin-1 attractive signaling. J Cell Sci *137*. 10.1242/jcs.261244.

103. Chen, X., Widmer, L.A., Stangier, M.M., Steinmetz, M.O., Stelling, J., and Barral, Y. (2019). Remote control of microtubule plus-end dynamics and function from the minus-end. eLife *8*, e48627. 10.7554/eLife.48627.

104. Sallee, M.D., Zonka, J.C., Skokan, T.D., Raftrey, B.C., and Feldman, J.L. (2018). Tissue-specific degradation of essential centrosome components reveals distinct microtubule populations at microtubule organizing centers. PLoS Biol *16*, e2005189. 10.1371/journal.pbio.2005189.

bioRxiv preprint doi: https://doi.org/10.1101/2025.05.02.651978; this version posted May 3, 2025. The copyright holder for this preprint (which was not certified by peer review) is the author/funder. All rights reserved. No reuse allowed without permission.

105. Zhang, T., Li, L., Fan, X., Shou, X., Ruan, Y., and Xie, X. (2025). Metaxin-2 tunes mitochondrial transportation and neuronal function in Drosophila. Genetics *229*. 10.1093/genetics/iyae204.
106. Zhao, Y., Song, E., Wang, W., Hsieh, C.-H., Wang, X., Feng, W., Wang, X., and Shen, K. (2021). Metaxins are core components of mitochondrial transport adaptor complexes. Nature Communications *12*, 83. 10.1038/s41467-020-20346-2.
107. Qu, C., Dwyer, T., Shao, Q., Yang, T., Huang, H., and Liu, G. (2013). Direct binding of TUBB3 with DCC couples netrin-1 signaling to intracellular microtubule dynamics in axon outgrowth and guidance. J Cell Sci *126*, 3070-3081. 10.1242/jcs.122184.
108. Bai, X., Green, R., Cai, T., Oegema, K., and Golden, A. (2023). A missense mutation in the C. elegans src-2 tyrosine-protein kinase reduces brood size and enhances embryonic morphogenesis defects in src-1(RNAi) conditions. MicroPubl Biol *2023*. 10.17912/micropub.biology.000872.
109. Sheng, Z.H., and Cai, Q. (2012). Mitochondrial transport in neurons: impact on synaptic homeostasis and neurodegeneration. Nat Rev Neurosci *13*, 77-93. 10.1038/nrn3156.
110. Sheng, Z.H. (2014). Mitochondrial trafficking and anchoring in neurons: New insight and implications. J Cell Biol *204*, 1087-1098. 10.1083/jcb.201312123.
111. Rintoul, G.L., and Reynolds, I.J. (2010). Mitochondrial trafficking and morphology in neuronal injury. Biochim Biophys Acta *1802*, 143-150. 10.1016/j.bbadis.2009.09.005.
112. Granath-Panelo, M., and Kajimura, S. (2024). Mitochondrial heterogeneity and adaptations to cellular needs. Nat Cell Biol *26*, 674-686. 10.1038/s41556-024-01410-1.
113. Johnson, D.T., Harris, R.A., French, S., Blair, P.V., You, J., Bemis, K.G., Wang, M., and Balaban, R.S. (2007). Tissue heterogeneity of the mammalian mitochondrial proteome. American Journal of Physiology-Cell Physiology *292*, C689-C697. 10.1152/ajpcell.00108.2006.
114. Rodríguez-Nuevo, A., Torres-Sanchez, A., Duran, J.M., De Guirior, C., Martínez-Zamora, M.A., and Böke, E. (2022). Oocytes maintain ROS-free mitochondrial metabolism by suppressing complex I. Nature *607*, 756-761. 10.1038/s41586-022-04979-5.
115. Ryu, K.W., Fung, T.S., Baker, D.C., Saoi, M., Park, J., Febres-Aldana, C.A., Aly, R.G., Cui, R., Sharma, A., Fu, Y., et al. (2024). Cellular ATP demand creates metabolically distinct subpopulations of mitochondria. Nature *635*, 746-754. 10.1038/s41586-024-08146-w.
116. Garcia, G.C., Gupta, K., Bartol, T.M., Sejnowski, T.J., and Rangamani, P. (2023). Mitochondrial morphology governs ATP production rate. J Gen Physiol *155*. 10.1085/jgp.202213263.
117. McLaughlin, K.L., Hagen, J.T., Coalson, H.S., Nelson, M.A.M., Kew, K.A., Wooten, A.R., and Fisher-Wellman, K.H. (2020). Novel approach to quantify mitochondrial content and intrinsic bioenergetic efficiency across organs. Sci Rep *10*, 17599. 10.1038/s41598-020-74718-1.

bioRxiv preprint doi: https://doi.org/10.1101/2025.05.02.651978; this version posted May 3, 2025. The copyright holder for this preprint (which was not certified by peer review) is the author/funder. All rights reserved. No reuse allowed without permission.

118. Graham, L.C., Eaton, S.L., Brunton, P.J., Atrih, A., Smith, C., Lamont, D.J., Gillingwater, T.H., Pennetta, G., Skehel, P., and Wishart, T.M. (2017). Proteomic profiling of neuronal mitochondria reveals modulators of synaptic architecture. Mol Neurodegener *12*, 77. 10.1186/s13024-017-0221-9.
119. Cserép, C., Pósfai, B., Schwarcz, A.D., and Dénes, Á. (2018). Mitochondrial Ultrastructure Is Coupled to Synaptic Performance at Axonal Release Sites. eNeuro *5*. 10.1523/eneuro.0390-17.2018.
120. Sanz-Morello, B., Pfisterer, U., Winther Hansen, N., Demharter, S., Thakur, A., Fujii, K., Levitskii, S.A., Montalant, A., Korshunova, I., Mammen, P.P., et al. (2020). Complex IV subunit isoform COX6A2 protects fast-spiking interneurons from oxidative stress and supports their function. EMBO J *39*, e105759. 10.15252/embj.2020105759.
121. Benador, I.Y., Veliova, M., Mahdaviani, K., Petcherski, A., Wikstrom, J.D., Assali, E.A., Acín-Pérez, R., Shum, M., Oliveira, M.F., Cinti, S., et al. (2018). Mitochondria Bound to Lipid Droplets Have Unique Bioenergetics, Composition, and Dynamics that Support Lipid Droplet Expansion. Cell Metab *27*, 869-885.e866. 10.1016/j.cmet.2018.03.003.
122. Chia, M.L., Bulat, F., Gaunt, A., Ros, S., Wright, A.J., Sawle, A., Porcu, L., Vias, M., Brenton, J.D., and Brindle, K.M. (2025). Metabolic imaging distinguishes ovarian cancer subtypes and detects their early and variable responses to treatment. Oncogene *44*, 563-574. 10.1038/s41388-024-03231-w.
123. Gentric, G., Kieffer, Y., Mieulet, V., Goundiam, O., Bonneau, C., Nemati, F., Hurbain, I., Raposo, G., Popova, T., Stern, M.H., et al. (2019). PML-Regulated Mitochondrial Metabolism Enhances Chemosensitivity in Human Ovarian Cancers. Cell Metab *29*, 156-173.e110. 10.1016/j.cmet.2018.09.002.
124. Jones, R.A., Robinson, T.J., Liu, J.C., Shrestha, M., Voisin, V., Ju, Y., Chung, P.E., Pellecchia, G., Fell, V.L., Bae, S., et al. (2016). RB1 deficiency in triple-negative breast cancer induces mitochondrial protein translation. J Clin Invest *126*, 3739-3757. 10.1172/jci81568.
125. Birkenmeier, K., Dröse, S., Wittig, I., Winkelmann, R., Käfer, V., Döring, C., Hartmann, S., Wenz, T., Reichert, A.S., Brandt, U., and Hansmann, M.L. (2016). Hodgkin and Reed-Sternberg cells of classical Hodgkin lymphoma are highly dependent on oxidative phosphorylation. Int J Cancer *138*, 2231-2246. 10.1002/ijc.29934.
126. Caro, P., Kishan, A.U., Norberg, E., Stanley, I.A., Chapuy, B., Ficarro, S.B., Polak, K., Tondera, D., Gounarides, J., Yin, H., et al. (2012). Metabolic signatures uncover distinct targets in molecular subsets of diffuse large B cell lymphoma. Cancer Cell *22*, 547-560. 10.1016/j.ccr.2012.08.014.
127. Ashton, T.M., McKenna, W.G., Kunz-Schughart, L.A., and Higgins, G.S. (2018). Oxidative Phosphorylation as an Emerging Target in Cancer Therapy. Clin Cancer Res *24*, 2482-2490. 10.1158/1078-0432.Ccr-17-3070.
128. Whitaker-Menezes, D., Martinez-Outschoorn, U.E., Flomenberg, N., Birbe, R.C., Witkiewicz, A.K., Howell, A., Pavlides, S., Tsirigos, A., Ertel, A., Pestell, R.G., et al. (2011). Hyperactivation of oxidative mitochondrial metabolism in epithelial cancer

bioRxiv preprint doi: https://doi.org/10.1101/2025.05.02.651978; this version posted May 3, 2025. The copyright holder for this preprint (which was not certified by peer review) is the author/funder. All rights reserved. No reuse allowed without permission.

cells in situ: visualizing the therapeutic effects of metformin in tumor tissue. Cell Cycle *10*, 4047-4064. 10.4161/cc.10.23.18151.

129. Masoud, R., Reyes-Castellanos, G., Lac, S., Garcia, J., Dou, S., Shintu, L., Abdel Hadi, N., Gicquel, T., El Kaoutari, A., Diémé, B., et al. (2020). Targeting Mitochondrial Complex I Overcomes Chemoresistance in High OXPHOS Pancreatic Cancer. Cell Rep Med *1*, 100143. 10.1016/j.xcrm.2020.100143.
130. Schwarz, T.L. (2013). Mitochondrial trafficking in neurons. Cold Spring Harb Perspect Biol *5*. 10.1101/cshperspect.a011304.
131. Altieri, D.C. (2019). Mitochondrial dynamics and metastasis. Cell Mol Life Sci *76*, 827-835. 10.1007/s00018-018-2961-2.
132. Huang, H., Majumder, T., Khot, B., Suriyaarachchi, H., Yang, T., Shao, Q., Tirukovalluru, S., and Liu, G. (2024). The role of microtubule-associated protein tau in netrin-1 attractive signaling. J Cell Sci *137*. 10.1242/jcs.261244.
133. Qu, C., Dwyer, T., Shao, Q., Yang, T., Huang, H., and Liu, G. (2013). Direct binding of TUBB3 with DCC couples netrin-1 signaling to intracellular microtubule dynamics in axon outgrowth and guidance. J Cell Sci *126*, 3070-3081. 10.1242/jcs.122184.
134. Höhr, A.I., Straub, S.P., Warscheid, B., Becker, T., and Wiedemann, N. (2015). Assembly of β-barrel proteins in the mitochondrial outer membrane. Biochim Biophys Acta *1853*, 74-88. 10.1016/j.bbamcr.2014.10.006.
135. Cartron, P.F., Petit, E., Bellot, G., Oliver, L., and Vallette, F.M. (2014). Metaxins 1 and 2, two proteins of the mitochondrial protein sorting and assembly machinery, are essential for Bak activation during TNF alpha triggered apoptosis. Cell Signal *26*, 1928-1934. 10.1016/j.cellsig.2014.04.021.
136. Zala, D., Schlattner, U., Desvignes, T., Bobe, J., Roux, A., Chavrier, P., and Boissan, M. (2017). The advantage of channeling nucleotides for very processive functions. F1000Res *6*, 724. 10.12688/f1000research.11561.2.
137. Gilbert, S.P., Webb, M.R., Brune, M., and Johnson, K.A. (1995). Pathway of processive ATP hydrolysis by kinesin. Nature *373*, 671-676. 10.1038/373671a0.
138. Saha, S., Weber, C.A., Nousch, M., Adame-Arana, O., Hoege, C., Hein, M.Y., Osborne-Nishimura, E., Mahamid, J., Jahnel, M., Jawerth, L., et al. (2016). Polar Positioning of Phase-Separated Liquid Compartments in Cells Regulated by an mRNA Competition Mechanism. Cell *166*, 1572-1584.e1516. 10.1016/j.cell.2016.08.006.
139. De Vos, D., Bruggeman, F.J., Westerhoff, H.V., and Bakker, B.M. (2011). How molecular competition influences fluxes in gene expression networks. PLoS ONE *6*, e28494. 10.1371/journal.pone.0028494.
140. Zhao, R.Z., Jiang, S., Zhang, L., and Yu, Z.B. (2019). Mitochondrial electron transport chain, ROS generation and uncoupling (Review). Int J Mol Med *44*, 3-15. 10.3892/ijmm.2019.4188.
141. Brand, M.D., Orr, A.L., Perevoshchikova, I.V., and Quinlan, C.L. (2013). The role of mitochondrial function and cellular bioenergetics in ageing and disease. Br J Dermatol *169 Suppl 2*, 1-8. 10.1111/bjd.12208.
142. Girard, L.R., Fiedler, T.J., Harris, T.W., Carvalho, F., Antoshechkin, I., Han, M., Sternberg, P.W., Stein, L.D., and Chalfie, M. (2007). WormBook: the online review of

bioRxiv preprint doi: https://doi.org/10.1101/2025.05.02.651978; this version posted May 3, 2025. The copyright holder for this preprint (which was not certified by peer review) is the author/funder. All rights reserved. No reuse allowed without permission.

Caenorhabditis elegans biology. Nucleic Acids Res *35*, D472-475. 10.1093/nar/gkl894.

143. Cogliati, S., Lorenzi, I., Rigoni, G., Caicci, F., and Soriano, M.E. (2018). Regulation of Mitochondrial Electron Transport Chain Assembly. Journal of Molecular Biology *430*, 4849-4873. https://doi.org/10.1016/j.jmb.2018.09.016.

144. Porta-de-la-Riva, M., Fontrodona, L., Villanueva, A., and Cerón, J. (2012). Basic Caenorhabditis elegans methods: synchronization and observation. J Vis Exp, e4019. 10.3791/4019.

145. Dickinson, D.J., and Goldstein, B. (2016). CRISPR-Based Methods for Caenorhabditis elegans Genome Engineering. Genetics *202*, 885-901. 10.1534/genetics.115.182162.

146. Keeley, D.P., Hastie, E., Jayadev, R., Kelley, L.C., Chi, Q., Payne, S.G., Jeger, J.L., Hoffman, B.D., and Sherwood, D.R. (2020). Comprehensive Endogenous Tagging of Basement Membrane Components Reveals Dynamic Movement within the Matrix Scaffolding. Developmental Cell *54*, 60-74.e67. 10.1016/j.devcel.2020.05.022.

147. Dickinson, D.J., Ward, J.D., Reiner, D.J., and Goldstein, B. (2013). Engineering the Caenorhabditis elegans genome using Cas9-triggered homologous recombination. Nat Methods *10*, 1028-1034. 10.1038/nmeth.2641.

148. Sherwood, D.R., Butler, J.A., Kramer, J.M., and Sternberg, P.W. (2005). FOS-1 promotes basement-membrane removal during anchor-cell invasion in C. elegans. Cell *121*, 951-962. 10.1016/j.cell.2005.03.031.

149. Luz, A.L., Smith, L.L., Rooney, J.P., and Meyer, J.N. (2015). Seahorse Xfe 24 Extracellular Flux Analyzer-Based Analysis of Cellular Respiration in Caenorhabditis elegans. Curr Protoc Toxicol *66*, 25.27.21-25.27.15. 10.1002/0471140856.tx2507s66.

150. Kelley, L.C., Wang, Z., Hagedorn, E.J., Wang, L., Shen, W., Lei, S., Johnson, S.A., and Sherwood, D.R. (2017). Live-cell confocal microscopy and quantitative 4D image analysis of anchor-cell invasion through the basement membrane in Caenorhabditis elegans. Nat Protoc *12*, 2081-2096. 10.1038/nprot.2017.093.

151. Kim, W., Underwood, R.S., Greenwald, I., and Shaye, D.D. (2018). OrthoList 2: A New Comparative Genomic Analysis of Human and Caenorhabditis elegans Genes. Genetics *210*, 445-461. 10.1534/genetics.118.301307.

152. Updates to the Alliance of Genome Resources central infrastructure. (2024). Genetics *227*. 10.1093/genetics/iyae049.

153. Subramanian, A., Tamayo, P., Mootha, V.K., Mukherjee, S., Ebert, B.L., Gillette, M.A., Paulovich, A., Pomeroy, S.L., Golub, T.R., Lander, E.S., and Mesirov, J.P. (2005). Gene set enrichment analysis: A knowledge-based approach for interpreting genome-wide expression profiles. Proceedings of the National Academy of Sciences *102*, 15545-15550. doi:10.1073/pnas.0506580102.

154. Mootha, V.K., Lindgren, C.M., Eriksson, K.-F., Subramanian, A., Sihag, S., Lehar, J., Puigserver, P., Carlsson, E., Ridderstråle, M., Laurila, E., et al. (2003). PGC-1α-responsive genes involved in oxidative phosphorylation are coordinately downregulated in human diabetes. Nat Genet *34*, 267-273. 10.1038/ng1180.

bioRxiv preprint doi: https://doi.org/10.1101/2025.05.02.651978; this version posted May 3, 2025. The copyright holder for this preprint (which was not certified by peer review) is the author/funder. All rights reserved. No reuse allowed without permission.

155. Reimand, J., Isserlin, R., Voisin, V., Kucera, M., Tannus-Lopes, C., Rostamianfar, A., Wadi, L., Meyer, M., Wong, J., Xu, C., et al. (2019). Pathway enrichment analysis and visualization of omics data using g:Profiler, GSEA, Cytoscape and EnrichmentMap. Nat Protoc *14*, 482-517. 10.1038/s41596-018-0103-9.
156. Chaudhry, A., Shi, R., and Luciani, D.S. (2020). A pipeline for multidimensional confocal analysis of mitochondrial morphology, function, and dynamics in pancreatic β-cells. American Journal of Physiology-Endocrinology and Metabolism *318*, E87-E101. 10.1152/ajpendo.00457.2019.
157. Schwartz, A.Z.A., Tsyba, N., Abdu, Y., Patel, M.R., and Nance, J. (2022). Independent regulation of mitochondrial DNA quantity and quality in Caenorhabditis elegans primordial germ cells. eLife *11*, e80396. 10.7554/eLife.80396.

bioRxiv preprint doi: https://doi.org/10.1101/2025.05.02.651978; this version posted May 3, 2025. The copyright holder for this preprint (which was not certified by peer review) is the author/funder. All rights reserved. No reuse allowed without permission.

Figure 1. An increase in ATP accompanies AC invasion. (**A**) A timeline of anchor cell (AC) invasion through the basement membrane (BM) in L3 *C. elegans* larva (top image). Schematics (top panel) and micrographs (bottom panel; differential interference contrast (DIC, gray) microscopy with the AC (magenta, *lin-29p*::2xmKate2::PLCδPH) and the BM (green, laminin::mNG) of the lateral view of AC invasion from the P6.p early 1-cell stage of the 1° vulval precursor cells (VPCs) to the P6.p 4-cell stage. (**B**) (Left) Spectral fluorescence intensity maps of the ATP:ADP ratio as visualized by PercevalHR (*eef-1A.1p*::PercevalHR) in the AC (arrowhead) before (P6.p early 1-cell (E1C) and 1-cell stage (1C)) and during (P6.p 2-cell (2C), 2-4 cell (2-4C) and 4-cell (4C) stages) BM breaching. This and all subsequent color calibration bar represent the minimum and maximum pixel value range of the acquired data. (Right) Quantification of total ATP:ADP ratio over time, n ≥ 19 animals per time point. One-way ANOVA with Tukey's post hoc test for multiple comparisons, **** $p < 0.0001$. (**C**) (Left) ATP levels as visualized by the ATP biosensor iATPSnFR1.0 (*eef-1A.1p*::iATPSnFR1.0) in the AC (arrowhead) before (E1C and 1C), during (2C, 2-4C), and after (4C) stages, BM breaching. Scale bar, 5 μm. (Right) Quantification of normalized iATPSnFR levels over time, n ≥ 12 animals per time point. One-way ANOVA with Tukey's post hoc test for multiple comparisons, **** $p < 0.0001$. (**D**) (Left) ATP levels (*eef-1A.1p*::iATPSnFR1.0) at the P6.p 2-cell stage in the AC (yellow outline) and uterine cell (UC, blue outline). (Right) Quantification of normalized iATPSnFR levels in AC versus UC at the P6.p 2-cell stage, n = 13 animals. Paired two-tailed t-test, **** $p < 0.0001$. (**E**) (Left) ATP levels (*eef-1A.1p*::iATPSnFR1.0) in the AC of control and rotenone-treated animals at the P6.p 2-cell stage. (Right) Quantification of normalized iATPSnFR levels in AC of control and rotenone-treated animals, n ≥ 16 animals per condition. Unpaired two-tailed t-test, ** $p < 0.01$. (**F**) (Left) Control and rotenone-treated animals were scored for AC (magenta, *cdh-3p*::2xmKate2mCherrry::PLCδPH) invasion through the BM (green, laminin::GFP) at the P6.p early 4-cell stage. Arrowheads indicate site of BM breaching. (Right) Quantification of invasion defects of control and rotenone-treated animals, n = 42 animals per condition. (**G**) (Left) Glycolytic ratiometric sensor, HYlight (*eef-1A.1p*::HYlight), in the AC of control and rotenone-treated animals at the P6.p 2-cell stage. (Right) Quantification of HYlight and HYlight-RA (HYlight control) ratiometric levels in the AC of control and rotenone-treated animals, n ≥ 10 animals per condition. One-way ANOVA with Tukey's post hoc test for multiple comparisons, ** $p < 0.01$, **** $p < 0.0001$. Representative ratiometric images of HYlight-RA control in Figure S1D.Scale bar, 5 μm.

bioRxiv preprint doi: https://doi.org/10.1101/2025.05.02.651978; this version posted May 3, 2025. The copyright holder for this preprint (which was not certified by peer review) is the author/funder. All rights reserved. No reuse allowed without permission.

Figure 2. ETC components are enriched in the AC mitochondria. (**A**) Schematic of mitochondrial membrane structure and electron transport chain (ETC) localization and composition in the inner mitochondrial membrane (IMM). The ETC is comprised of five multi-protein complexes (CI-CV) that generate an electrochemical proton gradient (red H+, arrows depict proton movement) used by Complex V (ATP synthase) to phosphorylate ADP to ATP. (**B**) (Left) Empty RNAi vector control and *nuo-1* RNAi-treated animals were scored for AC (magenta, *cdh-3p*::mCherry::PLCδPH) invasion through the BM (green, laminin::dendra) at the P6.p 4-cell stage. Arrowheads indicate site of BM breaching. Note smaller breach in *nuo-1* RNAi treated animals compared to empty vector control animals. (Right) Quantification of invasion defects of empty vector control and *nuo-1*, *nduv-2*, *ucr-2.1,* and *ant-1.1* RNAi-treated animals, n = 20 animals per condition. (**C**) (Left) Spectral fluorescence intensity maps of the ATP:ADP ratio (*eef-1A.1p*::PercevalHR) in the AC (arrowhead) of empty vector control and *nuo-1* RNAi-treated animals at the P6.p 2-cell stage. (Right) Quantification of ATP:ADP ratio in the P6.p 2-cell stage AC of empty vector control and *nuo-1*, *nduv-2*, and *ucr-2.1* RNAi-treated animals, n ≥ 28 animals per condition. One-way ANOVA with Dunnett's test for multiple comparisons, **** $p < 0.0001$. (**D**) Waffle plot of fluorescence intensity of ETC components per mitochondrion in the P6.p 2-cell stage AC versus uterine cell (UC). Each square represents 1000 a.u., n ≥ 10 animals for each ETC component, AC and UC measurements made in the same animal. (**E**) Representative images of one endogenously tagged ETC components per ETC complex in the P6.p 2-cell stage AC (arrowhead). Note the enriched expression of ETC components in the AC. Scale bar, 5 μm

bioRxiv preprint doi: https://doi.org/10.1101/2025.05.02.651978; this version posted May 3, 2025. The copyright holder for this preprint (which was not certified by peer review) is the author/funder. All rights reserved. No reuse allowed without permission.

Figure 3. AC high-capacity mitochondria have enriched protein import machinery and dense cristae. (**A**) Schematic of cristae in the mitochondria that house the ETC complexes. Mitochondrial protein translocases (TOM complex) localize in the outer mitochondrial membrane (OMM), while MICOS proteins localize in the inner mitochondrial membrane (IMM) where they stabilize cristae formation. Cardiolipin, synthesized by cardiolipin synthase, is essential for the folding of the IMM. (**B**) (Left) NUO-1::mNG in the AC (arrowhead) at the P6.p early 2-cell stage in empty vector control and *tomm-20*, *immt-1*, and *crls-1* RNAi-treated animals. Note the loss of NUO-1::mNG enrichment in the RNAi treated animals. (Right) Quantification of fluorescence intensity NUO-1::mNG per mitochondrion in empty vector control and *tomm-20*, *immt-1*, and *crls-1* RNAi-treated animals, n ≥ 15 animals for each condition. One-way ANOVA followed by uncorrected Fisher's LSD post hoc test, * $p < 0.05$, ** $p < 0.01$, **** $p < 0.0001$. (**C**) (Left) Empty RNAi vector control and *tomm-20* RNAi-treated animals scored for AC (magenta, *cdh-3p*::mCherry::PLCδPH) invasion through the BM (green, laminin::dendra) at the P6.p 4-cell stage. Arrowheads indicate site of BM breaching. Note smaller breach in *tomm-20* RNAi treated animals compared to control animals. Scale bar, 5 μm. (Right) Quantification of invasion defects in empty vector control and *tomm-20*, *immt-1*, and *crls-1* RNAi-treated animals, n = 20 animals per condition. (**D**) (Left) Spectral fluorescence intensity maps of the ATP:ADP ratio (*eef-1A.1p*::PercevalHR) in the AC (arrowheads) of empty vector control and *tomm-20*, *immt-1*, and *crls-1* RNAi-treated animals at the P6.p 2-cell stage. (Right) Quantification of ATP:ADP ratio in the P6.p 2-cell stage AC of vector control and *tomm-20*, *immt-1*, and *crls-1* RNAi-treated animals, n > 20 animals per condition. One-way ANOVA with Dunnett's test for multiple comparisons, * $p < 0.05$, **** $p < 0.0001$. (**E**) Waffle plot of fluorescence intensity of IMMT-1::mNG, TOMM-20::mNG, and CRLS-1::mNG per mitochondrion in the P6.p 2-cell stage AC versus uterine cell (UC). NUO-1::mNG included as representative ETC component. Each square represents 1000 a.u., n ≥ 14 animals for each component, AC and UC measurements made in the same animal. (**F**) NUO-1::mNG, IMMT-1::mNG, TOMM-20::mNG, and CRLS-1::mNG in the AC (arrowheads) at the P6.p 2-cell stage. Scale bar, 5 μm

bioRxiv preprint doi: https://doi.org/10.1101/2025.05.02.651978; this version posted May 3, 2025. The copyright holder for this preprint (which was not certified by peer review) is the author/funder. All rights reserved. No reuse allowed without permission.

Figure 4. High-capacity mitochondria are established early during AC invasive differentiation. (**A**) (Left) NUO-1::mNG (grey) in P6.p early 2-cell AC (*cdh-3p*::moseinABD::mCherry, magenta) in empty vector control and *egl-43* RNAi-treated animals. (Right) Quantification of NUO-1::mNG and UCR-2.1::mNG fluorescence intensity per mitochondrion in control and *egl-43* RNAi-treated animals, n ≥ 14 animals per condition. Paired two-tailed t test, **** $p < 0.0001$. (**B**) Schematic of early AC and ventral uterine cell (VU) specification from two-proto-uterine cells (α1 and α2) via stochastic LAG-2 (Notch)/LIN-12 (Delta) signaling pre-AC specification (top) and post-AC specification (bottom). (**C**) (Left) α1 and α2 (*lag-2p*::2xmKate2::PH, magenta, top panels) and IMMT-1::mNG (grey, left panels) or TOMM-20::mNG (grey, right panels). (Right) Quantification of the *lag-2p*::2xmKate2::PH α1:α2 ratio correlated with the α1:α2 ratio of TOMM-20::mNG, IMMT-1::mNG, CRLS-1::mNG, NDUV-2::NG, or UCR-2.1::mNG, n ≥ 12 animals per strain. Simple linear regression to determine if slope is significantly non-zero, indicating a correlative relationship, * $p < 0.05$. (**D**) (Left) Developmental progression of IMMT-1::mNG (top panel) and TOMM-20::mNG (bottom panel) expression in the AC (arrowhead) from the P6.p early 1-cell (E1C) to the P6.p 4-cell (4C) stage. (Right) Quantification of IMMT-1::mNG (top graph) and TOMM-20::mNG (bottom graph) mean fluorescence intensity per AC mitochondria from the E1C to 4C stage, n ≥ 12 animals per stage for each strain. One-way ANOVA with Tukey's post hoc test for multiple comparisons, ** $p < 0.01$, **** $p < 0.0001$. Scale bar, 5 μm.

bioRxiv preprint doi: https://doi.org/10.1101/2025.05.02.651978; this version posted May 3, 2025. The copyright holder for this preprint (which was not certified by peer review) is the author/funder. All rights reserved. No reuse allowed without permission.

Figure 5. High-capacity mitochondria are basally enriched during invasion. (A) Schematic depicting mitochondria (teal) in both the apical and basal portions of the AC at the P6.p 2-cell stage (basement membrane, BM; vulval precursor cells, VPC). (**B**)Waffle plot of ETC components, CRLS-1, TOMM-20, and IMMT-1 fluorescence intensity per mitochondrion in the apical versus basal mitochondria in P6.p 2-cell stage AC. Each square represents 1000 a.u., n ≥ 10 animals for each protein, apical and basal measurements made in the same AC. (**C**) UCR-2.1::mNG (Left) and NUO-1::mNG (Right) expression in the P6.p early-1-cell and late-1-cell stage AC. Quantification of basal to apical UCR-2.1::mNG (Left) and NUO-1::mNG (Right) fluorescence intensity per mitochondrion in the early 1-cell and late 1-cell AC (yellow dashed outline), n ≥ 10 animals per stage. Unpaired two-tailed t-test, *** $p < 0.001$, **** $p < 0.0001$. (**D**) Schematic of FRAP experiment. (Left panel) Pre-bleach – apical mitochondria (magenta) are separate from basal mitochondria (green). (Middle panel) Bleach – 405nm laser (lightning bolt) photo-bleaches half of the basal mitochondria (blue outline). (Right panel) Recovery – determining if, and from where, the mitochondrial signal is recovered in the bleached basal region (blue outline). (**E**) (Left) NUO-1::mNG in the AC (top) and uterine cell (UC, bottom) mitochondria before, immediately after photobleaching, and 15 minutes post-photobleaching. Blue outline indicates bleached region, green outline indicates adjacent basal mitochondria, and magenta outline indicates apical mitochondria. (Right) Line graphs of normalized NUO-1::mNG fluorescence intensity pre-bleach, immediately after photobleaching, and 15 minutes after bleaching in the AC (top) and UC (bottom), n = 6 for each cell type. Scale bar, 5 μm.

bioRxiv preprint doi: https://doi.org/10.1101/2025.05.02.651978; this version posted May 3, 2025. The copyright holder for this preprint (which was not certified by peer review) is the author/funder. All rights reserved. No reuse allowed without permission.

Figure 6. Netrin polarizes high-capacity mitochondria to the BM breach site. (**A**) Time-lapse of AC mitochondria (NUO-1::mNG, gray) prior to BM (EMB-9::mRuby2, magenta) breaching, during the initial breach, and as the breach is expanded. Animals were imaged every 1 min for 31 minutes. Bottom panels show enlarged areas corresponding to boxed regions in top panel. Yellow arrowhead indicates site of BM breaching, white arrow indicates mitochondria within the invasive protrusion. (**B**) (Left) NUO-1::mNG with BM (EMB-9::mRuby2, magenta) in wild-type and netrin mutant (*unc-6 (ev400)*) animals at the P6.p 2-cell stage. Yellow arrowheads indicate site of NUO-1::mNG enrichment. (Right) Quantification of basal to apical NUO-1::mNG fluorescence intensity per mitochondrion in wild-type and *unc-6* (*ev400*) mutant animals, n ≥ 14. Unpaired t-test, ** $p < 0.01$. (**C**) (Left) Spectral fluorescence intensity maps of the AC-specific ATP:ADP ratio (*lin-29p*::PercevalHR) of wild-type and netrin mutant (*unc-6 (ev400)*) animals at the P6.p early 2-cell stage. Arrowheads indicate site of ATP:ADP enrichment. (Right) Quantification of ATP:ADP ratio in basal versus apical regions of wild-type and *unc-6* (*ev400*) mutant P6.p 2-cell AC, n ≥ 19. Unpaired t-test, **** $p < 0.0001$. Scale bar, 5 µm.

bioRxiv preprint doi: https://doi.org/10.1101/2025.05.02.651978; this version posted May 3, 2025. The copyright holder for this preprint (which was not certified by peer review) is the author/funder. All rights reserved. No reuse allowed without permission.

Figure 7. Netrin-mediated microtubule polarization directs mitochondria to the invasive front. (**A**) (Top) AC-specific microtubule marker (*lin-29p*::EMTB::GFP, top) in wild-type and netrin mutant (*unc-6 (ev400)*) animals at the P6.p 2-cell stage. (Bottom) Spectral fluorescence intensity maps applied to emphasize microtubule enriched areas (arrowheads). (Right) Quantification of basal to apical microtubule fluorescence intensity in wild-type versus *unc-6 (ev400)* mutant animals, n ≥ 20 animals. Unpaired two-tailed t-test, *** p <0.001. (**B**) (Top) Endogenously tagged plus-end (EBP-2::GFP) and minus-end (GFP::GIP-1) microtubule-associated proteins in the AC (yellow arrowhead) at the P6.p 2-cell stage. (Bottom) Spectral fluorescence intensity maps applied to emphasize microtubule-associated protein enriched areas (white arrowheads). (Right) Quantification of basal to apical microtubule plus-end and minus-end protein fluorescence intensity, n ≥ 11. Unpaired two-tailed t-test, **** p < 0.0001. (**C**) (Left) NUO-1::mNG in the AC of empty vector control and *mtx-1* and *mtx-2* RNAi-treated animals at the P6.p early 2-cell stage. Yellow arrowhead indicates NUO-1::mNG enriched mitochondria. (Right) Quantification of basal to apical NUO-1::mNG fluorescence intensity per mitochondrion in empty vector control and *mtx-1* and *mtx-2* RNAi-treated animals, n = 19 animals. One-way ANOVA with Dunnett's multiple comparison test, **** p < 0.0001. (**D**) (Top) Endogenously tagged MTX-1::mNG and MTX-2::mNG in P6.p 2-cell stage ACs (yellow arrowhead). (Bottom) Spectral fluorescence intensity maps of MTX-1::mNG and MTX-2::mNG to emphasize metaxin enriched areas (white arrowheads). (Right) Quantification of basal to apical MTX-1::mNG and MTX-2::mNG fluorescence intensity per mitochondrion, n = 15 animals for each strain. (**E**) (Top) SRC-1::GFP in the AC (yellow arrowhead) in wild-type and netrin mutant (*unc-6 (ev400)*) animals at the P6.p 2-cell stage. (Bottom) Spectral fluorescence intensity maps to emphasize SRC-1::GFP enriched areas (white arrowheads). (Right) Quantification of basal to apical SRC-1::GFP fluorescence intensity in wild-type versus *unc-6 (ev400)* mutant animals, n = 11 animals. Unpaired two-tailed t-test, **** p < 0.0001**.** (**F**) (Left) NUO-1::mNG in P6.p 2-cell ACs in wild-type and *src-1 (lq185)* mutant animals. Yellow arrowhead indicates NUO-1::mNG enriched mitochondria. (Right) Quantification of basal to apical NUO-1::mNG fluorescence intensity per mitochondrion in wild-type versus *src-1 (lq185)* mutant animals, n ≥ 15 animals. Unpaired two-tailed t-test, *** p < 0.001. (**G**) (Left) AC-specific microtubule marker (*lin-29p*::EMTB::GFP) in P6.p 2-cell ACs in wild-type and *src-1 (lq185)* mutant animals. Yellow arrowhead indicates microtubule enriched areas. (Right) Quantification of basal to apical microtubule fluorescence intensity in wild-type versus *src-1 (lq185)* mutant animals, n = 20 animals. Unpaired two-tailed t-test, ** p < 0.01. (**H**) (Left) UCR-2.1::mNG in P6.p 2-cell ACs in control and rotenone-treated animals. Yellow arrowhead indicates UCR-2.1::mNG enriched mitochondria. (Right) Quantification of basal to apical UCR-2.1::mNG fluorescence intensity per mitochondrion in control and rotenone-treated animals, n = 18 animals. Unpaired two-tailed t-test, ** p < 0.01. Scale bar, 5 μm.

bioRxiv preprint doi: https://doi.org/10.1101/2025.05.02.651978; this version posted May 3, 2025. The copyright holder for this preprint (which was not certified by peer review) is the author/funder. All rights reserved. No reuse allowed without permission.

Figure S1. ATP increase in the AC is not a result of glycolysis or mitochondrial abundance, related to Figure 1.

(**A**) (Left) Promoter-driven cytosolic GFP levels as visualized by *eef-1A.1p*::GFP as a control for *eef-1A.1p*::iATPSnFR1.0. Representative images of GFP in the AC (arrowheads) before (P6.p early 1-cell (E1C) and 1-cell (1C) stage) and during (P6.p 2-cell (2C), 2-4 cell (2-4C)) and after (4-cell (4C) stages) BM breaching. (Right) Quantification of normalized cytosolic GFP levels over developmental time, n ≥ 10 animals per time point. One-way ANOVA with Tukey's post hoc test for multiple comparisons. Note there is no significant differences in GFP levels between adjacent stages.

(**B**) (Left) HYlight ratiometric glycolytic sensor (*eef-1A.1p*::HYlight) and (Middle) HYlight-RA control (*eef-1A.1p*::HYlight-RA) and differential interference contrast (DIC) images of P6.p 2-cell AC (yellow outline) and uterine cell (UC, blue outline). The HYlight-RA control has reduced affinity for FBP and does not respond to changes in FBP concentration. (Right) Quantification of HYlight and HYlight-RA ratiometric levels in the P6.p 2-cell AC and UC, n ≥ 16 animals per condition. One-way ANOVA with Tukey's post hoc test for multiple comparisons, **** $p < 0.0001$.

(**C**) (Left) Spectral fluorescence intensity maps of the ATP:ADP ratio (*eef-1A.1p*::PercevalHR) in wild-type and UCP-4 overexpression worms (*lin-29p::UCP-4::SL2::mKate2::PH*).(Right) Quantification of ATP:ADP ratio in wildtype and UCP-4 overexpression P6.p 2-cell AC, n = 10 animals. Unpaired two-tailed t-test **** $p < 0.0001$.

(**D**) HYlight-RA (*eef-1A.1p*::HYlight-RA) glycolytic sensor control, in the AC of control and rotenone-treated animals that correspond to the data presented in Figure 1G. Note no difference in HYlight-RA in control and rotenone-treated animals.

(**E-F**) Mitochondrial morphology characterization in AC versus UC at the P6.p 2-cell stage. (**E**) (Left) Isosurface renderings of mitochondrial volume (visualized by *rpl-28p*::TOMM-20::mKate2, magenta) using Imaris. (Right) Mitochondrial volume quantification determined from isosurface renderings, n = 8 animals. Paired two-tailed t-test, ** $p < 0.01$. (**F**) Quantification of mitochondrial branch number and sphericity, n = 8 animals. Paired two-tailed t-test. Note no significant difference in branch number or sphericity between AC and UC.

(**G**) (Left) Mitochondrial DNA transcription factor, HMG-5, as visualized by HMG-5::GFP in AC (yellow outline) and UC (blue outline) at the P6.p 2-cell stage. (Right) Quantification of the number of HMG-5::GFP puncta in the AC and neighboring UC, n = 16 animals. Paired two-tailed t-test. Note no significant difference in HMG-5 puncta between AC and UC.

Scale bar, 5 μm.

bioRxiv preprint doi: https://doi.org/10.1101/2025.05.02.651978; this version posted May 3, 2025. The copyright holder for this preprint (which was not certified by peer review) is the author/funder. All rights reserved. No reuse allowed without permission.

Figure S2. AC mitochondria are enriched in ETC components as quantified via transcriptomics and visualized by endogenous tags, related to Figure 2.

(**A**) MitoCarta[78] Pathways gene-set enrichment analysis performed on transcriptome[50] comparing the AC and the whole body. Two-sided bar plot visualizes the normalized enrichment score (NES) for MitoCarta pathways. Pink box indicates the top ten enriched pathways in the AC. Note 7 of the 10 pathways (bolded) encode proteins involved in the ETC and OXPHOS.

(**B**) AC invasion defects in *ucr-2.1*, *nduv-2* and *ant-1.1* RNAi-treated animals. Arrowheads indicate sites of incomplete BM (green, laminin::dendra) breaching by the AC (magenta, *cdh-3p*::mCherry::PLCδPH) at the P6.p 4-cell stage, corresponding to the data quantified in Figure 2B. Note example of blocked invasion from *ant-1.1* RNAi treatment.

(**C**) Spectral fluorescence intensity map of the ATP:ADP ratio (*eef-1A.1p*::PercevalHR) in the AC (arrowhead) of empty vector control, *ucr-2.1,* and *nduv-2* RNAi-treated animals at the P6.p early 2-cell stage, corresponding to the data quantified in Figure 2C.

(**D**) (Left) HYlight (*eef-1A.1p*::HYlight) and HYlight-RA control (*eef-1A.1p*::HYlight-RA) in the AC (pink outline) in empty vector control and *nuo-1* RNAi-treated animals. (Right) Quantification of HYlight and HYlight-RA ratiometric levels in the AC of empty vector control and *nuo-1* RNAi-treated animals, n = 16 animals per condition. One-way ANOVA with Tukey's post hoc test for multiple comparisons, **** $p \leq 0.0001$, * $p < 0.05$.

(**E**) Seahorse measurements of mitochondrial oxygen consumption rate (OCR) parameters for 8 endogenously tagged ETC. Tagged strains compared to wild-type (N2) OCR. One-way ANOVA with Dunnett's multiple comparisons test, * $p < 0.05$, ** $p < 0.01$.

(**F**) Endogenously tagged ETC components within each complex in the P6.p 2-cell stage AC (arrowhead).

(**G**) Quantification of fluorescence intensity of mNG tagged ETC components per mitochondrion in the AC versus the uterine cell (UC), n ≥ 10 animals for each tagged component, AC and UC measurements made in the same animal. Mixed-effects ANOVA with Geisser-Greenhouse correction, followed by uncorrected Fisher's LSD post hoc test, * $p < 0.05$, *** $p < 0.001$, **** $p < 0.0001$.

(**H**) (Left) TMRE staining for mitochondrial membrane potential in the AC (top, yellow outline) versus UC (bottom, blue outline) of P6.p 2-cell stage wild-type (N2) animals. (Right) Quantification of TMRE mean fluorescence intensity per mitochondrion in the AC versus UC, n = 9 animals. Paired two-tailed t-test, **** $p < 0.0001$.

Scale bar, 5 μm.

bioRxiv preprint doi: https://doi.org/10.1101/2025.05.02.651978; this version posted May 3, 2025. The copyright holder for this preprint (which was not certified by peer review) is the author/funder. All rights reserved. No reuse allowed without permission.

Figure S3. Cristae and import machinery in the AC, related to Figure 3.

(**A**) (Left) Transmission electron microscopy (TEM) images of P6.p 2-cell stage AC (white outline), scale bar, 2 µm. Right panels show enlarged areas of AC mitochondria (blue box) and uterine cell (UC) mitochondria (yellow box) corresponding to boxed regions in left panel, scale bar 500 nm. (Right) Quantification of the ratio between inner membrane (IMM) area and outer membrane (OMM) area per mitochondrion in AC and UC. n = 15 mitochondria per cell type. Unpaired two-tailed t-test, ** $p < 0.01$.

(**B**) (Left) NDUV-2::mNG in the AC (arrowhead) at the P6.p early 2-cell stage in empty vector control and *tomm-20*, *immt-1*, and *crls-1* RNAi-treated animals. (Right) Quantification of NDUV-2::mNG fluorescence intensity per mitochondrion in empty vector control and *tomm-20*, *immt-1*, and *crls-1* RNAi-treated animals, n = 15 animals for each condition. One-way ANOVA with Dunnett's test for multiple comparisons, * $p < 0.05$.

(**C**) (Left) UCR-2.1::mNG in the AC (arrowhead) at the P6.p early 2-cell stage in empty vector control and *tomm-20*, *immt-1*, and *crls-1* RNAi-treated animals. (Right) Quantification of UCR-2.1::mNG fluorescence intensity per mitochondrion in empty vector control and *tomm-20*, *immt-1*, and *crls-1* RNAi-treated animals, n ≥ 16 animals for each condition. One-Way ANOVA with Dunnett's test for multiple comparisons, * $p < 0.05$, **** $p < 0.0001$.

(D) Quantification of IMMT-1::mNG, TOMM-20::mNG, CRLS-1::mNG, and NUO-1::mNG fluorescence intensity per mitochondrion in the AC versus the uterine cell (UC), n ≥ 14 animals for each tagged component, AC and UC measurements made in the same animal. Mixed-effects ANOVA with Geisser-Greenhouse correction, followed by uncorrected Fisher's LSD post hoc test, *** $p < 0.001$, **** $p < 0.0001$.

(E) (Left) NAO staining of cardiolipin in the AC (top, yellow outline) and UC (bottom, blue outline) of P6.p 2-cell stage wild-type (N2) animals. (Right) Quantification of NAO fluorescence intensity per mitochondrion in the AC versus UC, n = 10 animals. Paired two-tailed t test, *** $p < 0.001$.

Unless noted otherwise, scale bar, 5 µm.

bioRxiv preprint doi: https://doi.org/10.1101/2025.05.02.651978; this version posted May 3, 2025. The copyright holder for this preprint (which was not certified by peer review) is the author/funder. All rights reserved. No reuse allowed without permission.

Figure S4. High-capacity mitochondria are specialized early during AC differentiation, related to Figure 4.

(**A**) UCR-2.1::mNG in the AC (arrowhead) in empty vector control and *egl-43* RNAi-treated animals, corresponding to the quantification reported in Figure 4A.

(**B**) CRLS-1::mNG (gray, left panel), UCR-2.1::mNG (gray, middle panel) and NDUV-2::mNG (grey, right panel) with *lag-2p*::2xmKate2::PH (magenta) in α1 and α2 during AC specification.

(**C**) (Left) Developmental progression of CRLS-1::mNG (top panel), UCR-2.1::mNG (middle panel) and NDUV-2::mNG (bottom panel) expression in the AC (arrowhead) from the P6.p early 1-cell (E1C) to the P6.p 4-cell (4C) stage. (Right) Quantification of CRLS-1::mNG (top), UCR-2.1::mNG (middle) and NDUV-2::mNG (bottom) mean fluorescence intensity per AC mitochondria from the E1C to 4C stage, n ≥ 11 animals per stage for each strain. One-way ANOVA with Tukey's post hoc test for multiple comparisons, * $p < 0.05$, ** $p < 0.01$.

(**D**) Quantification of TOMM-20::mNG, IMMT-1::mNG, CRLS-1::mNG, NDUV-2::mNG, and UCR-2.1::mNG fluorescence intensity per mitochondrion in the AC versus uterine cell (UC) at the P6.p early 1-cell stage, n ≥ 12 animals per strain. Mixed-effects ANOVA with Geisser-Greenhouse correction, followed by uncorrected Fisher's LSD post hoc test, ** $p < 0.01$, *** $p < 0.001$.

(**E**) (Left) *nuo-1p*::mNG (top) and *nduv-2p*::mNG (bottom) transcriptional reporter in the AC (arrowhead) over developmental time from P6.p AC/VU decision to 4-cell stage. (Right) Quantification of *nuo-1p*::mNG (top) and *nduv-2p*::mNG (bottom) expression in the AC from the P6.p AC/VU decision to 4-cell stage, n ≥ 11 animals per strain per stage. At the AC/VU decision, both proto-uterine cells (α1 and α2) were measured because their cell fates are undetermined. One-way ANOVA with Tukey's post hoc test for multiple comparisons, * $p < 0.05$, ** $p < 0.01$, **** $p < 0.0001$.

Scale bar, 5 µm.

bioRxiv preprint doi: https://doi.org/10.1101/2025.05.02.651978; this version posted May 3, 2025. The copyright holder for this preprint (which was not certified by peer review) is the author/funder. All rights reserved. No reuse allowed without permission.

Figure S5. High-capacity mitochondria localize basally and remain separate from apical mitochondria, related to Figure 5.

(**A**) Quantification of apical and basal mitochondrial volume in the AC and uterine cell (UC), n = 30. RM one-way ANOVA, with the Geisser-Greenhouse correction, followed by Sidák's multiple comparisons test, with individual variances computed for each comparison, **** $p > 0.0001$.

(**B**) (Left) Spectral fluorescence intensity maps of TMRE staining in the AC of P6.p 2-cell stage animals. Note the basal enrichment of TMRE (arrowhead). (Right) Quantification of TMRE fluorescence intensity per mitochondrion in the apical versus basal mitochondria in the AC, n = 12 animals. Paired two-tailed t test, * $p < 0.05$.

(**C**) Quantification of fluorescence intensity of mNG tagged ETC components, CRLS-1::mNG, TOMM-20::mNG, and IMMT-1::mNG per mitochondrion in the apical versus basal mitochondria in P6.p 2-cell stage AC, n > 10 animals for each tagged component. Mixed-effects ANOVA with Geisser-Greenhouse correction, followed by uncorrected Fisher's LSD post hoc test, * $p < 0.05$, ** $p < 0.01$, *** $p < 0.001$, **** $p < 0.0001$.

(**D**) (Left) Additional examples of FRAP of NUO-1::mNG in the AC (top) and uterine cell (UC, bottom) mitochondria before, immediately after photobleaching, and 15 minutes post-photobleaching. Blue outline indicates bleached region, green outline indicates adjacent basal mitochondria, and magenta outline indicates apical mitochondria.

Scale bar, 5 μm

bioRxiv preprint doi: https://doi.org/10.1101/2025.05.02.651978; this version posted May 3, 2025. The copyright holder for this preprint (which was not certified by peer review) is the author/funder. All rights reserved. No reuse allowed without permission.

Figure S6. High-capacity mitochondria localize to the BM breach during invasion, related to Figure 6.

(**A**) Time-lapse of AC mitochondria (NUO-1::mNG, gray) prior to BM (EMB-9::mRuby2, magenta) breaching, during the initial breach, and as the breach is expanding. Animals were imaged every 1 minute for 25 minutes. Bottom panels show enlarged areas corresponding to boxed regions in top panel. Yellow arrowheads indicate site of BM breaching.

(**B**) Time-lapse of AC mitochondria (NUO-1::mNG, gray) during the BM (EMB-9::mRuby2, magenta) breaching, and as the breach is expanding. The BM underlying the AC is composed of two BM networks that are linked together during AC invasion[44]. Occasionally, the two previously linked BMs visibly separate. Animals were imaged every 1.5 minutes for 51 min. Bottom panels show enlarged areas corresponding to boxed regions in top panel. Yellow arrowheads indicate site of BM breaching. White arrow indicates mitochondria within the invasive protrusion.

Scale bars, 5 μm.

bioRxiv preprint doi: https://doi.org/10.1101/2025.05.02.651978; this version posted May 3, 2025. The copyright holder for this preprint (which was not certified by peer review) is the author/funder. All rights reserved. No reuse allowed without permission.

Figure S7. High-capacity mitochondria trafficking is dependent on metaxin adaptor complex, related to Figure 7.

(**A**) (Left) UCR-2.1::mNG in the AC of empty vector control and *mtx-1* and *mtx-2* RNAi-treated animals at the P6.p early 2-cell stage. Yellow arrowhead indicates UCR-2.1::mNG enriched mitochondria. (Right) Quantification of basal to apical UCR-2.1::mNG fluorescence intensity per mitochondrion in empty vector control and *mtx-1* and *mtx-2* RNAi-treated animals, n = 19 animals. One-way ANOVA with Dunnett's multiple comparison test, ** $p < 0.01$, * $p < 0.05$.

(**B**) (Left) MTX-2::mNG in the AC of wild-type and netrin mutant (*unc-6 (ev400)*) animals at the P6.p 2-cell stage. Yellow arrowhead indicates site of MTX-2::mNG enrichment. (Right) Quantification of basal to apical MTX-2::mNG fluorescence intensity in wild-type versus *unc-6 (ev400)* mutant animals, n ≥ 14. Unpaired two-tailed t-test,** $p < 0.01$.

(**C**) Quantification of basal to apical NUO-1::mNG fluorescence intensity per mitochondrion in empty vector control and AMPK subunit (*aak-1*, *aak-2*, *aakb-1*, and *aakb-2*) RNAi-treated animals, n =18. One-way ANOVA with Dunnett's multiple comparison test found no significant differences between the basal/apical ratio of the control and AMPK subunit RNAi-treated animals.

(**D**) (Left) UCR-2.1::mNG in the AC of empty vector and *nuo-1* RNAi-treated animals at the P6.p 2-cell stage. Yellow arrowhead indicates UCR-2.1::mNG enriched mitochondria. (Right) Quantification of basal to apical UCR-2.1::mNG fluorescence intensity in empty vector and *nuo-1* RNAi-treated animals, n ≥ 15 animals. Unpaired two-tailed t-test, * $p < 0.05$.

(**E**) Schematic of AC mitochondrial localization dependent on the netrin directional cue, microtubules, metaxins, and Src kinase. Basal localization of mitochondria results high levels of ATP at the invasive front.

Scale bar, 5 μm.

bioRxiv preprint doi: https://doi.org/10.1101/2025.05.02.651978; this version posted May 3, 2025. The copyright holder for this preprint (which was not certified by peer review) is the author/funder. All rights reserved. No reuse allowed without permission.

Movie S1. Time-lapse of mitochondria (NUO-1::mNG, gray) prior to and during AC invasion through the BM (EMB-9::mRuby2, magenta) and in the emerging protrusion. Animals were imaged every 1 min for 31 min.

Movie S2. Time-lapse of mitochondria (NUO-1::mNG, gray) prior to and during AC invasion through the BM (EMB-9::mRuby2, magenta) and in the emerging protrusion. Animals were imaged every 1 min for 25 min.

Movie S3 Mitochondria (NUO-1::mNG, gray) during AC invasion through the BM (EMB-9::mRuby2, magenta) and in the emerging protrusion. Animals were imaged every 1:30 min for 51 min.

Scale bar, 5 μm.

Figure 1

bioRxiv preprint doi: https://doi.org/10.1101/2025.05.02.651978; this version posted May 3, 2025. The copyright holder for this preprint (which was not certified by peer review) is the author/funder. All rights reserved. No reuse allowed without permission.

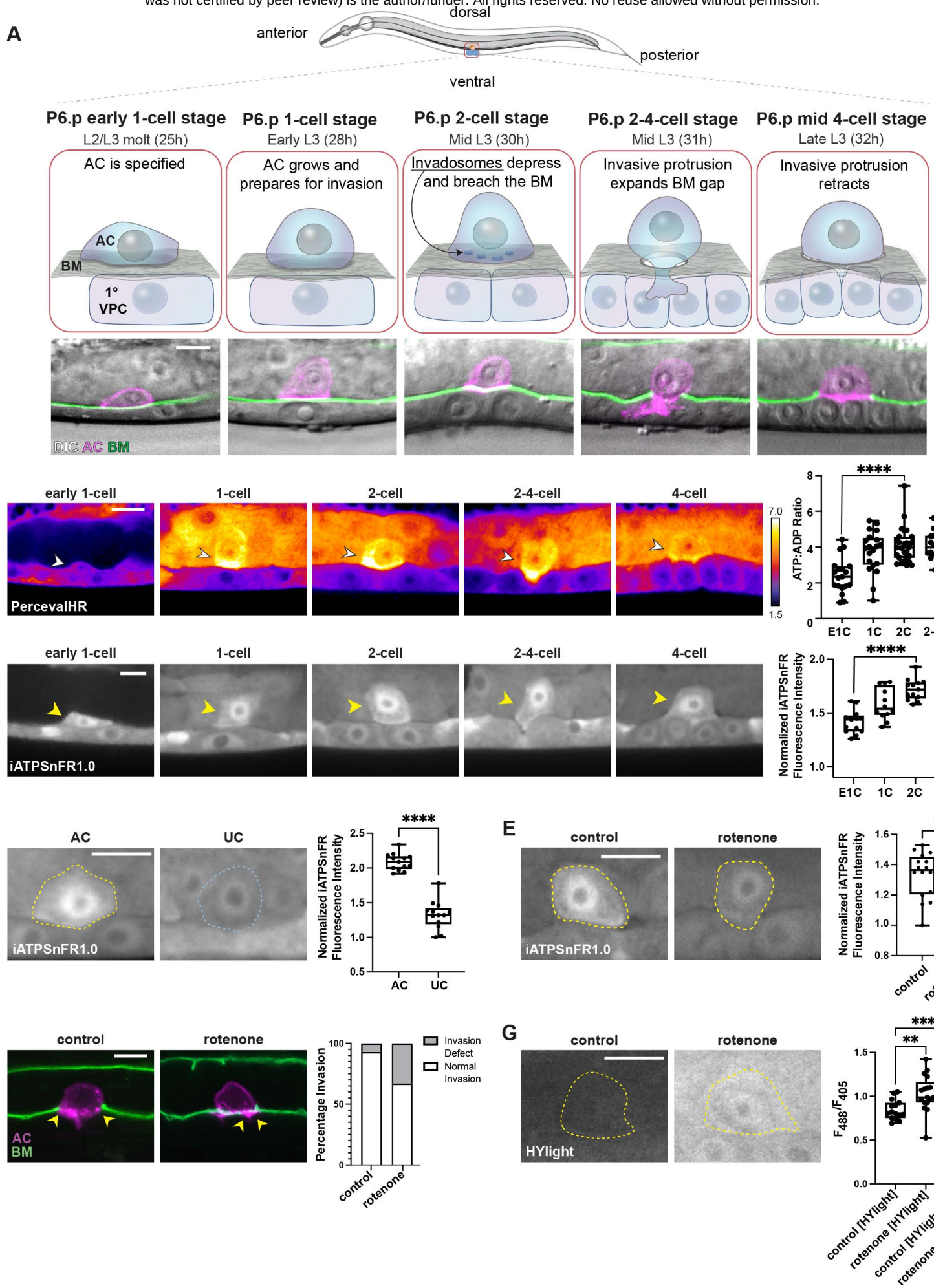

bioRxiv preprint doi: https://doi.org/10.1101/2025.05.02.651978; this version posted May 3, 2025. The copyright holder for this preprint (which was not certified by peer review) is the author/funder. All rights reserved. No reuse allowed without permission.

Figure 2

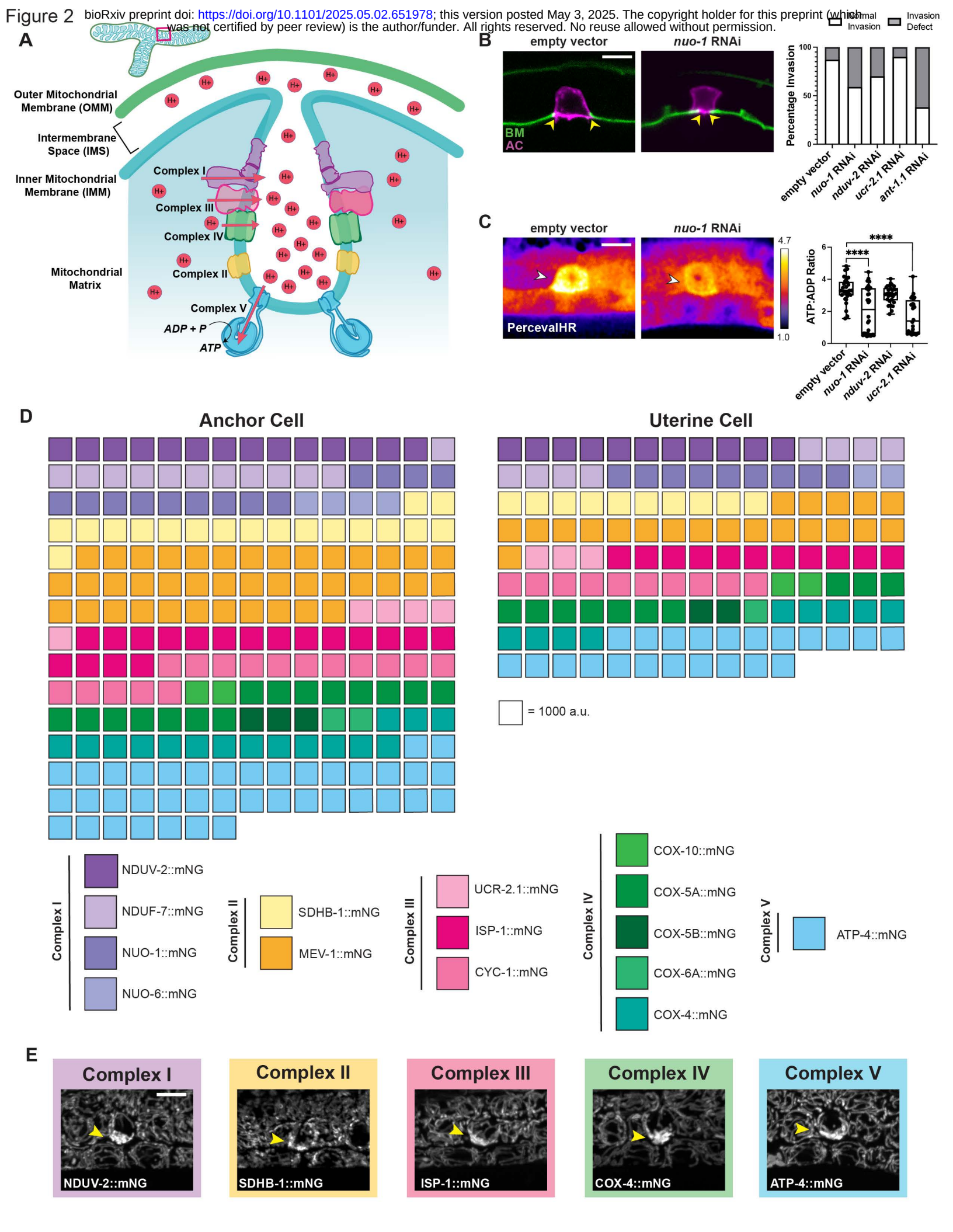

Figure 3

bioRxiv preprint doi: https://doi.org/10.1101/2025.05.02.651978; this version posted May 3, 2025. The copyright holder for this preprint (which was not certified by peer review) is the author/funder. All rights reserved. No reuse allowed without permission.

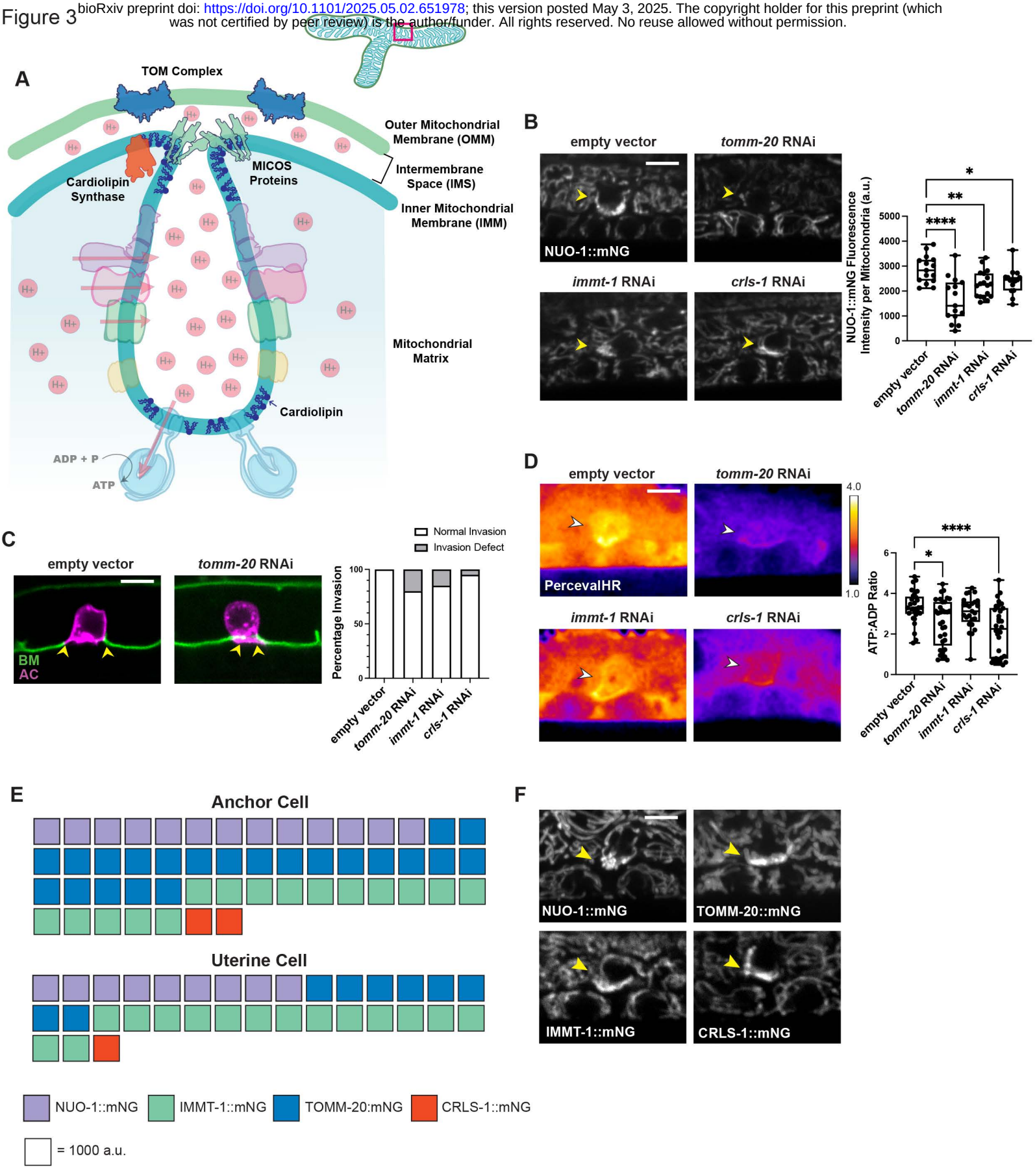

 bioRxiv preprint doi: https://doi.org/10.1101/2025.05.02.651978; this version posted May 3, 2025. The copyright holder for this preprint (which was not certified by peer review) is the author/funder. All rights reserved. No reuse allowed without permission.

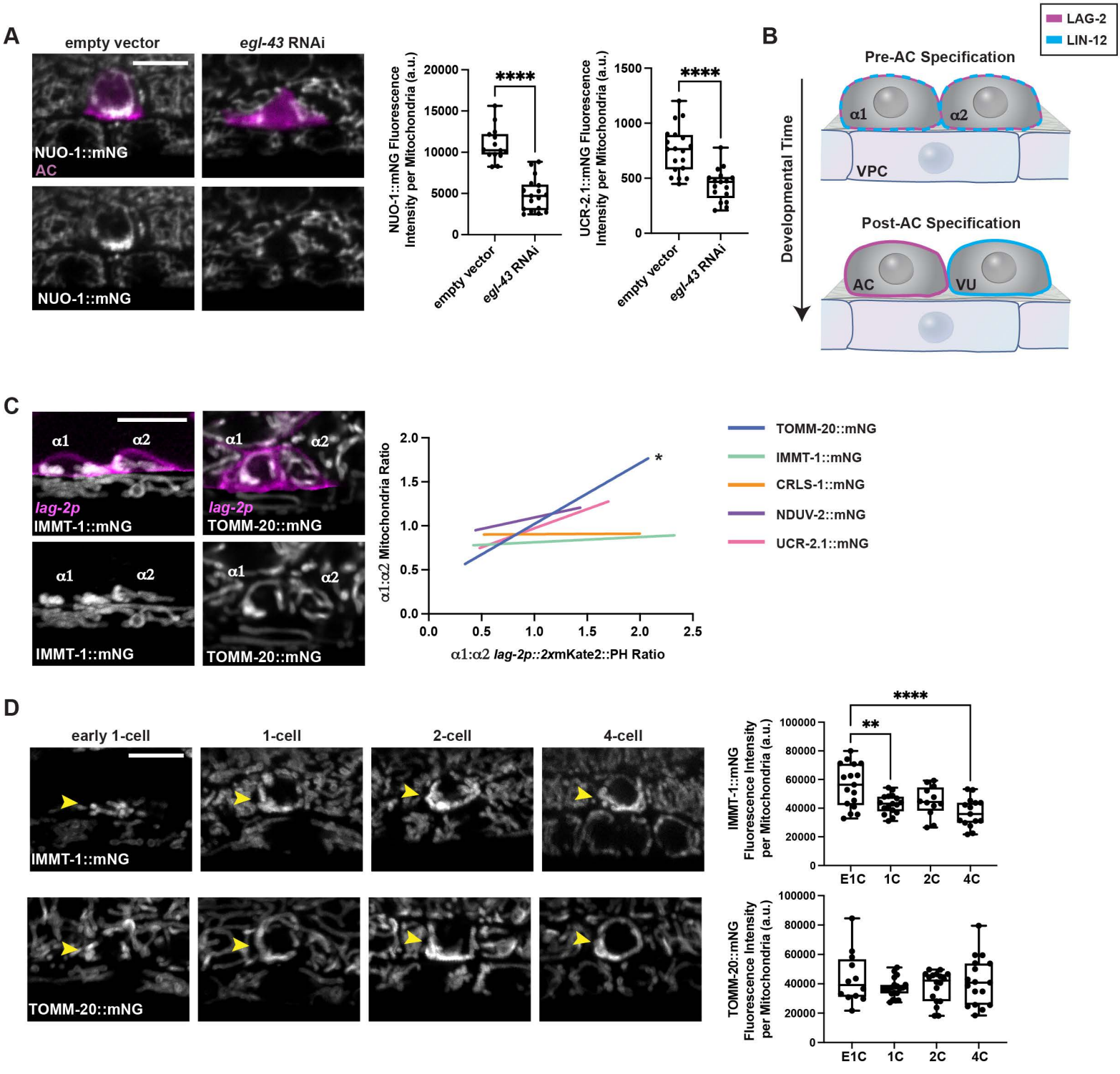

bioRxiv preprint doi: https://doi.org/10.1101/2025.05.02.651978; this version posted May 3, 2025. The copyright holder for this preprint (which was not certified by peer review) is the author/funder. All rights reserved. No reuse allowed without permission.

Figure 5

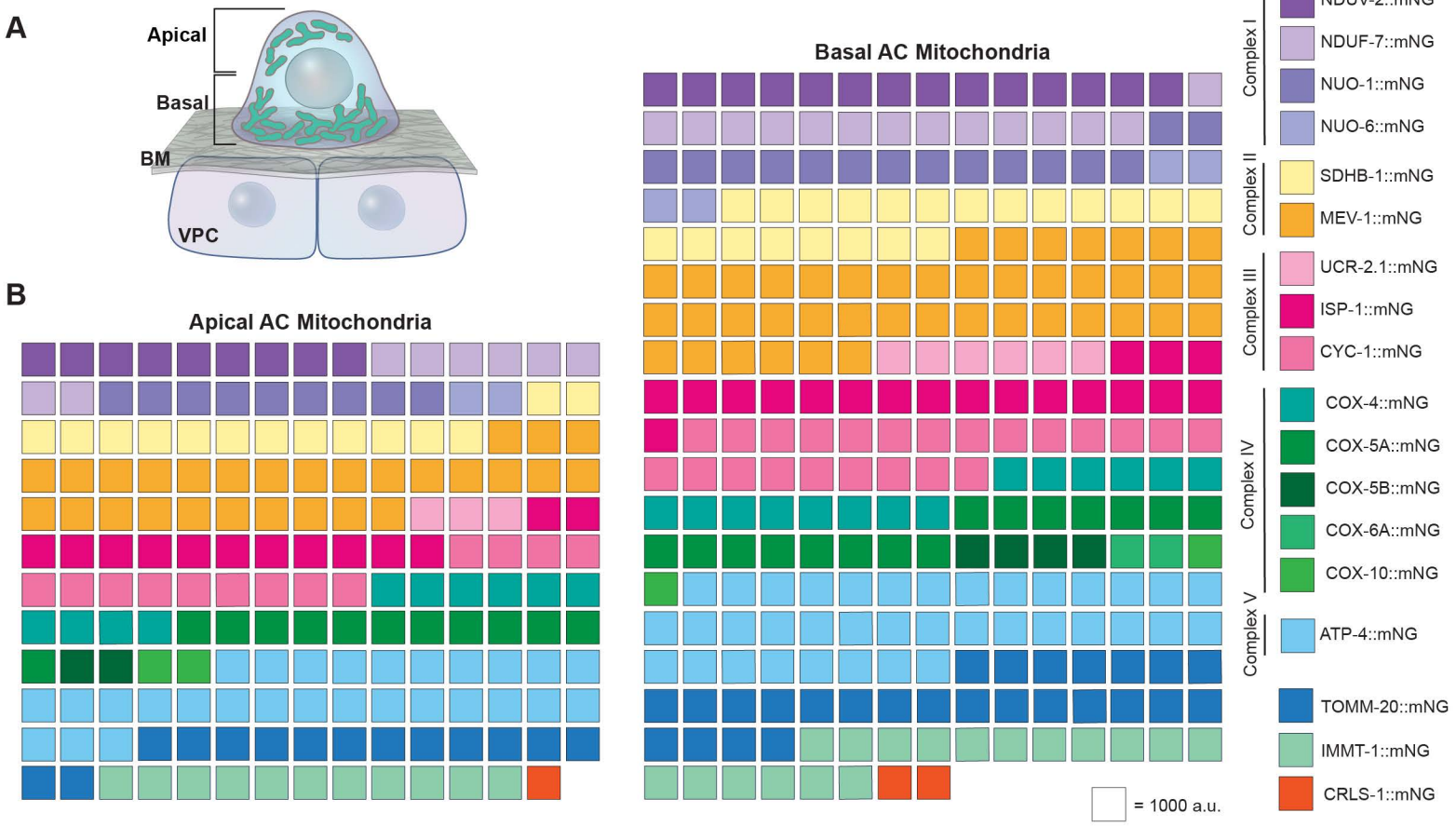

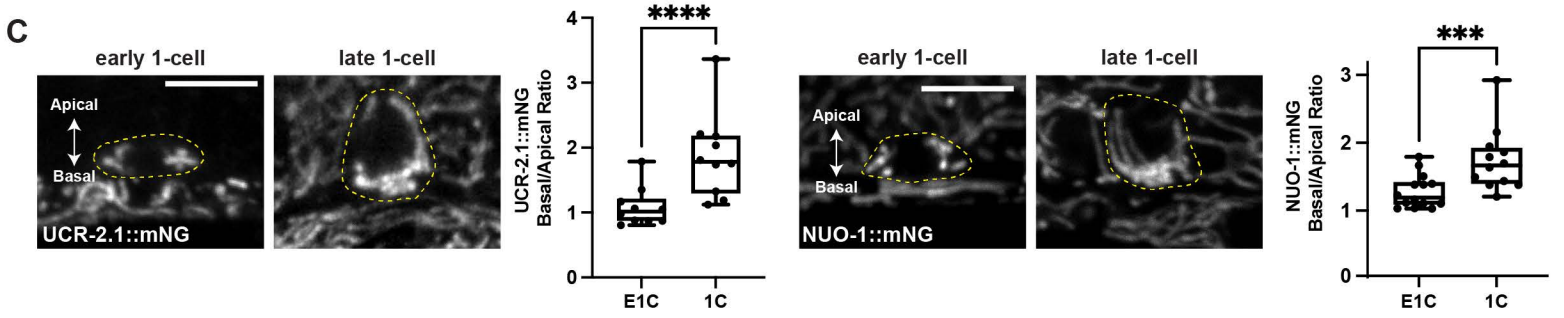

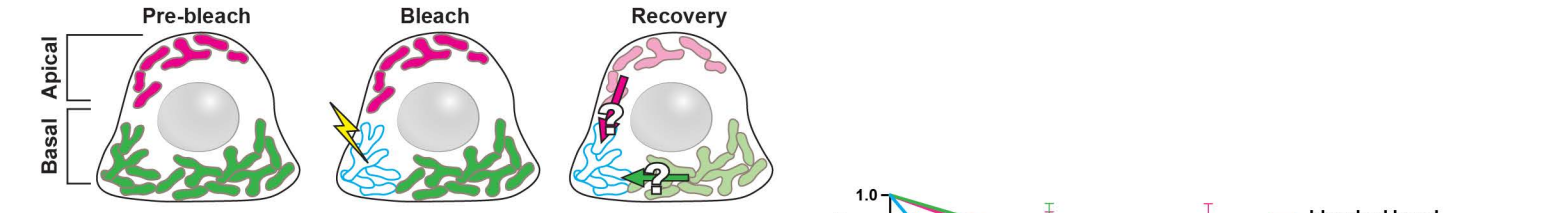

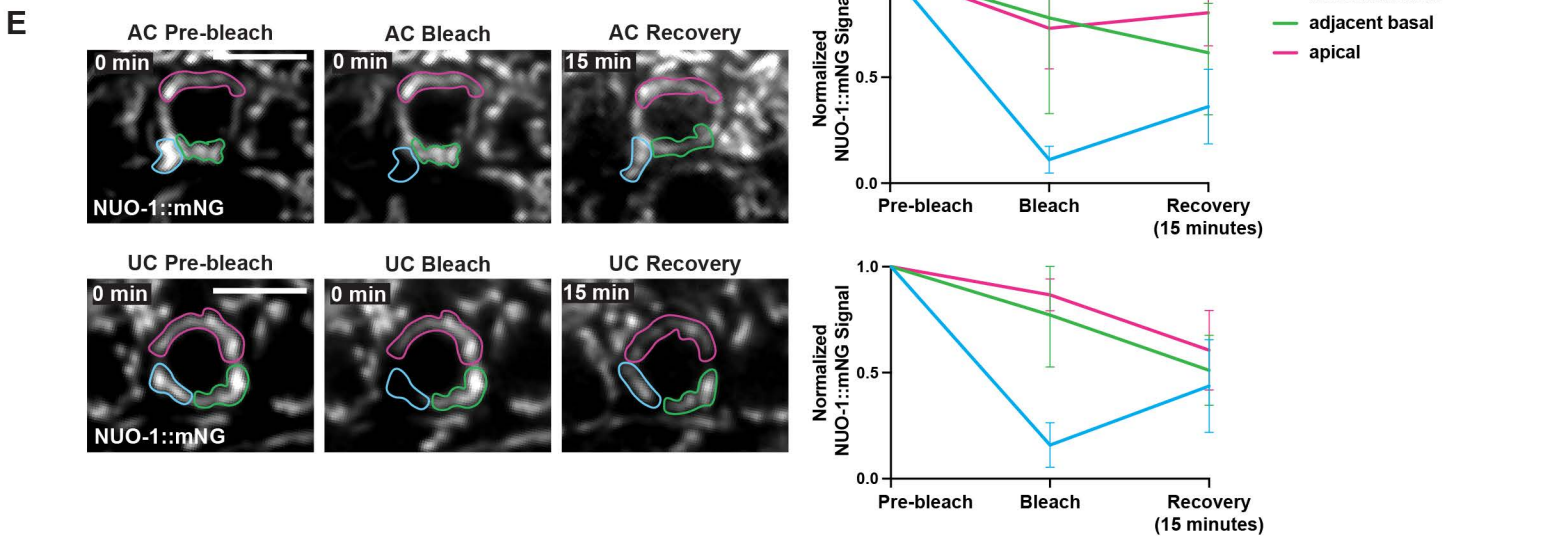

Figure 6

bioRxiv preprint doi: https://doi.org/10.1101/2025.05.02.651978; this version posted May 3, 2025. The copyright holder for this preprint (which was not certified by peer review) is the author/funder. All rights reserved. No reuse allowed without permission.

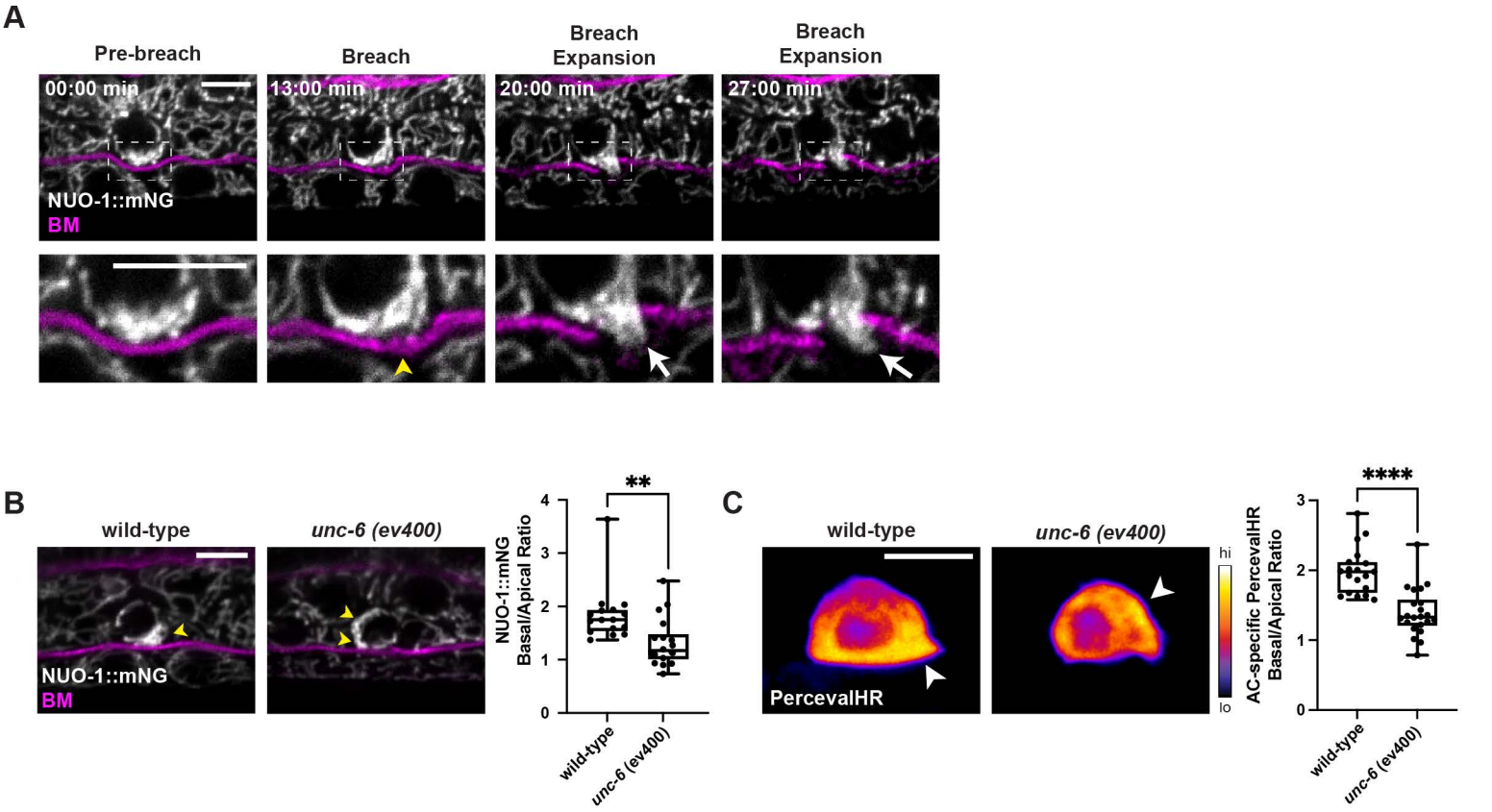

Figure 7 bioRxiv preprint doi: https://doi.org/10.1101/2025.05.02.651978; this version posted May 3, 2025. The copyright holder for this preprint (which was not certified by peer review) is the author/funder. All rights reserved. No reuse allowed without permission.

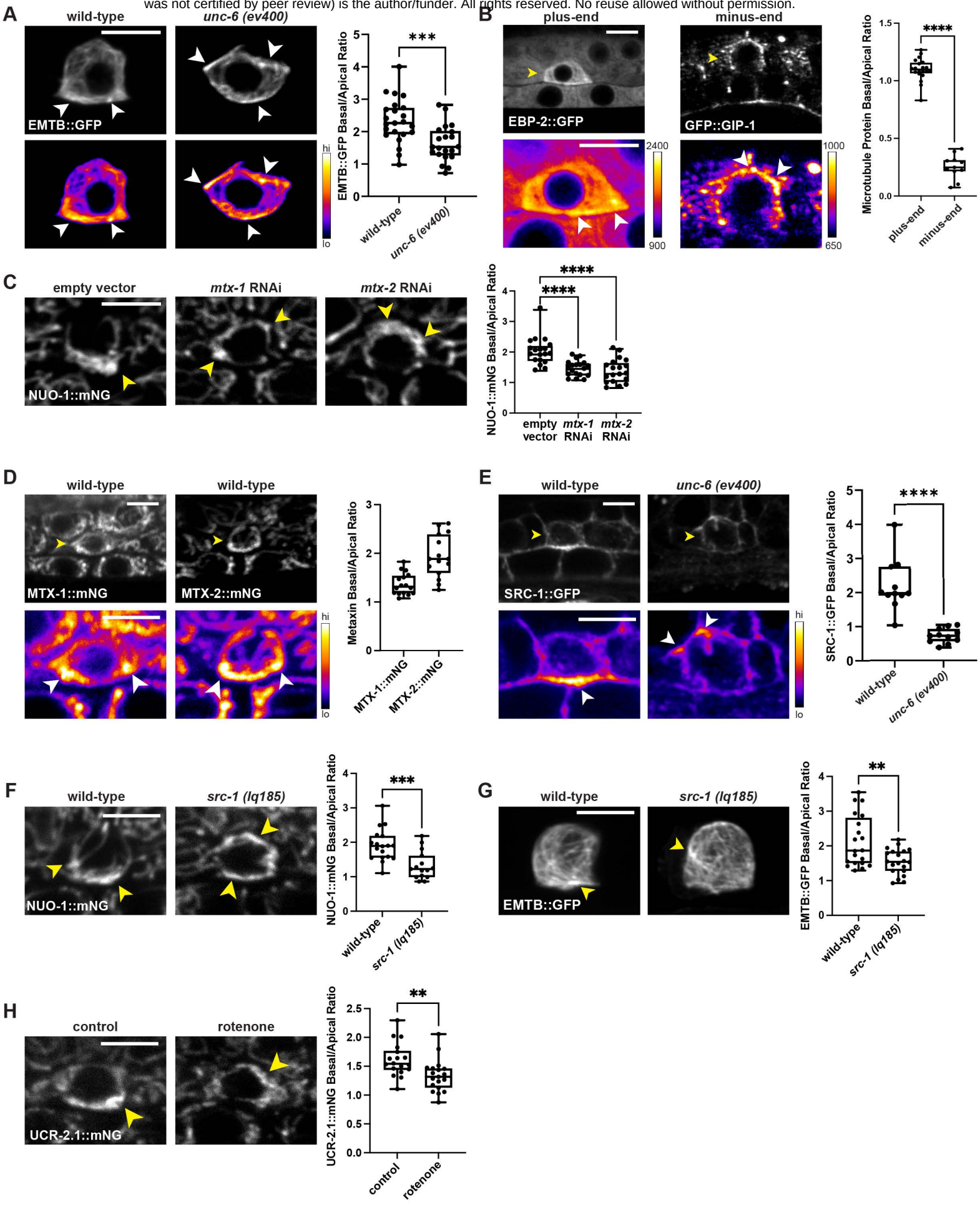

Figure S1

bioRxiv preprint doi: https://doi.org/10.1101/2025.05.02.651978; this version posted May 3, 2025. The copyright holder for this preprint (which was not certified by peer review) is the author/funder. All rights reserved. No reuse allowed without permission.

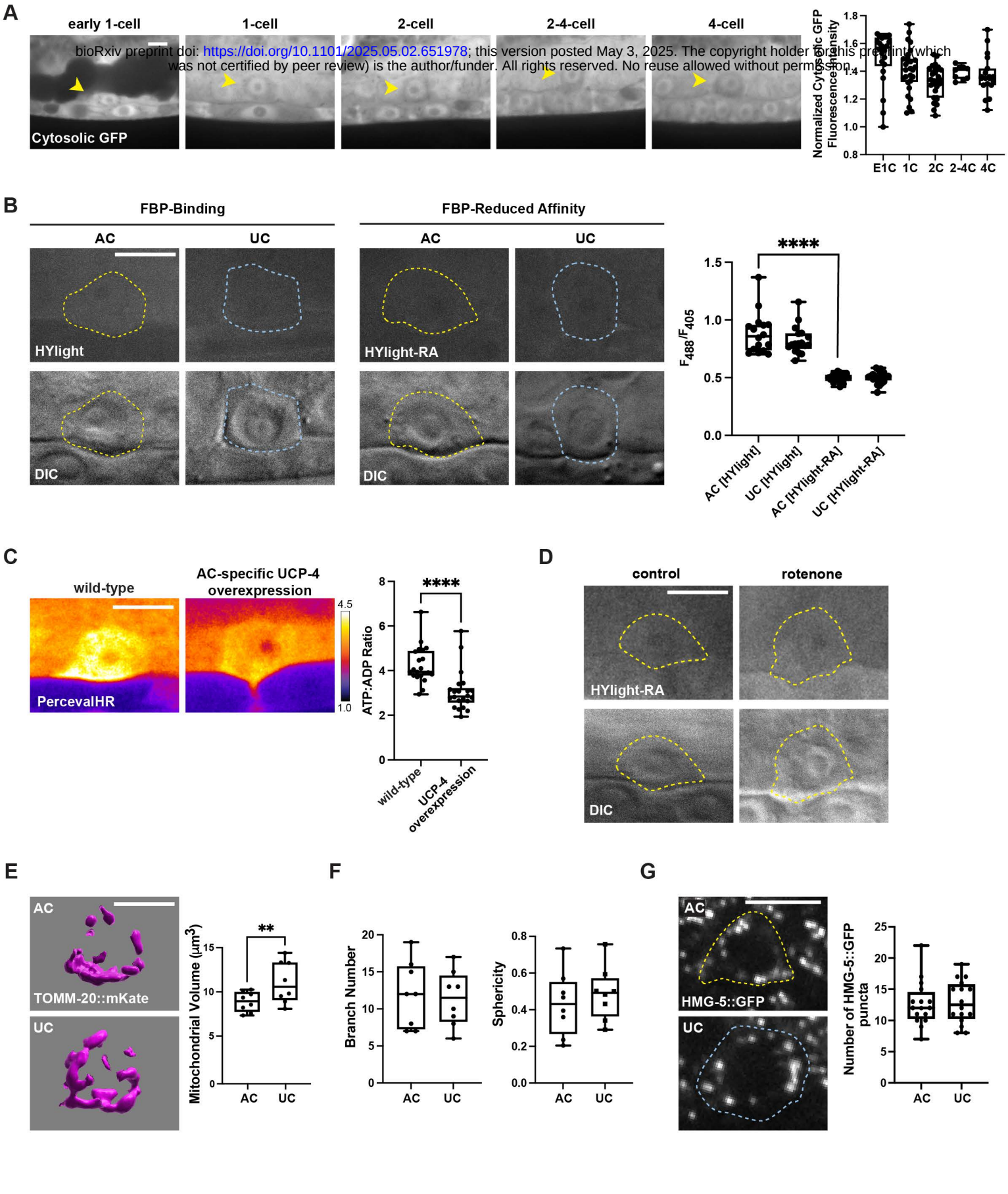

Figure S2

bioRxiv preprint doi: https://doi.org/10.1101/2025.05.02.651978; this version posted May 3, 2025. The copyright holder for this preprint (which was not certified by peer review) is the author/funder. All rights reserved. No reuse allowed without permission.

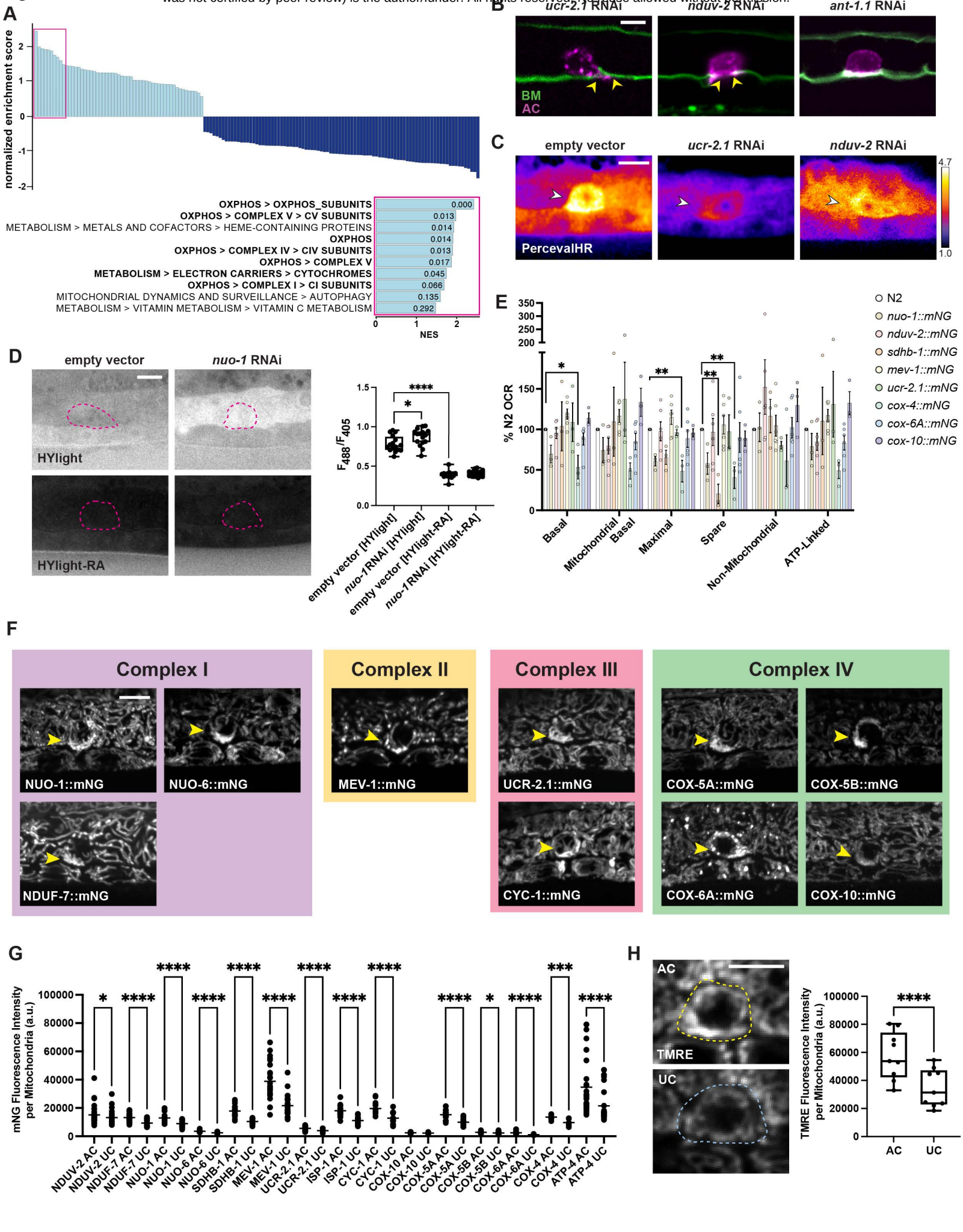

bioRxiv preprint doi: https://doi.org/10.1101/2025.05.02.651978; this version posted May 3, 2025. The copyright holder for this preprint (which was not certified by peer review) is the author/funder. All rights reserved. No reuse allowed without permission.

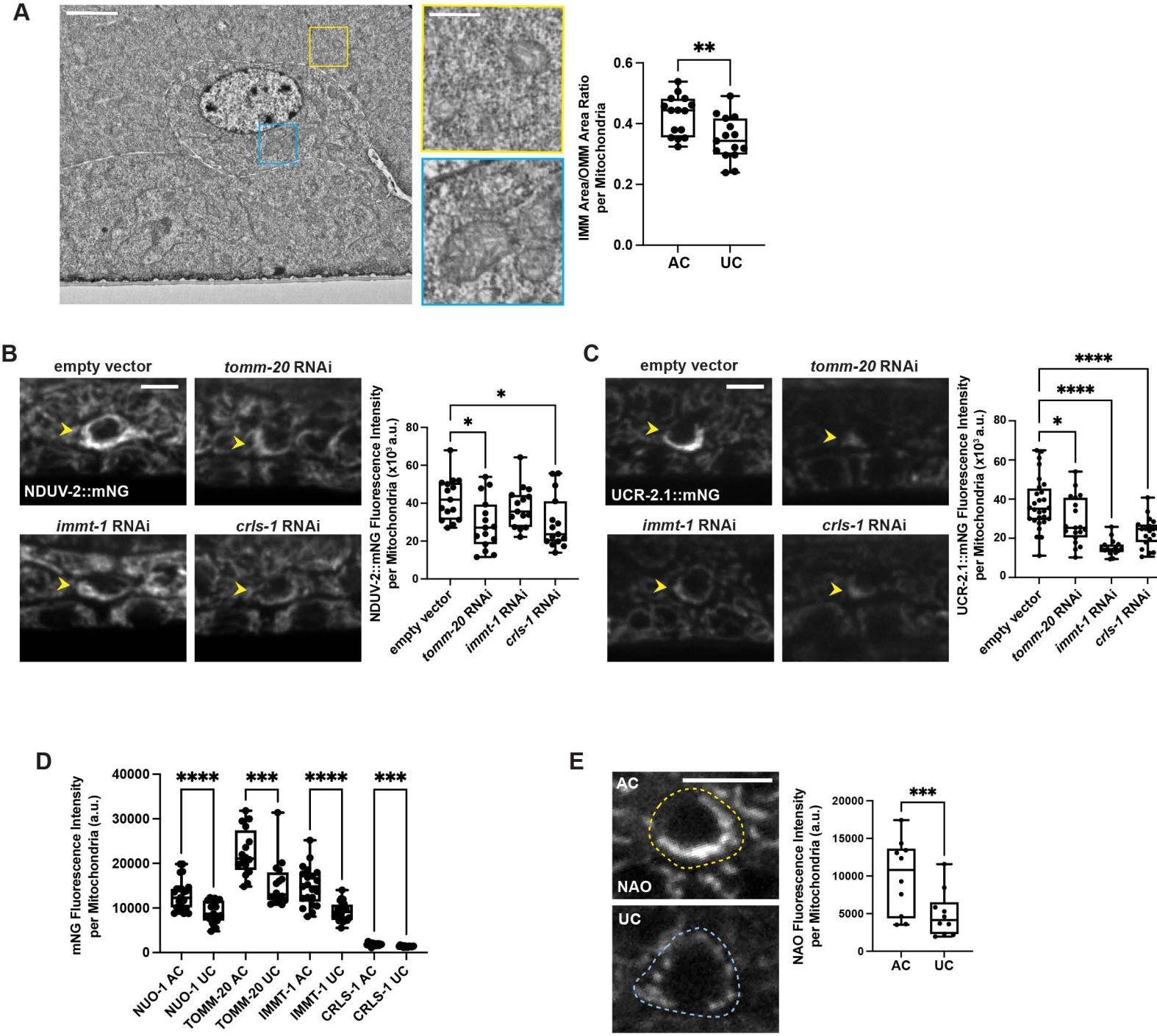

Figure S4

bioRxiv preprint doi: https://doi.org/10.1101/2025.05.02.651978; this version posted May 3, 2025. The copyright holder for this preprint (which was not certified by peer review) is the author/funder. All rights reserved. No reuse allowed without permission.

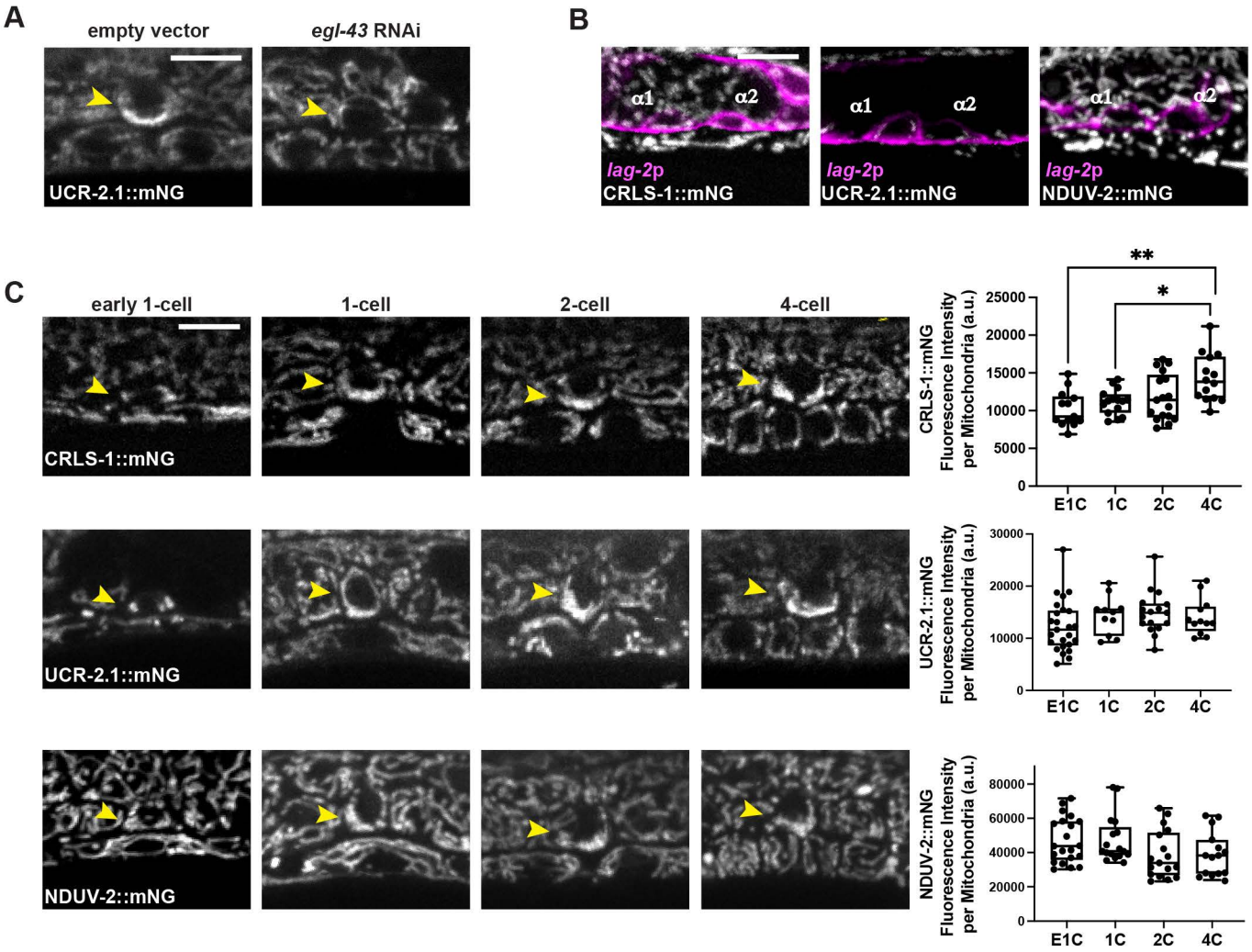

Figure S5

bioRxiv preprint doi: https://doi.org/10.1101/2025.05.02.651978; this version posted May 3, 2025. The copyright holder for this preprint (which was not certified by peer review) is the author/funder. All rights reserved. No reuse allowed without permission.

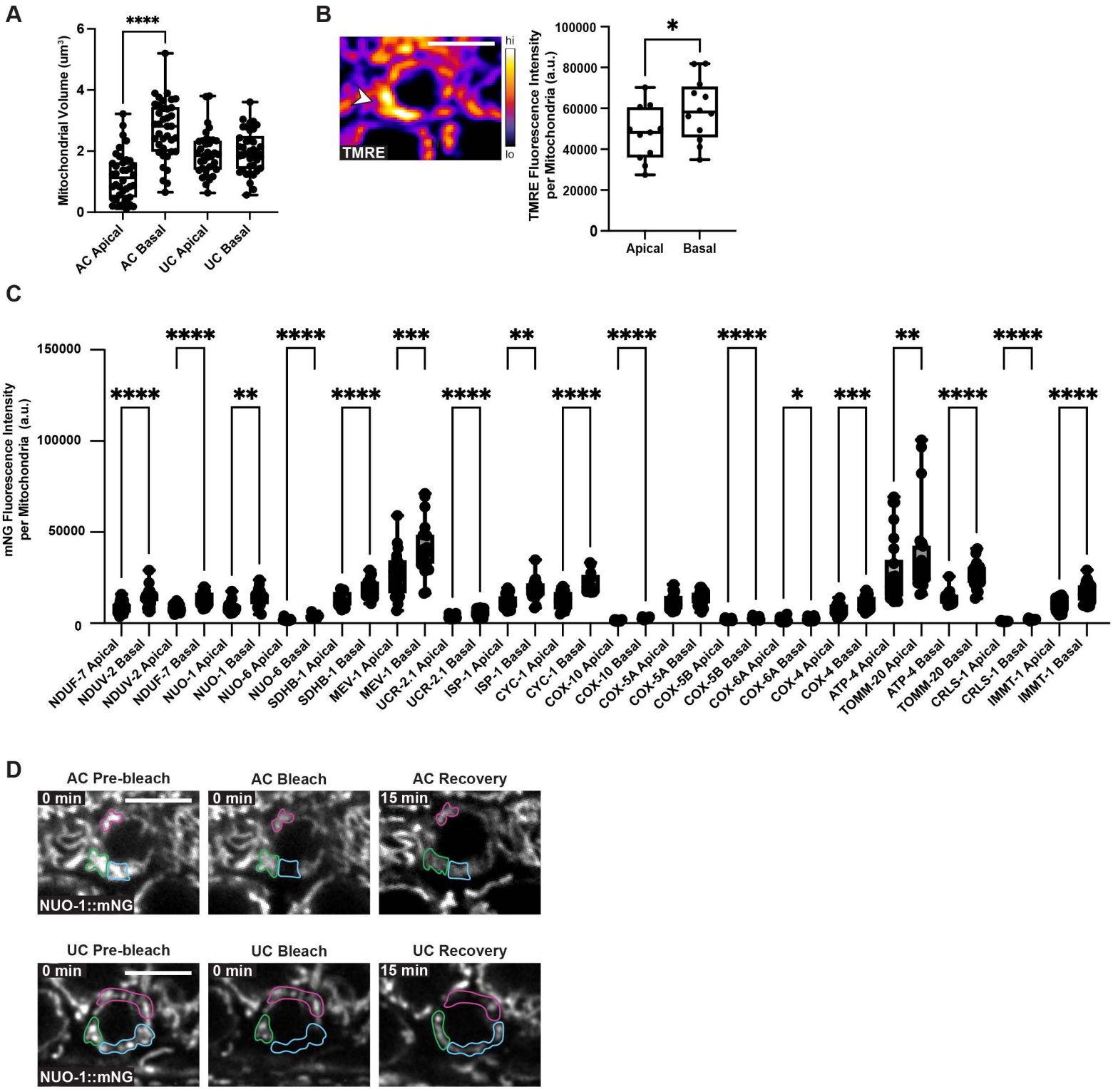

Figure S6

bioRxiv preprint doi: https://doi.org/10.1101/2025.05.02.651978; this version posted May 3, 2025. The copyright holder for this preprint (which was not certified by peer review) is the author/funder. All rights reserved. No reuse allowed without permission.

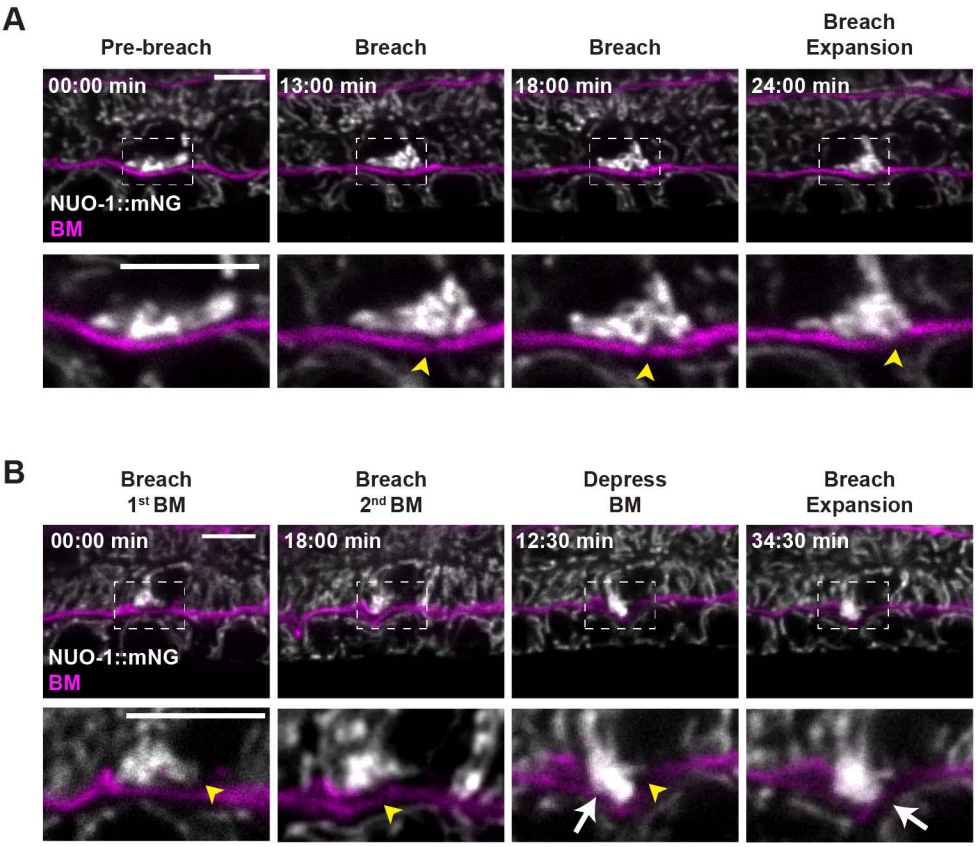

Figure S7

bioRxiv preprint doi: https://doi.org/10.1101/2025.05.02.651978; this version posted May 3, 2025. The copyright holder for this preprint (which was not certified by peer review) is the author/funder. All rights reserved. No reuse allowed without permission.

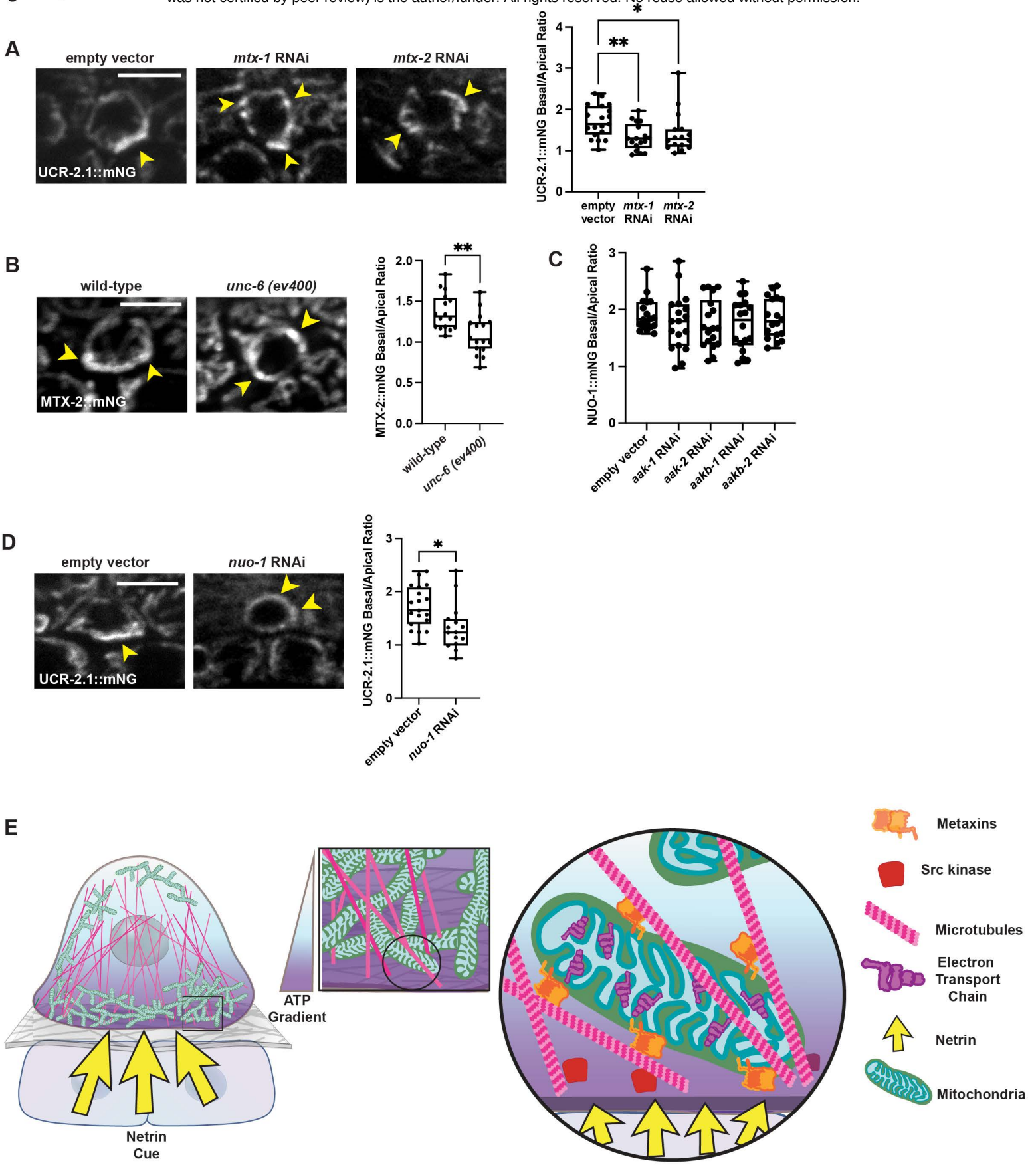

bioRxiv preprint doi: https://doi.org/10.1101/2025.05.02.651978; this version posted May 3, 2025. The copyright holder for this preprint (which was not certified by peer review) is the author/funder. All rights reserved. No reuse allowed without permission.

Key Resources Table

REAGENT or RESOURCE	SOURCE	IDENTIFIER
Bacterial and virus strains		
RNAi feeding strain	*Caenorhabditis* Genetics Center	HT115(DE3)
Vidal RNAi library	Open Biosystems	ORF RNAi Collection V1.1
Ahringer RNAi library	Source BioScience	*C.elegans* RNAi Collection (Ahringer)
E.coli OP50 standard food	*Caenorhabditis* Genetics Center	OP50
Chemicals, peptides, and recombinant proteins		
Gibson assembly	New England Biolabs	Cat. #10229799
NEBuilder HiFi DNA Assembly master mix	New England Biolabs	Cat. #E2621L
PureLink™ HiPure Plasmid Miniprep	Invitrogen	Cat.#K210002
Hygromycin B	Sigma-Aldrich	Cat. #H3274
Rotenone	EMD Millipore Corp.	Cat. # 557368
Isopropyl β-d-1-thiogalactopyranoside (IPTG)	Sigma-Aldrich	Cat. #I675
Sodium azide	Sigma-Aldrich	Cat. #S2002
Levamisole	Millipore Sigma	Cat. #L9756
Ampicillin	Sigma-Aldrich	Cat. #A0166
Tetramethylrhodamine, Ethyl Ester, Perchlorate	ThermoFisher Scientific	Cat. #T669
Nonyl Acridine Orange (NAO)	ThermoFisher Scientific	Cat. #A1372
Experimental models: Organisms/strains		
C. elegans wild-type strain N2	Caenorhabditis Genetics Center	N2
C. elegans unc-119 injection strain; Genotype: *unc-119 (ed4) III*	Caenorhabditis Genetics Center	PS3460
MMP- mutant animals with AC-specific plasma membrane marker and BM marker; Genotype: *lam-1::dendra (qyIs108); cdh-3p::mCherry::PLCΔPH (qyIs23); zmp-1 (cg115); zmp-3 (tm3482); zmp-4 (tm3484); zmp-5 (tm3209); zmp-6 (tm3073)*	Kelley et al. 2019	NK1267
Wild-type strain with AC-specific plasma membrane marker and BM marker; Genotype: *lam-1::dendra (qyIs108); cdh-3p::mCherry::PLCΔPH (qyIs23)*	Kelley et al. 2019	NK1588
Endogenously tagged mitochondria ETC (CIII) component; Genotype: *qy92[ucr-2.1::mNG] X.*	this study	NK2623

bioRxiv preprint doi: https://doi.org/10.1101/2025.05.02.651978; this version posted May 3, 2025. The copyright holder for this preprint (which was not certified by peer review) is the author/funder. All rights reserved. No reuse allowed without permission.

Wild-type strain with AC-specific ratiometric ATP biosensor PercevalHR; Genotype: *qyIs551[lin-29p::PercevalHR::unc-54 3'UTR]*	this study	NK2627
Wild-type strain with endogenously tagged mitochondria ETC (CI) component and AC-specific F-actin marker; Genotype: *qy143[nuo-1::mNG] II; qyIs50 [cdh-3p::moeABD::mCherry].*	this study	NK2657
Endogenously tagged mitochondria ETC (CI) component; Genotype: *qy131[nuo-6::mNG] I.*	this study	NK2733
Endogenously tagged mitochondria ETC (CIV) component (heterozygous); Genotype: *qy134[cox-4::mNG]/+ I.*	this study	NK2736
Endogenously tagged mitochondria ETC (CIV) component; Genotype: *qy136[cox-5A::mNG] III.*	this study	NK2738
Endogenously tagged mitochondria ETC (CIV) component; Genotype: *qy137[cox-5B::mNG] I.*	this study	NK2739
Endogenously tagged mitochondria ETC (CIV) component; Genotype: *qy141[cox-10::mNG] II.*	this study	NK2743
Endogenously tagged mitochondria ETC (CII) component; Genotype: *qy144[sdhb-1::mNG] II.*	this study	NK2746
Endogenously tagged strain TOMM complex component, balanced with nT1; Genotype: *qy132[tomm-20::mNG]/nT1 [qyIS51] (IV,V).*	this study	NK2747
Wild-type strain with ubiquitous expression of ATP biosensor iATPSnFR1.0; Genotype: *qy120[eef-1A.1p::iATPSnFR1.0::unc-54 3'UTR] I.*	this study	NK2765
Endogenously tagged mitochondria ETC(CI) component; Genotype: *qy157[nuo-1::mKate2] II.*	this study	NK2777
Wild-type strain with ubiquitous expression of cytosolic GFP; Genotype: *qy121[eef-1A.1p::GFP::unc-54 3'UTR] I.*	this study	NK2790
Wild-type strain with AC-specific microtubule marker; Genotype: *qyIs570[lin-29p::EMTB::GFP::unc-54 3'UTR] X.*	Garde et al. 2022	NK2799

bioRxiv preprint doi: https://doi.org/10.1101/2025.05.02.651978; this version posted May 3, 2025. The copyright holder for this preprint (which was not certified by peer review) is the author/funder. All rights reserved. No reuse allowed without permission.

Endogenously tagged mitochondria ETC (CII) component; Genotype: *qy169[mev-1::mNG] III.*	this study	NK2840
Endogenously tagged mitochondria ETC (CI) component; Genotype: *qy170[nduf-7::mNG] I.*	this study	NK2841
Wild-type strain with endogenously tagged microtubule plus-end marker and cell specific F-actin marker; Genotype: *ebp-2(wow47[ebp-2::GFP::3xFLAG]) II; qyIs250[exc-6p::mCh::moe-1 actin binding domain (ABD)]*	this study	NK2844
Endogenously tagged mitochondria ETC (CI) component; Genotype: *qy174[nduv-2::mNG] V.*	this study	NK2845
Endogenously tagged mitochondrial ETC (CIII) component; Genotype: *qy176[cyc-1::mNG] I.*	this study	NK2846
Endogenously tagged metaxin (plus-end adaptor); Genotype: *qy217[mtx-1::mNG] I.*	this study	NK3018
Wild-type strain with ubiquitous expression of mitochondria outermembrane marker; Genotype: *qy218[rpl-28p::tomm-20::mKate2::3xHA::unc-54 3'UTR] I.*	this study	NK3019
AC-specific overexpression of mitochondrial uncoupling protein with ubiquitous expression of ratiometric ATP:ADP biosensor PercevalHR; Genotype: qy314 [lin-29p::UCP-4::SL2::mKate2::PLC(delta)PH::3xHA::tbb-2 3'UTR] I; qyIS629[eef-1A.1p::PercevalHR::unc-54	this study	NK3027
Endogenously tagged mitochondrial ETC (CIII) component, balanced with nT1; Genotype: *qy133[isp-1::mNG]/nT1 [qyIS51] (IV,V).*	this study	NK3031
Endogenously tagged mitochondria ETC (CV) component, balanced with nT1; Genotype: *qy171[atp-4::mNG]/nT1 [qyIS51] (IV,V).*	this study	NK3032
Wild-type strain with endogenously tagged BM marker; Genotype: *qy244[emb-9::mRuby2] C-term III.*	Srinivasan et al. 2024	NK3072

bioRxiv preprint doi: https://doi.org/10.1101/2025.05.02.651978; this version posted May 3, 2025. The copyright holder for this preprint (which was not certified by peer review) is the author/funder. All rights reserved. No reuse allowed without permission.

Endogenously tagged metaxin (core adaptor); Genotype: *qy248[mtx-2::mNG] III.*	this study	NK3084
Wild-type strain with endogenously tagged MICOS marker and AC early cell fate marker; Genotype: *qy230[immt-1::mNG] X; cpIs91 [lag-2p::2xmKate2::PLC(delta)PH::3xHA::tbb-2 3'UTR LoxN] II.*	this study	NK3085
Wild-type strain with endogenously tagged ETC component (CIII) and AC early cell fate marker; Genotype: *qy92[ucr-2.1::mNG] X; cpIs91 [lag-2p::2xmKate2::PLC(delta)PH::3xHA::tbb-2 3'UTR LoxN] II.*	this study	NK3086
Wild-type strain with endogenously tagged ETC component (CI) and AC early cell fate marker; Genotype: *qy174[nduv-2::mNG] V; cpIs91 [lag-2p::2xmKate2::PLC(delta)PH::3xHA::tbb-2 3'UTR LoxN] II.*	this study	NK3087
Wild-type strain with endogenously tagged TOMM complex marker and AC early cell fate marker; Genotype: *qy132[tomm-20::mNG]/nT1 [qyIS51] V; cpIs91 [lag-2p::2xmKate2::PLC(delta)PH::3xHA::tbb-2 3'UTR LoxN] II.*	this study	NK3091
Endogenously tagged cardiolipin synthase; Genotype: *qy255[crls-1::mNG] III.*	this study	NK3114
Endogenously tagged mitochondria ETC (CI) component; Genotype: *qy275[nduv-2p::mNG::P2A::mKate2::unc-54 3'UTR] I.*	this study	NK3189
Wild-type strain with endogenously tagged mitochondria ETC(CI) component and BM marker; Genotype: *qy145[nuo-1::mNG] II; qy244[emb-9::mRuby2] III.*	this study	NK3210

bioRxiv preprint doi: https://doi.org/10.1101/2025.05.02.651978; this version posted May 3, 2025. The copyright holder for this preprint (which was not certified by peer review) is the author/funder. All rights reserved. No reuse allowed without permission.

Netrin null mutant *(ev400)* with endogenously tagged mitochondria marker and BM marker; Genotype: *qy145[nuo-1::mNG] II; qy244[emb-9::mRuby2] III; unc-6(ev400) X.*	this study	NK3211
Endogenously tagged mitochondria ETC (CIV) component; Genotype: *qy134[cox-4::mNG] I.*	this study	NK3212
Wild-type strain with endogenously tagged cardiolipin synthase and AC early fate marker; Genotype: *qy255[crls-1::mNG] III; cpIs91 [lag-2p::2xmKate2::PLC(delta)PH::3xHA::tbb-2 3'UTR LoxN] II.*	this study	NK3234
Netrin null mutant *(ev400)* with endogenously tagged metaxin; Genotype: *qy248[mtx-2::mNG] III; unc-6(ev400) X.*	this study	NK3255
Wild-type strain with ubiquitous expression of glycolysis ratiometric biosensor HYlight; Genotype: *qy296[eef-1A.1p::SL2::HYlight::tbb-2 3'UTR] I.*	this study	NK3271
Wild-type strain with ubiquitous expression of glycolysis ratiometric biosensor HYlight-RA control; Genotype: *qy312 [eef-1A.1p::SL2::HYlight-RA::tbb-2 3'UTR] I.*	this study	NK3299
Src kinase null mutant *(lp185)* with endogenously tagged mitochondria ETC (CI) component; Genotype: *qy143[nuo-1::mNG] II; src-1(lq185)/tmC20 [unc-14(tmIs1219) dpy-5(tm9715)] I.*	this study	NK3300
Src kinase null mutant *(lp185)* with AC-specific microtubule marker; Genotype: *src-1(lq185)/tmC20 [unc-14(tmIs1219) dpy-5(tm9715)] I; qyIS570 [lin-29p::EMTB::GFP::unc-54 3'UTR] X.*	this study	NK3302

bioRxiv preprint doi: https://doi.org/10.1101/2025.05.02.651978; this version posted May 3, 2025. The copyright holder for this preprint (which was not certified by peer review) is the author/funder. All rights reserved. No reuse allowed without permission.

AC-specific overexpression of mitochondrial uncoupling protein with ubiquitous expression of ratiometric ATP:ADP biosensor PercevalHR; Genotype: *qy314 [lin-29p::UCP-4::SL2::mKate2::PLC(delta)PH::3xHA::tbb-2 3'UTR] I; qyIS629[eef-1A.1p::PercevalHR::unc-54 3'UTR].*	this study	NK3304
Netrin null mutant *(ev400)* with AC-specific microtubule marker; Genotype: *qyIS636 [lin-29p::EMTB::GFP::unc-54 3'UTR]; unc-6(ev400) X.*	this study	NK3306
Transcriptional reporter of *nuo-1;* Genotype: *qy316[nuo-1p::mNG::P2A::mKate2::unc-54 3'UTR] I.*	this study	NK3325
Wild-type strain with ubiquitous expression of ratiometric ATP:ADP biosensor PercevalHR; Genotype: *qyIS629[eef-1A.1p::PercevalHR::unc-54 3'UTR].*	this study	NK3329
Netrin null mutant *(ev400)* with endogenously tagged Src kinase; Genotype: *ccp1[src-1::gfp]/+ I; unc-6(ev400) X.*	this study	NK3350
Wild-type strain with AC-specific overexpression of mitochondria uncoupling protein; Genotype: *qyIS636[lin-29p::EMTB::GFP::unc-54 3'UTR].*	Garde et al. 2022	NK3352
Wild-type strain with AC-specific plasma membrane marker and BM marker; Genotype: q*yIs10(lam-1::GFP) IV; qyIs23(cdh-3p::mCherry::PLCdPH) II.*	Naegeli et al. 2017	NK361
Netrin null mutant *(ev400);* Genotype: u*nc-6(ev400) X.*	Ziel et al. 2009	NW434
Endogenously tagged Src kinase; Genotype: *src-1(ccp1[src-1::gfp]) I; unc-119(ed3) III; ltIs37 IV.*	CGC and acknowledgement	PLG1
Endogenously tagged microtubule plus-end binding protein; Genotype: *ebp-2(wow47[ebp-2::GFP::3xFLAG]) II; qyIs250[exc-6p::mCh::moe-1 actin binding domain (ABD)]*	Costa et al. 2023	SBW292

bioRxiv preprint doi: https://doi.org/10.1101/2025.05.02.651978; this version posted May 3, 2025. The copyright holder for this preprint (which was not certified by peer review) is the author/funder. All rights reserved. No reuse allowed without permission.

Endogenously tagged mitochondria transcription factor-A (TFAM); Genotype: *xn107[hmg-5::GFP] IV.*	Schwartz et al. 2022	FT2064
Endogenously tagged microtubule minus-end binding protein; Genotype: *wow3[GFP::gip-1] III.*	Sallee et al. 2018	JLF14
Src kinase null mutant *(lp185);* Genotype: *src-1(lq185)/tmC20 [unc-14(tmIs1219) dpy-5(tm9715)] I; juIs76 II.*	Mahadik et al. 2023	LE6273
Oligonucleotides		
See Table S5 for details		
Recombinant DNA		
PercevalHR (C. elegans codon optimized)	Bohnert and Kenyon, 2017	Calico Labs pDONR221
T444T RNAi vector	Sturm et al., 2018	Addgene (#113081); RRID: Addgene_113081
Microtubule binding domain of ensconsin	Richardson et al., 2014	PCR8-EMTP::GFP entry vector
eef-1A.1::PercevalHR::unc-54 3'UTR	this study	*eef-1A.1::PercevalHR::unc-54 3'UTR*
eef-1A.1::HYlight::unc-54 3'UTR	this study	*eef-1A.1::HYlight::unc-54 3'UTR*
eef-1A.1::HYlight-RA::unc-54 3'UTR	this study	*eef-1A.1::HYlight-RA::unc-54 3'UTR*
pDD122 - *Peft-3::Cas9 + ttTi5605 sgRNA*	Bob Goldstein	Cat. #47550
pCFJ90 - *Pmyo-2::mCherry::unc-54utr*	Erik Jorgensen	Cat. #19327
pCFJ104 - *Pmyo-3::mCherry::unc-54utr*	Erik Jorgensen	Cat. #19328
pCFJ352 - MCS(ttTi4348, I)	Erik Jorgensen	Addgene plasmid # 30539
eef-1A.1p::iATPSnFR1.0::unc-54 3' UTR	this study	*eef-1A.1p::iATPSnFR1.0::unc-54 3' UTR*
iATPSnFR1.0 (codon-optimized gene block)	this study	ceIATPSnFR1.0
Software and algorithms		
GraphPad Prism	GraphPad	Version 10
µManager	Edelstein et al., 2014	Version 1.4.23 and Version 2.0.1
Fiji	Schneider et al., 2012	Version ImageJ 1.54p
Metamorph	Molecular Devices	7.10.3.279

bioRxiv preprint doi: https://doi.org/10.1101/2025.05.02.651978; this version posted May 3, 2025. The copyright holder for this preprint (which was not certified by peer review) is the author/funder. All rights reserved. No reuse allowed without permission.

Illustrator	Adobe	Version 28.7.1
Imaris	Bitplane	Version 9.9.1
OrthoList 2 (OL2)	Kim, Underwood et al. 2018	Version 2.0
Gene Set Enrichment Analysis (GSEA)	Subramanian et al., 2005	Version 4.4.0
R Studio		Version 4.4.0

bioRxiv preprint doi: https://doi.org/10.1101/2025.05.02.651978; this version posted May 3, 2025. The copyright holder for this preprint (which was not certified by peer review) is the author/funder. All rights reserved. No reuse allowed without permission.

Table S1 - AC invasion scoring

Genotye	Mitochondrial ETC Complex, Structure, Function	Condition	Sequence ID	% ACs with incomplete invasion[b]	n	p-value[c]
Sensitized RNAi screen of ETC components						
NK1267 -- *lam-1::dendra (qyIs108); cdh-3p::mCherry::PLCΔPH (qyIs23); zmp-1 (cg115); zmp-3 (tm3482); zmp-4 (tm3484); zmp-5 (tm3209); zmp-6 (tm3073)*	n/a	empty vector	L4440	12.6%	142	n/a
	n/a	positive control[a]	F29G9.4	82.8%	146	<0.0001
	ETC - CI	*nuo-1*	C09H10.3	41.5%	41	0.0002
	ETC - CI	*nuo-2*	T10E9.7	40.0%	20	0.0052
	ETC - CI	*nuo-3*	Y57G11C.12	35.0%	20	0.0176
	ETC - CI	*nuo-4*	K04G7.4	19.1%	21	0.491
	ETC - CI	*nuo-5*	Y45G12B.1	31.6%	19	0.0414
	ETC - CI	*nuo-6*	W01A8.4	40.0%	40	0.0003
	ETC - CI	*C16A3.5*	C16A3.5	34.8%	23	0.0127
	ETC - CI	*nduf-2.2*	T26A5.3	25.0%	20	0.1675
	ETC - CI	*gas-1*	K09A9.5	25.0%	20	0.1675
	ETC - CI	*ndua-13*	C34B2.8	45.5%	22	0.0007
	ETC - CI	*ndub-10*	F59C6.5	20.0%	20	0.4818
	ETC - CI	*ndub-2*	F44G4.2	25.0%	20	0.1675
	ETC - CI	*ndub-8*	Y51H1A.3	30.0%	20	0.0839
	ETC - CI	*nduf-5*	Y54E10BL.5	14.3%	21	0.7368
	ETC - CI	*nduf-6*	F22D6.4	14.3%	21	0.7368
	ETC - CI	*nduf-7*	W10D5.2	28.6%	21	0.0907
	ETC - CI	*ndus-8*	T20H4.5	20.0%	20	0.4818
	ETC - CI	*nduv-2*	F53F4.10	30.0%	20	0.0839
	ETC - CI	*ndua-7*	F45H10.3	25.0%	20	0.1675
	ETC - CII	*F25H9.7*	F25H9.7	10.0%	20	>0.9999
	ETC - CII	*sdha-2*	C34B2.7	14.3%	21	0.7368
	ETC - CII	*sdhb-1*	F42A8.2	15.0%	20	0.7267
	ETC - CII	*sdhd-1*	F33A8.5	30.0%	20	0.0839
	ETC - CII	*Y57A10A.29*	Y57A10A.29	20.0%	20	0.4818
	ETC - CIII	*F45H10.2*	F45H10.2	25.0%	20	0.1675
	ETC - CIII	*ucr-2.1*	VW06B3R.1	10.0%	20	>0.9999
	ETC - CIII	*isp-1*	F42G8.12	65.0%	20	0.0001
	ETC - CIV	*cox-5B*	F26E4.9	20.0%	20	0.4818
	ETC - CIV	*cox-6A*	F54D8.2	20.0%	20	0.4818
	Import	*tomm-20*	F23H12.2	20.0%	20	0.4818

bioRxiv preprint doi: https://doi.org/10.1101/2025.05.02.651978; this version posted May 3, 2025. The copyright holder for this preprint (which was not certified by peer review) is the author/funder. All rights reserved. No reuse allowed without permission.

	MICOS	*immt-1*	T14G11.3	15.0%	20	0.7267
	CL Synthesis	*crls-1*	F23H11.9	5.0%	20	>0.9999
	ANT	*ant-1.1*	T27E9.1	62.4%	125	<0.0001
Wildtype screen of ETC Components						
NK1588 -- *lam-1::dendra (qyIs108); cdh-3p::mCherry::PLCΔ PH (qyIs23)*	n/a	empty vector	L4440	3.0%	40	n/a
	n/a	positive control[a]	*F29G9.4*	87.5%	40	<0.0001
	ETC - CI	*nuo-1*	*C09H10.3*	15.0%	20	0.0383
	ETC - CI	*nduv-2*	*F53F4.10*	5.0%	20	>0.9999
	ETC - CIII	*ucr-2.1*	*VW06B3R.1*	5.0%	20	>0.9999
	Import	*tomm-22*	W10D9.5	5.0%	20	>0.9999
	Import	*tomm-7*	ZK370.8	5.0%	20	>0.9999
	Import	*tomm-20*	F23H12.2	15.0%	20	0.0383
	Import	*tin-13*	DY3.1	15.0%	20	0.1034
	Import	tin-44	T09B4.9	30.0%	20	0.0042
	MICOS	*immt-1*	T14G11.3	15.0%	20	0.1034
	CL Synthesis	*crls-1*	F23H11.9	5.0%	20	>0.9999
	ANT	*ant-1.1*	T27E9.1	25.0%	20	0.0132
Pharmacological inhibition of OXPHOS						
NK361 -- *lam-1::GFP (qyIs10); cdh-3p::mCherry::PLCΔ PH (qyIs23)*	n/a	Vehicle (DMSO)	n/a	7.0%	42	n/a
	n/a	40uM Rotenone	n/a	33.0%	42	0.0055
Characterization of AC invasion in ETC tagged strains						
N2	n/a	n/a	n/a	0.0%	45	n/a
NDUV-2::LL::mNG	ETC - CI	n/a	n/a	0.0%	15	>0.9999
NDUF-7::LL::mNG	ETC - CI	n/a	n/a	0.0%	15	>0.9999
NUO-1::LL::mNG	ETC - CI	n/a	n/a	0.0%	15	>0.9999
NUO-6::LL::mNG	ETC - CI	n/a	n/a	0.0%	15	>0.9999
SDHB-1::LL::mNG	ETC - CII	n/a	n/a	0.0%	15	>0.9999
MEV-1::LL::mNG	ETC - CII	n/a	n/a	0.0%	15	>0.9999
UCR-2.1::LL::mNG	ETC - CII	n/a	n/a	0.0%	15	>0.9999
ISP-1::LL::mNG	ETC - CII	n/a	n/a	0.0%	15	>0.9999
CYC-1::LL::mNG	ETC - CII	n/a	n/a	0.0%	15	>0.9999
COX-10::LL::mNG	ETC - CIV	n/a	n/a	0.0%	15	>0.9999
COX-5A::LL::mNG	ETC - CIV	n/a	n/a	0.0%	15	>0.9999
COX-5B::LL::mNG	ETC - CIV	n/a	n/a	0.0%	15	>0.9999
COX-6A::LL::mNG	ETC - CIV	n/a	n/a	0.0%	15	>0.9999
COX-4::LL::mNG	ETC - CIV	n/a	n/a	0.0%	15	>0.9999
ATP-4::LL::mNG	ETC - CV	n/a	n/a	0.0%	15	>0.9999
TOMM-20::LL::mNG	Import	n/a	n/a	0.0%	15	>0.9999

bioRxiv preprint doi: https://doi.org/10.1101/2025.05.02.651978; this version posted May 3, 2025. The copyright holder for this preprint (which was not certified by peer review) is the author/funder. All rights reserved. No reuse allowed without permission.

IMMT-1::LL::mNG	MICOS	n/a	n/a	0.0%	15	>0.9999
CRLS-1::LL::mNG	CL Synthesis	n/a	n/a	0.0%	15	>0.9999
MTX-1::LL::mNG	Metaxin	n/a	n/a	0.0%	15	>0.9999
MTX-2::LL::mNG	Metaxin	n/a	n/a	0.0%	15	>0.9999

[a] RNAi targeting *fos-1* gives a penetrant invasion defect (Sherwood, Butler et al. 2005)

[b] Incomplete invasion refers to ACs that have failed to fully remove the underlying BM by the late P6.p 4-cell stage.

[c] Two-sided Fisher's exact test for significance

ETC - Electron Transport Chain; MICOS - Mitochondrial Contact Site and Cristae Organizing System; CL - Cardiolipin; ANT - Adenine Nucleotide Translocase

Table S2 - *C.elegans* MitoCarta

Human Gene Symbol	Gene Systematic Name	Worm Gene Name	Orthology Surce	Orthology Algorithm	Best Orthology Score (Forward)	Best Orthology Score (Reverse)	Number of Orthology Algorithms	AC Log2 Fold	MitoCarta3.0 MitoPathways
AARS2	HGNC:21022	aars-1	Alliance+Orth	Ensembl Com	Yes	Yes	4	-0.79	Mitochondrial cen
AARS2	NA	aars-2	OrthoList	OrthoMCL	NA	NA	1	0.69	Mitochondrial cen
AASS	HGNC:17366	aass-1	Alliance+Orth	Ensembl Com	Yes	Yes	11	-0.73	Metabolism > Ami
ABAT	HGNC:23	gta-1	Alliance+Orth	Ensembl Com	Yes	Yes	11	-0.68	Metabolism > Ami
ABCA9	NA	abt-2	OrthoList	Ensembl Com	NA	NA	2	0.22	Small molecule tra
ABCA9	NA	abt-4	OrthoList	Ensembl Com	NA	NA	2	-3.41	Small molecule tra
ABCA9	NA	abt-5	OrthoList	Ensembl Com	NA	NA	2	-0.41	Small molecule tra
ABCA9	NA	ced-7	OrthoList	Ensembl Com	NA	NA	2	0.29	Small molecule tra
ABCB10	HGNC:41	haf-1	Alliance+Orth	Hieranoid|Ho	Yes	Yes	9	0.8	Metabolism > Meta
ABCB10	HGNC:41	haf-3	Alliance+Orth	Hieranoid|Ho	Yes	Yes	9	-1.2	Metabolism > Meta
ABCB10	NA	haf-6	OrthoList	OrthoMCL	NA	NA	1	-2.61	Metabolism > Meta
ABCB10	NA	haf-7	OrthoList	OrthoMCL	NA	NA	1	0.47	Metabolism > Meta
ABCB10	NA	haf-8	OrthoList	OrthoMCL	NA	NA	1	#N/A	Metabolism > Meta
ABCB6	HGNC:47	hmt-1	Alliance+Orth	Ensembl Com	Yes	Yes	11	-2.89	Metabolism > Meta
ABCB6	NA	abtm-1	OrthoList	OrthoMCL	NA	NA	1	-1.97	Metabolism > Meta
ABCB7	NA	hmt-1	OrthoList	OrthoMCL	NA	NA	1	-2.89	Metabolism > Meta
ABCB7	HGNC:48	abtm-1	Alliance+Orth	Ensembl Com	Yes	Yes	11	-1.97	Metabolism > Meta
ABCB8	NA	haf-1	OrthoList	OrthoMCL	NA	NA	1	0.8	Small molecule tra
ABCB8	NA	haf-3	OrthoList	OrthoMCL	NA	NA	1	-1.2	Small molecule tra
ABCB8	HGNC:49	haf-6	Alliance+Orth	Ensembl Com	Yes	Yes	11	-2.61	Small molecule tra
ABCB8	NA	haf-7	OrthoList	OrthoMCL	NA	NA	1	0.47	Small molecule tra
ABCB8	NA	haf-8	OrthoList	OrthoMCL	NA	NA	1	#N/A	Small molecule tra
ABCD1	NA	pmp-1	OrthoList	OrthoMCL	NA	NA	1	-0.89	Small molecule tra
ABCD1	NA	pmp-2	OrthoList	OrthoMCL	NA	NA	1	-0.85	Small molecule tra
ABCD1	NA	pmp-3	OrthoList	OrthoMCL	NA	NA	1	0.96	Small molecule tra

ABCD1	HGNC:61	pmp-4	Alliance+Orth	Ensembl Com	Yes	Yes	10	-1.15	Small molecule tra
ABCD2	NA	pmp-1	OrthoList	OrthoMCL	NA	NA	1	-0.89	Small molecule tra
ABCD2	NA	pmp-2	OrthoList	OrthoMCL	NA	NA	1	-0.85	Small molecule tra
ABCD2	NA	pmp-3	OrthoList	OrthoMCL	NA	NA	1	0.96	Small molecule tra
ABCD2	HGNC:66	pmp-4	Alliance+Orth	Ensembl Com	Yes	Yes	10	-1.15	Small molecule tra
ABCD3	HGNC:67	pmp-1	Alliance+Orth	Ensembl Com	Yes	Yes	11	-0.89	Small molecule tra
ABCD3	HGNC:67	pmp-2	Alliance+Orth	Ensembl Com	Yes	Yes	11	-0.85	Small molecule tra
ABCD3	NA	pmp-3	OrthoList	OrthoMCL	NA	NA	1	0.96	Small molecule tra
ABCD3	NA	pmp-4	OrthoList	OrthoMCL	NA	NA	1	-1.15	Small molecule tra
ABHD10	HGNC:25656	C50B6.9	Alliance+Orth	Hieranoid|InP	Yes	Yes	5	0.99	Metabolism > Deto
ABHD11	HGNC:16407	abhd-11.1	Alliance+Orth	Ensembl Com	No	Yes	8	#N/A	Metabolism > Carb
ABHD11	HGNC:16407	abhd-11.2	Alliance+Orth	Ensembl Com	Yes	Yes	11	-2.34	Metabolism > Carb
ACAA2	NA	kat-1	OrthoList	OrthoMCL	NA	NA	1	-1.43	Metabolism > Carb
ACAA2	HGNC:83	acaa-2	Alliance+Orth	Ensembl Com	Yes	Yes	11	-0.71	Metabolism > Carb
ACAA2	NA	T02G5.7	OrthoList	OrthoMCL	NA	NA	1	-0.97	Metabolism > Carb
ACACA	HGNC:84	pod-2	Alliance+Orth	Ensembl Com	Yes	Yes	9	-1.27	Metabolism > Lipid
ACACA	HGNC:84	T28F3.5	Alliance+Orth	Ensembl Com	No	Yes	6	1.36	Metabolism > Lipid
ACACB	HGNC:85	pod-2	Alliance+Orth	Ensembl Com	Yes	Yes	10	-1.27	Metabolism > Lipid
ACACB	HGNC:85	T28F3.5	Alliance+Orth	Ensembl Com	No	Yes	7	1.36	Metabolism > Lipid
ACAD10	HGNC:21597	acds-10	Alliance+Orth	Ensembl Com	Yes	Yes	11	-3.09	Metabolism > Lipid
ACAD11	NA	K09H11.1	OrthoList	OrthoMCL	NA	NA	1	#N/A	Metabolism > Lipid
ACAD8	HGNC:87	acdh-9	Alliance+Orth	Ensembl Com	Yes	Yes	11	-1.37	Metabolism > Amin
ACAD9	HGNC:21497	acdh-13	Alliance	OrthoFinder|I	Yes	Yes	3	#N/A	OXPHOS > Compl
ACAD9	NA	acdh-12	OrthoList	OrthoMCL	NA	NA	1	-1.4	OXPHOS > Compl
ACADM	HGNC:89	acdh-8	Alliance+Orth	Ensembl Com	Yes	Yes	11	-5.43	Metabolism > Lipid
ACADM	HGNC:89	acdh-10	Alliance+Orth	Ensembl Com	Yes	Yes	10	0.82	Metabolism > Lipid
ACADM	HGNC:89	acdh-7	Alliance+Orth	Ensembl Com	No	Yes	10	0.33	Metabolism > Lipid
ACADS	NA	acdh-1	OrthoList	OrthoMCL	NA	NA	1	-1.93	Metabolism > Lipid
ACADS	NA	acdh-3	OrthoList	OrthoMCL	NA	NA	1	-0.01	Metabolism > Lipid
ACADSB	HGNC:91	acdh-2	Alliance+Orth	Ensembl Com	No	Yes	4	-2.14	Metabolism > Lipid

ACADSB	HGNC:91	acdh-1	Alliance+Orth	Ensembl Com	Yes	Yes	11	-1.93	Metabolism > Lipic
ACADSB	HGNC:91	acdh-3	Alliance+Orth	Ensembl Com	Yes	Yes	11	-0.01	Metabolism > Lipic
ACADSB	HGNC:91	acdh-4	Alliance+Orth	Ensembl Com	No	Yes	8	1.07	Metabolism > Lipic
ACADVL	HGNC:92	acdh-12	Alliance+Orth	Ensembl Com	Yes	Yes	11	-1.4	Metabolism > Lipic
ACAT1	HGNC:93	kat-1	Alliance+Orth	Ensembl Com	Yes	Yes	11	-1.43	Metabolism > Carb
ACAT1	NA	acaa-2	OrthoList	OrthoMCL	NA	NA	1	-0.71	Metabolism > Carb
ACAT1	HGNC:93	T02G5.7	Alliance+Orth	Ensembl Com	No	Yes	5	-0.97	Metabolism > Carb
ACCS	HGNC:23989	T04F3.1	Alliance+Orth	Ensembl Com	Yes	Yes	5	1.24	Unknown
ACLY	HGNC:115	acly-2	Alliance+Orth	Ensembl Com	Yes	Yes	11	-0.32	Metabolism > Carb
ACLY	HGNC:115	acly-1	Alliance+Orth	Ensembl Com	Yes	Yes	11	-0.12	Metabolism > Carb
ACO2	NA	aco-1	OrthoList	OrthoMCL	NA	NA	1	-0.58	Metabolism > Carb
ACO2	HGNC:118	aco-2	Alliance+Orth	Ensembl Com	Yes	Yes	11	-0.77	Metabolism > Carb
ACOT13	HGNC:20999	C25H3.3	Alliance+Orth	Ensembl Com	No	Yes	9	1.18	Metabolism > Lipic
ACOT13	HGNC:20999	C25H3.14	Alliance+Orth	Ensembl Com	Yes	Yes	10	1.49	Metabolism > Lipic
ACOT13	HGNC:20999	F42H10.6	Alliance+Orth	Ensembl Com	No	Yes	6	0.61	Metabolism > Lipic
ACOT2	HGNC:18431	C31H5.6	Alliance+Orth	Ensembl Com	Yes	Yes	10	-1.09	Metabolism > Lipic
ACOT2	HGNC:18431	K05B2.4	Alliance+Orth	Ensembl Com	Yes	Yes	10	-6.3	Metabolism > Lipic
ACOT2	NA	T05E7.1	OrthoList	Ensembl Com	NA	NA	4	-0.41	Metabolism > Lipic
ACOT2	HGNC:18431	W03D8.8	Alliance+Orth	Ensembl Com	Yes	Yes	9	-2.9	Metabolism > Lipic
ACOT9	HGNC:17152	F57F4.1	Alliance+Orth	Ensembl Com	Yes	Yes	11	-0.81	Metabolism > Lipic
ACOT9	NA	T07D3.3	OrthoList	Ensembl Com	NA	NA	1	#N/A	Metabolism > Lipic
ACOT9	HGNC:17152	T07D3.9	Alliance+Orth	Ensembl Com	Yes	Yes	11	-1.85	Metabolism > Lipic
ACOT9	HGNC:17152	T22B7.7	Alliance+Orth	Ensembl Com	No	Yes	4	3.15	Metabolism > Lipic
ACP6	HGNC:29609	pho-10	Alliance	Ensembl Com	Yes	Yes	2	#N/A	Metabolism > Lipic
ACP6	HGNC:29609	pho-11	Alliance	Ensembl Com	Yes	Yes	2	#N/A	Metabolism > Lipic
ACP6	HGNC:29609	acp-3	Alliance	Ensembl Com	Yes	Yes	2	#N/A	Metabolism > Lipic
ACP6	HGNC:29609	acp-2	Alliance	Ensembl Com	Yes	Yes	2	#N/A	Metabolism > Lipic
ACP6	HGNC:29609	acp-4	Alliance	Ensembl Com	Yes	Yes	2	#N/A	Metabolism > Lipic
ACP6	NA	pho-8	OrthoList	Ensembl Com	NA	NA	1	0.98	Metabolism > Lipic
ACP6	NA	pho-7	OrthoList	Ensembl Com	NA	NA	1	-2.68	Metabolism > Lipic

ACP6	NA	pho-6	OrthoList	Ensembl Com	NA	NA	1	-0.67	Metabolism > Lipid
ACP6	NA	pho-9	OrthoList	Ensembl Com	NA	NA	1	0.36	Metabolism > Lipid
ACP6	HGNC:29609	acp-1	Alliance	Ensembl Com	Yes	Yes	2	#N/A	Metabolism > Lipid
ACSF2	NA	acs-7	OrthoList	OrthoMCL	NA	NA	1	-0.26	Metabolism > Lipid
ACSF2	NA	acs-14	OrthoList	OrthoMCL	NA	NA	1	-1.93	Metabolism > Lipid
ACSF2	NA	acs-12	OrthoList	OrthoMCL	NA	NA	1	0.15	Metabolism > Lipid
ACSF2	HGNC:26101	acs-2	Alliance+Orth	Ensembl Com	Yes	Yes	10	-5.38	Metabolism > Lipid
ACSF2	HGNC:26101	acs-1	Alliance+Orth	Ensembl Com	Yes	Yes	11	0.08	Metabolism > Lipid
ACSF3	HGNC:27288	acs-21	Alliance+Orth	Ensembl Com	Yes	Yes	8	1.79	Metabolism > Lipid
ACSF3	HGNC:27288	acs-11	Alliance+Orth	Ensembl Com	Yes	Yes	8	0.06	Metabolism > Lipid
ACSL1	NA	acs-5	OrthoList	Ensembl Com	NA	NA	2	-1.29	Metabolism > Lipid
ACSL1	NA	acs-17	OrthoList	OrthoMCL	NA	NA	1	-1.17	Metabolism > Lipid
ACSL1	NA	acs-4	OrthoList	OrthoMCL	NA	NA	1	-0.84	Metabolism > Lipid
ACSL1	HGNC:3569	acs-13	Alliance+Orth	Ensembl Com	Yes	No	9	0.41	Metabolism > Lipid
ACSL6	NA	acs-5	OrthoList	Ensembl Com	NA	NA	2	-1.29	Metabolism > Lipid
ACSL6	NA	acs-17	OrthoList	OrthoMCL	NA	NA	1	-1.17	Metabolism > Lipid
ACSL6	NA	acs-4	OrthoList	OrthoMCL	NA	NA	1	-0.84	Metabolism > Lipid
ACSL6	HGNC:16496	acs-13	Alliance+Orth	Ensembl Com	Yes	No	9	0.41	Metabolism > Lipid
ACSS1	NA	acs-19	OrthoList	OrthoMCL	NA	NA	1	0.48	Metabolism > Lipid
ACSS3	NA	acs-19	OrthoList	OrthoMCL	NA	NA	1	0.48	Metabolism > Lipid
ADCK1	HGNC:19038	D2023.6	Alliance+Orth	Ensembl Com	Yes	Yes	11	-2.24	Unknown
ADCK2	HGNC:19039	Y32H12A.7	Alliance+Orth	Ensembl Com	Yes	Yes	11	-1.72	Unknown
ADCK5	NA	D2023.6	OrthoList	OrthoMCL	NA	NA	1	-2.24	Unknown
ADHFE1	HGNC:16354	hphd-1	Alliance+Orth	Ensembl Com	Yes	Yes	11	-1.48	Metabolism > Amin
AFG1L	HGNC:16411	C30F12.2	Alliance+Orth	Ensembl Com	Yes	Yes	11	-3.79	Protein import, sor
AFG3L2	HGNC:315	spg-7	Alliance+Orth	Ensembl Com	Yes	Yes	11	-1.06	Protein import, sor
AFG3L2	NA	ymel-1	OrthoList	OrthoMCL	NA	NA	1	-0.16	Protein import, sor
AFG3L2	NA	ppgn-1	OrthoList	OrthoMCL	NA	NA	1	-0.33	Protein import, sor
AGK	HGNC:21869	F52C9.3	Alliance+Orth	Ensembl Com	Yes	Yes	9	0.73	Protein import, sor
AGMAT	NA	T21F4.1	OrthoList	Ensembl Com	NA	NA	1	#N/A	Metabolism > Amin

AGPAT5	HGNC:20886	acl-11	Alliance+Orth	Ensembl Com	Yes	Yes	11	0.45	Metabolism > Lipic
AGXT	HGNC:341	agxt-1	Alliance+Orth	Ensembl Com	Yes	Yes	11	0.47	Metabolism > Amir
AGXT2	HGNC:14412	T09B4.8	Alliance+Orth	Ensembl Com	Yes	Yes	11	-1.34	Metabolism > Amir
AHCYL1	NA	ahcy-1	OrthoList	Ensembl Com	NA	NA	1	-0.8	Mitochondrial dyn
AIFM1	HGNC:8768	wah-1	Alliance+Orth	Ensembl Com	Yes	Yes	11	-1.13	Protein import, sor
AIFM3	HGNC:26398	F20D6.11	Alliance+Orth	Ensembl Com	Yes	Yes	10	0.12	Metabolism > Met
AK2	HGNC:362	let-754	Alliance+Orth	Ensembl Com	Yes	Yes	11	-0.43	Metabolism > Nuc
AK3	HGNC:17376	ZK673.2	Alliance+Orth	Ensembl Com	Yes	Yes	8	0.32	Metabolism > Nuc
AK4	HGNC:363	ZK673.2	Alliance+Orth	Ensembl Com	Yes	No	5	0.32	Metabolism > Nuc
AKAP1	HGNC:367	akap-1	Alliance+Orth	Ensembl Com	Yes	Yes	7	-0.68	Signaling > cAMP-I
AKAP10	HGNC:368	rgs-5	Alliance+Orth	Ensembl Com	Yes	Yes	9	1.5	Signaling > cAMP-I
AKR1B10	HGNC:382	F53F1.2	Alliance+Orth	Ensembl Com	No	Yes	4	0.89	Metabolism > Vitar
AKR1B10	HGNC:382	Y39G8B.1	Alliance+Orth	Ensembl Com	Yes	Yes	8	1.31	Metabolism > Vitar
AKR1B10	HGNC:382	Y39G8B.2	Alliance+Orth	Ensembl Com	No	Yes	4	0.39	Metabolism > Vitar
AKR1B10	HGNC:382	ZC443.1	Alliance+Orth	Ensembl Com	No	Yes	5	2.18	Metabolism > Vitar
AKR1B10	HGNC:382	C01G5.5	Alliance+Orth	Ensembl Com	No	Yes	4	-1.74	Metabolism > Vitar
AKR1B10	NA	C07D8.5	OrthoList	Ensembl Com	NA	NA	1	-4.87	Metabolism > Vitar
AKR1B10	HGNC:382	C07D8.6	Alliance+Orth	Ensembl Com	No	Yes	6	0.99	Metabolism > Vitar
AKR1B10	NA	C35D10.6	OrthoList	OrthoMCL	NA	NA	1	0.51	Metabolism > Vitar
AKR1B10	HGNC:382	C56G3.2	Alliance	Ensembl Com	No	Yes	3	-2.4	Metabolism > Vitar
AKR1B10	HGNC:382	exc-15	Alliance+Orth	Ensembl Com	No	Yes	4	0.09	Metabolism > Vitar
AKR1B10	NA	ZK1290.5	OrthoList	OrthoMCL	NA	NA	1	-0.47	Metabolism > Vitar
AKR7A2	HGNC:389	ZK1290.5	Alliance	Ensembl Com	Yes	Yes	2	-0.47	Metabolism > Amir
ALAS1	NA	T25B9.1	OrthoList	OrthoMCL	NA	NA	1	-0.72	Metabolism > Met
ALAS2	NA	T25B9.1	OrthoList	OrthoMCL	NA	NA	1	-0.72	Metabolism > Met
ALDH18A1	HGNC:9722	alh-13	Alliance+Orth	Ensembl Com	Yes	Yes	11	0.79	Metabolism > Amir
ALDH1B1	HGNC:407	alh-1	Alliance+Orth	Ensembl Com	Yes	Yes	10	-1.43	Metabolism > Deto
ALDH1B1	HGNC:407	alh-2	Alliance+Orth	Ensembl Com	Yes	Yes	10	#N/A	Metabolism > Deto
ALDH1L1	HGNC:3978	alh-3	Alliance+Orth	Ensembl Com	Yes	Yes	11	0.88	Metabolism > Vitar
ALDH1L2	HGNC:26777	alh-3	Alliance+Orth	Ensembl Com	Yes	Yes	10	0.88	Metabolism > Vitar

ALDH2	HGNC:404	alh-1	Alliance+Orth	Ensembl Com	Yes	No	11	-1.43	Metabolism > Deto
ALDH2	HGNC:404	alh-2	Alliance+Orth	Ensembl Com	Yes	No	11	#N/A	Metabolism > Deto
ALDH3A2	HGNC:403	alh-4	Alliance+Orth	Ensembl Com	Yes	Yes	11	-0.24	Metabolism > Deto
ALDH3A2	HGNC:403	alh-5	Alliance+Orth	Ensembl Com	Yes	Yes	11	-3.1	Metabolism > Deto
ALDH4A1	HGNC:406	alh-6	Alliance+Orth	Ensembl Com	Yes	Yes	10	-1.69	Metabolism > Amir
ALDH5A1	HGNC:408	alh-7	Alliance+Orth	Ensembl Com	Yes	Yes	11	-0.11	Metabolism > Amir
ALDH6A1	HGNC:7179	alh-8	Alliance+Orth	Ensembl Com	Yes	Yes	11	-0.56	Metabolism > Amir
ALDH7A1	HGNC:877	alh-9	Alliance+Orth	Ensembl Com	Yes	Yes	11	0.18	Metabolism > Amir
ALDH9A1	HGNC:412	alh-11	Alliance+Orth	Ensembl Com	Yes	Yes	11	-0.3	Metabolism > Amir
ALDH9A1	HGNC:412	alh-12	Alliance+Orth	Ensembl Com	No	Yes	8	-1.52	Metabolism > Amir
ALKBH1	HGNC:17911	alkb-1	Alliance+Orth	Ensembl Com	Yes	Yes	11	0.31	Mitochondrial cen
ALKBH7	HGNC:21306	alkb-7	Alliance+Orth	Ensembl Com	Yes	Yes	11	0.77	Unknown
AMACR	HGNC:451	ZK892.4	Alliance+Orth	Ensembl Com	Yes	Yes	11	0.85	Metabolism > Lipic
AMACR	HGNC:451	C24A3.4	Alliance+Orth	Ensembl Com	Yes	Yes	11	-0.82	Metabolism > Lipic
AMT	HGNC:473	gcst-1	Alliance+Orth	Ensembl Com	Yes	Yes	11	-0.15	Metabolism > Amir
ANGEL2	HGNC:30534	angl-1	Alliance+Orth	Ensembl Com	Yes	Yes	8	0.2	Mitochondrial cen
ANTKMT	HGNC:14152	Y39A1A.21	Alliance	Ensembl Com	Yes	No	3	-1.54	Metabolism > Nuc
APEX1	HGNC:587	exo-3	Alliance+Orth	Ensembl Com	Yes	Yes	9	0.05	Mitochondrial cen
APOO	HGNC:28727	moma-1	Alliance	Ensembl Com	Yes	No	5	0.71	Mitochondrial dyn
APOOL	HGNC:24009	moma-1	Alliance	Ensembl Com	Yes	Yes	7	0.71	Mitochondrial dyn
ARF5	NA	arf-1.2	OrthoList	Ensembl Com	NA	NA	2	#N/A	Unknown
ARF5	HGNC:658	arf-5	Alliance+Orth	Ensembl Com	Yes	Yes	11	2.2	Unknown
ARG2	HGNC:664	argn-1	Alliance+Orth	Ensembl Com	Yes	Yes	8	-0.96	Metabolism > Amir
ARL2	HGNC:693	evl-20	Alliance+Orth	Ensembl Com	Yes	Yes	11	-0.18	Mitochondrial dyn
ARMC10	HGNC:21706	Y67A10A.7	Alliance	Ensembl Com	Yes	Yes	3	1.71	Mitochondrial dyn
ARMCX1	HGNC:18073	Y67A10A.7	Alliance	Ensembl Com	Yes	Yes	3	1.71	Mitochondrial dyn
ARMCX2	HGNC:16869	Y67A10A.7	Alliance	Ensembl Com	Yes	Yes	3	1.71	Unknown
ARMCX3	HGNC:24065	Y67A10A.7	Alliance	Ensembl Com	Yes	Yes	3	1.71	Mitochondrial dyn
ATAD1	HGNC:25903	mspn-1	Alliance+Orth	Ensembl Com	Yes	Yes	10	-0.97	Protein import, sor
ATAD3A	HGNC:25567	atad-3	Alliance+Orth	Ensembl Com	Yes	Yes	11	-1.36	Mitochondrial cen

ATAD3B	HGNC:24007	atad-3	Alliance+Orth	Ensembl Com	Yes	No	9	-1.36	Mitochondrial cen
ATP5F1A	HGNC:823	atp-1	Alliance	Ensembl Com	Yes	Yes	9	0.18	OXPHOS > Compl
ATP5F1B	HGNC:830	atp-2	Alliance	Ensembl Com	Yes	Yes	9	0.31	OXPHOS > Compl
ATP5F1C	HGNC:833	Y69A2AR.18	Alliance	Ensembl Com	Yes	Yes	9	0.74	OXPHOS > Compl
ATP5F1D	HGNC:837	F58F12.1	Alliance	Ensembl Com	Yes	Yes	9	0.81	OXPHOS > Compl
ATP5F1E	HGNC:838	hpo-18	Alliance	Hieranoid | InP	Yes	Yes	6	1.81	OXPHOS > Compl
ATP5F1E	HGNC:838	ZC262.5	Alliance	Hieranoid | InP	Yes	Yes	6	#N/A	OXPHOS > Compl
ATP5IF1	HGNC:871	mai-1	Alliance	OrthoFinder | I	No	Yes	3	1.14	OXPHOS > Compl
ATP5IF1	HGNC:871	mai-2	Alliance	Ensembl Com	Yes	Yes	6	1.15	OXPHOS > Compl
ATP5MC1	HGNC:841	Y82E9BR.3	Alliance	Ensembl Com	Yes	Yes	9	0.98	OXPHOS > Compl
ATP5MC2	HGNC:842	Y82E9BR.3	Alliance	Ensembl Com	Yes	No	8	0.98	OXPHOS > Compl
ATP5MC3	HGNC:843	Y82E9BR.3	Alliance	Ensembl Com	Yes	No	8	0.98	OXPHOS > Compl
ATP5ME	HGNC:846	R04F11.2	Alliance	Ensembl Com	Yes	Yes	6	1.36	OXPHOS > Compl
ATP5MF	HGNC:848	R53.4	Alliance	Ensembl Com	Yes	Yes	6	1.33	OXPHOS > Compl
ATP5MG	HGNC:14247	asg-1	Alliance	Ensembl Com	Yes	Yes	8	0.67	OXPHOS > Compl
ATP5MG	HGNC:14247	asg-2	Alliance	Ensembl Com	Yes	Yes	8	1.29	OXPHOS > Compl
ATP5PB	HGNC:840	asb-1	Alliance	Ensembl Com	Yes	Yes	7	-1.03	OXPHOS > Compl
ATP5PB	HGNC:840	asb-2	Alliance	Ensembl Com	Yes	Yes	7	1	OXPHOS > Compl
ATP5PD	HGNC:845	atp-5	Alliance	Ensembl Com	Yes	Yes	6	2.12	OXPHOS > Compl
ATP5PF	HGNC:847	atp-4	Alliance	OrthoFinder | I	Yes	Yes	2	1.25	OXPHOS > Compl
ATP5PO	HGNC:850	atp-3	Alliance	Ensembl Com	Yes	Yes	9	0.7	OXPHOS > Compl
ATPAF2	HGNC:18802	Y116A8C.27	Alliance+Orth	Ensembl Com	Yes	Yes	11	0.82	OXPHOS > Compl
ATPSCKMT	HGNC:27029	Y39A1A.21	Alliance	Ensembl Com	Yes	Yes	9	-1.54	OXPHOS > Compl
AUH	HGNC:890	ech-5	Alliance+Orth	Ensembl Com	Yes	Yes	11	0.56	Metabolism > Carb
BBC3	NA	col-124	OrthoList	OMA	NA	NA	1	3.11	Mitochondrial dyn
BBC3	NA	col-176	OrthoList	OMA	NA	NA	1	-0.46	Mitochondrial dyn
BCAT2	HGNC:977	bcat-1	Alliance+Orth	Ensembl Com	Yes	Yes	10	-0.43	Metabolism > Amin
BCAT2	HGNC:977	Y44A6D.5	Alliance+Orth	Ensembl Com	No	Yes	6	0.59	Metabolism > Amin
BCKDHA	HGNC:986	bckd-1A	Alliance+Orth	Ensembl Com	Yes	Yes	10	-0.44	Metabolism > Amin
BCKDHB	HGNC:987	bckd-1B	Alliance+Orth	Ensembl Com	Yes	Yes	11	-0.26	Metabolism > Amin

BCL2	HGNC:990	ced-9	Alliance	OrthoFinder|I	Yes	No	4	0.95	Mitochondrial dyna
BCL2L1	HGNC:992	ced-9	Alliance+Orth	OrthoFinder|(	Yes	No	5	0.95	Mitochondrial dyna
BCL2L2	HGNC:995	ced-9	Alliance	OrthoFinder|(	Yes	Yes	5	0.95	Mitochondrial dyna
BCO2	HGNC:18503	bcmo-1	Alliance+Orth	Ensembl Com	Yes	Yes	10	-3.63	Metabolism > Vitar
BCO2	HGNC:18503	bcmo-2	Alliance+Orth	Ensembl Com	Yes	Yes	10	-2.79	Metabolism > Vitar
BCS1L	HGNC:1020	bcs-1	Alliance+Orth	Ensembl Com	Yes	Yes	11	-2.28	OXPHOS > Compl
BDH1	NA	dhs-2	OrthoList	OrthoMCL	NA	NA	1	-1.54	Metabolism > Carb
BDH1	NA	dhs-16	OrthoList	OrthoMCL	NA	NA	1	-1.2	Metabolism > Carb
BDH1	NA	dhs-20	OrthoList	OrthoMCL	NA	NA	1	-1.07	Metabolism > Carb
BLOC1S1	HGNC:4200	blos-1	Alliance+Orth	Ensembl Com	Yes	Yes	10	1.88	Signaling
BNIP3	HGNC:1084	dct-1	Alliance+Orth	Ensembl Com	Yes	Yes	8	1.83	Mitochondrial dyna
BNIP3L	HGNC:1085	dct-1	Alliance+Orth	Ensembl Com	Yes	No	6	1.83	Mitochondrial dyna
BOLA1	HGNC:24263	K11H12.1	Alliance+Orth	Ensembl Com	Yes	Yes	11	0.04	Metabolism > Meta
BOLA1	NA	T12D8.10	OrthoList	Ensembl Com	NA	NA	1	2.31	Metabolism > Meta
BOLA3	HGNC:24415	Y105E8A.11	Alliance+Orth	Ensembl Com	Yes	Yes	10	0.53	Metabolism > Meta
BOLA3	NA	T12D8.10	OrthoList	OrthoMCL	NA	NA	1	2.31	Metabolism > Meta
BPHL	HGNC:1094	parg-1	Alliance	Ensembl Com	No	Yes	6	#N/A	Metabolism > Deto
BPHL	HGNC:1094	parg-2	Alliance	Ensembl Com	No	Yes	6	#N/A	Metabolism > Deto
BPHL	HGNC:1094	K01A2.5	Alliance+Orth	Ensembl Com	Yes	Yes	11	-0.09	Metabolism > Deto
C12orf65	NA	T23B5.4	OrthoList	InParanoid|O	NA	NA	2	0.39	Mitochondrial cen
C1QBP	HGNC:1243	cri-3	Alliance+Orth	Ensembl Com	Yes	Yes	11	0.63	Signaling > Immun
C3orf33	HGNC:26434	F32A11.1	Alliance+Orth	Ensembl Com	Yes	Yes	9	0.21	Unknown
C3orf33	HGNC:26434	W09H1.3	Alliance+Orth	Ensembl Com	No	Yes	4	#N/A	Unknown
C6orf136	HGNC:21301	C27B7.2	Alliance+Orth	Ensembl Com	Yes	Yes	5	0.57	Unknown
C8orf82	HGNC:33826	F59C6.12	Alliance+Orth	Ensembl Com	Yes	Yes	10	2.42	Unknown
CA5A	NA	cah-3	OrthoList	Ensembl Com	NA	NA	2	-0.28	Metabolism > Amin
CA5A	HGNC:1377	cah-4	Alliance+Orth	Ensembl Com	No	Yes	4	0.76	Metabolism > Amin
CA5A	HGNC:1377	cah-5	Alliance+Orth	Ensembl Com	Yes	No	4	0.69	Metabolism > Amin
CA5A	HGNC:1377	cah-6	Alliance	Ensembl Com	Yes	No	4	#N/A	Metabolism > Amin
CA5B	NA	cah-3	OrthoList	Ensembl Com	NA	NA	2	-0.28	Metabolism > Amin

CA5B	HGNC:1378	cah-4	Alliance	Ensembl Com	No	Yes	3	0.76	Metabolism > Ami
CA5B	HGNC:1378	cah-5	Alliance+Orth	Ensembl Com	Yes	No	4	0.69	Metabolism > Ami
CA5B	HGNC:1378	cah-6	Alliance	Ensembl Com	Yes	No	4	#N/A	Metabolism > Ami
CARS2	NA	cars-1	OrthoList	OrthoMCL	NA	NA	1	-0.93	Mitochondrial cen
CASP3	HGNC:1504	ced-3	Alliance+Orth	Hieranoid | Or	Yes	Yes	6	-4.44	Protein import, sor
CASP3	NA	csp-1	OrthoList	OrthoInspect	NA	NA	1	-1.88	Protein import, sor
CASP8	HGNC:1509	ced-3	Alliance+Orth	Ensembl Com	Yes	No	4	-4.44	Protein import, sor
CASP8	NA	csp-1	OrthoList	OrthoInspect	NA	NA	1	-1.88	Protein import, sor
CASP8	HGNC:1509	csp-3	Alliance	Ensembl Com	No	Yes	3	4.48	Protein import, sor
CASP9	NA	ced-3	OrthoList	Ensembl Com	NA	NA	1	-4.44	Protein import, sor
CASP9	NA	csp-1	OrthoList	Ensembl Com	NA	NA	1	-1.88	Protein import, sor
CASP9	NA	csp-2	OrthoList	Ensembl Com	NA	NA	1	-1.72	Protein import, sor
CASP9	NA	csp-3	OrthoList	Ensembl Com	NA	NA	1	4.48	Protein import, sor
CAT	HGNC:1516	ctl-1	Alliance+Orth	Ensembl Com	Yes	Yes	11	#N/A	Metabolism > Deto
CAT	HGNC:1516	ctl-2	Alliance+Orth	Ensembl Com	Yes	Yes	11	-1.26	Metabolism > Deto
CAT	HGNC:1516	ctl-3	Alliance+Orth	Ensembl Com	Yes	Yes	11	1.48	Metabolism > Deto
CBR3	HGNC:1549	C55A6.6	Alliance	Ensembl Com	Yes	Yes	2	#N/A	Metabolism > Deto
CBR3	HGNC:1549	F20G2.1	Alliance	Ensembl Com	Yes	Yes	2	#N/A	Metabolism > Deto
CBR3	NA	dhs-31	OrthoList	Legacy Ortho	NA	NA	1	0.29	Metabolism > Deto
CBR4	NA	dhs-11	OrthoList	OrthoMCL	NA	NA	1	-4.9	Metabolism > Lipio
CBR4	NA	dhs-25	OrthoList	OrthoMCL	NA	NA	1	0.54	Metabolism > Lipio
CBR4	NA	Y47G6A.22	OrthoList	OrthoMCL	NA	NA	1	-0.22	Metabolism > Lipio
CCDC51	HGNC:25714	ZC477.3	Alliance+Orth	Ensembl Com	Yes	Yes	11	-1.16	Small molecule tra
CDK5RAP1	HGNC:15880	F25B5.5	Alliance+Orth	Ensembl Com	Yes	Yes	11	-0.57	Mitochondrial cen
CDK5RAP1	NA	Y92H12BL.1	OrthoList	OrthoMCL	NA	NA	1	0.65	Mitochondrial cen
CEP89	NA	C14H10.2	OrthoList	OMA	NA	NA	1	1.14	OXPHOS > Compl
CHCHD1	HGNC:23518	C24D10.6	Alliance+Orth	Ensembl Com	Yes	Yes	9	0.41	Mitochondrial cen
CHCHD10	HGNC:15559	har-1	Alliance+Orth	Ensembl Com	Yes	Yes	8	0.7	Unknown
CHCHD2	HGNC:21645	har-1	Alliance+Orth	Ensembl Com	Yes	No	9	0.7	Mitochondrial dyn
CHCHD3	HGNC:21906	chch-3	Alliance	Ensembl Com	Yes	Yes	5	1.09	Mitochondrial dyn

CHCHD4	HGNC:26467	F11C1.1	Alliance+Orth	Ensembl Com	No	Yes	6	2.25	Protein import, sor
CHCHD4	HGNC:26467	F42H10.2	Alliance+Orth	Ensembl Com	No	Yes	5	0.79	Protein import, sor
CHCHD4	HGNC:26467	ZK616.2	Alliance+Orth	Ensembl Com	No	Yes	7	-0.99	Protein import, sor
CHCHD4	HGNC:26467	ZK616.3	Alliance+Orth	Ensembl Com	Yes	Yes	9	-3.93	Protein import, sor
CHDH	HGNC:24288	chdh-1	Alliance+Orth	Ensembl Com	Yes	Yes	10	-0.26	Metabolism > Amir
CHPT1	HGNC:17852	cept-1	Alliance+Orth	Ensembl Com	Yes	Yes	9	-1.99	Metabolism > Lipic
CHPT1	HGNC:17852	cept-2	Alliance+Orth	Ensembl Com	Yes	Yes	9	0.42	Metabolism > Lipic
CISD1	HGNC:30880	cisd-1	Alliance+Orth	Ensembl Com	Yes	No	8	-0.86	Metabolism > Meta
CISD3	HGNC:27578	cisd-3.1	Alliance+Orth	Ensembl Com	Yes	Yes	7	-0.04	Metabolism > Meta
CISD3	HGNC:27578	cisd-3.2	Alliance+Orth	Ensembl Com	No	Yes	4	0.31	Metabolism > Meta
CKMT1A	HGNC:31736	argk-1	Alliance+Orth	Ensembl Com	Yes	Yes	8	-0.29	Metabolism > Nuc
CKMT1A	HGNC:31736	ZC434.8	Alliance+Orth	Ensembl Com	Yes	Yes	7	-6.76	Metabolism > Nuc
CKMT1A	NA	F11G11.13	OrthoList	Ensembl Com	NA	NA	1	#N/A	Metabolism > Nuc
CKMT1A	HGNC:31736	F32B5.1	Alliance+Orth	Ensembl Com	No	Yes	6	#N/A	Metabolism > Nuc
CKMT1A	HGNC:31736	F46H5.3	Alliance+Orth	Ensembl Com	No	Yes	7	0.34	Metabolism > Nuc
CKMT1A	HGNC:31736	W10C8.5	Alliance+Orth	Ensembl Com	Yes	Yes	7	0.11	Metabolism > Nuc
CKMT1B	HGNC:1995	argk-1	Alliance+Orth	Ensembl Com	Yes	Yes	7	-0.29	Metabolism > Nuc
CKMT1B	HGNC:1995	ZC434.8	Alliance+Orth	Ensembl Com	Yes	Yes	7	-6.76	Metabolism > Nuc
CKMT1B	NA	F11G11.13	OrthoList	Ensembl Com	NA	NA	1	#N/A	Metabolism > Nuc
CKMT1B	HGNC:1995	F32B5.1	Alliance+Orth	Ensembl Com	No	Yes	6	#N/A	Metabolism > Nuc
CKMT1B	HGNC:1995	F46H5.3	Alliance+Orth	Ensembl Com	No	Yes	7	0.34	Metabolism > Nuc
CKMT1B	HGNC:1995	W10C8.5	Alliance+Orth	Ensembl Com	Yes	Yes	7	0.11	Metabolism > Nuc
CKMT2	HGNC:1996	argk-1	Alliance+Orth	Ensembl Com	Yes	Yes	7	-0.29	Metabolism > Nuc
CKMT2	HGNC:1996	ZC434.8	Alliance+Orth	Ensembl Com	Yes	Yes	7	-6.76	Metabolism > Nuc
CKMT2	NA	F11G11.13	OrthoList	Ensembl Com	NA	NA	1	#N/A	Metabolism > Nuc
CKMT2	HGNC:1996	F32B5.1	Alliance+Orth	Ensembl Com	No	Yes	6	#N/A	Metabolism > Nuc
CKMT2	HGNC:1996	F46H5.3	Alliance+Orth	Ensembl Com	No	Yes	7	0.34	Metabolism > Nuc
CKMT2	HGNC:1996	W10C8.5	Alliance+Orth	Ensembl Com	Yes	Yes	7	0.11	Metabolism > Nuc
CLPP	HGNC:2084	clpp-1	Alliance+Orth	Ensembl Com	Yes	Yes	11	-0.57	Protein import, sor
CLPX	HGNC:2088	D2030.2	Alliance+Orth	Ensembl Com	Yes	Yes	11	0.47	Protein import, sor

CLPX	HGNC:2088	K07A3.3	Alliance+Orth	Ensembl Com	No	Yes	5	-1.1	Protein import, so
CLYBL	HGNC:18355	C01G10.7	Alliance+Orth	Ensembl Com	Yes	Yes	10	-4.14	Metabolism > Carb
CMC1	HGNC:28783	F01F1.2	Alliance+Orth	Hieranoid | InP	Yes	Yes	7	-0.01	OXPHOS > Compl
CMC2	HGNC:24447	C35D10.17	Alliance+Orth	Ensembl Com	Yes	Yes	9	-2.12	OXPHOS > Compl
COA1	HGNC:21868	coa-1	Alliance+Orth	Hieranoid | InP	Yes	Yes	7	-0.54	OXPHOS > Compl
COA3	HGNC:24990	coa-3	Alliance+Orth	Ensembl Com	Yes	Yes	5	-6.27	Mitochondrial cen
COA4	NA	T20D3.3	OrthoList	OMA	NA	NA	1	#N/A	OXPHOS > Compl
COA4	HGNC:24604	T20D3.14	Alliance	OMA | OrthoFi	Yes	Yes	6	#N/A	OXPHOS > Compl
COA5	HGNC:33848	coa-5	Alliance+Orth	Ensembl Com	Yes	Yes	10	1.36	OXPHOS > Compl
COA7	HGNC:25716	coa-7	Alliance+Orth	Ensembl Com	Yes	Yes	11	-0.01	OXPHOS > Compl
COA8	HGNC:20492	Y39B6A.34	Alliance	Ensembl Com	Yes	Yes	8	-3.28	OXPHOS > Compl
COASY	HGNC:29932	Y65B4A.8	Alliance+Orth	Ensembl Com	Yes	Yes	11	-0.13	Metabolism > Meta
COMTD1	HGNC:26309	comt-2	Alliance+Orth	Ensembl Com	Yes	Yes	11	-2.94	Unknown
COMTD1	NA	comt-1	OrthoList	Ensembl Com	NA	NA	1	-1.54	Unknown
COMTD1	HGNC:26309	comt-3	Alliance+Orth	Ensembl Com	Yes	Yes	11	-0.48	Unknown
COMTD1	HGNC:26309	comt-4	Alliance+Orth	Ensembl Com	Yes	Yes	11	1.38	Unknown
COMTD1	HGNC:26309	comt-5	Alliance+Orth	Ensembl Com	Yes	Yes	11	-3.25	Unknown
COQ10A	HGNC:26515	R144.13	Alliance+Orth	Ensembl Com	Yes	Yes	11	0.44	Metabolism > Meta
COQ10B	HGNC:25819	R144.13	Alliance+Orth	Ensembl Com	Yes	Yes	9	0.44	Metabolism > Meta
COQ2	HGNC:25223	coq-2	Alliance+Orth	Ensembl Com	Yes	Yes	11	-1.77	Metabolism > Meta
COQ3	HGNC:18175	coq-3	Alliance+Orth	Ensembl Com	Yes	Yes	11	0.49	Metabolism > Meta
COQ4	HGNC:19693	coq-4	Alliance+Orth	Ensembl Com	Yes	Yes	11	3.38	Metabolism > Meta
COQ5	HGNC:28722	coq-5	Alliance+Orth	Ensembl Com	Yes	Yes	11	-0.09	Metabolism > Meta
COQ6	HGNC:20233	coq-6	Alliance+Orth	Ensembl Com	Yes	Yes	11	-0.36	Metabolism > Meta
COQ7	HGNC:2244	clk-1	Alliance+Orth	Ensembl Com	Yes	Yes	11	1.9	Metabolism > Meta
COQ8A	HGNC:16812	coq-8	Alliance+Orth	Ensembl Com	Yes	Yes	10	-1.34	Metabolism > Meta
COQ8B	HGNC:19041	coq-8	Alliance+Orth	Ensembl Com	Yes	Yes	9	-1.34	Metabolism > Meta
COX10	HGNC:2260	cox-10	Alliance+Orth	Ensembl Com	Yes	Yes	10	-0.87	OXPHOS > Compl
COX11	HGNC:2261	cox-11	Alliance+Orth	Ensembl Com	Yes	Yes	11	-2.28	OXPHOS > Compl
COX15	HGNC:2263	cox-15	Alliance+Orth	Ensembl Com	Yes	Yes	11	-0.93	OXPHOS > Compl

COX16	HGNC:20213	cox-16	Alliance	Hieranoid|InP	Yes	Yes	7	#N/A	OXPHOS > Compl
COX17	HGNC:2264	cox-17	Alliance+Orth	Ensembl Com	Yes	Yes	10	0.29	OXPHOS > Compl
COX18	HGNC:26801	cox-18	Alliance+Orth	Ensembl Com	Yes	Yes	8	0.64	OXPHOS > Compl
COX19	HGNC:28074	cox-19	Alliance+Orth	Ensembl Com	Yes	Yes	10	3.03	OXPHOS > Compl
COX4I1	HGNC:2265	cox-4	Alliance+Orth	Ensembl Com	Yes	Yes	10	1.05	OXPHOS > Compl
COX4I2	HGNC:16232	cox-4	Alliance+Orth	Ensembl Com	Yes	Yes	9	1.05	OXPHOS > Compl
COX5A	HGNC:2267	cox-5A	Alliance+Orth	Ensembl Com	Yes	Yes	10	1.04	OXPHOS > Compl
COX5B	HGNC:2269	cox-5B	Alliance+Orth	Ensembl Com	Yes	Yes	10	1.2	OXPHOS > Compl
COX6A1	HGNC:2277	cox-6A	Alliance+Orth	Ensembl Com	Yes	Yes	9	0.6	OXPHOS > Compl
COX6A2	HGNC:2279	cox-6A	Alliance+Orth	Ensembl Com	Yes	Yes	9	0.6	OXPHOS > Compl
COX6B1	HGNC:2280	cox-6B	Alliance+Orth	Ensembl Com	Yes	Yes	9	2.59	OXPHOS > Compl
COX6B2	HGNC:24380	cox-6B	Alliance+Orth	Ensembl Com	Yes	No	8	2.59	OXPHOS > Compl
COX7C	HGNC:2292	cox-7C	Alliance	Ensembl Com	Yes	Yes	6	1.87	OXPHOS > Compl
CPS1	NA	pyr-1	OrthoList	Ensembl Com	NA	NA	2	-0.94	Metabolism > Ami
CPT1A	HGNC:2328	cpt-1	Alliance+Orth	Ensembl Com	Yes	Yes	10	-0.61	Metabolism > Lipid
CPT1A	HGNC:2328	W03F9.4	Alliance	OrthoFinder|I	No	Yes	4	#N/A	Metabolism > Lipid
CPT1B	HGNC:2329	cpt-1	Alliance+Orth	Ensembl Com	Yes	No	10	-0.61	Metabolism > Lipid
CPT1B	HGNC:2329	W03F9.4	Alliance	OrthoFinder|I	No	Yes	4	#N/A	Metabolism > Lipid
CPT1C	HGNC:18540	cpt-1	Alliance+Orth	Ensembl Com	Yes	Yes	10	-0.61	Metabolism > Lipid
CPT1C	HGNC:18540	W03F9.4	Alliance	OrthoFinder|I	No	Yes	4	#N/A	Metabolism > Lipid
CPT2	HGNC:2330	cpt-2	Alliance+Orth	Ensembl Com	Yes	Yes	11	-0.04	Metabolism > Lipid
CRAT	HGNC:2342	B0395.3	Alliance+Orth	Ensembl Com	Yes	Yes	11	0.3	Metabolism > Lipid
CRLS1	HGNC:16148	crls-1	Alliance+Orth	Ensembl Com	Yes	Yes	10	0.59	Metabolism > Lipid
CROT	HGNC:2366	F41E7.6	Alliance+Orth	Ensembl Com	Yes	Yes	11	-1	Metabolism > Lipid
CROT	HGNC:2366	T20B3.1	Alliance+Orth	Ensembl Com	Yes	Yes	11	-1.75	Metabolism > Lipid
CRYZ	HGNC:2419	F39B2.3	Alliance+Orth	Ensembl Com	Yes	Yes	11	-1.34	Unknown
CS	HGNC:2422	cts-1	Alliance+Orth	Ensembl Com	Yes	Yes	11	-0.05	Metabolism > Carb
CSKMT	HGNC:33113	F52F12.9	Alliance	Ensembl Com	Yes	Yes	2	2.13	Signaling
CSKMT	HGNC:33113	Y34B4A.7	Alliance	Ensembl Com	Yes	Yes	2	-2.96	Signaling
CYB5B	HGNC:24374	cytb-5.1	Alliance+Orth	Ensembl Com	Yes	Yes	9	1.51	Metabolism > Meta

CYB5B	NA	D2023.1	OrthoList	OrthoMCL	NA	NA	1	1.52	Metabolism > Meta
CYB5B	NA	cytb-5.2	OrthoList	Homologene	NA	NA	3	1.7	Metabolism > Meta
CYB5R3	HGNC:2873	T05H4.4	Alliance+Orth	Ensembl Com	Yes	Yes	9	-3.11	Metabolism > Deto
CYB5R3	HGNC:2873	hpo-19	Alliance+Orth	Ensembl Com	Yes	Yes	9	0.74	Metabolism > Deto
CYC1	HGNC:2579	cyc-1	Alliance+Orth	Ensembl Com	Yes	Yes	11	0.2	OXPHOS > Compl
CYCS	HGNC:19986	cyc-2.2	Alliance+Orth	Ensembl Com	No	Yes	10	#N/A	Metabolism > Meta
CYCS	HGNC:19986	cyc-2.1	Alliance+Orth	Ensembl Com	Yes	Yes	11	2.43	Metabolism > Meta
CYP11A1	HGNC:2590	cyp-44A1	Alliance+Orth	Ensembl Com	Yes	No	4	0.61	Metabolism > Lipid
CYP11B1	NA	cyp-44A1	OrthoList	Ensembl Com	NA	NA	2	0.61	Metabolism > Lipid
CYP11B2	NA	cyp-44A1	OrthoList	Ensembl Com	NA	NA	2	0.61	Metabolism > Lipid
CYP24A1	HGNC:2602	cyp-44A1	Alliance+Orth	Ensembl Com	Yes	Yes	8	0.61	Metabolism > Meta
CYP24A1	NA	ZK177.4	OrthoList	OrthoMCL	NA	NA	1	#N/A	Metabolism > Meta
CYP27A1	HGNC:2605	cyp-44A1	Alliance+Orth	Ensembl Com	Yes	No	6	0.61	Metabolism > Lipid
CYP27A1	NA	ZK177.4	OrthoList	OrthoMCL	NA	NA	1	#N/A	Metabolism > Lipid
CYP27B1	HGNC:2606	cyp-44A1	Alliance+Orth	Ensembl Com	Yes	No	5	0.61	Metabolism > Meta
D2HGDH	HGNC:28358	dhgd-1	Alliance+Orth	Ensembl Com	Yes	Yes	11	-0.28	Metabolism > Carb
DAP3	HGNC:2673	dap-3	Alliance+Orth	Ensembl Com	Yes	Yes	11	0.5	Mitochondrial cen
DARS2	HGNC:25538	dars-2	Alliance+Orth	Ensembl Com	Yes	Yes	11	-1.65	Mitochondrial cen
DBI	NA	acbp-3	OrthoList	OrthoMCL	NA	NA	1	3.62	Metabolism > Lipid
DBI	NA	acbp-6	OrthoList	Legacy Ortho	NA	NA	1	0.28	Metabolism > Lipid
DBI	HGNC:2690	acbp-1	Alliance+Orth	Ensembl Com	Yes	Yes	9	0.66	Metabolism > Lipid
DBT	HGNC:2698	dbt-1	Alliance+Orth	Ensembl Com	Yes	Yes	11	-0.23	Metabolism > Amin
DCAKD	HGNC:26238	T05G5.5	Alliance+Orth	Ensembl Com	Yes	Yes	11	1.15	Unknown
DCXR	HGNC:18985	dhs-21	Alliance+Orth	Ensembl Com	Yes	Yes	11	-0.15	Metabolism > Carb
DECR1	HGNC:2753	decr-1.1	Alliance+Orth	Ensembl Com	Yes	Yes	10	-1.43	Metabolism > Lipid
DECR1	HGNC:2753	decr-1.3	Alliance+Orth	Ensembl Com	Yes	Yes	9	-4.53	Metabolism > Lipid
DECR1	HGNC:2753	decr-1.2	Alliance+Orth	Ensembl Com	Yes	Yes	9	-3.32	Metabolism > Lipid
DHODH	HGNC:2867	dhod-1	Alliance+Orth	Ensembl Com	Yes	Yes	11	0.19	Metabolism > Nuc
DHRS1	HGNC:16445	dhs-9	Alliance+Orth	Ensembl Com	Yes	Yes	11	1.76	Metabolism > Lipid
DHRS1	HGNC:16445	dhs-26	Alliance+Orth	Ensembl Com	No	Yes	8	-1.89	Metabolism > Lipid

DHRS1	HGNC:16445	F59E11.2	Alliance+Orth	Ensembl Com	Yes	Yes	10	3.17	Metabolism > Lipic
DHRS2	HGNC:18349	dhs-13	Alliance+Orth	Ensembl Com	Yes	Yes	9	-0.15	Metabolism > Deto
DHRS2	HGNC:18349	dhrs-4	Alliance+Orth	Ensembl Com	No	Yes	5	-1.42	Metabolism > Deto
DHRS4	HGNC:16985	dhs-13	Alliance+Orth	Ensembl Com	Yes	Yes	11	-0.15	Metabolism > Vita
DHRS4	HGNC:16985	dhrs-4	Alliance+Orth	Ensembl Com	No	Yes	6	-1.42	Metabolism > Vita
DHRS7B	HGNC:24547	dhs-30	Alliance+Orth	Ensembl Com	Yes	Yes	11	-1.46	Unknown
DHRS7B	HGNC:24547	C33E10.10	Alliance+Orth	Ensembl Com	No	Yes	5	4.6	Unknown
DHRS7B	NA	T25G12.2	OrthoList	OrthoMCL	NA	NA	1	#N/A	Unknown
DHRS7B	HGNC:24547	T25G12.13	Alliance+Orth	Ensembl Com	Yes	Yes	10	#N/A	Unknown
DHTKD1	HGNC:23537	ogdh-2	Alliance+Orth	Ensembl Com	Yes	Yes	11	-0.1	Metabolism > Amir
DHTKD1	NA	ogdh-1	OrthoList	OrthoMCL	NA	NA	1	-0.71	Metabolism > Amir
DLAT	HGNC:2896	dlat-1	Alliance+Orth	Ensembl Com	Yes	Yes	11	0.31	Metabolism > Carb
DLD	HGNC:2898	dld-1	Alliance+Orth	Ensembl Com	Yes	Yes	11	-0.23	Metabolism > Carb
DLST	HGNC:2911	dlst-1	Alliance+Orth	Ensembl Com	Yes	Yes	11	0.29	Metabolism > Carb
DMAC2	HGNC:25496	Y53G8AR.8	Alliance	Ensembl Com	Yes	Yes	5	0.31	OXPHOS > Compl
DMAC2L	HGNC:18799	C05C8.1	Alliance	Ensembl Com	Yes	Yes	5	0.59	OXPHOS > Compl
DMAC2L	HGNC:18799	R02D5.8	Alliance	Ensembl Com	Yes	Yes	5	3.47	OXPHOS > Compl
DMGDH	HGNC:24475	Y37E3.17	Alliance+Orth	Ensembl Com	Yes	Yes	11	-5.12	Metabolism > Amir
DMPK	NA	mrck-1	OrthoList	Ensembl Com	NA	NA	1	0.55	Unknown
DNA2	HGNC:2939	dna-2	Alliance+Orth	Ensembl Com	Yes	Yes	11	-1.64	Mitochondrial cen
DNAJA3	HGNC:11808	dnj-10	Alliance+Orth	Ensembl Com	Yes	Yes	10	-0.49	Protein import, sor
DNAJA3	NA	dnj-18	OrthoList	Ensembl Com	NA	NA	1	-0.76	Protein import, sor
DNAJC11	HGNC:25570	dnj-9	Alliance+Orth	Ensembl Com	Yes	Yes	11	-2.17	Protein import, sor
DNAJC15	HGNC:20325	dnj-21	Alliance+Orth	Ensembl Com	Yes	No	8	-0.28	Protein import, sor
DNAJC19	HGNC:30528	dnj-21	Alliance+Orth	Ensembl Com	Yes	Yes	11	-0.28	Protein import, sor
DNAJC30	HGNC:16410	dnj-18	Alliance	Hieranoid | Or	Yes	Yes	2	-0.76	Unknown
DNAJC4	HGNC:5271	dnj-4	Alliance+Orth	Ensembl Com	Yes	Yes	9	-0.85	Protein import, sor
DNLZ	HGNC:33879	F53A3.7	Alliance+Orth	Ensembl Com	Yes	Yes	8	1.41	Protein import, sor
DNM1L	HGNC:2973	drp-1	Alliance+Orth	Ensembl Com	Yes	Yes	11	-0.54	Mitochondrial dyn
DNM1L	NA	dyn-1	OrthoList	OrthoMCL	NA	NA	1	0.81	Mitochondrial dyn

DTYMK	HGNC:3061	dtmk-1	Alliance+Orth	Ensembl Com	Yes	Yes	11	-0.58	Metabolism > Nuc
DUS2	HGNC:26014	dus-2	Alliance+Orth	Ensembl Com	Yes	Yes	11	0.71	Mitochondrial cen
DUT	HGNC:3078	dut-1	Alliance+Orth	Ensembl Com	Yes	Yes	8	-0.65	Metabolism > Nuc
EARS2	HGNC:29419	ears-2	Alliance+Orth	Ensembl Com	Yes	Yes	11	-4.26	Mitochondrial cen
ECH1	HGNC:3149	F58A6.1	Alliance+Orth	Ensembl Com	Yes	Yes	11	-1.48	Metabolism > Lipic
ECH1	HGNC:3149	Y25C1A.13	Alliance+Orth	Ensembl Com	No	Yes	10	-0.04	Metabolism > Lipic
ECHDC1	HGNC:21489	C32E8.9	Alliance+Orth	Ensembl Com	Yes	Yes	11	-1.02	Metabolism > Lipic
ECHDC2	HGNC:23408	ech-5	Alliance+Orth	Ensembl Com	Yes	Yes	10	0.56	Unknown
ECHDC3	HGNC:23489	ech-2	Alliance+Orth	Ensembl Com	Yes	Yes	11	1.37	Unknown
ECHS1	HGNC:3151	ech-6	Alliance+Orth	Ensembl Com	Yes	Yes	11	-0.27	Metabolism > Lipic
ECHS1	HGNC:3151	ech-7	Alliance+Orth	Ensembl Com	No	Yes	7	-0.42	Metabolism > Lipic
ECI2	HGNC:14601	ech-4	Alliance+Orth	Ensembl Com	Yes	Yes	11	-0.6	Metabolism > Lipic
ECI2	HGNC:14601	B0272.4	Alliance+Orth	Ensembl Com	No	Yes	4	-2.15	Metabolism > Lipic
ECSIT	HGNC:29548	Y17G9B.5	Alliance+Orth	Ensembl Com	Yes	Yes	11	-1.06	OXPHOS > Compl
EFHD1	HGNC:29556	efhd-1	Alliance+Orth	Ensembl Com	Yes	Yes	7	0.5	Signaling > Calciu
EHHADH	NA	ech-1.1	OrthoList	OrthoMCL	NA	NA	1	-5	Metabolism > Lipic
EHHADH	HGNC:3247	ech-8	Alliance+Orth	Ensembl Com	Yes	Yes	4	0.56	Metabolism > Lipic
EHHADH	HGNC:3247	ech-9	Alliance+Orth	Ensembl Com	Yes	Yes	4	-1.5	Metabolism > Lipic
EHHADH	NA	ech-1.2	OrthoList	OrthoMCL	NA	NA	1	-0.88	Metabolism > Lipic
ELAC2	HGNC:14198	elac-2	Alliance+Orth	Ensembl Com	Yes	Yes	11	#N/A	Mitochondrial cen
ENDOG	HGNC:3346	cps-6	Alliance+Orth	Ensembl Com	Yes	Yes	11	-0.9	Mitochondrial cen
EPHX2	NA	ceeh-2	OrthoList	Ensembl Com	NA	NA	1	-1.86	Metabolism > Deto
EPHX2	NA	ceeh-1	OrthoList	Ensembl Com	NA	NA	1	-0.46	Metabolism > Deto
ERAL1	HGNC:3424	eral-1	Alliance+Orth	Ensembl Com	Yes	Yes	11	-0.53	Mitochondrial cen
ETFA	HGNC:3481	etfa-1	Alliance+Orth	Ensembl Com	Yes	Yes	11	#N/A	Metabolism > Lipic
ETFB	HGNC:3482	etfb-1	Alliance+Orth	Ensembl Com	Yes	Yes	11	#N/A	Metabolism > Lipic
ETFBKMT	HGNC:28739	etfm-1	Alliance+Orth	Ensembl Com	Yes	Yes	11	#N/A	Metabolism > Elec
ETFDH	HGNC:3483	let-721	Alliance+Orth	Ensembl Com	Yes	Yes	11	-0.53	Metabolism > Lipic
ETFRF1	HGNC:27052	etfr-1	Alliance+Orth	Ensembl Com	Yes	Yes	10	#N/A	Metabolism > Elec
ETHE1	HGNC:23287	ethe-1	Alliance+Orth	Ensembl Com	Yes	Yes	11	1.63	Metabolism > Sulf

EXOG	NA	cps-6	OrthoList	OrthoMCL	NA	NA	1	-0.9	Mitochondrial cen
FAHD1	HGNC:14169	fahd-1	Alliance+Orth	Ensembl Com	Yes	Yes	11	0.76	Metabolism > Carb
FAHD2A	NA	fahd-1	OrthoList	OrthoMCL	NA	NA	1	0.76	Unknown
FAM136A	HGNC:25911	famh-136	Alliance+Orth	Ensembl Com	Yes	Yes	10	-0.28	Unknown
FAM162A	HGNC:17865	taap-1	Alliance	Ensembl Com	Yes	Yes	2	0.45	Unknown
FAM210A	HGNC:28346	Y56A3A.22	Alliance+Orth	Ensembl Com	Yes	Yes	8	-1.13	Unknown
FARS2	HGNC:21062	fars-2	Alliance+Orth	Ensembl Com	Yes	Yes	11	-1.23	Mitochondrial cen
FASN	HGNC:3594	fasn-1	Alliance+Orth	Ensembl Com	Yes	Yes	11	-0.18	Metabolism > Lipid
FASN	HGNC:3594	F32H2.6	Alliance+Orth	Ensembl Com	No	Yes	3	#N/A	Metabolism > Lipid
FASN	NA	C41A3.1	OrthoList	OrthoMCL	NA	NA	1	#N/A	Metabolism > Lipid
FBXL4	HGNC:13601	fbxl-2	Alliance	InParanoid|P	Yes	Yes	2	#N/A	Unknown
FDPS	HGNC:3631	fdps-1	Alliance+Orth	Ensembl Com	Yes	Yes	10	0.01	Metabolism > Lipid
FDX1	NA	Y73F8A.27	OrthoList	OrthoMCL	NA	NA	1	-1.99	Metabolism > Lipid
FDX2	HGNC:30546	fdx-2	Alliance+Orth	Ensembl Com	Yes	Yes	10	#N/A	Metabolism > Meta
FDXR	HGNC:3642	Y62E10A.6	Alliance+Orth	Ensembl Com	Yes	Yes	10	-0.71	Metabolism > Lipid
FECH	HGNC:3647	fecl-1	Alliance	Hieranoid|Or	Yes	Yes	3	0.51	Metabolism > Meta
FH	HGNC:3700	fum-1	Alliance+Orth	Ensembl Com	Yes	Yes	11	-0.24	Metabolism > Carb
FIS1	HGNC:21689	fis-1	Alliance+Orth	Ensembl Com	No	Yes	5	-4.37	Mitochondrial dyn
FIS1	HGNC:21689	fis-2	Alliance+Orth	Ensembl Com	Yes	Yes	10	1.54	Mitochondrial dyn
FKBP10	HGNC:18169	fkb-3	Alliance+Orth	Ensembl Com	No	Yes	7	1.76	Protein import, sor
FKBP10	HGNC:18169	fkb-4	Alliance+Orth	Ensembl Com	Yes	Yes	6	1.94	Protein import, sor
FKBP10	HGNC:18169	fkb-5	Alliance+Orth	Ensembl Com	Yes	Yes	7	-0.52	Protein import, sor
FKBP8	NA	fkb-2	OrthoList	Ensembl Com	NA	NA	1	1.68	Mitochondrial dyn
FKBP8	NA	fkb-6	OrthoList	Ensembl Com	NA	NA	1	1.25	Mitochondrial dyn
FKBP8	NA	fkb-8	OrthoList	Ensembl Com	NA	NA	1	4.24	Mitochondrial dyn
FLAD1	HGNC:24671	flad-1	Alliance+Orth	Ensembl Com	Yes	Yes	11	0.48	Metabolism > Vita
FMC1	HGNC:26946	C29E4.12	Alliance+Orth	Ensembl Com	Yes	Yes	9	0.43	OXPHOS > Compl
FOXRED1	HGNC:26927	M04B2.4	Alliance+Orth	Ensembl Com	Yes	Yes	10	-1.2	OXPHOS > Compl
FPGS	HGNC:3824	F25B5.6	Alliance+Orth	Ensembl Com	Yes	Yes	11	-1.25	Metabolism > Vita
FTH1	HGNC:3976	ftn-1	Alliance+Orth	Ensembl Com	No	Yes	9	#N/A	Metabolism > Meta

FTH1	HGNC:3976	ftn-2	Alliance+Orth	Ensembl Com	Yes	Yes	10	-0.59	Metabolism > Meta
FTMT	HGNC:17345	ftn-1	Alliance+Orth	Ensembl Com	No	Yes	8	#N/A	Metabolism > Meta
FTMT	HGNC:17345	ftn-2	Alliance+Orth	Ensembl Com	Yes	Yes	9	-0.59	Metabolism > Meta
FUNDC1	HGNC:28746	fndc-1	Alliance+Orth	Ensembl Com	Yes	Yes	8	1.14	Mitochondrial dyna
FUNDC2	HGNC:24925	fndc-1	Alliance+Orth	Ensembl Com	Yes	Yes	7	1.14	Mitochondrial dyna
FXN	HGNC:3951	frh-1	Alliance+Orth	Ensembl Com	Yes	Yes	8	-2.11	Metabolism > Meta
GADD45GIP1	HGNC:29996	K07A1.10	Alliance+Orth	Ensembl Com	Yes	Yes	9	-0.2	Mitochondrial cent
GARS1	HGNC:4162	gars-1	Alliance	Ensembl Com	Yes	Yes	9	0.02	Mitochondrial cent
GATB	HGNC:8849	C39B5.6	Alliance+Orth	Ensembl Com	Yes	Yes	9	-0.88	Mitochondrial cent
GATC	HGNC:25068	Y66D12A.7	Alliance+Orth	Ensembl Com	Yes	Yes	8	-4.55	Mitochondrial cent
GCAT	HGNC:4188	T25B9.1	Alliance+Orth	Ensembl Com	Yes	Yes	10	-0.72	Metabolism > Amin
GCDH	HGNC:4189	F54D5.7	Alliance+Orth	Ensembl Com	Yes	Yes	11	-1.48	Metabolism > Amin
GCSH	HGNC:4208	gcsh-1	Alliance+Orth	Ensembl Com	Yes	Yes	11	-0.22	Metabolism > Lipid
GCSH	HGNC:4208	gcsh-2	Alliance+Orth	Ensembl Com	Yes	Yes	11	1.04	Metabolism > Lipid
GFER	HGNC:4236	F56C11.3	Alliance+Orth	Ensembl Com	Yes	Yes	10	0.66	Protein import, sor
GFM1	HGNC:13780	gfm-1	Alliance+Orth	Ensembl Com	Yes	Yes	11	-1.46	Mitochondrial cent
GFM1	NA	F58G1.8	OrthoList	Ensembl Com	NA	NA	1	#N/A	Mitochondrial cent
GFM1	NA	Y119D3B.14	OrthoList	OrthoMCL	NA	NA	1	0.06	Mitochondrial cent
GFM2	NA	gfm-1	OrthoList	OrthoMCL	NA	NA	1	-1.46	Mitochondrial cent
GFM2	HGNC:29682	Y119D3B.14	Alliance+Orth	Ensembl Com	Yes	Yes	11	0.06	Mitochondrial cent
GHITM	HGNC:17281	K11H12.8	Alliance+Orth	Ensembl Com	Yes	Yes	11	0.12	Mitochondrial dyna
GLDC	HGNC:4313	gldc-1	Alliance+Orth	Ensembl Com	Yes	Yes	11	0.13	Metabolism > Amin
GLOD4	HGNC:14111	glod-4	Alliance+Orth	Ensembl Com	Yes	Yes	11	-0.48	Unknown
GLRX2	NA	glrx-10	OrthoList	OrthoMCL	NA	NA	1	1.48	Metabolism > Meta
GLRX2	HGNC:16065	glrx-21	Alliance+Orth	InParanoid|O	Yes	Yes	5	2.13	Metabolism > Meta
GLRX2	HGNC:16065	glrx-22	Alliance+Orth	InParanoid|O	Yes	Yes	4	2.72	Metabolism > Meta
GLRX5	HGNC:20134	glrx-5	Alliance+Orth	Ensembl Com	Yes	Yes	11	2.43	Metabolism > Meta
GLS	HGNC:4331	glna-1	Alliance+Orth	Ensembl Com	No	Yes	10	1.13	Metabolism > Amin
GLS	HGNC:4331	glna-2	Alliance+Orth	Ensembl Com	Yes	Yes	11	3.47	Metabolism > Amin
GLS	HGNC:4331	glna-3	Alliance+Orth	Ensembl Com	No	Yes	8	0.07	Metabolism > Amin

GLS2	HGNC:29570	glna-1	Alliance+Orth	Ensembl Com	No	Yes	9	1.13	Metabolism > Ami
GLS2	HGNC:29570	glna-2	Alliance+Orth	Ensembl Com	Yes	Yes	10	3.47	Metabolism > Ami
GLS2	HGNC:29570	glna-3	Alliance+Orth	Ensembl Com	No	Yes	7	0.07	Metabolism > Ami
GLUD1	HGNC:4335	gdh-1	Alliance+Orth	Ensembl Com	Yes	No	10	0	Metabolism > Ami
GLUD2	HGNC:4336	gdh-1	Alliance+Orth	Ensembl Com	Yes	Yes	9	0	Metabolism > Ami
GLYAT	HGNC:13734	T10B10.4	Alliance	Ensembl Com	Yes	No	3	1.16	Metabolism > Ami
GLYAT	HGNC:13734	F43H9.4	Alliance	Ensembl Com	Yes	Yes	3	0.83	Metabolism > Ami
GLYAT	HGNC:13734	ZK185.3	Alliance	Ensembl Com	Yes	Yes	3	0.22	Metabolism > Ami
GLYCTK	HGNC:24247	C13B9.2	Alliance+Orth	Ensembl Com	Yes	Yes	11	-4.37	Metabolism > Carb
GOLPH3	HGNC:15452	Y47G6A.18	Alliance+Orth	Ensembl Com	Yes	Yes	11	0.68	Unknown
GOT2	HGNC:4433	got-2.2	Alliance+Orth	Ensembl Com	Yes	Yes	11	0.84	Metabolism > Carb
GOT2	HGNC:4433	got-2.1	Alliance+Orth	Ensembl Com	No	Yes	8	-2.3	Metabolism > Carb
GOT2	NA	got-1.2	OrthoList	OrthoMCL	NA	NA	1	0.43	Metabolism > Carb
GPAM	HGNC:24865	acl-6	Alliance+Orth	Ensembl Com	Yes	Yes	9	-1.61	Metabolism > Lipic
GPAT2	HGNC:27168	acl-6	Alliance+Orth	Ensembl Com	Yes	Yes	6	-1.61	Metabolism > Lipic
GPD2	HGNC:4456	gpdh-3	Alliance+Orth	Ensembl Com	Yes	Yes	11	-0.59	Metabolism > Carb
GPD2	HGNC:4456	Y50E8A.6	Alliance+Orth	Ensembl Com	No	Yes	4	3.15	Metabolism > Carb
GPT2	HGNC:18062	C32F10.8	Alliance+Orth	Ensembl Com	Yes	Yes	11	-1.21	Metabolism > Ami
GPX1	NA	gpx-5	OrthoList	Ensembl Com	NA	NA	4	0.21	Metabolism > Deto
GPX1	HGNC:4553	gpx-3	Alliance+Orth	Ensembl Com	Yes	No	8	-0.38	Metabolism > Deto
GPX1	NA	gpx-4	OrthoList	Ensembl Com	NA	NA	3	-0.87	Metabolism > Deto
GPX4	HGNC:4556	gpx-1	Alliance+Orth	Hieranoid | Or	No	Yes	5	1.82	Metabolism > Deto
GPX4	HGNC:4556	gpx-2	Alliance+Orth	Hieranoid | InP	No	Yes	8	0.29	Metabolism > Deto
GPX4	HGNC:4556	gpx-7	Alliance+Orth	Ensembl Com	Yes	Yes	10	#N/A	Metabolism > Deto
GPX4	HGNC:4556	gpx-6	Alliance+Orth	Ensembl Com	No	Yes	9	#N/A	Metabolism > Deto
GRPEL1	HGNC:19696	C34C12.8	Alliance+Orth	Ensembl Com	Yes	Yes	10	0.32	Protein import, sor
GRPEL2	HGNC:21060	C34C12.8	Alliance+Orth	Ensembl Com	Yes	Yes	8	0.32	Protein import, sor
GRSF1	NA	hrpf-1	OrthoList	Ensembl Com	NA	NA	1	2.34	Mitochondrial cen
GRSF1	HGNC:4610	hrpf-2	Alliance+Orth	Ensembl Com	Yes	No	6	1.29	Mitochondrial cen
GSR	HGNC:4623	gsr-1	Alliance+Orth	Ensembl Com	Yes	Yes	11	-0.46	Metabolism > Deto

GSR	NA	trxr-2	OrthoList	OrthoMCL	NA	NA	1	0.5	Metabolism > Deto
GSR	NA	trxr-1	OrthoList	OrthoMCL	NA	NA	1	0.37	Metabolism > Deto
GSTK1	HGNC:16906	gstk-1	Alliance+Orth	Ensembl Com	Yes	Yes	10	-1.97	Metabolism > Deto
GSTK1	HGNC:16906	gstk-2	Alliance+Orth	Ensembl Com	No	Yes	6	-1.81	Metabolism > Deto
GSTZ1	HGNC:4643	gst-42	Alliance+Orth	Ensembl Com	Yes	Yes	11	1.95	Metabolism > Deto
GSTZ1	HGNC:4643	gst-43	Alliance+Orth	Ensembl Com	No	Yes	11	0.88	Metabolism > Deto
GSTZ1	HGNC:4643	Y53G8B.1	Alliance+Orth	Ensembl Com	No	Yes	10	3.22	Metabolism > Deto
GTPBP10	HGNC:25106	C26E6.12	Alliance+Orth	Ensembl Com	Yes	Yes	10	0.11	Mitochondrial cen
GTPBP3	HGNC:14880	mtcu-1	Alliance+Orth	Ensembl Com	Yes	Yes	11	-0.55	Mitochondrial cen
GTPBP6	HGNC:30189	F46B6.4	Alliance+Orth	Ensembl Com	Yes	Yes	10	-0.74	Unknown
GUF1	HGNC:25799	ZK1236.1	Alliance+Orth	Ensembl Com	Yes	Yes	11	-1.7	Mitochondrial cen
GUK1	HGNC:4693	guk-1	Alliance+Orth	Ensembl Com	Yes	Yes	10	1.94	Metabolism > Nuc
HADH	NA	ech-8	OrthoList	Ensembl Com	NA	NA	1	0.56	Metabolism > Lipic
HADH	NA	ech-9	OrthoList	Ensembl Com	NA	NA	1	-1.5	Metabolism > Lipic
HADH	HGNC:4799	B0272.3	Alliance+Orth	Ensembl Com	Yes	Yes	11	1.69	Metabolism > Lipic
HADH	HGNC:4799	F54C8.1	Alliance+Orth	Ensembl Com	No	Yes	9	-2.11	Metabolism > Lipic
HADH	NA	hacd-1	OrthoList	Ensembl Com	NA	NA	1	0.84	Metabolism > Lipic
HADHA	HGNC:4801	ech-1.1	Alliance+Orth	Ensembl Com	Yes	Yes	11	-5	Metabolism > Lipic
HADHA	HGNC:4801	ech-1.2	Alliance+Orth	Ensembl Com	Yes	Yes	11	-0.88	Metabolism > Lipic
HADHB	HGNC:4803	hadb-1	Alliance+Orth	Ensembl Com	Yes	Yes	11	0.07	Metabolism > Carb
HAGH	HGNC:4805	Y17G7B.3	Alliance+Orth	Ensembl Com	Yes	Yes	11	0.12	Metabolism > Deto
HAO2	HGNC:4810	F41E6.5	Alliance+Orth	Ensembl Com	Yes	No	7	-0.63	Metabolism > Lipic
HARS2	HGNC:4817	hars-1	Alliance+Orth	Ensembl Com	Yes	Yes	10	0.28	Mitochondrial cen
HCCS	HGNC:4837	cchl-1	Alliance+Orth	Ensembl Com	Yes	Yes	10	-1.07	Metabolism > Meta
HDHD3	HGNC:28171	K01G5.10	Alliance+Orth	Ensembl Com	Yes	Yes	11	-0.32	Unknown
HDHD5	HGNC:1843	H32C10.1	Alliance+Orth	Ensembl Com	Yes	Yes	11	-0.69	Unknown
HIBADH	HGNC:4907	B0250.5	Alliance+Orth	Ensembl Com	Yes	Yes	11	1.05	Metabolism > Amir
HIBCH	HGNC:4908	hach-1	Alliance+Orth	Ensembl Com	Yes	Yes	11	-1.89	Metabolism > Amir
HIGD1A	HGNC:29527	T20D3.6	Alliance	Ensembl Com	Yes	No	3	-0.41	OXPHOS > Compl
HIGD2A	HGNC:28311	T20D3.6	Alliance+Orth	Ensembl Com	Yes	Yes	7	-0.41	OXPHOS > OXPHO

HINT1	HGNC:4912	hint-1	Alliance+Orth	Ensembl Com	Yes	Yes	11	2.42	Metabolism > Nuc
HINT2	NA	hint-1	OrthoList	Ensembl Com	NA	NA	2	2.42	Metabolism > Lipic
HINT3	HGNC:18468	hint-3	Alliance+Orth	Ensembl Com	Yes	Yes	10	0.93	Unknown
HMGCL	HGNC:5005	Y71G12B.10	Alliance+Orth	Ensembl Com	Yes	Yes	11	-3.54	Metabolism > Carb
HMGCS2	HGNC:5008	hmgs-1	Alliance+Orth	Ensembl Com	Yes	Yes	10	-0.14	Metabolism > Carb
HPDL	NA	C31H2.4	OrthoList	Ensembl Com	NA	NA	1	-3.27	Unknown
HSCB	HGNC:28913	dnj-15	Alliance+Orth	Ensembl Com	Yes	Yes	11	-3.28	Metabolism > Meta
HSD17B10	HGNC:4800	ard-1	Alliance+Orth	Ensembl Com	Yes	Yes	11	0.21	Mitochondrial cen
HSD17B4	HGNC:5213	dhs-28	Alliance+Orth	Ensembl Com	Yes	Yes	8	-0.36	Metabolism > Lipic
HSD17B4	NA	nlt-1	OrthoList	Ensembl Com	NA	NA	1	1.91	Metabolism > Lipic
HSD17B4	HGNC:5213	maoc-1	Alliance+Orth	Ensembl Com	No	Yes	5	-0.4	Metabolism > Lipic
HSD17B8	HGNC:3554	dhs-11	Alliance+Orth	Ensembl Com	No	Yes	10	-4.9	Metabolism > Lipic
HSD17B8	HGNC:3554	dhs-25	Alliance+Orth	Ensembl Com	Yes	Yes	11	0.54	Metabolism > Lipic
HSD17B8	NA	Y47G6A.22	OrthoList	OrthoMCL	NA	NA	1	-0.22	Metabolism > Lipic
HSDL1	NA	dhs-5	OrthoList	Ensembl Com	NA	NA	1	-0.16	Unknown
HSDL1	NA	dhs-27	OrthoList	Ensembl Com	NA	NA	2	2.84	Unknown
HSDL1	HGNC:16475	let-767	Alliance+Orth	Ensembl Com	Yes	No	6	-0.22	Unknown
HSDL1	HGNC:16475	stdh-4	Alliance+Orth	Ensembl Com	Yes	No	6	#N/A	Unknown
HSDL1	HGNC:16475	stdh-1	Alliance+Orth	Ensembl Com	Yes	No	5	-2.28	Unknown
HSDL1	HGNC:16475	stdh-3	Alliance+Orth	Ensembl Com	Yes	No	5	-3.98	Unknown
HSDL1	HGNC:16475	stdh-2	Alliance+Orth	Ensembl Com	Yes	No	5	-5.49	Unknown
HSDL2	HGNC:18572	dhs-6	Alliance+Orth	Ensembl Com	Yes	Yes	11	0.15	Unknown
HSDL2	HGNC:18572	dhs-18	Alliance+Orth	Ensembl Com	No	Yes	10	-1.21	Unknown
HSDL2	NA	maoc-1	OrthoList	Ensembl Com	NA	NA	1	-0.4	Unknown
HSPA9	HGNC:5244	hsp-6	Alliance+Orth	Ensembl Com	Yes	Yes	11	-1.02	Metabolism > Meta
HSPD1	HGNC:5261	hsp-60	Alliance+Orth	Ensembl Com	Yes	Yes	11	-2.05	Protein import, sor
HSPE1	HGNC:5269	Y22D7AL.10	Alliance+Orth	Ensembl Com	Yes	Yes	11	0.56	Protein import, sor
HTATIP2	HGNC:16637	C33F10.14	Alliance+Orth	Ensembl Com	Yes	Yes	11	1.05	Unknown
IARS2	NA	iars-1	OrthoList	OrthoMCL	NA	NA	1	-0.21	Mitochondrial cen
IARS2	HGNC:29685	iars-2	Alliance+Orth	Ensembl Com	Yes	Yes	11	-1	Mitochondrial cen

IBA57	HGNC:27302	F39H2.3	Alliance+Orth	Ensembl Com	Yes	Yes	11	-1.08	Metabolism > Meta
IDE	HGNC:5381	Y70C5C.1	Alliance+Orth	Ensembl Com	Yes	Yes	11	-2.01	Protein import, sor
IDE	NA	C02G6.1	OrthoList	Ensembl Com	NA	NA	5	#N/A	Protein import, sor
IDE	HGNC:5381	C02G6.2	Alliance+Orth	Ensembl Com	Yes	Yes	11	-2.22	Protein import, sor
IDE	HGNC:5381	C28F5.4	Alliance+Orth	Ensembl Com	No	Yes	10	#N/A	Protein import, sor
IDE	HGNC:5381	F44E7.4	Alliance+Orth	Ensembl Com	Yes	Yes	11	-0.72	Protein import, sor
IDH2	HGNC:5383	idh-2	Alliance+Orth	Ensembl Com	Yes	Yes	11	0.71	Metabolism > Carb
IDH2	NA	idh-1	OrthoList	OrthoMCL	NA	NA	1	-0.21	Metabolism > Carb
IDH3A	HGNC:5384	idha-1	Alliance+Orth	Ensembl Com	Yes	Yes	11	-0.22	Metabolism > Carb
IDH3B	HGNC:5385	idhb-1	Alliance+Orth	Ensembl Com	Yes	Yes	11	-1.11	Metabolism > Carb
IDH3B	NA	idhg-1	OrthoList	OrthoMCL	NA	NA	1	0.64	Metabolism > Carb
IDH3B	NA	idhg-2	OrthoList	OrthoMCL	NA	NA	1	-1.74	Metabolism > Carb
IDH3G	NA	idhb-1	OrthoList	OrthoMCL	NA	NA	1	-1.11	Metabolism > Carb
IDH3G	HGNC:5386	idhg-1	Alliance+Orth	Ensembl Com	Yes	Yes	11	0.64	Metabolism > Carb
IDH3G	HGNC:5386	idhg-2	Alliance+Orth	Ensembl Com	Yes	Yes	11	-1.74	Metabolism > Carb
IDI1	HGNC:5387	idi-1	Alliance+Orth	Ensembl Com	Yes	Yes	10	-1.42	Metabolism > Lipic
IMMP1L	HGNC:26317	immp-1	Alliance+Orth	Ensembl Com	Yes	Yes	11	1.81	Protein import, sor
IMMP2L	HGNC:14598	immp-2	Alliance+Orth	Ensembl Com	Yes	Yes	11	#N/A	Protein import, sor
IMMT	HGNC:6047	immt-2	Alliance+Orth	Ensembl Com	No	Yes	9	-4.62	Mitochondrial dyn
IMMT	HGNC:6047	immt-1	Alliance+Orth	Ensembl Com	Yes	Yes	11	-0.28	Mitochondrial dyn
ISCA1	HGNC:28660	Y39B6A.3	Alliance+Orth	Ensembl Com	Yes	Yes	11	2.26	Metabolism > Meta
ISCA2	HGNC:19857	Y54G11A.9	Alliance+Orth	Ensembl Com	Yes	Yes	11	0.34	Metabolism > Meta
ISCU	HGNC:29882	iscu-1	Alliance+Orth	Ensembl Com	Yes	Yes	11	0.33	Metabolism > Meta
ISOC2	HGNC:26278	marb-1	Alliance+Orth	Ensembl Com	Yes	Yes	10	0.57	Unknown
IVD	HGNC:6186	ivd-1	Alliance+Orth	Ensembl Com	Yes	Yes	11	-0.12	Metabolism > Amir
KARS1	HGNC:6215	kars-1	Alliance	Ensembl Com	Yes	Yes	9	-0.95	Mitochondrial cen
KMO	HGNC:6381	kmo-2	Alliance+Orth	Ensembl Com	No	Yes	4	-5.08	Metabolism > Amir
KMO	HGNC:6381	kmo-1	Alliance+Orth	Ensembl Com	Yes	Yes	11	0.23	Metabolism > Amir
KYAT3	HGNC:33238	nkat-1	Alliance+Orth	Ensembl Com	Yes	Yes	11	-1.49	Metabolism > Amir
KYAT3	HGNC:33238	nkat-3	Alliance+Orth	Ensembl Com	Yes	Yes	11	-0.83	Metabolism > Amir

L2HGDH	HGNC:20499	Y45G12B.3	Alliance+Orth	Ensembl Com	Yes	Yes	11	-2.36	Metabolism > Carb
LACTB	HGNC:16468	lact-9	Alliance+Orth	Ensembl Com	Yes	Yes	11	0.56	Protein import, sor
LACTB2	HGNC:18512	Y53F4B.39	Alliance+Orth	Ensembl Com	Yes	Yes	11	-0.71	Mitochondrial cen
LAP3	NA	lap-2	OrthoList	Ensembl Com	NA	NA	1	0.75	Protein import, sor
LARS2	HGNC:17095	lars-2	Alliance+Orth	Ensembl Com	Yes	Yes	11	-1.42	Mitochondrial cen
LDHAL6B	HGNC:21481	ldh-1	Alliance+Orth	Ensembl Com	Yes	No	8	1.09	Metabolism > Carb
LDHB	HGNC:6541	ldh-1	Alliance+Orth	Ensembl Com	Yes	Yes	10	1.09	Metabolism > Ami
LDHD	NA	ego-1	OrthoList	Legacy Ortho	NA	NA	1	-4.77	Metabolism > Carb
LDHD	NA	rrf-1	OrthoList	Legacy Ortho	NA	NA	1	-1.47	Metabolism > Carb
LDHD	NA	rrf-2	OrthoList	Legacy Ortho	NA	NA	1	1.04	Metabolism > Carb
LDHD	NA	rrf-3	OrthoList	Legacy Ortho	NA	NA	1	-1.04	Metabolism > Carb
LDHD	HGNC:19708	F32D8.12	Alliance+Orth	Ensembl Com	Yes	Yes	11	-1.56	Metabolism > Carb
LETM1	HGNC:6556	letm-1	Alliance+Orth	Ensembl Com	Yes	Yes	11	-1.04	Signaling > Calciu
LETM2	HGNC:14648	letm-1	Alliance+Orth	Ensembl Com	Yes	No	4	-1.04	Unknown
LETMD1	HGNC:24241	F30F8.9	Alliance	Ensembl Com	Yes	Yes	6	0.61	Small molecule tra
LIAS	HGNC:16429	lias-1	Alliance+Orth	Ensembl Com	Yes	Yes	11	-0.45	Metabolism > Lipid
LIG3	NA	lig-1	OrthoList	Ensembl Com	NA	NA	1	-1.01	Mitochondrial cen
LIG3	HGNC:6600	K07C5.3	Alliance+Orth	Ensembl Com	Yes	Yes	5	0.66	Mitochondrial cen
LIG3	HGNC:6600	Y73B6BL.14	Alliance	Ensembl Com	No	Yes	3	#N/A	Mitochondrial cen
LIPT1	HGNC:29569	lipt-1	Alliance+Orth	Ensembl Com	Yes	Yes	11	-1.61	Metabolism > Lipid
LIPT2	HGNC:37216	lpl-1	Alliance	Ensembl Com	Yes	Yes	9	-0.09	Metabolism > Lipid
LONP1	NA	Y75B8A.4	OrthoList	OrthoMCL	NA	NA	1	#N/A	Protein import, sor
LONP1	HGNC:9479	lonp-1	Alliance+Orth	Ensembl Com	Yes	Yes	11	-0.74	Protein import, sor
LRPPRC	NA	mma-1	OrthoList	InParanoid	NA	NA	1	-0.52	Mitochondrial cen
LRPPRC	HGNC:15714	lrpr-1	Alliance+Orth	Ensembl Com	Yes	Yes	4	#N/A	Mitochondrial cen
LYPLA1	HGNC:6737	ath-1	Alliance+Orth	Ensembl Com	Yes	Yes	11	0.78	Metabolism > Lipid
LYRM4	HGNC:21365	F53G2.12	Alliance	Hieranoid | InP	Yes	Yes	8	#N/A	Metabolism > Meta
MACROD1	HGNC:29598	B0035.3	Alliance+Orth	Ensembl Com	Yes	Yes	8	0.63	Signaling
MAIP1	HGNC:26198	Y62E10A.20	Alliance	Ensembl Com	Yes	Yes	3	-1.19	Protein import, sor
MALSU1	HGNC:21721	mals-1	Alliance+Orth	OrthoFinder | (	Yes	Yes	3	#N/A	Mitochondrial cen

MAOA	HGNC:6833	amx-2	Alliance+Orth	Ensembl Com	Yes	Yes	5	1.14	Metabolism > Ami
MAOB	HGNC:6834	amx-2	Alliance+Orth	Ensembl Com	Yes	Yes	5	1.14	Metabolism > Ami
MARCHF5	HGNC:26025	M110.3	Alliance	Ensembl Com	Yes	Yes	4	-1.48	Mitochondrial dyn
MARS2	HGNC:25133	Y105E8A.20	Alliance+Orth	Ensembl Com	Yes	Yes	10	-2.64	Mitochondrial cen
MCAT	HGNC:29622	mcat-1	Alliance+Orth	Ensembl Com	Yes	Yes	10	-0.67	Metabolism > Lipi
MCCC1	NA	pyc-1	OrthoList	OrthoMCL	NA	NA	1	-1.05	Metabolism > Ami
MCCC1	HGNC:6936	mccc-1	Alliance+Orth	Ensembl Com	Yes	Yes	11	-2.19	Metabolism > Ami
MCCC1	NA	pcca-1	OrthoList	OrthoMCL	NA	NA	1	-0.72	Metabolism > Ami
MCCC2	NA	F02A9.4	OrthoList	Ensembl Com	NA	NA	6	#N/A	Metabolism > Ami
MCCC2	HGNC:6937	mccc-2	Alliance	Ensembl Com	Yes	Yes	9	#N/A	Metabolism > Ami
MCEE	HGNC:16732	mce-1	Alliance+Orth	Ensembl Com	Yes	Yes	11	-0.39	Metabolism > Carb
MCU	HGNC:23526	mcu-1	Alliance+Orth	Ensembl Com	Yes	Yes	11	0.68	Signaling > Calciu
MCUB	HGNC:26076	mcu-1	Alliance+Orth	Ensembl Com	Yes	No	7	0.68	Signaling > Calciu
MDH2	HGNC:6971	mdh-2	Alliance+Orth	Ensembl Com	Yes	Yes	11	0.31	Metabolism > Carb
ME2	HGNC:6984	men-1	Alliance+Orth	Ensembl Com	Yes	No	8	-0.19	Metabolism > Carb
ME3	HGNC:6985	men-1	Alliance+Orth	Ensembl Com	Yes	Yes	11	-0.19	Metabolism > Carb
MECR	HGNC:19691	mecr-1	Alliance+Orth	Ensembl Com	Yes	Yes	11	0.64	Metabolism > Lipi
MECR	HGNC:19691	Y48A6B.9	Alliance+Orth	Ensembl Com	No	Yes	6	-1.8	Metabolism > Lipi
METAP1D	NA	map-1	OrthoList	OrthoMCL	NA	NA	1	-0.82	Mitochondrial cen
METTL17	NA	F32A7.4	OrthoList	Ensembl Com	NA	NA	6	#N/A	Mitochondrial cen
METTL4	HGNC:24726	damt-1	Alliance+Orth	Ensembl Com	Yes	Yes	8	-1.94	Mitochondrial cen
METTL5	HGNC:25006	metl-5	Alliance+Orth	Ensembl Com	Yes	Yes	11	-2.66	Mitochondrial cen
METTL8	NA	ZK1058.5	OrthoList	OrthoMCL	NA	NA	1	#N/A	Mitochondrial cen
METTL8	HGNC:25856	metl-2	Alliance+Orth	Ensembl Com	Yes	No	7	0.34	Mitochondrial cen
MFF	HGNC:24858	mff-2	Alliance	Ensembl Com	Yes	Yes	2	0.1	Mitochondrial dyn
MFN1	HGNC:18262	fzo-1	Alliance+Orth	Ensembl Com	Yes	Yes	10	-0.17	Mitochondrial dyn
MFN2	HGNC:16877	fzo-1	Alliance+Orth	Ensembl Com	Yes	No	11	-0.17	Mitochondrial dyn
MGME1	HGNC:16205	C27H6.9	Alliance+Orth	Ensembl Com	Yes	Yes	8	-1.12	Mitochondrial cen
MICOS10	HGNC:32068	F54A3.5	Alliance	Hieranoid | InP	Yes	Yes	8	1.92	Mitochondrial dyn
MICOS13	HGNC:33702	W04C9.2	Alliance	OrthoFinder | I	Yes	Yes	2	2.03	Mitochondrial dyn

MICU1	HGNC:1530	micu-1	Alliance+Orth	Ensembl Com	Yes	Yes	11	-0.93	Signaling > Calciu
MICU2	HGNC:31830	micu-3	Alliance+Orth	Ensembl Com	Yes	No	5	#N/A	Signaling > Calciu
MICU3	HGNC:27820	micu-3	Alliance+Orth	Ensembl Com	Yes	Yes	11	#N/A	Signaling > Calciu
MIGA1	HGNC:24741	miga-1	Alliance+Orth	Ensembl Com	Yes	No	8	0.59	Mitochondrial dyn
MIGA2	HGNC:23621	miga-1	Alliance+Orth	Ensembl Com	Yes	Yes	8	0.59	Mitochondrial dyn
MIPEP	HGNC:7104	Y67H2A.7	Alliance+Orth	Ensembl Com	Yes	Yes	11	-0.63	Protein import, so
MLYCD	HGNC:7150	mlcd-1	Alliance+Orth	Ensembl Com	Yes	Yes	11	-1.87	Metabolism > Lipi
MMAA	HGNC:18871	mmaa-1	Alliance+Orth	Ensembl Com	Yes	Yes	11	-0.35	Metabolism > Vita
MMAB	HGNC:19331	mmab-1	Alliance+Orth	Ensembl Com	Yes	Yes	10	1.55	Metabolism > Vita
MMADHC	HGNC:25221	mmad-1	Alliance+Orth	Ensembl Com	Yes	Yes	10	#N/A	Metabolism > Vita
MMUT	HGNC:7526	mmcm-1	Alliance	Ensembl Com	Yes	Yes	9	-1.35	Metabolism > Carb
MOCS1	HGNC:7190	moc-5	Alliance+Orth	Ensembl Com	Yes	Yes	10	2.65	Metabolism > Met
MOCS1	HGNC:7190	F49H6.5	Alliance+Orth	Ensembl Com	No	Yes	10	#N/A	Metabolism > Met
MPC1	HGNC:21606	mpc-1	Alliance+Orth	Ensembl Com	Yes	Yes	11	1.93	Metabolism > Carb
MPC1L	HGNC:44205	mpc-1	Alliance+Orth	Ensembl Com	Yes	No	7	1.93	Metabolism > Carb
MPC2	HGNC:24515	mpc-2	Alliance+Orth	Ensembl Com	Yes	Yes	10	0.05	Metabolism > Carb
MPST	HGNC:7223	mpst-1	Alliance+Orth	Ensembl Com	Yes	No	7	-2.31	Metabolism > Det
MPST	HGNC:7223	mpst-2	Alliance+Orth	Ensembl Com	Yes	No	8	#N/A	Metabolism > Det
MPST	HGNC:7223	mpst-3	Alliance+Orth	Ensembl Com	Yes	No	8	-3.02	Metabolism > Det
MPST	HGNC:7223	mpst-7	Alliance+Orth	Ensembl Com	Yes	Yes	8	1.02	Metabolism > Det
MPST	NA	mpst-4	OrthoList	Ensembl Com	NA	NA	1	-4.23	Metabolism > Det
MPST	NA	mpst-5	OrthoList	Ensembl Com	NA	NA	2	#N/A	Metabolism > Det
MPST	NA	mpst-6	OrthoList	Ensembl Com	NA	NA	3	#N/A	Metabolism > Det
MPV17	HGNC:7224	T18D3.9	Alliance+Orth	Ensembl Com	Yes	Yes	11	2.73	Small molecule tra
MPV17L2	HGNC:28177	ZK470.1	Alliance+Orth	Ensembl Com	Yes	Yes	10	-0.23	Mitochondrial cen
MRM1	HGNC:26202	Y45F3A.9	Alliance+Orth	Ensembl Com	Yes	Yes	10	0.85	Mitochondrial cen
MRM2	HGNC:16352	F45G2.9	Alliance+Orth	Ensembl Com	Yes	Yes	10	-0.71	Mitochondrial cen
MRM2	NA	R74.7	OrthoList	InParanoid	NA	NA	1	-0.17	Mitochondrial cen
MRM2	NA	H06I04.3	OrthoList	OrthoMCL	NA	NA	1	-1.27	Mitochondrial cen
MRPL1	HGNC:14275	mrpl-1	Alliance+Orth	Ensembl Com	Yes	Yes	10	-0.2	Mitochondrial cen

MRPL10	HGNC:14055	mrpl-10	Alliance+Orth	InParanoid|O	Yes	Yes	6	0.72	Mitochondrial cen
MRPL11	HGNC:14042	mrpl-11	Alliance+Orth	Ensembl Com	Yes	Yes	11	1.37	Mitochondrial cen
MRPL12	HGNC:10378	mrpl-12	Alliance+Orth	Ensembl Com	Yes	Yes	10	1.29	Mitochondrial cen
MRPL13	HGNC:14278	mrpl-13	Alliance+Orth	Ensembl Com	Yes	Yes	11	-1.47	Mitochondrial cen
MRPL14	NA	mrpl-14	OrthoList	OMA|OrthoIn	NA	NA	2	#N/A	Mitochondrial cen
MRPL15	HGNC:14054	mrpl-15	Alliance+Orth	Ensembl Com	Yes	Yes	11	-2.73	Mitochondrial cen
MRPL16	HGNC:14476	mrpl-16	Alliance+Orth	Ensembl Com	Yes	Yes	11	-0.56	Mitochondrial cen
MRPL17	HGNC:14053	mrpl-17	Alliance+Orth	Ensembl Com	Yes	Yes	10	1.84	Mitochondrial cen
MRPL18	HGNC:14477	mrpl-18	Alliance+Orth	Ensembl Com	Yes	Yes	10	0.01	Mitochondrial cen
MRPL19	HGNC:14052	mrpl-19	Alliance+Orth	Ensembl Com	Yes	Yes	10	0.48	Mitochondrial cen
MRPL2	NA	rpl-2	OrthoList	OrthoMCL	NA	NA	1	0.63	Mitochondrial cen
MRPL2	HGNC:14056	mrpl-2	Alliance+Orth	Ensembl Com	Yes	Yes	11	0.61	Mitochondrial cen
MRPL20	HGNC:14478	mrpl-20	Alliance	Ensembl Com	Yes	Yes	6	2.2	Mitochondrial cen
MRPL21	HGNC:14479	mrpl-21	Alliance+Orth	Ensembl Com	Yes	Yes	10	1.63	Mitochondrial cen
MRPL22	HGNC:14480	mrpl-22	Alliance+Orth	Ensembl Com	Yes	Yes	11	-1.12	Mitochondrial cen
MRPL23	HGNC:10322	mrpl-23	Alliance+Orth	Ensembl Com	Yes	Yes	10	0.52	Mitochondrial cen
MRPL24	HGNC:14037	mrpl-24	Alliance+Orth	Ensembl Com	Yes	Yes	11	-0.36	Mitochondrial cen
MRPL27	HGNC:14483	Y54G11A.17	Alliance	Hieranoid|Or	Yes	Yes	2	0.51	Mitochondrial cen
MRPL28	HGNC:14484	mrpl-28	Alliance+Orth	Ensembl Com	Yes	Yes	11	-0.57	Mitochondrial cen
MRPL3	HGNC:10379	mrps-18C	Alliance+Orth	Ensembl Com	Yes	Yes	10	-1.86	Mitochondrial cen
MRPL30	HGNC:14036	mrpl-30	Alliance+Orth	Hieranoid|Or	Yes	Yes	5	0.31	Mitochondrial cen
MRPL32	HGNC:14035	mrpl-32	Alliance+Orth	Ensembl Com	Yes	Yes	9	0.16	Mitochondrial cen
MRPL35	HGNC:14489	mrpl-35	Alliance+Orth	Ensembl Com	Yes	Yes	7	-5.51	Mitochondrial cen
MRPL36	HGNC:14490	mrpl-36	Alliance+Orth	Ensembl Com	Yes	Yes	7	1.06	Mitochondrial cen
MRPL37	HGNC:14034	mrpl-37	Alliance+Orth	Ensembl Com	Yes	Yes	9	-1.6	Mitochondrial cen
MRPL38	HGNC:14033	mrpl-38	Alliance+Orth	Ensembl Com	Yes	Yes	9	-0.91	Mitochondrial cen
MRPL39	NA	tars-1	OrthoList	Ensembl Com	NA	NA	1	-0.31	Mitochondrial cen
MRPL39	HGNC:14027	mrpl-39	Alliance+Orth	Ensembl Com	Yes	Yes	6	-1.59	Mitochondrial cen
MRPL4	HGNC:14276	mrpl-4	Alliance+Orth	Ensembl Com	Yes	Yes	11	0.09	Mitochondrial cen
MRPL40	HGNC:14491	mrpl-40	Alliance+Orth	Ensembl Com	Yes	Yes	11	0.58	Mitochondrial cen

MRPL41	HGNC:14492	mrpl-41	Alliance	Ensembl Com	Yes	Yes	6	0.15	Mitochondrial cen
MRPL42	NA	lpl-1	OrthoList	InParanoid|O	NA	NA	2	-0.09	Mitochondrial cen
MRPL42	HGNC:14493	mrpl-42	Alliance	Hieranoid|InP	Yes	Yes	6	#N/A	Mitochondrial cen
MRPL43	HGNC:14517	mrpl-34	Alliance+Orth	Ensembl Com	Yes	Yes	11	0.57	Mitochondrial cen
MRPL44	HGNC:16650	mrpl-44	Alliance	Ensembl Com	Yes	Yes	9	-1	Mitochondrial cen
MRPL45	HGNC:16651	mrpl-45	Alliance+Orth	Ensembl Com	Yes	Yes	9	-0.36	Mitochondrial cen
MRPL46	HGNC:1192	mrpl-46	Alliance+Orth	Ensembl Com	Yes	Yes	10	-4.06	Mitochondrial cen
MRPL47	HGNC:16652	mrpl-47	Alliance+Orth	Ensembl Com	Yes	Yes	9	0.01	Mitochondrial cen
MRPL48	HGNC:16653	mrpl-48	Alliance+Orth	Ensembl Com	Yes	Yes	9	0.8	Mitochondrial cen
MRPL49	HGNC:1176	mrpl-49	Alliance+Orth	Ensembl Com	Yes	Yes	10	0.44	Mitochondrial cen
MRPL50	HGNC:16654	mrpl-50	Alliance+Orth	Ensembl Com	Yes	Yes	5	0.92	Mitochondrial cen
MRPL51	HGNC:14044	mrpl-51	Alliance+Orth	Ensembl Com	Yes	Yes	9	-0.58	Mitochondrial cen
MRPL53	HGNC:16684	mrpl-53	Alliance+Orth	Hieranoid|InP	Yes	Yes	8	1.25	Mitochondrial cen
MRPL54	HGNC:16685	mrpl-54	Alliance+Orth	Ensembl Com	Yes	Yes	9	-0.2	Mitochondrial cen
MRPL55	HGNC:16686	mrpl-55	Alliance+Orth	Ensembl Com	Yes	Yes	10	0.35	Mitochondrial cen
MRPL58	HGNC:5359	mrpl-58	Alliance+Orth	Ensembl Com	Yes	Yes	11	#N/A	Mitochondrial cen
MRPL9	HGNC:14277	mrpl-9	Alliance+Orth	Ensembl Com	Yes	Yes	9	0.21	Mitochondrial cen
MRPS10	HGNC:14502	mrps-10	Alliance+Orth	Ensembl Com	Yes	Yes	10	0.14	Mitochondrial cen
MRPS11	NA	rps-14	OrthoList	OrthoMCL	NA	NA	1	1.22	Mitochondrial cen
MRPS11	HGNC:14050	mrps-11	Alliance+Orth	Ensembl Com	Yes	Yes	9	1.53	Mitochondrial cen
MRPS12	HGNC:10380	mrps-12	Alliance+Orth	Ensembl Com	Yes	Yes	10	1.83	Mitochondrial cen
MRPS14	HGNC:14049	mrps-14	Alliance+Orth	Ensembl Com	Yes	Yes	9	-2.07	Mitochondrial cen
MRPS15	HGNC:14504	mrps-15	Alliance	Ensembl Com	Yes	Yes	7	1.17	Mitochondrial cen
MRPS16	HGNC:14048	mrps-16	Alliance+Orth	Ensembl Com	Yes	Yes	11	1.46	Mitochondrial cen
MRPS17	HGNC:14047	mrps-17	Alliance+Orth	Ensembl Com	Yes	Yes	9	0.5	Mitochondrial cen
MRPS18A	HGNC:14515	mrps-18A	Alliance+Orth	Ensembl Com	Yes	Yes	8	0.29	Mitochondrial cen
MRPS18B	HGNC:14516	mrps-18B	Alliance+Orth	Ensembl Com	Yes	Yes	8	-0.19	Mitochondrial cen
MRPS18C	HGNC:16633	mrps-18.C	Alliance+Orth	Ensembl Com	Yes	Yes	11	0.65	Mitochondrial cen
MRPS2	HGNC:14495	mrps-2	Alliance+Orth	Ensembl Com	Yes	Yes	11	0.13	Mitochondrial cen
MRPS21	HGNC:14046	mrps-21	Alliance+Orth	Ensembl Com	Yes	Yes	9	-0.11	Mitochondrial cen

MRPS22	HGNC:14508	mrps-22	Alliance+Orth	Ensembl Com	Yes	Yes	11	-0.24	Mitochondrial cen
MRPS23	HGNC:14509	mrps-23	Alliance+Orth	Ensembl Com	Yes	Yes	10	-0.61	Mitochondrial cen
MRPS24	HGNC:14510	mrps-24	Alliance+Orth	Ensembl Com	Yes	Yes	11	-0.08	Mitochondrial cen
MRPS25	HGNC:14511	mrps-25	Alliance+Orth	Ensembl Com	Yes	Yes	11	0.25	Mitochondrial cen
MRPS26	HGNC:14045	mrps-26	Alliance+Orth	Ensembl Com	Yes	Yes	7	-1.22	Mitochondrial cen
MRPS27	HGNC:14512	mrps-27	Alliance+Orth	Ensembl Com	Yes	Yes	8	-0.41	Mitochondrial cen
MRPS28	HGNC:14513	mrps-28	Alliance+Orth	Ensembl Com	Yes	Yes	8	0.17	Mitochondrial cen
MRPS30	HGNC:8769	mrps-30	Alliance	Ensembl Com	Yes	Yes	6	-0.83	Mitochondrial cen
MRPS31	HGNC:16632	mrps-31	Alliance+Orth	Ensembl Com	Yes	Yes	6	0.81	Mitochondrial cen
MRPS33	HGNC:16634	mrps-33	Alliance+Orth	Ensembl Com	Yes	Yes	10	-0.64	Mitochondrial cen
MRPS34	HGNC:16618	mrps-34	Alliance+Orth	Ensembl Com	Yes	Yes	8	-0.38	Mitochondrial cen
MRPS35	HGNC:16635	mrps-35	Alliance+Orth	Ensembl Com	Yes	Yes	11	-0.58	Mitochondrial cen
MRPS5	HGNC:14498	mrps-5	Alliance+Orth	Ensembl Com	Yes	Yes	11	0.9	Mitochondrial cen
MRPS6	HGNC:14051	mrps-6	Alliance+Orth	Hieranoid | InP	Yes	Yes	8	-1.57	Mitochondrial cen
MRPS7	HGNC:14499	mrps-7	Alliance+Orth	Ensembl Com	Yes	Yes	11	0.33	Mitochondrial cen
MRPS9	HGNC:14501	mrps-9	Alliance+Orth	Ensembl Com	Yes	Yes	11	-1.81	Mitochondrial cen
MRRF	HGNC:7234	mrrf-1	Alliance+Orth	Ensembl Com	Yes	Yes	9	1.44	Mitochondrial cen
MSRA	HGNC:7377	msra-1	Alliance+Orth	Ensembl Com	Yes	Yes	7	-2.25	Metabolism > Deto
MSRB2	HGNC:17061	F44E2.6	Alliance+Orth	Ensembl Com	Yes	Yes	10	-1.27	Metabolism > Deto
MSRB3	HGNC:27375	F44E2.6	Alliance+Orth	Ensembl Com	Yes	No	7	-1.27	Metabolism > Deto
MT-ATP6	NA	atp-6	OrthoList	InParanoid	NA	NA	1	4.93	OXPHOS > Compl
MT-CO1	NA	ctc-1	OrthoList	Ensembl Com	NA	NA	5	4.35	OXPHOS > Compl
MT-CO2	NA	ctc-2	OrthoList	Ensembl Com	NA	NA	5	5.57	OXPHOS > Compl
MT-CO3	NA	ctc-3	OrthoList	Ensembl Com	NA	NA	4	4.32	OXPHOS > Compl
MT-CYB	NA	ctb-1	OrthoList	Ensembl Com	NA	NA	4	4.04	OXPHOS > Compl
MT-ND1	NA	nduo-1	OrthoList	Ensembl Com	NA	NA	5	3.6	OXPHOS > Compl
MT-ND4	NA	nduo-4	OrthoList	Ensembl Com	NA	NA	5	4.31	OXPHOS > Compl
MT-ND5	NA	nduo-5	OrthoList	Ensembl Com	NA	NA	3	4	OXPHOS > Compl
MTARC1	HGNC:26189	F22B8.7	Alliance	Ensembl Com	Yes	Yes	9	-0.59	Metabolism > Meta
MTARC1	HGNC:26189	F53E10.1	Alliance	Ensembl Com	Yes	Yes	9	2.92	Metabolism > Meta

MTARC1	HGNC:26189	F56A11.5	Alliance	Ensembl Com	Yes	Yes	9	-1.18	Metabolism > Meta
MTARC2	HGNC:26064	F22B8.7	Alliance	Ensembl Com	Yes	Yes	9	-0.59	Metabolism > Meta
MTARC2	HGNC:26064	F53E10.1	Alliance	Ensembl Com	Yes	Yes	9	2.92	Metabolism > Meta
MTARC2	HGNC:26064	F56A11.5	Alliance	Ensembl Com	Yes	Yes	9	-1.18	Metabolism > Meta
MTCH1	HGNC:17586	mtch-1	Alliance+Orth	Ensembl Com	Yes	Yes	10	0.39	Small molecule tra
MTCH1	HGNC:17586	F43E2.11	Alliance	Ensembl Com	No	Yes	3	#N/A	Small molecule tra
MTCH2	HGNC:17587	mtch-1	Alliance+Orth	Ensembl Com	Yes	Yes	11	0.39	Small molecule tra
MTCH2	HGNC:17587	F43E2.11	Alliance	Ensembl Com	No	Yes	3	#N/A	Small molecule tra
MTERF3	HGNC:24258	C50F4.12	Alliance+Orth	Ensembl Com	Yes	Yes	10	-2.48	Mitochondrial cen
MTERF4	HGNC:28785	mter-4	Alliance+Orth	Ensembl Com	Yes	Yes	7	0.71	Mitochondrial cen
MTFP1	HGNC:26945	mtp-18	Alliance+Orth	Ensembl Com	Yes	Yes	11	-1.17	Mitochondrial dyn
MTG1	HGNC:32159	mtg-1	Alliance+Orth	Ensembl Com	Yes	Yes	11	-1.59	Mitochondrial cen
MTG2	HGNC:16239	M01E5.2	Alliance+Orth	Ensembl Com	Yes	Yes	11	-2.37	Mitochondrial cen
MTHFD1L	NA	dao-3	OrthoList	Ensembl Com	NA	NA	2	1.72	Metabolism > Vita
MTHFD1L	HGNC:21055	K07E3.4	Alliance+Orth	Ensembl Com	Yes	Yes	8	-0.84	Metabolism > Vita
MTHFD2	HGNC:7434	dao-3	Alliance+Orth	Ensembl Com	Yes	Yes	7	1.72	Metabolism > Vita
MTHFD2	NA	K07E3.4	OrthoList	OrthoMCL	NA	NA	1	-0.84	Metabolism > Vita
MTHFD2L	HGNC:31865	dao-3	Alliance+Orth	Ensembl Com	Yes	No	7	1.72	Metabolism > Vita
MTHFD2L	NA	K07E3.4	OrthoList	OrthoMCL	NA	NA	1	-0.84	Metabolism > Vita
MTHFS	HGNC:7437	Y106G6E.4	Alliance+Orth	Ensembl Com	Yes	Yes	11	0.54	Metabolism > Vita
MTIF2	HGNC:7441	F46B6.6	Alliance+Orth	Ensembl Com	Yes	Yes	11	-2.04	Mitochondrial cen
MTO1	HGNC:19261	mtcu-2	Alliance+Orth	Ensembl Com	Yes	Yes	11	-0.84	Mitochondrial cen
MTPAP	NA	mut-2	OrthoList	Legacy Ortho	NA	NA	1	-2.49	Mitochondrial cen
MTPAP	NA	usip-1	OrthoList	InParanoid	NA	NA	1	0.18	Mitochondrial cen
MTPAP	HGNC:25532	C53A5.16	Alliance	Ensembl Com	Yes	Yes	3	#N/A	Mitochondrial cen
MTRES1	HGNC:17971	C47B2.9	Alliance	Ensembl Com	Yes	Yes	3	-0.71	Mitochondrial cen
MTRF1	HGNC:7469	mtrf-1L	Alliance+Orth	Ensembl Com	Yes	No	8	-0.31	Mitochondrial cen
MTRF1L	HGNC:21051	mtrf-1L	Alliance+Orth	Ensembl Com	Yes	Yes	11	-0.31	Mitochondrial cen
MTX1	HGNC:7504	mtx-1	Alliance+Orth	Ensembl Com	Yes	No	10	0.87	Protein import, so
MTX2	HGNC:7506	mtx-2	Alliance+Orth	Ensembl Com	Yes	Yes	11	-0.65	Protein import, so

MTX3	HGNC:24812	mtx-1	Alliance+Orth	Ensembl Com	Yes	Yes	9	0.87	Mitochondrial dyn
MUL1	HGNC:25762	exc-14	Alliance	Ensembl Com	Yes	Yes	2	1.91	Protein import, so
MYG1	HGNC:17590	C27H6.8	Alliance	Ensembl Com	Yes	Yes	9	0.26	Mitochondrial cen
MYO19	NA	hum-2	OrthoList	Ensembl Com	NA	NA	1	0.57	Mitochondrial dyn
NADK2	HGNC:26404	nadk-2	Alliance+Orth	Ensembl Com	Yes	Yes	11	-1.8	Metabolism > Met
NADK2	HGNC:26404	nadk-1	Alliance+Orth	Ensembl Com	No	Yes	4	-0.74	Metabolism > Met
NARS2	NA	nars-1	OrthoList	OrthoMCL	NA	NA	1	0.45	Mitochondrial cen
NARS2	HGNC:26274	nars-2	Alliance+Orth	Ensembl Com	Yes	Yes	10	0.74	Mitochondrial cen
NAXD	HGNC:25576	R107.2	Alliance+Orth	Ensembl Com	Yes	Yes	10	0.23	Metabolism > Met
NAXE	HGNC:18453	Y18D10A.3	Alliance+Orth	Ensembl Com	Yes	Yes	11	2.79	Metabolism > Met
NDUFA1	HGNC:7683	ndua-1	Alliance	OrthoFinder |	Yes	Yes	2	0.73	OXPHOS > Compl
NDUFA10	HGNC:7684	nuo-4	Alliance+Orth	Ensembl Com	Yes	Yes	10	0.78	OXPHOS > Compl
NDUFA12	HGNC:23987	ndua-12	Alliance+Orth	Ensembl Com	Yes	Yes	11	1.7	OXPHOS > Compl
NDUFA13	HGNC:17194	ndua-13	Alliance+Orth	Ensembl Com	Yes	Yes	9	0.42	OXPHOS > Compl
NDUFA2	HGNC:7685	ndua-2	Alliance+Orth	Ensembl Com	Yes	Yes	10	-1.11	OXPHOS > Compl
NDUFA5	HGNC:7688	ndua-5	Alliance+Orth	Ensembl Com	Yes	Yes	10	0.64	OXPHOS > Compl
NDUFA6	HGNC:7690	nuo-3	Alliance+Orth	Ensembl Com	Yes	Yes	8	1.28	OXPHOS > Compl
NDUFA7	HGNC:7691	ndua-7	Alliance	Ensembl Com	Yes	Yes	5	0.21	OXPHOS > Compl
NDUFA8	HGNC:7692	ndua-8	Alliance+Orth	Ensembl Com	Yes	Yes	11	0.72	OXPHOS > Compl
NDUFA9	HGNC:7693	nduf-9	Alliance+Orth	Ensembl Com	Yes	Yes	10	0.58	OXPHOS > Compl
NDUFAB1	HGNC:7694	ndab-1	Alliance+Orth	Ensembl Com	Yes	Yes	10	0.6	OXPHOS > Compl
NDUFAB1	NA	Y79H2A.4	OrthoList	Legacy Ortho	NA	NA	1	-0.96	OXPHOS > Compl
NDUFAB1	NA	F16B4.6	OrthoList	Legacy Ortho	NA	NA	1	-1.54	OXPHOS > Compl
NDUFAB1	HGNC:7694	ndab-2	Alliance+Orth	Ensembl Com	No	Yes	4	0.34	OXPHOS > Compl
NDUFAF1	HGNC:18828	nuaf-1	Alliance+Orth	Ensembl Com	Yes	Yes	10	0.18	OXPHOS > Compl
NDUFAF2	HGNC:28086	Y116A8C.30	Alliance+Orth	Ensembl Com	Yes	Yes	5	2.21	OXPHOS > Compl
NDUFAF3	HGNC:29918	nuaf-3	Alliance+Orth	Ensembl Com	Yes	Yes	9	-0.93	OXPHOS > Compl
NDUFAF4	HGNC:21034	B0035.15	Alliance	Ensembl Com	Yes	Yes	2	-1.34	OXPHOS > Compl
NDUFAF5	HGNC:15899	K09E4.3	Alliance+Orth	Ensembl Com	Yes	Yes	11	1.11	OXPHOS > Compl
NDUFAF6	HGNC:28625	B0334.5	Alliance+Orth	Ensembl Com	Yes	Yes	11	0.68	OXPHOS > Compl

NDUFAF7	HGNC:28816	ZK1128.1	Alliance+Orth	Ensembl Com	Yes	Yes	11	-2.66	OXPHOS > Compl
NDUFB10	HGNC:7696	ndub-10	Alliance+Orth	Ensembl Com	Yes	Yes	10	0.33	OXPHOS > Compl
NDUFB11	HGNC:20372	ndub-11	Alliance+Orth	Ensembl Com	Yes	Yes	5	-0.74	OXPHOS > Compl
NDUFB2	HGNC:7697	ndub-2	Alliance	Ensembl Com	Yes	Yes	6	1.3	OXPHOS > Compl
NDUFB3	HGNC:7698	ndub-3	Alliance+Orth	Ensembl Com	Yes	Yes	5	1.45	OXPHOS > Compl
NDUFB4	HGNC:7699	nuo-6	Alliance+Orth	Ensembl Com	Yes	Yes	8	0.68	OXPHOS > Compl
NDUFB5	HGNC:7700	ndub-5	Alliance+Orth	Ensembl Com	Yes	Yes	9	-0.56	OXPHOS > Compl
NDUFB6	HGNC:7701	ndub-6	Alliance	Hieranoid|So	Yes	Yes	2	#N/A	OXPHOS > Compl
NDUFB7	HGNC:7702	ndub-7	Alliance+Orth	Ensembl Com	Yes	Yes	10	1.47	OXPHOS > Compl
NDUFB8	HGNC:7703	ndub-8	Alliance+Orth	Ensembl Com	Yes	Yes	10	1.76	OXPHOS > Compl
NDUFB9	HGNC:7704	C16A3.5	Alliance+Orth	Ensembl Com	Yes	Yes	11	0.54	OXPHOS > Compl
NDUFC2	HGNC:7706	nduc-2	Alliance	Ensembl Com	Yes	Yes	4	2.74	OXPHOS > Compl
NDUFS1	HGNC:7707	nuo-5	Alliance+Orth	Ensembl Com	Yes	Yes	10	-0.55	OXPHOS > Compl
NDUFS2	HGNC:7708	gas-1	Alliance+Orth	Ensembl Com	Yes	Yes	11	0.44	OXPHOS > Compl
NDUFS2	HGNC:7708	nduf-2.2	Alliance+Orth	Ensembl Com	Yes	Yes	11	-5.42	OXPHOS > Compl
NDUFS3	HGNC:7710	nuo-2	Alliance+Orth	Ensembl Com	Yes	Yes	11	1.14	OXPHOS > Compl
NDUFS4	HGNC:7711	lpd-5	Alliance+Orth	Ensembl Com	Yes	Yes	11	1.46	OXPHOS > Compl
NDUFS5	HGNC:7712	nduf-5	Alliance+Orth	InParanoid|O	Yes	Yes	5	2.15	OXPHOS > Compl
NDUFS6	HGNC:7713	nduf-6	Alliance+Orth	Ensembl Com	Yes	Yes	11	1.84	OXPHOS > Compl
NDUFS7	HGNC:7714	nduf-7	Alliance+Orth	Ensembl Com	Yes	Yes	10	1.01	OXPHOS > Compl
NDUFS8	HGNC:7715	ndus-8	Alliance+Orth	Ensembl Com	Yes	Yes	11	0.39	OXPHOS > Compl
NDUFV1	HGNC:7716	nuo-1	Alliance+Orth	Ensembl Com	Yes	Yes	11	0.5	OXPHOS > Compl
NDUFV2	HGNC:7717	nduv-2	Alliance+Orth	Ensembl Com	Yes	Yes	11	-0.14	OXPHOS > Compl
NFS1	HGNC:15910	nfs-1	Alliance+Orth	Ensembl Com	Yes	Yes	11	-0.73	Metabolism > Meta
NFU1	HGNC:16287	nfu-1	Alliance+Orth	Ensembl Com	Yes	Yes	11	2.96	Metabolism > Meta
NIPSNAP1	HGNC:7827	K02D10.1	Alliance+Orth	Ensembl Com	Yes	Yes	6	0.47	Mitochondrial dyn
NIPSNAP2	HGNC:4179	K02D10.1	Alliance+Orth	Ensembl Com	Yes	Yes	6	0.47	Mitochondrial dyn
NIT1	HGNC:7828	nft-1	Alliance+Orth	Ensembl Com	Yes	Yes	10	0.75	Metabolism > Deto
NIT2	NA	nft-1	OrthoList	OrthoMCL	NA	NA	1	0.75	Metabolism > Deto
NLN	NA	ZK550.3	OrthoList	Ensembl Com	NA	NA	3	#N/A	Protein import, so

NME3	HGNC:7851	ndk-1	Alliance+Orth	Ensembl Com	Yes	No	6	2.12	Metabolism > Nuc
NME4	HGNC:7852	ndk-1	Alliance+Orth	Ensembl Com	Yes	No	5	2.12	Metabolism > Nuc
NME6	NA	ndk-1	OrthoList	Ensembl Com	NA	NA	1	2.12	Metabolism > Nuc
NME6	NA	R05G6.5	OrthoList	InParanoid	NA	NA	1	-0.52	Metabolism > Nuc
NME6	HGNC:20567	Y48G8AL.15	Alliance+Orth	OrthoFinder |	Yes	Yes	3	0.87	Metabolism > Nuc
NMNAT3	HGNC:20989	nmat-2	Alliance+Orth	Ensembl Com	Yes	Yes	10	-0.4	Metabolism > Meta
NMNAT3	HGNC:20989	nmat-1	Alliance+Orth	Ensembl Com	Yes	Yes	10	-2.42	Metabolism > Meta
NNT	HGNC:7863	nnt-1	Alliance+Orth	Ensembl Com	Yes	Yes	11	-1.83	Metabolism > Meta
NOA1	HGNC:28473	noa-1	Alliance+Orth	Ensembl Com	Yes	Yes	11	-1.42	Mitochondrial cen
NRDC	NA	Y70C5C.1	OrthoList	OrthoMCL	NA	NA	1	-2.01	Protein import, sor
NRDC	NA	C02G6.1	OrthoList	OrthoMCL	NA	NA	1	#N/A	Protein import, sor
NRDC	NA	C02G6.2	OrthoList	OrthoMCL	NA	NA	1	-2.22	Protein import, sor
NRDC	NA	C28F5.4	OrthoList	OrthoMCL	NA	NA	1	#N/A	Protein import, sor
NRDC	NA	F44E7.4	OrthoList	OrthoMCL	NA	NA	1	-0.72	Protein import, sor
NSUN2	HGNC:25994	nsun-2	Alliance+Orth	Ensembl Com	Yes	Yes	11	-1.04	Mitochondrial cen
NSUN4	HGNC:31802	nsun-4	Alliance+Orth	Ensembl Com	Yes	Yes	10	-1.17	Mitochondrial cen
NTHL1	HGNC:8028	nth-1	Alliance+Orth	Ensembl Com	Yes	Yes	11	1.05	Metabolism > Meta
NUBPL	NA	nubp-1	OrthoList	Ensembl Com	NA	NA	2	-0.04	OXPHOS > Compl
NUDT13	HGNC:18827	ndx-9	Alliance+Orth	Ensembl Com	Yes	Yes	9	-0.54	Metabolism > Meta
NUDT19	HGNC:32036	ndx-7	Alliance+Orth	Ensembl Com	Yes	Yes	11	-0.83	Metabolism > Meta
NUDT2	HGNC:8049	ndx-4	Alliance+Orth	Ensembl Com	Yes	Yes	11	3.01	Metabolism > Nuc
NUDT5	HGNC:8052	ndx-2	Alliance+Orth	Ensembl Com	Yes	Yes	11	2.99	Metabolism > Nuc
NUDT8	HGNC:8055	ndx-3	Alliance+Orth	Ensembl Com	Yes	Yes	11	0.7	Metabolism > Meta
NUDT8	NA	ndx-8	OrthoList	OrthoMCL	NA	NA	1	0.91	Metabolism > Meta
NUDT9	HGNC:8056	ndx-6	Alliance+Orth	Ensembl Com	Yes	Yes	11	1.37	Metabolism > Nuc
OAT	HGNC:8091	oatr-1	Alliance+Orth	Ensembl Com	Yes	Yes	11	-0.6	Metabolism > Ami
OGDH	NA	ZK836.2	OrthoList	OrthoMCL	NA	NA	1	#N/A	Metabolism > Carb
OGDH	HGNC:8124	ogdh-1	Alliance+Orth	Ensembl Com	Yes	Yes	11	-0.71	Metabolism > Carb
OGDHL	NA	ZK836.2	OrthoList	OrthoMCL	NA	NA	1	#N/A	Metabolism > Carb
OGDHL	HGNC:25590	ogdh-1	Alliance+Orth	Ensembl Com	Yes	Yes	10	-0.71	Metabolism > Carb

OPA1	HGNC:8140	eat-3	Alliance+Orth	Ensembl Com	Yes	Yes	11	-1.07	Mitochondrial dyn
OPA3	HGNC:8142	H43I07.1	Alliance+Orth	Ensembl Com	Yes	Yes	7	-1.2	Unknown
OSBPL1A	HGNC:16398	obr-2	Alliance+Orth	Ensembl Com	Yes	No	8	2.77	Metabolism > Lipid
OSBPL1A	NA	obr-1	OrthoList	OrthoMCL	NA	NA	1	-0.61	Metabolism > Lipid
OSGEPL1	HGNC:23075	C01G10.10	Alliance+Orth	Ensembl Com	Yes	Yes	10	0.64	Mitochondrial cen
OSGEPL1	NA	Y71H2AM.1	OrthoList	OrthoMCL	NA	NA	1	-0.72	Mitochondrial cen
OXA1L	HGNC:8526	oxa-1	Alliance+Orth	Hieranoid | Ho	Yes	Yes	10	0.65	Protein import, sor
OXCT1	HGNC:8527	C05C10.3	Alliance+Orth	Ensembl Com	Yes	Yes	11	-1.2	Metabolism > Carb
OXCT2	HGNC:18606	C05C10.3	Alliance+Orth	Ensembl Com	Yes	No	8	-1.2	Metabolism > Carb
OXLD1	HGNC:27901	C49A9.10	Alliance+Orth	Ensembl Com	Yes	Yes	5	-1.82	Unknown
OXR1	HGNC:15822	lmd-3	Alliance+Orth	Ensembl Com	Yes	Yes	10	0.58	Metabolism > Deto
OXSM	HGNC:26063	F10G8.9	Alliance+Orth	Ensembl Com	Yes	Yes	10	-0.21	Metabolism > Lipid
PABPC5	NA	pab-1	OrthoList	Ensembl Com	NA	NA	1	0.27	Unknown
PABPC5	HGNC:13629	pab-2	Alliance+Orth	Ensembl Com	Yes	No	3	0.93	Unknown
PAICS	HGNC:8587	paic-1	Alliance+Orth	Ensembl Com	Yes	Yes	10	#N/A	Metabolism > Nuc
PAM16	HGNC:29679	F45G2.8	Alliance+Orth	Ensembl Com	Yes	Yes	11	1.63	Protein import, sor
PANK2	HGNC:15894	pnk-1	Alliance+Orth	Ensembl Com	Yes	Yes	5	0.5	Metabolism > Meta
PANK2	NA	pnk-4	OrthoList	OrthoMCL	NA	NA	1	-1.23	Metabolism > Meta
PARK7	HGNC:16369	djr-1.1	Alliance+Orth	Ensembl Com	Yes	Yes	11	2.65	Protein import, sor
PARK7	HGNC:16369	djr-1.2	Alliance+Orth	Ensembl Com	No	Yes	10	-2.9	Protein import, sor
PARL	HGNC:18253	rom-5	Alliance+Orth	Ensembl Com	Yes	Yes	8	-0.62	Protein import, sor
PARS2	HGNC:30563	pars-2	Alliance+Orth	Ensembl Com	Yes	Yes	11	1.15	Mitochondrial cen
PC	HGNC:8636	pyc-1	Alliance+Orth	Ensembl Com	Yes	Yes	11	-1.05	Metabolism > Carb
PC	NA	mccc-1	OrthoList	OrthoMCL	NA	NA	1	-2.19	Metabolism > Carb
PC	NA	pcca-1	OrthoList	OrthoMCL	NA	NA	1	-0.72	Metabolism > Carb
PCBD2	HGNC:24474	pcbd-1	Alliance+Orth	Ensembl Com	Yes	No	10	2.05	Metabolism > Meta
PCCA	NA	pyc-1	OrthoList	OrthoMCL	NA	NA	1	-1.05	Metabolism > Carb
PCCA	NA	mccc-1	OrthoList	OrthoMCL	NA	NA	1	-2.19	Metabolism > Carb
PCCA	HGNC:8653	pcca-1	Alliance+Orth	Ensembl Com	Yes	Yes	11	-0.72	Metabolism > Carb
PCCB	HGNC:8654	pccb-1	Alliance+Orth	Ensembl Com	Yes	Yes	11	-0.14	Metabolism > Carb

PCK2	HGNC:8725	pck-2	Alliance+Orth	Ensembl Com	Yes	No	10	-0.51	Metabolism > Carb
PCK2	NA	pck-3	OrthoList	Ensembl Com	NA	NA	1	-2.46	Metabolism > Carb
PCK2	HGNC:8725	pck-1	Alliance+Orth	Ensembl Com	Yes	No	10	-0.44	Metabolism > Carb
PDE12	HGNC:25386	pde-12	Alliance+Orth	Ensembl Com	Yes	Yes	9	-3.06	Mitochondrial cen
PDE2A	HGNC:8777	pde-2	Alliance+Orth	Ensembl Com	Yes	Yes	9	0.93	Signaling > cAMP-I
PDHA1	HGNC:8806	pdha-1	Alliance+Orth	Ensembl Com	Yes	Yes	11	-0.04	Metabolism > Carb
PDHA2	HGNC:8807	pdha-1	Alliance+Orth	Ensembl Com	Yes	Yes	10	-0.04	Metabolism > Carb
PDHB	HGNC:8808	pdhb-1	Alliance+Orth	Ensembl Com	Yes	Yes	11	-0.67	Metabolism > Carb
PDHX	HGNC:21350	dlat-2	Alliance+Orth	Ensembl Com	Yes	Yes	3	0.21	Metabolism > Carb
PDK1	HGNC:8809	pdhk-2	Alliance+Orth	Ensembl Com	Yes	Yes	10	-0.08	Metabolism > Carb
PDK2	HGNC:8810	pdhk-2	Alliance+Orth	Ensembl Com	Yes	No	10	-0.08	Metabolism > Carb
PDK3	HGNC:8811	pdhk-2	Alliance+Orth	Ensembl Com	Yes	No	11	-0.08	Metabolism > Carb
PDK4	HGNC:8812	pdhk-2	Alliance+Orth	Ensembl Com	Yes	Yes	10	-0.08	Metabolism > Carb
PDP1	HGNC:9279	pdp-1	Alliance+Orth	Ensembl Com	Yes	Yes	11	-0.62	Metabolism > Carb
PDP2	HGNC:30263	pdp-1	Alliance+Orth	Ensembl Com	Yes	Yes	10	-0.62	Metabolism > Carb
PDPR	HGNC:30264	pdpr-1	Alliance+Orth	Ensembl Com	Yes	Yes	11	-0.36	Metabolism > Carb
PDSS1	HGNC:17759	coq-1	Alliance+Orth	Ensembl Com	Yes	Yes	11	-0.72	Metabolism > Meta
PET100	HGNC:40038	Y53F4B.14	Alliance+Orth	Ensembl Com	Yes	Yes	6	1.05	OXPHOS > Compl
PGAM5	HGNC:28763	pgam-5	Alliance+Orth	Ensembl Com	Yes	Yes	10	0.11	Mitochondrial dyn
PGS1	HGNC:30029	pgs-1	Alliance+Orth	Ensembl Com	Yes	Yes	11	-2.28	Metabolism > Lipid
PHB	NA	phb-1	OrthoList	Ensembl Com	NA	NA	6	-0.7	Protein import, sor
PHB2	HGNC:30306	phb-2	Alliance+Orth	Ensembl Com	Yes	Yes	11	-0.63	Protein import, sor
PHYH	HGNC:8940	phyh-1	Alliance+Orth	Ensembl Com	No	Yes	6	-1.65	Metabolism > Lipid
PHYH	HGNC:8940	ZK550.6	Alliance+Orth	Ensembl Com	Yes	Yes	11	-0.29	Metabolism > Lipid
PICK1	HGNC:9394	Y57G11C.22	Alliance+Orth	Ensembl Com	Yes	Yes	11	0.05	Unknown
PIF1	HGNC:26220	pif-1	Alliance+Orth	Ensembl Com	Yes	Yes	10	-2.18	Mitochondrial cen
PINK1	HGNC:14581	pink-1	Alliance+Orth	Ensembl Com	Yes	Yes	9	0.16	Mitochondrial dyn
PISD	HGNC:8999	psd-1	Alliance+Orth	Ensembl Com	Yes	Yes	11	0.59	Metabolism > Lipid
PITRM1	HGNC:17663	C05D11.1	Alliance+Orth	OrthoInspect	Yes	Yes	2	-0.2	Protein import, sor
PLGRKT	HGNC:23633	tag-280	Alliance+Orth	Ensembl Com	Yes	Yes	7	#N/A	Unknown

PLGRKT	HGNC:23633	tag-281	Alliance	Ensembl Com	No	Yes	5	#N/A	Unknown
PLPBP	NA	F09E5.7	OrthoList	OrthoMCL	NA	NA	1	0.55	Metabolism > Vita
PLPBP	HGNC:9457	F09E5.8	Alliance+Orth	Ensembl Com	Yes	Yes	11	0.54	Metabolism > Vita
PLSCR3	HGNC:16495	scrm-4	Alliance+Orth	Ensembl Com	No	Yes	4	-1.22	Metabolism > Lipic
PLSCR3	NA	scrm-6	OrthoList	Ensembl Com	NA	NA	1	-2.61	Metabolism > Lipic
PLSCR3	HGNC:16495	scrm-1	Alliance+Orth	Ensembl Com	Yes	Yes	6	3.91	Metabolism > Lipic
PLSCR3	NA	scrm-7	OrthoList	Ensembl Com	NA	NA	1	-5	Metabolism > Lipic
PLSCR3	HGNC:16495	scrm-2	Alliance+Orth	Ensembl Com	Yes	Yes	6	-2.36	Metabolism > Lipic
PLSCR3	HGNC:16495	scrm-3	Alliance+Orth	Ensembl Com	Yes	Yes	6	1.46	Metabolism > Lipic
PLSCR3	NA	scrm-8	OrthoList	Ensembl Com	NA	NA	1	-7.64	Metabolism > Lipic
PLSCR3	NA	scrm-5	OrthoList	Ensembl Com	NA	NA	1	#N/A	Metabolism > Lipic
PLSCR3	NA	K08D10.18	OrthoList	Ensembl Com	NA	NA	1	#N/A	Metabolism > Lipic
PMPCA	HGNC:18667	mppa-1	Alliance+Orth	Ensembl Com	Yes	Yes	11	-1.51	Protein import, sor
PMPCB	HGNC:9119	mppb-1	Alliance+Orth	Ensembl Com	Yes	Yes	10	-0.59	Protein import, sor
PMPCB	NA	ucr-1	OrthoList	Ensembl Com	NA	NA	1	0.79	Protein import, sor
PNPLA8	HGNC:28900	ipla-6	Alliance+Orth	Ensembl Com	Yes	Yes	10	-3.03	Metabolism > Lipic
PNPO	HGNC:30260	F57B9.1	Alliance+Orth	Ensembl Com	Yes	Yes	11	-1.52	Metabolism > Vita
PNPT1	HGNC:23166	pnpt-1	Alliance+Orth	Ensembl Com	Yes	Yes	11	#N/A	Mitochondrial cen
POLDIP2	HGNC:23781	tag-307	Alliance+Orth	Ensembl Com	Yes	Yes	10	0.01	Mitochondrial cen
POLG	HGNC:9179	polg-1	Alliance+Orth	Ensembl Com	Yes	Yes	10	1.56	Mitochondrial cen
POLQ	HGNC:9186	polq-1	Alliance+Orth	Ensembl Com	Yes	Yes	9	-2.99	Mitochondrial cen
POLQ	NA	helq-1	OrthoList	OrthoMCL	NA	NA	1	-0.78	Mitochondrial cen
POLRMT	HGNC:9200	rpom-1	Alliance+Orth	Ensembl Com	Yes	Yes	8	-0.95	Mitochondrial cen
PPA2	HGNC:28883	pyp-1	Alliance+Orth	Ensembl Com	Yes	Yes	9	1.13	Mitochondrial cen
PPIF	NA	cyn-1	OrthoList	InParanoid|O	NA	NA	4	1.39	Signaling > Calciu
PPIF	HGNC:9259	cyn-2	Alliance+Orth	InParanoid|O	Yes	Yes	6	0.06	Signaling > Calciu
PPIF	NA	cyn-3	OrthoList	InParanoid|O	NA	NA	3	1.86	Signaling > Calciu
PPIF	NA	cyn-7	OrthoList	InParanoid|O	NA	NA	3	1.25	Signaling > Calciu
PPIF	NA	Y17G9B.4	OrthoList	Ensembl Com	NA	NA	1	-2.88	Signaling > Calciu
PPIF	NA	T22F3.12	OrthoList	Ensembl Com	NA	NA	1	#N/A	Signaling > Calciu

PPTC7	HGNC:30695	W09D10.4	Alliance+Orth	Ensembl Com	Yes	Yes	11	0.2	Signaling
PRDX2	HGNC:9353	prdx-2	Alliance+Orth	Ensembl Com	Yes	Yes	10	0.82	Metabolism > Deto
PRDX2	NA	prdx-3	OrthoList	OrthoMCL	NA	NA	1	0.8	Metabolism > Deto
PRDX2	NA	prdx-6	OrthoList	OrthoMCL	NA	NA	1	-3.43	Metabolism > Deto
PRDX3	NA	prdx-2	OrthoList	OrthoMCL	NA	NA	1	0.82	Metabolism > Deto
PRDX3	HGNC:9354	prdx-3	Alliance+Orth	Ensembl Com	Yes	Yes	10	0.8	Metabolism > Deto
PRDX3	NA	prdx-6	OrthoList	OrthoMCL	NA	NA	1	-3.43	Metabolism > Deto
PRDX4	NA	prdx-2	OrthoList	OrthoMCL	NA	NA	1	0.82	Metabolism > Deto
PRDX4	NA	prdx-3	OrthoList	OrthoInspect	NA	NA	2	0.8	Metabolism > Deto
PRDX4	NA	prdx-6	OrthoList	OrthoMCL	NA	NA	1	-3.43	Metabolism > Deto
PRDX6	NA	prdx-2	OrthoList	OrthoMCL	NA	NA	1	0.82	Metabolism > Lipid
PRDX6	NA	prdx-3	OrthoList	OrthoMCL	NA	NA	1	0.8	Metabolism > Lipid
PRDX6	HGNC:16753	prdx-6	Alliance+Orth	Ensembl Com	Yes	Yes	11	-3.43	Metabolism > Lipid
PRELID1	HGNC:30255	prel-1	Alliance+Orth	Ensembl Com	Yes	Yes	11	#N/A	Metabolism > Lipid
PRELID2	NA	F15D3.6	OrthoList	Ensembl Com	NA	NA	1	-0.48	Unknown
PRELID3A	HGNC:24639	prel-3	Alliance+Orth	Ensembl Com	Yes	No	10	#N/A	Metabolism > Lipid
PRELID3B	HGNC:15892	prel-3	Alliance+Orth	Ensembl Com	Yes	Yes	11	#N/A	Metabolism > Lipid
PRKACA	HGNC:9380	kin-1	Alliance+Orth	Ensembl Com	Yes	Yes	10	-0.04	Signaling > cAMP-I
PRKACA	NA	F47F2.1	OrthoList	OrthoMCL	NA	NA	1	2.01	Signaling > cAMP-I
PRKN	HGNC:8607	pdr-1	Alliance+Orth	Ensembl Com	Yes	Yes	10	1.14	Mitochondrial dyn
PRODH	HGNC:9453	prdh-1	Alliance+Orth	Ensembl Com	Yes	Yes	11	-1.23	Metabolism > Amir
PRXL2A	HGNC:28651	R53.5	Alliance	Hieranoid | InP	Yes	Yes	8	-0.89	Metabolism > Deto
PTCD3	HGNC:24717	let-630	Alliance+Orth	Ensembl Com	Yes	Yes	8	-3.66	Mitochondrial cen
PTGES2	HGNC:17822	pges-2	Alliance+Orth	Ensembl Com	Yes	Yes	11	-2.34	Metabolism > Lipid
PTPMT1	HGNC:26965	F28C6.8	Alliance+Orth	Ensembl Com	Yes	Yes	10	2.05	Metabolism > Lipid
PTRH2	HGNC:24265	C24G6.8	Alliance+Orth	Ensembl Com	Yes	Yes	5	1	Unknown
PUS1	HGNC:15508	pus-1	Alliance+Orth	Ensembl Com	Yes	Yes	11	-0.96	Mitochondrial cen
PUSL1	NA	tag-124	OrthoList	OrthoMCL	NA	NA	1	-2.43	Mitochondrial cen
PUSL1	HGNC:26914	Y73B6BL.29	Alliance+Orth	Hieranoid | InP	Yes	Yes	8	-2.71	Mitochondrial cen
PXMP2	NA	pgam-5	OrthoList	OrthoMCL	NA	NA	1	0.11	Unknown

PXMP4	HGNC:15920	pxmp-4	Alliance+Orth	Ensembl Com	Yes	Yes	11	-0.38	Unknown
PYCR1	HGNC:9721	pycr-1	Alliance+Orth	Ensembl Com	Yes	Yes	9	3.04	Metabolism > Ami
PYCR2	HGNC:30262	pycr-1	Alliance+Orth	Ensembl Com	Yes	Yes	8	3.04	Metabolism > Ami
QDPR	HGNC:9752	qdpr-1	Alliance+Orth	Ensembl Com	Yes	Yes	11	0.95	Metabolism > Met
QRSL1	HGNC:21020	Y41D4A.6	Alliance+Orth	Ensembl Com	Yes	Yes	11	0.2	Mitochondrial cen
QTRT1	HGNC:23797	tgt-1	Alliance+Orth	Ensembl Com	Yes	Yes	11	-4.33	Mitochondrial cen
RAB5IF	HGNC:15870	F44E7.9	Alliance	Ensembl Com	Yes	Yes	9	0.69	OXPHOS > OXPHC
RARS2	NA	rars-1	OrthoList	OrthoMCL	NA	NA	1	-0.24	Mitochondrial cen
RARS2	HGNC:21406	rars-2	Alliance+Orth	Ensembl Com	Yes	Yes	10	0.65	Mitochondrial cen
RBFA	HGNC:26120	C25G4.3	Alliance	Ensembl Com	Yes	Yes	3	1.57	Mitochondrial cen
RCC1L	HGNC:14948	W09G3.7	Alliance+Orth	Ensembl Com	Yes	Yes	10	0.95	Mitochondrial cen
RDH13	HGNC:19978	dhs-22	Alliance+Orth	Hieranoid | InP	Yes	Yes	5	1.55	Metabolism > Vita
RDH13	HGNC:19978	dhs-24	Alliance	OrthoFinder | I	No	Yes	3	#N/A	Metabolism > Vita
RDH14	HGNC:19979	dhs-22	Alliance+Orth	InParanoid | O	Yes	No	4	1.55	Metabolism > Vita
REXO2	HGNC:17851	C08B6.8	Alliance+Orth	Ensembl Com	Yes	Yes	11	-1.24	Mitochondrial cen
RFK	HGNC:30324	rfk-1	Alliance+Orth	Ensembl Com	Yes	Yes	11	-0.34	Metabolism > Vita
RHOT1	NA	miro-2	OrthoList	Ensembl Com	NA	NA	1	#N/A	Signaling > Calciu
RHOT1	HGNC:21168	miro-1	Alliance+Orth	Ensembl Com	Yes	Yes	11	-0.23	Signaling > Calciu
RHOT2	NA	miro-2	OrthoList	Ensembl Com	NA	NA	1	#N/A	Signaling > Calciu
RHOT2	HGNC:21169	miro-1	Alliance+Orth	Ensembl Com	Yes	Yes	10	-0.23	Signaling > Calciu
RIDA	HGNC:16897	C23G10.2	Alliance+Orth	Ensembl Com	Yes	Yes	11	0.31	Unknown
RMDN1	HGNC:24285	F33H2.6	Alliance+Orth	Ensembl Com	Yes	Yes	11	-0.27	Unknown
RMDN3	HGNC:25550	rmd-3	Alliance+Orth	Ensembl Com	Yes	No	5	-3.84	Mitochondrial dyn
RMDN3	HGNC:25550	rmd-2	Alliance+Orth	Ensembl Com	Yes	No	5	1.28	Mitochondrial dyn
RMDN3	HGNC:25550	rmd-1	Alliance+Orth	Ensembl Com	Yes	Yes	5	-0.66	Mitochondrial dyn
RMDN3	NA	sup-35	OrthoList	Ensembl Com	NA	NA	1	#N/A	Mitochondrial dyn
RMDN3	NA	C16C8.18	OrthoList	Ensembl Com	NA	NA	1	-2.18	Mitochondrial dyn
RMDN3	HGNC:25550	rmd-6	Alliance+Orth	Ensembl Com	Yes	No	5	#N/A	Mitochondrial dyn
RMND1	HGNC:21176	ZK1010.2	Alliance+Orth	Ensembl Com	Yes	Yes	10	0.61	Mitochondrial cen
RNASEH1	HGNC:18466	rnh-1.0	Alliance+Orth	Ensembl Com	Yes	Yes	10	-0.42	Mitochondrial cen

RNASEH1	NA	rnh-1.3	OrthoList	Ensembl Com	NA	NA	2	0.82	Mitochondrial cen
ROMO1	HGNC:16185	romo-1	Alliance+Orth	Ensembl Com	Yes	Yes	10	1.51	Protein import, so
ROMO1	HGNC:16185	Y94A7B.11	Alliance+Orth	Ensembl Com	No	Yes	4	1.84	Protein import, so
RPIA	HGNC:10297	rpia-1	Alliance+Orth	Ensembl Com	Yes	Yes	11	0.87	Metabolism > Carb
RPUSD3	HGNC:28437	ZK287.7	Alliance+Orth	Ensembl Com	Yes	Yes	5	-0.85	Mitochondrial cen
RPUSD4	HGNC:25898	ZK287.7	Alliance+Orth	Ensembl Com	Yes	No	4	-0.85	Mitochondrial cen
RTN4IP1	HGNC:18647	rad-8	Alliance+Orth	Ensembl Com	Yes	Yes	11	0.31	Unknown
SAMM50	HGNC:24276	gop-3	Alliance+Orth	Ensembl Com	Yes	Yes	11	-0.09	Protein import, so
SARDH	NA	Y37E3.17	OrthoList	OrthoMCL	NA	NA	1	-5.12	Metabolism > Ami
SARS2	HGNC:17697	sars-2	Alliance+Orth	Ensembl Com	Yes	Yes	10	0.6	Mitochondrial cen
SARS2	NA	sars-1	OrthoList	OrthoMCL	NA	NA	1	-0.25	Mitochondrial cen
SCO1	HGNC:10603	sco-1	Alliance+Orth	Ensembl Com	Yes	Yes	11	-1.58	OXPHOS > Compl
SCO2	HGNC:10604	sco-1	Alliance+Orth	Ensembl Com	Yes	No	5	-1.58	OXPHOS > Compl
SCP2	HGNC:10606	daf-22	Alliance+Orth	Ensembl Com	Yes	Yes	10	-2.3	Metabolism > Lipi
SDHA	HGNC:10680	sdha-1	Alliance+Orth	Ensembl Com	Yes	Yes	11	-0.31	OXPHOS > Compl
SDHA	HGNC:10680	sdha-2	Alliance+Orth	Ensembl Com	Yes	Yes	11	-2.43	OXPHOS > Compl
SDHAF2	HGNC:26034	Y57A10A.29	Alliance+Orth	Ensembl Com	Yes	Yes	8	4.78	OXPHOS > Compl
SDHAF3	HGNC:21752	F25H9.7	Alliance+Orth	Ensembl Com	Yes	Yes	10	0.11	OXPHOS > Compl
SDHAF4	HGNC:20957	W02D3.12	Alliance+Orth	Ensembl Com	Yes	Yes	9	1.6	OXPHOS > Compl
SDHB	HGNC:10681	sdhb-1	Alliance+Orth	Ensembl Com	Yes	Yes	11	1.18	OXPHOS > Compl
SDHC	HGNC:10682	mev-1	Alliance+Orth	Ensembl Com	Yes	Yes	9	0.89	OXPHOS > Compl
SDHD	HGNC:10683	sdhd-1	Alliance+Orth	Ensembl Com	Yes	Yes	10	1.18	OXPHOS > Compl
SDSL	HGNC:30404	cysl-1	Alliance	Ensembl Com	Yes	Yes	2	0.78	Metabolism > Ami
SDSL	HGNC:30404	cysl-2	Alliance	Ensembl Com	Yes	Yes	2	0.77	Metabolism > Ami
SDSL	HGNC:30404	cysl-4	Alliance	Ensembl Com	Yes	Yes	2	#N/A	Metabolism > Ami
SEPTIN4	HGNC:9165	unc-59	Alliance	InParanoid|O	Yes	No	5	-0.16	Mitochondrial dyn
SERAC1	HGNC:21061	F17H10.1	Alliance+Orth	Ensembl Com	Yes	Yes	6	-1.47	Metabolism > Lipi
SFXN1	NA	sfxn-1.1	OrthoList	Ensembl Com	NA	NA	3	-1.47	Metabolism > Ami
SFXN1	NA	sfxn-1.4	OrthoList	Ensembl Com	NA	NA	3	-6.35	Metabolism > Ami
SFXN1	NA	sfxn-1.2	OrthoList	Ensembl Com	NA	NA	3	-1.66	Metabolism > Ami

SFXN1	HGNC:16085	sfxn-1.5	Alliance+Orth	Ensembl Com	Yes	Yes	11	1.46	Metabolism > Ami
SFXN1	NA	sfxn-1.3	OrthoList	Ensembl Com	NA	NA	1	#N/A	Metabolism > Ami
SFXN1	NA	sfxn-5	OrthoList	OrthoMCL	NA	NA	1	-1.02	Metabolism > Ami
SFXN2	NA	sfxn-1.1	OrthoList	OrthoInspect	NA	NA	1	-1.47	Small molecule tra
SFXN2	NA	sfxn-1.4	OrthoList	OrthoInspect	NA	NA	1	-6.35	Small molecule tra
SFXN2	NA	sfxn-1.2	OrthoList	OrthoInspect	NA	NA	1	-1.66	Small molecule tra
SFXN2	NA	sfxn-1.5	OrthoList	OrthoInspect	NA	NA	1	1.46	Small molecule tra
SFXN2	HGNC:16086	sfxn-2	Alliance+Orth	Ensembl Com	Yes	Yes	9	-0.73	Small molecule tra
SFXN3	HGNC:16087	sfxn-1.1	Alliance+Orth	Ensembl Com	No	Yes	8	-1.47	Metabolism > Ami
SFXN3	HGNC:16087	sfxn-1.4	Alliance+Orth	Ensembl Com	No	Yes	8	-6.35	Metabolism > Ami
SFXN3	HGNC:16087	sfxn-1.2	Alliance+Orth	Ensembl Com	No	Yes	8	-1.66	Metabolism > Ami
SFXN3	HGNC:16087	sfxn-1.5	Alliance+Orth	Ensembl Com	Yes	No	9	1.46	Metabolism > Ami
SFXN3	HGNC:16087	sfxn-1.3	Alliance+Orth	Ensembl Com	No	Yes	7	#N/A	Metabolism > Ami
SFXN3	NA	sfxn-5	OrthoList	OrthoMCL	NA	NA	1	-1.02	Metabolism > Ami
SFXN4	NA	sfxn-5	OrthoList	Ensembl Com	NA	NA	1	-1.02	Small molecule tra
SFXN5	NA	sfxn-1.5	OrthoList	OrthoMCL	NA	NA	1	1.46	Metabolism > Carb
SFXN5	HGNC:16073	sfxn-5	Alliance+Orth	Ensembl Com	Yes	Yes	11	-1.02	Metabolism > Carb
SHMT2	HGNC:10852	mel-32	Alliance+Orth	Ensembl Com	Yes	No	6	-0.21	Metabolism > Ami
SIRT4	HGNC:14932	sir-2.2	Alliance+Orth	Ensembl Com	No	Yes	11	-1.54	Metabolism > Meta
SIRT4	HGNC:14932	sir-2.3	Alliance+Orth	Ensembl Com	Yes	Yes	11	-2.34	Metabolism > Meta
SLC25A1	HGNC:10979	K11H3.3	Alliance+Orth	Ensembl Com	Yes	Yes	10	-0.13	Metabolism > Carb
SLC25A1	HGNC:10979	Y37B11A.3	Alliance+Orth	Ensembl Com	No	Yes	3	-1.23	Metabolism > Carb
SLC25A10	HGNC:10980	slc-25A10	Alliance+Orth	Ensembl Com	Yes	Yes	9	0	Metabolism > Carb
SLC25A11	HGNC:10981	misc-1	Alliance+Orth	Ensembl Com	Yes	Yes	11	-0.16	Metabolism > Carb
SLC25A12	HGNC:10982	K02F3.2	Alliance+Orth	Ensembl Com	Yes	Yes	11	-0.32	Metabolism > Carb
SLC25A13	HGNC:10983	K02F3.2	Alliance+Orth	Ensembl Com	Yes	No	10	-0.32	Metabolism > Carb
SLC25A15	HGNC:10985	T10F2.2	Alliance+Orth	Ensembl Com	Yes	Yes	11	-1.47	Metabolism > Ami
SLC25A16	NA	slc-25A42	OrthoList	OrthoMCL	NA	NA	1	0.16	Small molecule tra
SLC25A18	HGNC:10988	slc-25A18.1	Alliance+Orth	Ensembl Com	Yes	Yes	10	-1.42	Small molecule tra
SLC25A18	HGNC:10988	slc-25A18.2	Alliance+Orth	Ensembl Com	No	Yes	9	-0.72	Small molecule tra

SLC25A19	NA	F47B8.10	OrthoList	Ensembl Com	NA	NA	1	#N/A	Metabolism > Vita
SLC25A19	HGNC:14409	hpo-12	Alliance+Orth	Ensembl Com	Yes	Yes	11	1.87	Metabolism > Vita
SLC25A20	HGNC:1421	dif-1	Alliance+Orth	Ensembl Com	Yes	Yes	11	0.65	Metabolism > Lipic
SLC25A21	HGNC:14411	slc-25A21	Alliance+Orth	Ensembl Com	Yes	Yes	11	-1.42	Metabolism > Ami
SLC25A22	HGNC:19954	slc-25A18.1	Alliance+Orth	Ensembl Com	Yes	Yes	11	-1.42	Small molecule tra
SLC25A22	HGNC:19954	slc-25A18.2	Alliance+Orth	Ensembl Com	No	Yes	10	-0.72	Small molecule tra
SLC25A23	HGNC:19375	F17E5.2	Alliance+Orth	Ensembl Com	Yes	Yes	10	-0.6	Metabolism > Nuc
SLC25A23	NA	F55A11.4	OrthoList	Ensembl Com	NA	NA	3	-1.34	Metabolism > Nuc
SLC25A24	HGNC:20662	F17E5.2	Alliance+Orth	Ensembl Com	Yes	No	10	-0.6	Metabolism > Nuc
SLC25A24	NA	F55A11.4	OrthoList	Ensembl Com	NA	NA	3	-1.34	Metabolism > Nuc
SLC25A25	HGNC:20663	F17E5.2	Alliance+Orth	Ensembl Com	Yes	Yes	11	-0.6	Metabolism > Nuc
SLC25A25	NA	F55A11.4	OrthoList	Ensembl Com	NA	NA	5	-1.34	Metabolism > Nuc
SLC25A26	HGNC:20661	slc-25A26	Alliance+Orth	Ensembl Com	Yes	Yes	11	-0.28	Small molecule tra
SLC25A27	HGNC:21065	ucp-4	Alliance+Orth	Ensembl Com	Yes	Yes	11	-2.47	Small molecule tra
SLC25A28	HGNC:23472	mfn-1	Alliance+Orth	Ensembl Com	Yes	Yes	9	-1.61	Metabolism > Meta
SLC25A29	HGNC:20116	slc-25A29	Alliance+Orth	Ensembl Com	Yes	Yes	10	-1.21	Metabolism > Ami
SLC25A3	HGNC:10989	C14C10.1	Alliance+Orth	Ensembl Com	No	Yes	5	-4.25	Metabolism > Meta
SLC25A3	HGNC:10989	F01G4.6	Alliance+Orth	Ensembl Com	Yes	Yes	11	0	Metabolism > Meta
SLC25A3	HGNC:10989	T05F1.8	Alliance+Orth	Ensembl Com	No	Yes	10	4.97	Metabolism > Meta
SLC25A3	HGNC:10989	C33F10.12	Alliance+Orth	Ensembl Com	No	Yes	10	-2.15	Metabolism > Meta
SLC25A31	HGNC:25319	ant-1.1	Alliance+Orth	Ensembl Com	Yes	No	9	0.94	Metabolism > Nuc
SLC25A31	HGNC:25319	ant-1.2	Alliance+Orth	Ensembl Com	Yes	No	9	-5.17	Metabolism > Nuc
SLC25A31	NA	C47E12.2	OrthoList	Ensembl Com	NA	NA	1	-0.99	Metabolism > Nuc
SLC25A31	HGNC:25319	ant-1.3	Alliance+Orth	Ensembl Com	Yes	No	9	-2.03	Metabolism > Nuc
SLC25A31	NA	R07E3.4	OrthoList	Ensembl Com	NA	NA	1	0.4	Metabolism > Nuc
SLC25A31	NA	F25B4.7	OrthoList	Ensembl Com	NA	NA	1	-0.31	Metabolism > Nuc
SLC25A31	HGNC:25319	ant-1.4	Alliance+Orth	Ensembl Com	Yes	No	9	0.54	Metabolism > Nuc
SLC25A32	HGNC:29683	slc-25A32	Alliance+Orth	Ensembl Com	Yes	Yes	11	-5.6	Metabolism > Vita
SLC25A33	HGNC:29681	T09F3.2	Alliance+Orth	Ensembl Com	Yes	Yes	10	-0.85	Metabolism > Nuc
SLC25A36	HGNC:25554	T09F3.2	Alliance+Orth	Ensembl Com	Yes	Yes	11	-0.85	Metabolism > Nuc

SLC25A37	HGNC:29786	mfn-1	Alliance+Orth	Ensembl Com	Yes	No	9	-1.61	Metabolism > Meta
SLC25A39	HGNC:24279	C16C10.1	Alliance+Orth	Ensembl Com	Yes	No	9	-1.27	Small molecule tra
SLC25A4	HGNC:10990	ant-1.1	Alliance+Orth	Ensembl Com	Yes	Yes	9	0.94	Metabolism > Nuc
SLC25A4	HGNC:10990	ant-1.2	Alliance+Orth	Ensembl Com	Yes	Yes	9	-5.17	Metabolism > Nuc
SLC25A4	NA	C47E12.2	OrthoList	Ensembl Com	NA	NA	1	-0.99	Metabolism > Nuc
SLC25A4	HGNC:10990	ant-1.3	Alliance+Orth	Ensembl Com	Yes	Yes	9	-2.03	Metabolism > Nuc
SLC25A4	NA	R07E3.4	OrthoList	Ensembl Com	NA	NA	1	0.4	Metabolism > Nuc
SLC25A4	NA	F25B4.7	OrthoList	Ensembl Com	NA	NA	1	-0.31	Metabolism > Nuc
SLC25A4	HGNC:10990	ant-1.4	Alliance+Orth	Ensembl Com	Yes	Yes	9	0.54	Metabolism > Nuc
SLC25A40	HGNC:29680	C16C10.1	Alliance+Orth	Ensembl Com	Yes	Yes	11	-1.27	Small molecule tra
SLC25A41	HGNC:28533	F17E5.2	Alliance+Orth	Ensembl Com	Yes	No	3	-0.6	Metabolism > Nuc
SLC25A41	NA	F55A11.4	OrthoList	Ensembl Com	NA	NA	1	-1.34	Metabolism > Nuc
SLC25A42	HGNC:28380	slc-25A42	Alliance+Orth	Ensembl Com	Yes	Yes	11	0.16	Metabolism > Meta
SLC25A44	HGNC:29036	F13G3.7	Alliance+Orth	Ensembl Com	Yes	Yes	11	-1.57	Metabolism > Amin
SLC25A44	HGNC:29036	Y43C5B.3	Alliance+Orth	Ensembl Com	No	Yes	11	-5.16	Metabolism > Amin
SLC25A45	HGNC:27442	R07B7.10	Alliance+Orth	Ensembl Com	Yes	Yes	8	1.6	Small molecule tra
SLC25A46	HGNC:25198	slc-25A46	Alliance+Orth	Ensembl Com	Yes	Yes	11	-0.73	Small molecule tra
SLC25A47	HGNC:20115	R07B7.10	Alliance+Orth	Ensembl Com	Yes	Yes	7	1.6	Small molecule tra
SLC25A48	HGNC:30451	R07B7.10	Alliance+Orth	Ensembl Com	Yes	Yes	7	1.6	Small molecule tra
SLC25A5	HGNC:10991	ant-1.1	Alliance+Orth	Ensembl Com	Yes	Yes	9	0.94	Metabolism > Nuc
SLC25A5	HGNC:10991	ant-1.2	Alliance+Orth	Ensembl Com	Yes	Yes	9	-5.17	Metabolism > Nuc
SLC25A5	NA	C47E12.2	OrthoList	Ensembl Com	NA	NA	1	-0.99	Metabolism > Nuc
SLC25A5	HGNC:10991	ant-1.3	Alliance+Orth	Ensembl Com	Yes	Yes	9	-2.03	Metabolism > Nuc
SLC25A5	NA	R07E3.4	OrthoList	Ensembl Com	NA	NA	1	0.4	Metabolism > Nuc
SLC25A5	NA	F25B4.7	OrthoList	Ensembl Com	NA	NA	1	-0.31	Metabolism > Nuc
SLC25A5	HGNC:10991	ant-1.4	Alliance+Orth	Ensembl Com	Yes	Yes	9	0.54	Metabolism > Nuc
SLC25A51	HGNC:23323	T20D3.5	Alliance+Orth	Ensembl Com	Yes	Yes	11	0.92	Metabolism > Meta
SLC25A52	HGNC:23324	T20D3.5	Alliance+Orth	Ensembl Com	Yes	No	8	0.92	Metabolism > Meta
SLC25A53	NA	T20D3.5	OrthoList	Ensembl Com	NA	NA	1	0.92	Small molecule tra
SLC25A6	HGNC:10992	ant-1.1	Alliance+Orth	Ensembl Com	Yes	Yes	10	0.94	Metabolism > Nuc

SLC25A6	HGNC:10992	ant-1.2	Alliance+Orth	Ensembl Com	Yes	Yes	10	-5.17	Metabolism > Nuc
SLC25A6	NA	C47E12.2	OrthoList	Ensembl Com	NA	NA	1	-0.99	Metabolism > Nuc
SLC25A6	HGNC:10992	ant-1.3	Alliance+Orth	Ensembl Com	Yes	Yes	10	-2.03	Metabolism > Nuc
SLC25A6	NA	R07E3.4	OrthoList	Ensembl Com	NA	NA	1	0.4	Metabolism > Nuc
SLC25A6	NA	F25B4.7	OrthoList	Ensembl Com	NA	NA	1	-0.31	Metabolism > Nuc
SLC25A6	HGNC:10992	ant-1.4	Alliance+Orth	Ensembl Com	Yes	Yes	10	0.54	Metabolism > Nuc
SLC30A9	HGNC:1329	slc-30A9	Alliance+Orth	Ensembl Com	Yes	Yes	11	2.3	Small molecule tra
SLC8B1	HGNC:26175	ncx-6	Alliance+Orth	Ensembl Com	Yes	Yes	11	0.51	Signaling > Calciu
SLC8B1	HGNC:26175	ncx-7	Alliance+Orth	Ensembl Com	Yes	Yes	11	-1.17	Signaling > Calciu
SLC8B1	HGNC:26175	ncx-8	Alliance+Orth	Ensembl Com	Yes	Yes	11	-2.72	Signaling > Calciu
SLC8B1	HGNC:26175	ncx-9	Alliance+Orth	Ensembl Com	Yes	Yes	11	#N/A	Signaling > Calciu
SLC8B1	HGNC:26175	ncx-10	Alliance+Orth	Ensembl Com	No	Yes	11	-0.42	Signaling > Calciu
SLIRP	HGNC:20495	slrp-1	Alliance+Orth	Hieranoid | InP	Yes	Yes	8	0.56	Mitochondrial cen
SMDT1	HGNC:25055	emre-1	Alliance+Orth	Ensembl Com	Yes	Yes	8	1.52	Signaling > Calciu
SNAP29	HGNC:11133	snap-29	Alliance+Orth	Ensembl Com	Yes	Yes	10	1.72	Mitochondrial dyn
SND1	HGNC:30646	tsn-1	Alliance+Orth	Ensembl Com	Yes	Yes	11	0.8	Unknown
SOD1	HGNC:11179	sod-1	Alliance+Orth	Hieranoid | Ho	Yes	Yes	9	1.32	Metabolism > Deto
SOD1	NA	sod-4	OrthoList	Ensembl Com	NA	NA	2	1.39	Metabolism > Deto
SOD1	HGNC:11179	sod-5	Alliance+Orth	Hieranoid | Ho	Yes	Yes	9	#N/A	Metabolism > Deto
SOD2	HGNC:11180	sod-2	Alliance+Orth	Ensembl Com	Yes	Yes	11	0.36	Metabolism > Deto
SOD2	HGNC:11180	sod-3	Alliance+Orth	Ensembl Com	Yes	Yes	11	-0.79	Metabolism > Deto
SPATA20	HGNC:26125	B0495.5	Alliance+Orth	Ensembl Com	Yes	Yes	11	-0.29	Unknown
SPG7	NA	spg-7	OrthoList	OrthoMCL	NA	NA	1	-1.06	Protein import, sor
SPG7	NA	ymel-1	OrthoList	OrthoMCL	NA	NA	1	-0.16	Protein import, sor
SPG7	HGNC:11237	ppgn-1	Alliance+Orth	Ensembl Com	Yes	Yes	11	-0.33	Protein import, sor
SPG7	HGNC:11237	Y47C4A.1	Alliance+Orth	Ensembl Com	No	Yes	4	#N/A	Protein import, sor
SPG7	NA	Y108F1.1	OrthoList	Ensembl Com	NA	NA	1	#N/A	Protein import, sor
SPHK2	HGNC:18859	sphk-1	Alliance+Orth	Ensembl Com	Yes	No	10	-1	Metabolism > Lipic
SPTLC2	HGNC:11278	sptl-3	Alliance+Orth	Ensembl Com	No	Yes	6	-1.53	Metabolism > Lipic
SPTLC2	HGNC:11278	sptl-2	Alliance+Orth	Ensembl Com	Yes	Yes	11	-3.71	Metabolism > Lipic

SQOR	HGNC:20390	sqrd-1	Alliance+Orth	Ensembl Com	Yes	Yes	11	-0.7	Metabolism > Elec
SQOR	HGNC:20390	Y9C9A.16	Alliance+Orth	Ensembl Com	Yes	Yes	11	3.51	Metabolism > Elec
SSBP1	HGNC:11317	mtss-1	Alliance+Orth	Ensembl Com	Yes	Yes	9	-1.04	Mitochondrial cen
STAR	HGNC:11359	strl-1	Alliance+Orth	Hieranoid | In	Yes	Yes	7	-0.32	Metabolism > Lipic
STAR	NA	tag-340	OrthoList	Ensembl Com	NA	NA	1	-0.97	Metabolism > Lipic
STARD7	HGNC:18063	C06H2.2	Alliance+Orth	Ensembl Com	Yes	Yes	8	0.11	Metabolism > Lipic
STOM	NA	mec-2	OrthoList	Ensembl Com	NA	NA	3	0.67	Unknown
STOM	NA	stl-1	OrthoList	OrthoMCL	NA	NA	1	-0.2	Unknown
STOM	NA	sto-1	OrthoList	Ensembl Com	NA	NA	2	0.48	Unknown
STOM	HGNC:3383	sto-2	Alliance+Orth	Ensembl Com	Yes	Yes	10	-0.03	Unknown
STOM	NA	sto-3	OrthoList	Ensembl Com	NA	NA	1	2.07	Unknown
STOM	NA	sto-4	OrthoList	Ensembl Com	NA	NA	1	0.5	Unknown
STOM	NA	sto-5	OrthoList	Ensembl Com	NA	NA	1	-2.84	Unknown
STOM	NA	sto-6	OrthoList	Ensembl Com	NA	NA	1	0.01	Unknown
STOM	NA	unc-1	OrthoList	Ensembl Com	NA	NA	1	0.87	Unknown
STOML2	NA	mec-2	OrthoList	OrthoMCL	NA	NA	1	0.67	Protein import, sor
STOML2	HGNC:14559	stl-1	Alliance+Orth	Ensembl Com	Yes	Yes	11	-0.2	Protein import, sor
STOML2	NA	sto-1	OrthoList	OrthoMCL	NA	NA	1	0.48	Protein import, sor
STOML2	NA	sto-2	OrthoList	OrthoMCL	NA	NA	1	-0.03	Protein import, sor
STX17	HGNC:11432	syx-17	Alliance+Orth	Ensembl Com	Yes	Yes	5	-0.15	Mitochondrial dyn
SUCLA2	HGNC:11448	suca-1	Alliance+Orth	Ensembl Com	Yes	Yes	11	0.12	Metabolism > Carb
SUCLA2	NA	sucg-1	OrthoList	OrthoMCL	NA	NA	1	-2.08	Metabolism > Carb
SUCLG1	HGNC:11449	sucl-1	Alliance+Orth	Ensembl Com	Yes	Yes	11	0.62	Metabolism > Carb
SUCLG1	HGNC:11449	sucl-2	Alliance+Orth	Ensembl Com	Yes	Yes	11	0.71	Metabolism > Carb
SUCLG2	NA	suca-1	OrthoList	OrthoMCL	NA	NA	1	0.12	Metabolism > Carb
SUCLG2	HGNC:11450	sucg-1	Alliance+Orth	Ensembl Com	Yes	Yes	11	-2.08	Metabolism > Carb
SUOX	HGNC:11460	suox-1	Alliance+Orth	Ensembl Com	Yes	Yes	11	-0.71	Metabolism > Met
SUPV3L1	HGNC:11471	C08F8.2	Alliance+Orth	Ensembl Com	Yes	Yes	11	-1.6	Mitochondrial cen
SURF1	HGNC:11474	sft-1	Alliance+Orth	Ensembl Com	Yes	Yes	11	-2.69	OXPHOS > Compl
SYNJ2BP	HGNC:18955	mics-1	Alliance+Orth	Ensembl Com	Yes	Yes	3	1.93	Mitochondrial dyn

TACO1	HGNC:24316	taco-1	Alliance+Orth	Ensembl Com	Yes	Yes	11	1.21	Mitochondrial cen
TAMM41	HGNC:25187	Y71F9B.2	Alliance+Orth	Ensembl Com	Yes	Yes	11	0.81	Metabolism > Lipid
TARS2	HGNC:30740	tars-1	Alliance+Orth	Ensembl Com	Yes	No	5	-0.31	Mitochondrial cen
TAZ	NA	acl-3	OrthoList	Ensembl Com	NA	NA	6	1.06	Metabolism > Lipid
TBRG4	HGNC:17443	fask-1	Alliance	Ensembl Com	Yes	Yes	3	-2.26	Mitochondrial cen
TCAIM	HGNC:25241	C35B8.3	Alliance+Orth	Ensembl Com	Yes	Yes	11	0.72	Unknown
TFAM	HGNC:11741	hmg-5	Alliance+Orth	InParanoid|O	Yes	Yes	8	1.05	Mitochondrial cen
TFB1M	NA	E02H1.1	OrthoList	OrthoMCL	NA	NA	1	-1.16	Mitochondrial cen
TFB1M	HGNC:17037	tfbm-1	Alliance+Orth	Ensembl Com	Yes	Yes	11	1.11	Mitochondrial cen
TIMM10	HGNC:11814	tin-10	Alliance+Orth	Ensembl Com	Yes	Yes	11	0.38	Protein import, sor
TIMM10B	HGNC:4022	tin-9.2	Alliance+Orth	OrthoFinder|	Yes	Yes	3	#N/A	Protein import, sor
TIMM13	HGNC:11816	tin-13	Alliance+Orth	Ensembl Com	Yes	Yes	10	0.98	Protein import, sor
TIMM17A	HGNC:17315	timm-17B.2	Alliance+Orth	Ensembl Com	No	Yes	4	-2.97	Protein import, sor
TIMM17A	HGNC:17315	timm-17B.1	Alliance+Orth	Ensembl Com	Yes	Yes	10	0	Protein import, sor
TIMM17B	HGNC:17310	timm-17B.2	Alliance+Orth	Ensembl Com	No	Yes	4	-2.97	Protein import, sor
TIMM17B	HGNC:17310	timm-17B.1	Alliance+Orth	Ensembl Com	Yes	Yes	11	0	Protein import, sor
TIMM21	HGNC:25010	F56B3.11	Alliance+Orth	Ensembl Com	Yes	Yes	10	-0.33	Mitochondrial cen
TIMM22	HGNC:17317	C47G2.3	Alliance+Orth	Ensembl Com	Yes	Yes	11	-1.25	Protein import, sor
TIMM23	HGNC:17312	timm-23	Alliance+Orth	Ensembl Com	Yes	Yes	9	-0.19	Protein import, sor
TIMM29	HGNC:25152	R04F11.5	Alliance+Orth	Ensembl Com	Yes	Yes	10	0.81	Protein import, sor
TIMM44	HGNC:17316	tin-44	Alliance+Orth	Ensembl Com	Yes	Yes	11	-1.89	Protein import, sor
TIMM50	HGNC:23656	scpl-4	Alliance+Orth	Ensembl Com	Yes	Yes	9	-1.67	Protein import, sor
TIMM8A	HGNC:11817	ddp-1	Alliance+Orth	Ensembl Com	Yes	Yes	10	1.56	Protein import, sor
TIMM8B	HGNC:11818	ddp-1	Alliance+Orth	Ensembl Com	Yes	No	7	1.56	Protein import, sor
TIMM9	HGNC:11819	tin-9.1	Alliance+Orth	Ensembl Com	Yes	Yes	10	0.15	Protein import, sor
TIMMDC1	HGNC:1321	Y38F2AR.3	Alliance+Orth	Ensembl Com	Yes	Yes	8	-4.04	OXPHOS > Compl
TMEM177	HGNC:28143	R144.11	Alliance	Ensembl Com	Yes	Yes	6	-0.69	OXPHOS > Compl
TMEM177	HGNC:28143	R144.12	Alliance	Ensembl Com	No	Yes	3	-4.42	OXPHOS > Compl
TMEM65	HGNC:25203	tag-321	Alliance+Orth	Ensembl Com	Yes	Yes	8	0.29	Unknown
TMEM70	HGNC:26050	F32D8.5	Alliance	Ensembl Com	Yes	Yes	6	0.63	OXPHOS > Compl

TMLHE	HGNC:18308	gbh-2	Alliance+Orth	Ensembl Com	Yes	Yes	11	1.74	Metabolism > Meta
TOMM20	HGNC:20947	tomm-20	Alliance+Orth	Ensembl Com	Yes	Yes	11	-1.59	Protein import, sor
TOMM20L	HGNC:33752	tomm-20	Alliance+Orth	Ensembl Com	Yes	No	4	-1.59	Protein import, sor
TOMM20L	HGNC:33752	F32B4.2	Alliance	OrthoFinder|I	No	Yes	3	#N/A	Protein import, sor
TOMM22	HGNC:18002	tomm-22	Alliance+Orth	Ensembl Com	Yes	Yes	10	-0.5	Protein import, sor
TOMM40	HGNC:18001	tomm-40	Alliance+Orth	Ensembl Com	Yes	No	11	-1.02	Protein import, sor
TOMM40L	HGNC:25756	tomm-40	Alliance+Orth	Ensembl Com	Yes	Yes	10	-1.02	Protein import, sor
TOMM7	HGNC:21648	tomm-7	Alliance+Orth	InParanoid|O	Yes	Yes	8	2.55	Protein import, sor
TOP1MT	HGNC:29787	top-1	Alliance+Orth	Ensembl Com	Yes	Yes	10	0.32	Mitochondrial cen
TOP3A	HGNC:11992	top-3A	Alliance+Orth	Ensembl Com	Yes	Yes	10	#N/A	Mitochondrial cen
TRAP1	HGNC:16264	hsp-75	Alliance+Orth	Ensembl Com	Yes	Yes	11	-1.56	Protein import, sor
TRIAP1	HGNC:26937	mdmh-35	Alliance+Orth	Hieranoid|Or	Yes	Yes	3	#N/A	Metabolism > Lipid
TRIT1	HGNC:20286	gro-1	Alliance+Orth	Ensembl Com	Yes	Yes	11	0.94	Mitochondrial cen
TRMT1	HGNC:25980	trm-1	Alliance+Orth	Ensembl Com	Yes	Yes	11	-1.76	Mitochondrial cen
TRMT10C	NA	F25H8.1	OrthoList	Ensembl Com	NA	NA	1	#N/A	Mitochondrial cen
TRMT10C	HGNC:26022	trmt-10C.1	Alliance+Orth	Ensembl Com	Yes	Yes	7	-2.68	Mitochondrial cen
TRMT2B	HGNC:25748	trm-2A	Alliance+Orth	Ensembl Com	Yes	No	8	-1.2	Mitochondrial cen
TRMT5	NA	C53A5.2	OrthoList	OrthoMCL	NA	NA	1	#N/A	Mitochondrial cen
TRMT5	HGNC:23141	C53A5.17	Alliance+Orth	Ensembl Com	Yes	Yes	10	-0.55	Mitochondrial cen
TRMU	HGNC:25481	mttu-1	Alliance+Orth	Ensembl Com	Yes	Yes	11	1.19	Mitochondrial cen
TRNT1	HGNC:17341	hpo-31	Alliance+Orth	Ensembl Com	Yes	Yes	11	0.42	Mitochondrial cen
TRUB2	HGNC:17170	Y43B11AR.3	Alliance+Orth	Ensembl Com	Yes	Yes	10	-0.56	Mitochondrial cen
TSFM	HGNC:12367	tsfm-1	Alliance+Orth	Ensembl Com	Yes	Yes	11	-0.68	Mitochondrial cen
TSPO	HGNC:1158	tspo-1	Alliance+Orth	Ensembl Com	Yes	Yes	9	0.58	Metabolism > Lipid
TST	HGNC:12388	mpst-1	Alliance+Orth	Ensembl Com	Yes	Yes	7	-2.31	Metabolism > Deto
TST	HGNC:12388	mpst-2	Alliance+Orth	Ensembl Com	Yes	Yes	8	#N/A	Metabolism > Deto
TST	HGNC:12388	mpst-3	Alliance+Orth	Ensembl Com	Yes	Yes	8	-3.02	Metabolism > Deto
TST	HGNC:12388	mpst-7	Alliance+Orth	Ensembl Com	No	Yes	9	1.02	Metabolism > Deto
TST	HGNC:12388	mpst-4	Alliance+Orth	Ensembl Com	No	Yes	4	-4.23	Metabolism > Deto
TST	HGNC:12388	mpst-5	Alliance+Orth	Ensembl Com	No	Yes	6	#N/A	Metabolism > Deto

TST	HGNC:12388	mpst-6	Alliance+Orth	Ensembl Com	No	Yes	6	#N/A	Metabolism > Deto
TTC19	HGNC:26006	ddl-3	Alliance+Orth	Ensembl Com	Yes	Yes	10	-1.08	OXPHOS > Compl
TUFM	HGNC:12420	tufm-1	Alliance+Orth	Ensembl Com	Yes	Yes	11	-0.99	Mitochondrial cen
TWNK	HGNC:1160	twnk-1	Alliance+Orth	Ensembl Com	Yes	Yes	11	-0.06	Mitochondrial cen
TXN2	HGNC:17772	trx-2	Alliance+Orth	Ensembl Com	Yes	Yes	11	-0.67	Metabolism > Vita
TXN2	NA	trx-1	OrthoList	OrthoMCL	NA	NA	1	-3.17	Metabolism > Vita
TXN2	NA	trx-4	OrthoList	OrthoMCL	NA	NA	1	2.31	Metabolism > Vita
TXN2	NA	Y55F3AR.2	OrthoList	OrthoMCL	NA	NA	1	2.73	Metabolism > Vita
TXNRD1	NA	gsr-1	OrthoList	OrthoMCL	NA	NA	1	-0.46	Metabolism > Deto
TXNRD1	NA	trxr-2	OrthoList	OrthoMCL	NA	NA	1	0.5	Metabolism > Deto
TXNRD1	HGNC:12437	trxr-1	Alliance+Orth	Ensembl Com	Yes	Yes	9	0.37	Metabolism > Deto
TXNRD2	NA	gsr-1	OrthoList	OrthoMCL	NA	NA	1	-0.46	Metabolism > Deto
TXNRD2	HGNC:18155	trxr-2	Alliance+Orth	Ensembl Com	Yes	Yes	8	0.5	Metabolism > Deto
TXNRD2	NA	trxr-1	OrthoList	OrthoMCL	NA	NA	1	0.37	Metabolism > Deto
UNG	HGNC:12572	ung-1	Alliance+Orth	Ensembl Com	Yes	Yes	8	-4.12	Mitochondrial cen
UQCC1	HGNC:15891	C35D10.5	Alliance+Orth	Ensembl Com	Yes	Yes	10	0.68	OXPHOS > Compl
UQCR10	HGNC:30863	C14B9.10	Alliance	OrthoFinder |	Yes	Yes	3	1.25	OXPHOS > Compl
UQCRB	HGNC:12582	T02H6.11	Alliance+Orth	Ensembl Com	Yes	Yes	9	1.7	OXPHOS > Compl
UQCRC1	HGNC:12585	mppb-1	Alliance+Orth	Ensembl Com	Yes	No	6	-0.59	Protein import, so
UQCRC1	HGNC:12585	ucr-1	Alliance+Orth	Ensembl Com	Yes	Yes	6	0.79	Protein import, so
UQCRC2	HGNC:12586	ucr-2.2	Alliance+Orth	Ensembl Com	Yes	Yes	9	0.52	Protein import, so
UQCRC2	HGNC:12586	ucr-2.1	Alliance+Orth	Ensembl Com	Yes	Yes	10	0.34	Protein import, so
UQCRC2	HGNC:12586	ucr-2.3	Alliance+Orth	Ensembl Com	No	Yes	9	-2.79	Protein import, so
UQCRFS1	HGNC:12587	isp-1	Alliance+Orth	Ensembl Com	Yes	Yes	11	1.27	OXPHOS > Compl
UQCRH	HGNC:12590	T27E9.2	Alliance+Orth	Ensembl Com	Yes	Yes	10	2.07	OXPHOS > Compl
UQCRQ	HGNC:29594	F45H10.2	Alliance+Orth	Ensembl Com	Yes	Yes	10	0.88	OXPHOS > Compl
UQCRQ	HGNC:29594	R07E4.3	Alliance+Orth	Ensembl Com	Yes	Yes	10	1.94	OXPHOS > Compl
USP30	HGNC:20065	Y67D2.2	Alliance+Orth	Ensembl Com	Yes	Yes	10	-2.42	Protein import, so
VARS2	HGNC:21642	vars-1	Alliance+Orth	Ensembl Com	Yes	Yes	4	-2.13	Mitochondrial cen
VARS2	HGNC:21642	glp-4	Alliance+Orth	Ensembl Com	Yes	No	4	-0.35	Mitochondrial cen

VDAC1	HGNC:12669	vdac-1	Alliance+Orth	Ensembl Com	Yes	Yes	10	0.36	Signaling > Calciu
VDAC2	HGNC:12672	vdac-1	Alliance+Orth	Ensembl Com	Yes	Yes	11	0.36	Small molecule tra
VDAC3	HGNC:12674	vdac-1	Alliance+Orth	Ensembl Com	Yes	No	10	0.36	Signaling > Calciu
VPS13D	NA	C25H3.8	OrthoList	Ensembl Com	NA	NA	5	#N/A	Mitochondrial dyn
VPS13D	HGNC:23595	vps-13D	Alliance	Ensembl Com	Yes	Yes	8	#N/A	Mitochondrial dyn
VWA8	HGNC:29071	vwa-8	Alliance+Orth	Ensembl Com	Yes	Yes	11	-0.78	Unknown
WARS2	HGNC:12730	prx-10	Alliance+Orth	Ensembl Com	Yes	Yes	11	-1.73	Mitochondrial cen
XPNPEP3	NA	pqn-59	OrthoList	OrthoMCL	NA	NA	1	0.51	Protein import, so
XPNPEP3	NA	K12C11.1	OrthoList	OrthoMCL	NA	NA	1	-0.16	Protein import, so
XPNPEP3	HGNC:28052	icpp-55	Alliance+Orth	Ensembl Com	Yes	Yes	10	#N/A	Protein import, so
YARS2	HGNC:24249	yars-2	Alliance+Orth	Ensembl Com	Yes	Yes	11	#N/A	Mitochondrial cen
YME1L1	NA	spg-7	OrthoList	OrthoMCL	NA	NA	1	-1.06	Protein import, so
YME1L1	HGNC:12843	ymel-1	Alliance+Orth	Ensembl Com	Yes	Yes	9	-0.16	Protein import, so
YME1L1	NA	ppgn-1	OrthoList	OrthoMCL	NA	NA	1	-0.33	Protein import, so
YRDC	HGNC:28905	Y48C3A.18	Alliance+Orth	Ensembl Com	Yes	Yes	10	0	Mitochondrial cen

bioRxiv preprint doi: https://doi.org/10.1101/2025.05.02.651978; this version posted May 3, 2025. The copyright holder for this preprint (which was not certified by peer review) is the author/funder. All rights reserved. No reuse allowed without permission.

Table S3 - Health of fluorescently tagged mitochondrial strains

Strain	Mitochondrial ETC Complex, Structure, Function	Homozygous Fertile	Additional days to starvation relative to wild-type[a]		
			Replicate 1	Replicate 2	Replicate 3
NDUV-2::LL::mNG	ETC - CI	yes	1	1	1
NDUF-7::LL::mNG	ETC - CI	yes	0	0	0
NUO-1::LL::mNG	ETC - CI	yes	3	3	3
NUO-6::LL::mNG	ETC - CI	no[b]	n/a	n/a	n/a
SDHB-1::LL::mNG	ETC - CII	yes	4	4	4
MEV-1::LL::mNG	ETC - CII	yes	5	9	6
UCR-2.1::LL::mNG	ETC - CIII	yes	1	1	1
ISP-1::LL::mNG	ETC - CIII	no[b]	n/a	n/a	n/a
CYC-1::LL::mNG	ETC - CIII	no[b]	n/a	n/a	n/a
COX-10::LL::mNG	ETC - CIV	yes	1	1	1
COX-5A::LL::mNG	ETC - CIV	yes	7	7	7
COX-5B::LL::mNG	ETC - CIV	yes	1	1	1
COX-6A::LL::mNG	ETC - CIV	yes	1	1	1
COX-4::LL::mNG	ETC - CIV	yes	1	1	1
ATP-4::LL::mNG	ETC - CIV	no[b]	n/a	n/a	n/a
TOMM-20::LL::mNG	Import	no[b]	n/a	n/a	n/a
IMMT-1::LL::mNG	MICOS	yes	0	0	0
CRLS-1::LL::mNG	CL Synthesis	yes	0	0	0
MTX-1::LL::mNG	Metaxin	yes	5	4	3
MTX-2::LL::mNG	Metaxin	yes	0	0	0

[a] NGM plates were seeded with 400 uL of E. coli OP50 from the same culture and 4 mid-L4s from each strain were picked onto each OP50 plate (in triplicate) and an intermediate NGM plate was used to avoid carrying over embryos/L1s/L2s. With every batch of experiments, wild-type N2 animals were also plated. Plates were checked twice a day and the time at which the food was depleted was reported (time to starvation). Numbers above indicates how much longer animals took to starve compared to wild-type. No strains starved faster than N2.

[b] Strains that are not homozygous fertile are balanced, and therefore not counted in this health assay

ETC - Electron Transport Chain; MICOS - Mitochondrial Contact Site and Cristae Organizing System; CL - Cardiolipin

bioRxiv preprint doi: https://doi.org/10.1101/2025.05.02.651978; this version posted May 3, 2025. The copyright holder for this preprint (which was not certified by peer review) is the author/funder. All rights reserved. No reuse allowed without permission.

Table S4 - Mitochondrial Import and Cristae Screen

Human Gene	Role	RNAi Condition	Sequence ID	Decreased AC NUO-1 enrichment[a]	n	p-value[b]
n/a	n/a	n/a	empty vector	1.2%	165	n/a
TOMM40	Import	*tomm-40*	C18E9.6	73.3%	30	<0.0001
TOMM70	Import	*tomm-70*	ZK370.8	46.7%	30	<0.0001
TOMM20	Import	*tomm-20*	F23H12.2	73.3%	15	<0.0001
TIMM23	Import	*timm-23*	F15D3.7	80.0%	15	<0.0001
APOOL	MICOS	*moma-1*	K02F3.10	6.7%	15	0.2309
MICOS13	MICOS	*W04C9.2*	W04C9.2	20.0%	15	0.0043
CHCHD3	MICOS	*chch-3*	M176.3	0.0%	15	>0.9999
MICOS10	MICOS	*F54A3.5*	F54A3.5	6.7%	15	0.2309
DNAJC11	MICOS	*dnj-9*	F11G11.7	40.0%	30	<0.0001
IMMT	MICOS	*F36D4.6*	F36D4.6	20.0%	15	0.0043
IMMT	MICOS	*immt-2*	W06H3.1	26.7%	15	0.0004
SAMM50	MICOS	*gop-3*	C34E10.1	0.0%	15	>0.9999
IMMT	MICOS	*immt-1*	T14G11.3	33.3%	30	<0.0001
SYNJ2BP	MICOS	*mics-1*	T21C9.1	33.3%	30	<0.0001
CRLS1	CL Synthesis	*crls-1*	F23H11.9	33.3%	30	<0.0001

[a] Decreased enrichment scored by eye on fluorescent compound microscope. If AC was not distinguishable from other uterine cells by NUO-1::mNG fluorescence intensity, then it was scored as having decreased NUO-1 enrichment

[b] One-way ANOVA with Tukey's post hoc test for multiple comparisons

MICOS - Mitochondrial Contact Site and Cristae Organizing System; CL - Cardiolipin

bioRxiv preprint doi: https://doi.org/10.1101/2025.05.02.651978; this version posted May 3, 2025. The copyright holder for this preprint (which was not certified by peer review) is the author/funder. All rights reserved. No reuse allowed without permission.

Primer type	Amplicon	Oligonucleotide Sequence (5' → 3')	Template
Forward	*nuo-1 sgRNA*	tcctattgcgagatgtcttggatctgcttggctccctgctgtttt agagctagaaatagc	pDD122
Forward	*nuo-1 5' homology arm*	gcatacattatacgaagttattttcagggagccggatcttga aggccgttttagtgtttg	N2 genomic DNA
Reverse	*nuo-1 5' homology arm*	cccgatgctcctgaggcacccgatgcacctgaggcacctt gactaatttgtttcgcgcct	N2 genomic DNA
Forward	*nuo-1 3' homology arm*	tcatctgatcgtacatgtagttgcatgcaaagcggccgctg gagctccagcttttgttcc	N2 genomic DNA
Reverse	*nuo-1 3' homology arm*	ggaacaaaagctggagctccagcggccgctttgcatgca actacatgtacgatcagatga	N2 genomic DNA
Forward	*nuo-1 genotyping*	cttttctgcatctccggtcaa	qy143[nuo-1::mNG] genomic DNA
Reverse	*nuo-1 genotyping*	cgtcgtcgtagaagatcacac	qy143[nuo-1::mNG] genomic DNA
Forward	*nduv-2 sgRNA*	tcctattgcgagatgtcttggctgctcttaaataaacgctgttt tagagctagaaatagc	pDD122
Forward	*nduv-2 5' homology arm*	tacgactcactatagggcgaattgggtaccacaactagtc cttggtgaaatggtgatcaa	N2 genomic DNA
Reverse	*nduv-2 5' homology arm*	cccgatgctcctgaggcacccgatgcacctgaggcacctt taagagcagcttgcaaaccg	N2 genomic DNA
Forward	*nduv-2 3' homology arm*	gcatacattatacgaagttattttcagggagccggatcttaa acgcttggacatgcttga	N2 genomic DNA
Reverse	*nduv-2 3' homology arm*	ggaacaaaagctggagctccagcggccgctttgcatgcg agagcactaatagcttgtggt	N2 genomic DNA
Forward	*nduv-2 genotyping*	agatgtcgttggcatcgaacgt	qy174[nduv-2::mNG] genomic DNA
Reverse	*nduv-2 genotyping*	cttgatcggtggtgatagctga	qy174[nduv-2::mNG] genomic DNA
Forward	*nduf-7 sgRNA*	tcctattgcgagatgtcttggtaagcgagaagctcaacttgt tttagagctagaaatagc	pDD122
Forward	*nduf-7 5' homology arm*	tacgactcactatagggcgaattgggtaccacaactagta cagtaaccaacaaaatggca	N2 genomic DNA
Reverse	*nduf-7 5' homology arm*	cccgatgctcctgaggcacccgatgcacctgaggcaccg cgtctgtaccatagctgtgcc	N2 genomic DNA
Forward	*nduf-7 3' homology arm*	gcatacattatacgaagttattttcagggagccggatcttaa acagaacacgaggcgaaa	N2 genomic DNA
Reverse	*nduf-7 3' homology arm*	ggaacaaaagctggagctccagcggccgctttgcatgcg ttccgtgtggatttcccaatt	N2 genomic DNA

bioRxiv preprint doi: https://doi.org/10.1101/2025.05.02.651978; this version posted May 3, 2025. The copyright holder for this preprint (which was not certified by peer review) is the author/funder. All rights reserved. No reuse allowed without permission.

Forward	*nduf-7 genotyping*	gccgatttgattttcgttgccg	qy170[nduf-7::mNG] genomic DNA
Reverse	*nduf-7 genotyping*	ggcgaatttgaatggtccagt	qy170[nduf-7::mNG] genomic DNA
Forward	*nuo-6 sgRNA*	tcctattgcgagatgtcttgcgattagaagtcgattccgagtttagagctagaaatagc	pDD122
Forward	*nuo-6 5′ homology arm*	tacgactcactatagggcgaattgggtaccacaactagtatgaagttggcattaagactt	N2 genomic DNA
Reverse	*nuo-6 5′ homology arm*	cccgatgctcctgaggcacccgatgcacctgaggcaccgtcgattccgatggttggagca	N2 genomic DNA
Forward	*nuo-6 3′ homology arm*	gcatacattatacgaagttattttcagggagccggatctttctaatcgtctcgatctatc	N2 genomic DNA
Reverse	*nuo-6 3′ homology arm*	ggaacaaaagctggagctccagcggccgctttgcatgctgcatcaagtcaagttttcaaa	N2 genomic DNA
Forward	*nuo-6 genotyping*	acaaggcgctgttgcgaaata	qy131[nuo-6::mNG] genomic DNA
Reverse	*nuo-6 genotyping*	tgcttcacttatgcgagctc	qy131[nuo-6::mNG] genomic DNA
Forward	*sdhb-1 sgRNA*	tcctattgcgagatgtcttgatctctccgatggccttagcgttttagagctagaaatagc	pDD122
Forward	*sdhb-1 5′ homology arm*	tacgactcactatagggcgaattgggtaccacaactagttgatcttgaccaatgcggaac	N2 genomic DNA
Reverse	*sdhb-1 5′ homology arm*	tcccgatgctcctgaggcacccgatgcacctgaggcacctggcttcgatgtgaatccagt	N2 genomic DNA
Forward	*sdhb-1 3′ homology arm*	agcatacattatacgaagttattttcagggagccggatctgccgctgagccatcagcattt	N2 genomic DNA
Reverse	*sdhb-1 3′ homology arm*	agggaacaaaagctggagctccagcggccgctttgcatgctgcgccaaaactacagtacc	N2 genomic DNA
Forward	*sdhb-1 genotyping*	aactgatgatgtagccgccaag	qy144[sdhb-1::mNG] genomic DNA
Reverse	*sdhb-1 genotyping*	cagtgaaagtgcgtgtagga	qy144[sdhb-1::mNG] genomic DNA
Forward	*mev-1 sgRNA*	tcctattgcgagatgtcttgcaagagcaacaagactgcctgttttagagctagaaatagc	pDD122
Forward	*mev-1 5′ homology arm*	tacgactcactatagggcgaattgggtaccacaactagtgctgtccatttggaagcaccc	N2 genomic DNA
Reverse	*mev-1 5′ homology arm*	cccgatgctcctgaggcacccgatgcacctgaggcaccagctgtcttgttgctcttgttc	N2 genomic DNA

bioRxiv preprint doi: https://doi.org/10.1101/2025.05.02.651978; this version posted May 3, 2025. The copyright holder for this preprint (which was not certified by peer review) is the author/funder. All rights reserved. No reuse allowed without permission.

Forward	*mev-1 3′ homology arm*	gcatacattatacgaagttattttcagggagccggatcttag gcacagatgctccgcctt	N2 genomic DNA
Reverse	*mev-1 3′ homology arm*	ggaacaaaagctggagctccagcggccgctttgcatgct ctcccttaccaaacgtccata	N2 genomic DNA
Forward	*mev-1 genotyping*	tatccagacaaaccataggact	qy169[mev-1::mNG] genomic DNA
Reverse	*mev-1 genotyping*	gccgaacgagattagacctat	qy169[mev-1::mNG] genomic DNA
Forward	*ucr-2.1 sgRNA*	tcctattgcgagatgtcttgtttatagctcgtcgagatatgtttt agagctagaaatagc	pDD122
Forward	*ucr-2.1 5′ homology arm*	tacgactcactatagggcgaattgggtaccacaactagta gctaaatattttggaggaga	N2 genomic DNA
Reverse	*ucr-2.1 5′ homology arm*	cccgatgctcctgaggcacccgatgcacctgaggcacctt cgtccagatatgggacgagt	N2 genomic DNA
Forward	*ucr-2.1 3′ homology arm*	gcatacattatacgaagttattttcagggagccggatctcta taaattgttacaagtttt	N2 genomic DNA
Reverse	*ucr-2.1 3′ homology arm*	ggaacaaaagctggagctccagcggccgctttgcatgctt ggaatgtaagatcacgggtc	N2 genomic DNA
Forward	*ucr-2.1 genotyping*	tcagaaggaacgactcgttg	qy92[ucr-2.1::mNG] genomic DNA
Reverse	*ucr-2.1 genotyping*	cgaaagtagaatgctagtcaag	qy92[ucr-2.1::mNG] genomic DNA
Forward	*isp-1 sgRNA*	tcctattgcgagatgtcttgttagctcgatccaatgacgagtt ttagagctagaaatagc	pDD122
Forward	*isp-1 5′ homology arm*	tacgactcactatagggcgaattgggtaccacaactagttt tccaggctatggcagctga	N2 genomic DNA
Reverse	*isp-1 5′ homology arm*	cccgatgctcctgaggcacccgatgcacctgaggcacca atgacgatggtggcatccttg	N2 genomic DNA
Forward	*isp-1 3′ homology arm*	gcatacattatacgaagttattttcagggagccggatctgg atcgagctaaatattcaga	N2 genomic DNA
Reverse	*isp-1 3′ homology arm*	ggaacaaaagctggagctccagcggccgctttgcatgcc gtgaaacttacgaaaatgtgt	N2 genomic DNA
Forward	*isp-1 genotyping*	ctctttgagctcgtgccgcaga	qy133[isp-1::mNG] genomic DNA
Reverse	*isp-1 genotyping*	cacaaagatagaactcctccag	qy133[isp-1::mNG] genomic DNA
Forward	*cyc-1 sgRNA*	tcctattgcgagatgtcttgcaagggaagagagccacca agttttagagctagaaatagc	pDD122

bioRxiv preprint doi: https://doi.org/10.1101/2025.05.02.651978; this version posted May 3, 2025. The copyright holder for this preprint (which was not certified by peer review) is the author/funder. All rights reserved. No reuse allowed without permission.

Forward	*cyc-1 5′ homology arm*	tacgactcactatagggcgaattgggtaccacaactagtt gtacgacgtggatacgaagt	N2 genomic DNA
Reverse	*cyc-1 5′ homology arm*	cccgatgctcctgaggcacccgatgcacctgaggcaccc tgagctttaggaggttcccta	N2 genomic DNA
Forward	*cyc-1 3′ homology arm*	gcatacattatacgaagttattttcagggagccggatcttaa tcaccagctttccgctat	N2 genomic DNA
Reverse	*cyc-1 3′ homology arm*	ggaacaaaagctggagctccagcggccgctttgcatgct cgaaacatgatctttggcgtc	N2 genomic DNA
Forward	*cyc-1 genotyping*	aatgcagcgtgccgtggttcaa	qy176[cyc-1::mNG] genomic DNA
Reverse	*cyc-1 genotyping*	aggatatggacatgttacagc	qy176[cyc-1::mNG] genomic DNA
Forward	*cox-4 sgRNA*	tcctattgcgagatgtcttgttctcgtaatcgtagtgtgtgtttta gagctagaaatagc	pDD122
Forward	*cox-4 5′ homology arm*	tacgactcactatagggcgaattgggtaccacaactagtc cgtgtgttctgttgtttgtt	N2 genomic DNA
Reverse	*cox-4 5′ homology arm*	cccgatgctcctgaggcacccgatgcacctgaggcaccc ttccacttcttgttttcatag	N2 genomic DNA
Forward	*cox-4 3′ homology arm*	gcatacattatacgaagttattttcagggagccggatcttaa aatatagagattcagcag	N2 genomic DNA
Reverse	*cox-4 3′ homology arm*	ggaacaaaagctggagctccagcggccgctttgcatgcc gctgagcagattcaggttggc	N2 genomic DNA
Forward	*cox-4 genotyping*	cacgaagagagaacggtttttga	qy134[cox-4::mNG] genomic DNA
Reverse	*cox-4 genotyping*	tcgactggaaactctcgaaggt	qy134[cox-4::mNG] genomic DNA
Forward	*cox-5A sgRNA*	tcctattgcgagatgtcttgaagaagtggtacaaggactag ttttagagctagaaatagc	pDD122
Forward	*cox-5A 5′ homology arm*	tacgactcactatagggcgaattgggtaccacaactagta cacggtgacgacatcatgga	N2 genomic DNA
Reverse	*cox-5A 5′ homology arm*	cccgatgctcctgaggcacccgatgcacctgaggcacca atttggatatttgggtgtttg	N2 genomic DNA
Forward	*cox-5A 3′ homology arm*	gcatacattatacgaagttattttcagggagccggatcttaa attttccattctgcaaat	N2 genomic DNA
Reverse	*cox-5A 3′ homology arm*	ggaacaaaagctggagctccagcggccgctttgcatgca atgacacttccttctcgaatt	N2 genomic DNA
Forward	*cox-5A genotyping*	ggtaacatggcctcgttgacc	qy136[cox-5A::mNG] genomic DNA

bioRxiv preprint doi: https://doi.org/10.1101/2025.05.02.651978; this version posted May 3, 2025. The copyright holder for this preprint (which was not certified by peer review) is the author/funder. All rights reserved. No reuse allowed without permission.

Reverse	*cox-5A genotyping*	atattaggaggtctcagaggag	qy136[cox-5A::mNG] genomic DNA
Forward	*cox-5B sgRNA*	tcctattgcgagatgtcttgtgtttagatggattctgggtgtttt agagctagaaatagc	pDD122
Forward	*cox-5B 5′ homology arm*	tacgactcactatagggcgaattgggtaccacaactagtg tgtttcgtattgaggagcgt	N2 genomic DNA
Reverse	*cox-5B 5′ homology arm*	cccgatgctcctgaggcacccgatgcacctgaggcaccg atggattctgggtctgcgtcg	N2 genomic DNA
Forward	*cox-5B 3′ homology arm*	gcatacattatacgaagttattttcagggagccggatcttaa acaattttcaatgtagat	N2 genomic DNA
Reverse	*cox-5B 3′ homology arm*	ggaacaaaagctggagctccagcggccgctttgcatgcc gagacacacaaatactgagtt	N2 genomic DNA
Forward	*cox-5B genotyping*	tacagcatgtgtagacaacgag	qy137[cox-5B::mNG] genomic DNA
Reverse	*cox-5B genotyping*	aaagatgcgcacacagacaca	qy137[cox-5B::mNG] genomic DNA
Forward	*cox-6A sgRNA*	tcctattgcgagatgtcttgtcagcctcgaatccaactccgtt ttagagctagaaatagc	pDD122
Forward	*cox-6A 5′ homology arm*	tacgactcactatagggcgaattgggtaccacaactagttt ccaacgcaaatcctcagga	N2 genomic DNA
Reverse	*cox-6A 5′ homology arm*	cccgatgctcctgaggcacccgatgcacctgaggcaccg tgcttctcacgatctgcttca	N2 genomic DNA
Forward	*cox-6A 3′ homology arm*	gcatacattatacgaagttattttcagggagccggatcttaa acaatgctggacgataca	N2 genomic DNA
Reverse	*cox-6A 3′ homology arm*	ggaacaaaagctggagctccagcggccgctttgcatgcc ggaagtgagcatacaataaat	N2 genomic DNA
Forward	*cox-6A genotyping*	aaggtatccgacatgaaccgt	qy173[cox-6A::mNG] genomic DNA
Reverse	*cox-6A genotyping*	ccattcaagctttacagggttc	qy173[cox-6A::mNG] genomic DNA
Forward	*cox-10 sgRNA*	tcctattgcgagatgtcttggaacggctacaacaaaatgg gttttagagctagaaatagc	pDD122
Forward	*cox-10 5′ homology arm*	tacgactcactatagggcgaattgggtaccacaactagtc ggtaccgtatttttggagca	N2 genomic DNA
Reverse	*cox-10 5′ homology arm*	cccgatgctcctgaggcacccgatgcacctgaggcaccg ttgtagccgttctggaaaaaa	N2 genomic DNA
Forward	*cox-10 3′ homology arm*	gcatacattatacgaagttattttcagggagccggatctaa aatggtggattcggtgaag	N2 genomic DNA

bioRxiv preprint doi: https://doi.org/10.1101/2025.05.02.651978; this version posted May 3, 2025. The copyright holder for this preprint (which was not certified by peer review) is the author/funder. All rights reserved. No reuse allowed without permission.

Reverse	*cox-10 3′ homology arm*	ggaacaaaagctggagctccagcggccgctttgcatgcg gagctacaaagttggacatta	N2 genomic DNA
Forward	*cox-10 genotyping*	ggcactcacattttcgcgtta	qy141[cox-10::mNG] genomic DNA
Reverse	*cox-10 genotyping*	tgaagcgcgtctaacacgtt	qy141[cox-10::mNG] genomic DNA
Forward	*atp-4 sgRNA*	tcctattgcgagatgtcttgcttgagggcagcattacggggt tttagagctagaaatagc	pDD122
Forward	*atp-4 5′ homology arm*	tacgactcactatagggcgaattgggtaccacaactagtc aatcagtccgttctctttcg	N2 genomic DNA
Reverse	*atp-4 5′ homology arm*	cccgatgctcctgaggcacccgatgcacctgaggcacca gcattacgggcggcttgttcg	N2 genomic DNA
Forward	*atp-4 3′ homology arm*	gcatacattatacgaagttattttcagggagccggatctgc cctcaagcaataaatttaa	N2 genomic DNA
Reverse	*atp-4 3′ homology arm*	ggaacaaaagctggagctccagcggccgctttgcatgcc attcgaatcgaagaagttgca	N2 genomic DNA
Forward	*atp-4 genotyping*	attcaggtatgttccgcgcagtc	qy171[atp-4::mNG] genomic DNA
Reverse	*atp-4 genotyping*	cgctcaactcgagttccttct	qy171[atp-4::mNG] genomic DNA
Forward	*tomm-20 sgRNA*	tcctattgcgagatgtcttgacaccgacgacttggagtaag ttttagagctagaaatagc	pDD122
Forward	*tomm-20 5′ homology arm*	atacgactcactatagggcgaattgggtaccacaactagt acgctccagactacaaggac	N2 genomic DNA
Reverse	*tomm-20 5′ homology arm*	ctcccgatgctcctgaggcacccgatgcacctgaggcac cctccaagtcgtcggtgtcat	N2 genomic DNA
Forward	*tomm-20 3′ homology arm*	agcatacattatacgaagttattttcagggagccggatctta atggataatgatttaaaa	N2 genomic DNA
Reverse	*tomm-20 3′ homology arm*	agggaacaaaagctggagctccagcggccgctttgcatg cgtggtgcctaatttgaccga	N2 genomic DNA
Forward	*tomm-20 genotyping*	tcggctactgcatttacttcg	qy132[tomm-20::mNG] genomic DNA
Reverse	*tomm-20 genotyping*	gagcttcctacaggcttgaa	qy132[tomm-20::mNG] genomic DNA
Forward	*crls-1 sgRNA*	ctattgcgagatgtcttgcgggactacagtatgccagtgtttt agagctagaaatagcaa	pDD122
Forward	*crls-1 5′ homology arm*	ctatagggcgaattgggtaccacaactagtctagacggct tcatcgctcgcaacgtaccc	N2 genomic DNA

bioRxiv preprint doi: https://doi.org/10.1101/2025.05.02.651978; this version posted May 3, 2025. The copyright holder for this preprint (which was not certified by peer review) is the author/funder. All rights reserved. No reuse allowed without permission.

Reverse	*crls-1 5′ homology arm*	tcctgaggcacccgatgcacctgaggcaccaatttttttgatggcctttccgcttgcgtat	N2 genomic DNA
Forward	*crls-1 3′ homology arm*	atacgaagttattttcagggagccggatcttaattattatatgtttttcgctagactgtga	N2 genomic DNA
Reverse	*crls-1 3′ homology arm*	agctggagctccagcggccgctttgcatgcaattaaatttttgttttcaaaacttttcgg	N2 genomic DNA
Forward	*crls-1 genotyping*	agtcactaccaccggaagaacg	qy255[crls-1::mNG] genomic DNA
Reverse	*crls-1 genotyping*	cttggtttcggcactggtgtttc	qy255[crls-1::mNG] genomic DNA
Forward	*immt-1 sgRNA*	tcctattgcgagatgtcttgctaataagttgagcgaatcggttttagagctagaaatagc	pDD122
Forward	*immt-1 5′ homology arm*	atacgactcactatagggcgaattgggtaccacaactagtatcgatgagaacggaggaac	N2 genomic DNA
Reverse	*immt-1 5′ homology arm*	ctcccgatgctcctgaggcacccgatgcacctgaggcaccagttgagcgaatcgatgagacggc	N2 genomic DNA
Forward	*immt-1 3′ homology arm*	catacattatacgaagttattttcagggagccggatcttattagaacaattgattgtcttg	N2 genomic DNA
Reverse	*immt-1 3′ homology arm*	agggaacaaaagctggagctccagcggccgctttgcatgctgtgtgacacctattgcctc	N2 genomic DNA
Forward	*immt-1 genotyping*	gtcaatccagaagacgagtt	qy230[immt-1::mNG] genomic DNA
Reverse	*immt-1 genotyping*	atcgatgagaacggaggaac	qy230[immt-1::mNG] genomic DNA
Forward	*mtx-1 sgRNA*	cctcctattgcgagatgtcttggactgacacttgaatcagacgttttagagctagaaatagca	pDD122
Forward	*mtx-1 5′ homology arm*	aatacgactcactatagggcgaattgggtaccacaactagtcagacttcggtctcccaacta	N2 genomic DNA
Reverse	*mtx-1 5′ homology arm*	gctcccgatgctcctgaggcacccgatgcacctgaggcaccttgaatcagaccggtatgaatt	N2 genomic DNA
Forward	*mtx-1 3′ homology arm*	tagcatacattatacgaagttattttcagggagccggatctgtgtcagtcgaagaggagatc	N2 genomic DNA
Reverse	*mtx-1 3′ homology arm*	agggaacaaaagctggagctccagcggccgctttgcatgcatctttcttccttaaatgtatag	N2 genomic DNA
Forward	*mtx-1 genotyping*	atggaattacacatttggccg	qy217[mtx-1::mNG] genomic DNA
Reverse	*mtx-1 genotyping*	tgttgaggatctttcttcct	qy217[mtx-1::mNG] genomic DNA

bioRxiv preprint doi: https://doi.org/10.1101/2025.05.02.651978; this version posted May 3, 2025. The copyright holder for this preprint (which was not certified by peer review) is the author/funder. All rights reserved. No reuse allowed without permission.

Forward	*mtx-2 sgRNA*	tcctattgcgagatgtcttggaccaattgggttatcacccgtttagagctagaaatagc	pDD122
Forward	*mtx-2 5′ homology arm*	atacgactcactatagggcgaattgggtaccacaactagtactattcgtgcacagagcagg	N2 genomic DNA
Reverse	*mtx-2 5′ homology arm*	aggccatgttgtcctcctctcccttggagaccatgtggatctgaaaaagagcaaaaaagcgt	N2 genomic DNA
Forward	*mtx-2 3′ homology arm*	attttcagggagccggatcttcgacactcgagatgagcagctcaggggtgataacccaattggtcac	N2 genomic DNA
Reverse	*mtx-2 3′ homology arm*	agggaacaaaagctggagctccagcggccgctttgcatgcgatgttcgatcatcgaaatatt	N2 genomic DNA
Forward	*mtx-2 genotyping*	ctacaatttgcctgccgatga	qy248[mtx-2::mNG] genomic DNA
Reverse	*mtx-2 genotyping*	tacctcgacagtggtaagaa	qy248[mtx-2::mNG] genomic DNA
Forward	*ttTi5605 MosSCI genotyping*	gtgtatctgcattaaccaat	qy148[lin-29p::2xmKate2::PLC(delta)PH::3xHA::tbb-2 3'UTR] genomic DNA

bioRxiv preprint doi: https://doi.org/10.1101/2025.05.02.651978; this version posted May 3, 2025. The copyright holder for this preprint (which was not certified by peer review) is the author/funder. All rights reserved. No reuse allowed without permission.

Forward	*ttTi4348 MosSCI genotyping*	gtgccatatctcactcggtt	qy120[eef-1A.1p::iATPSnFR1.0::unc-54 3'UTR]; qy121[eef-1A.1p::GFP::unc-54 3'UTR]; qy296 [eef-1A.1p::SL2::HYlight::tbb-2 3'UTR];qy312 [eef-1A.1p::SL2::HYlight-RA::tbb-2 3'UTR]; qy314 [lin-29p::UCP-4::SL2::mKate2::PLC(delta)PH::3xHA::tbb-2 3'UTR] qy275[nduv-2p::mNG::P2A::mKate2::unc-54 3'UTR]; qy316[nuo-1p::mNG::P2A::mKate2::unc-54 3'UTR]; qy218 [rpl-28p::tomm-20::mKate2::3xHA::unc-54 3'UTR]
Forward	*lin-29 promoter with pAP087 overhang*	tgtaaaacgacggccagtgcggccgccggtaggtatggagagttgg	pBS-lin-29-2b-GFP
Reverse	*lin-29 promoter with mKate2 overhang*	cttgatcaactcggaaaccatcgattgcgttgaagaagttggctt	pBS-lin-29-2b-GFP
Reverse	*mKate2 genotyping*	tggtttgggttccctcgtat	qy148[lin-29p::2xmKate2::PLC(delta)PH::3xHA::tbb-2 3'UTR] genomic DNA
Forward	*eef-1A.1 promoter*	acgttggcgtcgatcatcc	pPA088 ttTi4348 eef-1A.1::PercevalHR::unc-54 3'UTR
Reverse	*M13R*	caggaaacagctatgaccatg	pPA088 ttTi4348 eef-1A.1::PercevalHR::unc-54 3'UTR

bioRxiv preprint doi: https://doi.org/10.1101/2025.05.02.651978; this version posted May 3, 2025. The copyright holder for this preprint (which was not certified by peer review) is the author/funder. All rights reserved. No reuse allowed without permission.

Forward	*eef-1A.1 promoter with pAP088 overhang*	cgacggccagtaaagctagctttattgtcaacttccattg	pDD122
Reverse	*eef-1A.1 promoter with iATPSnFR1.0 overhang*	agacgtggatggtcttcattttgggcccctgctacggagtgagcaaagtg	pDD122
Forward	*iATPSnFR1.0 with eef-1A.1 promoter overhang*	ctcactccgtagcaggggcccaaaatgaagaccatccacg	ceIATPSnFR1.0
Reverse	*iATPSnFR1.0 with unc-54 3'UTR overhang*	ggtaatggtagcgaccggcgctcagttggcggccgcctacttcatctcggcgacggagag	ceIATPSnFR1.0
Reverse	*eef-1A.1p::iATPSnFR1.0 genotyping*	cttcatctcggcgacggagagacggtt	qy120[eef-1A.1p::iATPSnFR1.0] genomic DNA
Forward	*GFP with eef-1A.1 promoter overhang*	actttgctcactccgtagcaggggcccaaaatgagtaaaggagaagaact	pBS-lin-29-2b-GFP
Reverse	*GFP with unc-54 3'UTR overhang*	tagcgaccggcgctcagttggcggccgcctatttgtatagttcatccatgcc	pBS-lin-29-2b-GFP
Reverse	*eef-1A.1p::GFP genotyping*	tcaccctctccactgacaga	qy121[eef-1A.1p::GFP] genomic DNA
Forward	*SL2::HYlight(-RA) with eef-1A.1 overhang*	cagttgggaaacactttgcgcatgcgctgtctcat	DACR3882; DACR3883
Reverse	*SL2::HYlight(-RA) with tbb-2 3'UTR overhang*	atgcttgaaaggattttgcatttatcttaagtcatcctgactcatctcggaggagc	DACR3882; DACR3883
Reverse	*HYlight(-RA) genotyping*	gtgcttctcccagataaccatt	qy296 [eef-1A.1p::SL2::HYlight::tbb-2 3'UTR];qy312 [eef-1A.1p::SL2::HYlight-RA::tbb-2 3'UTR] genomic DNA
Forward	*ucp-4*	gatagcggagtgtcgttgtt	N2 genomic DNA
Reverse	*ucp-4*	ttgacggaagctcgcaac	N2 genomic DNA
Forward	*ucp-4 with lin-29 promoter overhang*	tcaagccaacttcttcaacgcaatcgatgtcatcagcagtcacaagtacg	ucp-4 PCR product
Reverse	*ucp-4 with SL2 overhang*	aggatgagacagcctagaaacttgaagcgc	ucp-4 PCR product
Forward	*SL2 with ucp-4 overhang*	gcgcttcaagtttctaggctgtctcatcct	pSA120
Reverse	*SL2 with mKate2 overhang*	gatcaactcggaaaccatcgatgatgcgttgaagcagtttccctg	pSA120

bioRxiv preprint doi: https://doi.org/10.1101/2025.05.02.651978; this version posted May 3, 2025. The copyright holder for this preprint (which was not certified by peer review) is the author/funder. All rights reserved. No reuse allowed without permission.

Reverse	*mKate2_627 genotyping*	ccttgattctcatggtctgag	qy314[lin-29p::ucp-4::SL2::mKate2_627::3xHA::tbb-2 3'UTR]; qy218 [rpl-28P::tomm-20::mKate2::3xHA::unc-54 3'UTR] genomic DNA
Forward	*rpl-28 promoter with pAP088 overhang*	gtaaaacgacggccagtgcggccgcgtttgtgcaacaaattgaggaaggc	pWZ290
Reverse	*rpl-28 promoter with tomm-20 overhang*	aagaattgtgtccgacatgcatgcgggatccacga	pWZ290
Forward	*tomm-20 with rpl-28 promoter overhang*	tcgtggatcccgcatgcatgtcggacacaattctt	N2 genomic DNA
Reverse	*tomm-20 with mKate2 overhang*	ttgatcaactcggaaaccatctccaagtcgtcggtgtcatcgataagctc	N2 genomic DNA
Forward	*nduv-2 promoter*	atcgagaagtggaataagagcaccag	N2 genomic DNA
Reverse	*nduv-2 promoter*	gaaggtatgggtgactacgctgtt	N2 genomic DNA
Forward	*nduv-2 promoter with pAP088 overhang*	tgtaaaacgacggccagtaaagctagcaattcaagaaaagtatattcggacctgactgaa	nduv-2 promoter PCR product
Reverse	*nduv-2 promoter with mNG overhang*	catgttgtcctcctctcccttggagaccatcttttgcaggccgatcaccctgaaaattgat	nduv-2 promoter PCR product
Forward	*P2A with mNG overhang*	aatggacgagctctacaagggagccggaggcgccaccaacttctccctgctgaagcaggc	pBS-LL-mNG-P2A-mKate2-SEC
Reverse	*mKate2 with unc-54 3' UTR overhang*	accggcgctcagttggcggccgcttaacggtgtccgagcttgg	pBS-LL-mNG-P2A-mKate2-SEC
Forward	*nuo-1 promoter*	tgttgtgttgcatgtcgtcgtg	N2 genomic DNA
Reverse	*nuo-1 promoter*	caactcctccgatcaagcat	N2 genomic DNA
Forward	*nuo-1 promoter with pAP088 overhang*	catcctgtaaaacgacggccagtaaagctagcgattaaacttggtaatat	nuo-1 promoter PCR product
Reverse	*nuo-1 promoter with mNG overhang*	tcctcctctcccttggagaccatcgatgccctgaaaaaaatagttgagataaat	nuo-1 promoter PCR product
Forward	*M13F*	tgtaaaacgacggccagt	RNAi plasmid DNA

bioRxiv preprint doi: https://doi.org/10.1101/2025.05.02.651978; this version posted May 3, 2025. The copyright holder for this preprint (which was not certified by peer review) is the author/funder. All rights reserved. No reuse allowed without permission.

Table S6. RNAi knockdown efficiency

Gene targeted	Strain genotype[a]	Treatment	Percent protein knockdown (%)	n[b]
ucr-2.1	*qy92[ucr-2.1::mNG] X*	*ucr-2.1 RNAi*	63.8	≥ 27
nuo-1	*qy143[nuo-1::mNG] II*	*nuo-1 RNAi*	93.7	≥ 13
nduv-2	*qy174[nduv-2::mNG] V*	*nduv-2 RNAi*	66.7	≥ 11
immt-1	qy230[immt-1::mNG] X	*immt-1 RNAi*	71.1	13
mtx-1	qy217[mtx-1::mNG] I	*mtx-1 RNAi*	83.5	≥ 14
mtx-2	qy248[mtx-2::mNG] III	*mtx-2 RNAi*	61.3	8

[a] All RNAi knockdown efficiency was performed using strains endogenously editted with

[b] Number of animals imaged in each condition